Final Report

Project Title: Main Group Element Chemistry in Service of Hydrogen Storage and Activation

Date of Report: September 2010

Recipient: The University of Alabama
Award Number: DE-FC36-05GO15059

Working Partners: The University of Alabama
Cost-Sharing Partners: The University of Alabama

Contacts: Prof. Anthony J. Arduengo
phone: 205-348-3556
fax: 205-348-4704
email: ajarduengo@worldnet.att.net
And Prof. David A. Dixon
phone: 205-348-8441
fax: 205-348-4704
email: dadixon@bama.ua.edu

DOE Managers: DOE HQ Technology Manager: Dr. Grace Ordaz, DOE Field Project Officer: James Alkire

Part of the DOE Center of Excellence in Chemical Hydrogen Storage

Executive Summary

Replacing combustion of carbon-based fuels with alternative energy sources that have minimal environmental impact is one of the grand scientific and technological challenges of the early 21st century. Not only is it critical to capture energy from new, renewable sources, it is also necessary to store the captured energy efficiently and effectively for use at the point of service when and where it is needed, which may not be collocated with the collection site. The energy from a wind turbine must be stored for use on days when there is low wind velocity. Likewise, solar energy must be collected and stored to cover periods (night, cloudy days, winter) when there is insufficient sunlight. There are many potential storage media but we focus on the storage of energy in chemical bonds. For example, the energy density for organic compounds is in the range of ~ 20 to ~40 MJ/L, which is about 100 times more than that for current batteries and a factor of about 1000 times more than capacitors per cycle. It is more efficient to store energy on a per weight basis in chemical bonds. This is because it is hard to pack electrons into small volumes with low weight without the use of chemical bonds. The focus of the project was the development of new chemistries to enable DOE to meet its technical objectives for hydrogen storage using chemical hydrogen storage systems. We provided computational chemistry support in terms of thermodynamics, kinetics, and properties prediction in support of the experimental efforts of the DOE Center of Excellence for Chemical Hydrogen Storage. The goal of the Center is to store energy in chemical bonds involving hydrogen atoms. Once the hydrogen is stored in a set of X-H/Y-H bonds, the hydrogen has to be easily released and the depleted fuel regenerated very efficiently. This differs substantially from our current use of fossil fuel energy sources where the reactant is converted to energy plus CO_2 (coal) or CO_2 and H_2O (gasoline, natural gas), which are released into the atmosphere. In future energy storage scenarios, the spent fuel will be captured and the energy storage medium regenerated. This places substantial additional constraints on the chemistry. The goal of the computational chemistry work was to reduce the time to design new materials and develop materials that meet the 2010 and 2015 DOE objectives in terms of weight percent, volume, release time, and regeneration ability. This goal was met in terms of reducing the number of costly experiments and helping to focus the experimental effort on the potentially optimal targets.

We have used computational chemistry approaches to predict the thermodynamic properties of a wide range of compounds containing boron, nitrogen, hydrogen, and other elements as appropriate including carbon. These calculations were done in most cases with high level molecular orbital theory methods that have small error bars on the order of ± 1 to 2 kcal/mol. The results were used to benchmark more approximate methods such as density functional theory for larger systems and for database development. We predicted reliable thermodynamics for thousands of compounds for release and regeneration schemes to aid/guide materials design and process design and simulation. These are the first reliable computed values for these compounds and for many represent the only available values. For example, the first set of accurate thermodynamics for $B_xN_xH_y$ compounds up to x = 3 and y = 14, including rings and chains which are critical intermediates in the release of hydrogen for release and regeneration of ammonia borane in the gas and condensed phases, was developed. Accurate bond energy calculations show that the driving force for the release of H_2 is the conversion of a weak Lewis acid-base donor acceptor B-N bond to a strong B-N sigma bond in contrast to the endothermic C-C to C=C conversion in hydrocarbons. We developed a method to predict heats of vaporization which can be used with our calculated gas phase heats of formation to give liquid heats of

formation. Our approach was shown to give good values when compared to known values. The predicted values have been used for process simulations by Dow Chemical. Significant advances in the reliable prediction of the thermodynamics of new hydrogen chemical hydrogen storage systems to help focus experimental efforts, for example, for $C_xB_yN_zH_{12}$ (x+y+z = 6) chemistries, were made. We predicted the energetics for methyl substituted amine-boranes for improved fuel properties (liquids) with improved thermochemistry. We studied amine exchange reactions for regeneration schemes. We developed a good model for the prediction of the thermodynamics of spent fuel for "BNH_2" through "BNH". Reliable estimates of maximum process efficiency in terms of thermodynamics were made. We have studied catalytic H_2 release processes and predicted orders of magnitude improvement in kinetics. We identified the potential role of BH_3 as a Lewis acid catalyst as well as the role of strong Brönsted and Lewis acids in a cationic chain polymerization mechanism for the release of H_2. This work has led to new understanding of alane chemistries for metal hydride regeneration schemes based on amine complexation where we have identified multiple transition states and new complexes. These studies have been extended to reactions of hydrazine as the reagent for the regeneration of spent fuel derived from ammonia borane. An extensive set of calculations for the thermodynamics of metal substituted $M/BH_2NH_3^-$ and $M/NH_2BH_3^-$ complexes for M = Li, Mg, Ca, Al, Si, C, P, N, Ti were completed. A range of Lewis acidities were calculated for the design of new regeneration reagents. Overall, the computational results have provided us with new insights into the chemistry of main group and organic-base chemical hydrogen systems from the release of hydrogen to the regeneration of spent fuel.

A number of experimental accomplishments were also made in this project. The experimental work on hydrogen storage materials centered on activated polarized σ- or π-bonded frameworks that hold the potential for ready dihydrogen activation, uptake, and eventually release. To this end, a large number of non-traditional valence systems including carbenes, cyanocarbons, and C-B and and B-N systems were synthesized and examined. During the course of these studies an important lead arose from the novel valency of a class of stable organic singlet bi-radical systems. A new coupled bis(imidazolium) dication was discovered that facilitated studies on hydrogen uptake and release from carbene and C-N systems in general. Work on hydrazine-networked triazine (cyanocarbon) polymers was initiated as a variant on our original cyanocarbon paradigm. This chemistry resembles that used in the synthesis of the structural polymer melamine suggesting that, if successful, hydrogen storage systems could also provide additional structural integrity to the automotive structural frame. A synthetic strategy to an "endless" hydrogen storage polymer has been developed based on our cyanocarbon chemistry. Cyclization to pure cyclopentamers and cyclohexamers has been accomplished. In addition to the carbene and cyanocarbon related systems, work on a diphosphacyclobutadiendiyl proved quite effective for hydrogen storage. A key issue with the synthetic efforts was being able to link the kinetics of release with the size of the substituents as it was difficult to develop a low molecular weight molecule with the right kinetics. A novel hydrogen activation process has been developed which showed that Lewis acid-base pairs need not be "frustrated" in their reactivity towards activating H_2. Reaction can occur at temperatures as low as -80 ºC. We established that the interaction of H_2 with the electrophile is a key step in the activation process. Electrophiles to replace the initial $Fe(CO)_5$ reactant such as BBr_3, $B(OCH_3)_3$, 1-bora-adamantane, and trityl cation reacting with an imidazolylidene nucleophile have been investigated.

Project Objective: The focus of the completed work was the development of new chemistries to enable DOE to meet the technical objective: "By 2010, develop and verify on-board hydrogen storage systems achieving 2 kWh/kg (6 wt%), 1.5 kWh/L, and $4/kWh.; by 2015, 3 kWh/kg (9 wt%), 2.7 kWh/L, and $2/kWh" by using chemical hydrogen storage systems. We:

- developed and implemented new organic -based H_2 activation chemistry;
- developed and implemented chemical systems based on polyhydrides of main group elements;
- developed and implemented cyanocarbon systems for H_2 storage; and
- provided computational chemistry support (thermodynamics, kinetics, properties prediction) to the experimental efforts of the DOE Center of Excellence for Chemical Hydrogen Storage to reduce the time to design new materials and develop materials that meet the 2010 and 2015 DOE objectives.

Background: To achieve our project objectives, we:

- used novel chemistry approaches to synthesize compounds for easily reversible addition/elimination of H_2 based on our novel, stable carbene and cyanocarbon chemistry;
- used first principles computational chemistry approaches on advanced computer architectures to predict the electronic structure of molecules to obtain thermodynamic and kinetic information in support of the design of hydrogen storage materials and of catalysts to effect easy release and addition of H_2; and
- developed a thermodynamic approach for chemical H_2 storage based on exploiting ΔH and ΔG coupled with Le Chatelier's principle to manage H_2 addition and release in chemical compounds, which is a potential approach for dealing with cold-start issues.

Closely coupled with our experimental work were detailed, high-level, theoretical modeling studies to understand the thermodynamics and kinetics in the systems and provide guidance and insight for innovation and identify new targets for investigation for the overall Center efforts. We explored new chemistries from hydrogen storage. We provided computational support for efforts in Tiers 1, 2, and 3 in terms of predictions of reaction energies, structures and spectral properties. The computational effort including the electronic infrastructure and web-sites supports the entire Center with special interactions with LANL, PNNL, UW, UPenn, UC-Davis, and U Missouri. There has been a specific focus on the design of novel regeneration approaches.

Ammonia-Borane and Isoelectronic Compounds Thermodynamics

Thermodynamic Properties of Molecular Borane Amines and the $[BH_4^-][NH_4^+]$ Salt for Chemical Hydrogen Storage Systems from Ab Initio Electronic Structure Theory

The heats of formation for the boron amines BH_3NH_3, BH_2NH_2, and HBNH, tetrahedral BH_4^-, and the BN molecule have been calculated by using *ab initio* molecular orbital theory. Coupled cluster calculations with single and double excitations and perturbative triples (CCSD(T)) were employed for the total valence electronic energies. Correlation consistent basis sets were used, up through the augmented quadruple zeta, to extrapolate to the complete basis set limit. Core/valence, scalar relativistic, and spin-orbit corrections were included in an additive fashion to predict the atomization energies. Geometries were calculated at the CCSD(T) level up through

at least aug-cc-pVTZ and frequencies were calculated at the CCSD(T)/aug-cc-pVDZ level. The heats of formation at 0K in the gas phase are $\Delta H_f(BH_3NH_3)$ = -10.2, $\Delta H_f(BH_2NH_2)$ = -17.0, $\Delta H_f(BHNH)$ = 12.5, $\Delta H_f(BN)$ = 145.3, and $\Delta H_f(BH_4^-)$ = -12.7 kcal/mol. The reported experimental value for $\Delta H_f(BN)$ is clearly in error. The heat of formation of the salt $[BH_4^-]NH_4^+]$ (s) has been estimated by using an empirical expression for the lattice energy and the calculated heats of formation of the two component ions.

Based on the calculated values, we can calculate the energy for the sequential release of H_2 from these molecules in the gas phase at 298 K in kcal/mol:

$BH_3NH_3 \rightarrow BH_2NH_2 + H_2$ $\Delta H = -5.1$ (1)

$BH_2NH_2 \rightarrow HBNH + H_2$ $\Delta H = 31.4$ (2)

$HBNH \rightarrow BN + H_2$ $\Delta H = 134.3$ (3)

Clearly, BH_3NH_3 will be a good source of H_2 as the release of H_2 from this species is not far from thermoneutral. For comparison, we list the energies of the following gas phase reactions based on hydrocarbons at 298 K in kcal/mol:

$C_2H_6 \rightarrow C_2H_4 + H_2$ $\Delta H = 32.6$ (4)

$C_2H_4 \rightarrow C_2H_2 + H_2$ $\Delta H = 42.0$ (5)

$C_2H_2 \rightarrow C_2 + H_2$ $\Delta H = 145.7$ (6)

Based on these results, it is clear that the C_2 gaseous hydrocarbons cannot release H_2. What is surprising is how close the reaction energies are for reactions of BH_2NH_2 and C_2H_4 and the reactions of BHNH and C_2H_2. This is a manifestation of similarity of the isoelectronic CCH_m and BNH_m systems.

Another possibility for an H_2 storage system is the salt $[BH_4^-][NH_4^+]$. We can estimate the lattice energy of the salt by using an empirical expression and we calculate the heat of formation using the obtained lattice energy and the heats of formation of the component ions using our standard total atomization energy approach. We note that the error bars for using are probably ±5 kcal/mol. The reaction from the ionic solid to the gas phase products:

$[BH_4^-]NH_4^+]$ (s) $\rightarrow BH_3NH_3 + H_2$ $\Delta H(0K) = 0.2$ (7)

is essentially thermoneutral and the salt would be a good source of H_2. The hydride affinity of BH_3 is calculated to be 72.2 kcal/mol in excellent agreement with the experimental value at 298K of 74.2 ± 2.8 kcal/mol.

Thermodynamic Properties of Molecular Borane Phosphines, Alane Amines, and Phosphine Alanes and the $[BH_4^-][PH_4^+]$, $[AlH_4^-][NH_4^+]$, and $[AlH_4^-][PH_4^+]$ Salts for Chemical Hydrogen Storage Systems from Ab Initio Electronic Structure Theory

The heats of formation for the molecules BH_3PH_3, BH_2PH_2, HBPH, AlH_3NH_3, AlH_2NH_2, HAlNH, AlH_3PH_3, AlH_2PH_2, HAlPH, AlH_4^-, PH_3, PH_4, and PH_4^+, as well as the diatomics BP, AlN, and AlP, have been calculated by using *ab initio* molecular orbital theory. The coupled cluster with single and double excitations and perturbative triples method (CCSD(T)) was employed for the total valence electronic energies. Correlation consistent basis sets were used, up through the augmented quadruple zeta, to extrapolate to the complete basis set limit. Additional d core functions were used for Al and P. Core-valence, scalar relativistic, and spin-orbit corrections were included in an additive fashion to predict the atomization energies. Geometries were calculated at the CCSD(T) level up through at least aug-cc-pVTZ and frequencies were calculated at the CCSD(T)/aug-cc-pVDZ level. The heats of formation of the

salts $[BH_4^-][PH_4^+](s)$, $[AlH_4^-][NH_4^+](s)$, and $[AlH_4^-][PH_4^+](s)$ have been estimated by using an empirical expression for the lattice energy and the calculated heats of formation of the two component ions.

Table 1. Calculated heats of Formation (kcal/mol) at 0K and 298K[a]

Molecule	**$\Delta H_f(0K)_{theory}$**	**$\Delta H_f(298K)_{theory}$**
$BP(^3\Pi)$[b]	134.1	134.6
$AlN(^3\Pi)$[c]	133.7	133.7
$AlN(^3\Sigma)$	133.5	133.5
$AlP(^3\Pi)$[d]	102.9	102.8
$AlP(^3\Sigma)$	102.7	102.6
HBPH (non-linear)	52.5	52.1
HAlNH (non-linear)	60.4	58.6
HAlPH (non-linear)	58.6	57.2
BH_2PH_2 (non-planar)	23.3	20.7
AlH_2NH_2 (planar)	-0.3	-3.3
AlH_2PH_2 (non-planar)	25.4	22.6
BH_3PH_3	7.5	3.3
AlH_3NH_3	-3.8	-8.3
AlH_3PH_3	21.1	17.0
AlH_3	31.9	30.3
AlH_4^-	-3.4	-5.9
PH_3	3.28	1.4
PH_4	50.5	47.7
PH_4^+	182.7	179.8

Using the calculated values, we can calculate the energy for the sequential release of H_2 from these molecules in the gas phase in kcal/mol at 298 K.

$AlH_3NH_3 \rightarrow AlH_2NH_2 + H_2$	$\Delta H = 5.0$	(8)
$AlH_2NH_2 \rightarrow HAlNH + H_2$	$\Delta H = 61.9$	(9)
$AlHNH \rightarrow AlN + H_2$	$\Delta H = 74.9$	(10)
$BH_3PH_3 \rightarrow BH_2PH_2 + H_2$	$\Delta H = 17.4$	(11)
$BH_2PH_2 \rightarrow HBPH + H_2$	$\Delta H = 31.4$	(12)
$BHPH \rightarrow BP + H_2$	$\Delta H = 82.5$	(13)
$AlH_3PH_3 \rightarrow AlH_2PH_2 + H_2$	$\Delta H = 9.7$	(14)
$AlH_2PH_2 \rightarrow HAlPH + H_2$	$\Delta H = 30.5$	(15)
$AlHPH \rightarrow AlP + H_2$	$\Delta H = 45.4$	(16)

Based simply on the value of ΔH, only the reaction involving AlH_3NH_3 might be a possible source for H_2 release as it is close to thermoneutral. However, one must also consider the values of the free energy. The formation of two gas phase products will lead to a substantial $T\Delta S$ term which will make H_2 generation more favorable. The values of S for each molecule were calculated and the values of $-T\Delta S$ at T = 298K for reactions indicate that the reaction for the dehydrogenation of AlH_3PH_3 can also serve as a potential source for H_2.

Another possibility for an H_2 storage system are the salts $[BH_4^-][PH_4^+]$, $[AlH_4^-]$ $[NH_4^+]$, and $[AlH_4^-][PH_4^+]$. We have predicted that the salt $[BH_4^-][NH_4^+]$ can readily release H_2 to form either solid or gaseous BH_3NH_3 exothermically. We can estimate the lattice energy of the salts from an empirical modeling equation by using the volumes found in an ion volum database. Use of these values in the lattice empirical equation gives lattice energies for $[BH_4^-][PH_4^+]$, $[AlH_4^-][NH_4^+]$, and $[AlH_4^-][PH_4^+]$ of 149.3, 150.7, and 148.9 kcal/mol respectively and calculated heats of formation of the salts at 0 K of 21.8, -0.5, and 30.4 kcal/mol respectively. We note that the error bars for using the equation are probably ±5 kcal/mol. The reaction energies starting from the ionic solid to form the gas phase products are in kcal/mol at 0 K:

$$[BH_4^-][PH_4^+]\ (s) \rightarrow BH_3PH_3 + H_2 \qquad \Delta H = -13.2 \qquad (17)$$

$$[AlH_4^-][NH_4^+]\ (s) \rightarrow AlH_3NH_3 + H_2 \qquad \Delta H = -3.3 \qquad (18)$$

$$[AlH_4^-][PH_4^+]\ (s) \rightarrow AlH_3PH_3 + H_2 \qquad \Delta H = -9.3 \qquad (19)$$

All of the reactions involving the salts releasing H_2 are predicted to be exothermic as found for $[BH_4^-][NH_4^+]$. Thus, they may serve as H_2 storage systems. The reaction starting from $[AlH_4^-][NH_4^+](s)$ is close to thermoneutral so this salt might be a good source of H_2 as it will be easier to manage the heat release.The hydride affinity of AlH_3 is calculated to be -70.4 kcal/mol at 298 K. The proton affinity of PH_3 is calculated to be 187.8 kcal/mol at 298 K in excellent agreement with the experimental value of 188 kcal/mol. PH_4 is calculated to be barely stable with respect to loss of a hydrogen atom to form PH_3.

σ- and π-Bond strengths in the Borane Amines

In order to better understand the chemistry of the isoelectronic borane amines in terms of their energetics and thermodynamic forces driving hydrogen release, we calculated the σ- and π-bond strengths for the molecules BH_2NH_2, BH_2PH_2, AlH_2NH_2, and AlH_2PH_2 by using ab initio molecular electronic structure theory at the CCSD(T)/CBS level plus additional core-valence, scalar relativist, and atomic spin orbit corrections.

Table 2. Donor σ-Bond Strengths in AH_3XH_3 Compounds in kcal/mol.

Molecule	σ-Bond Energy (0K)	σ-Bond Energy (298K)
H_3BNH_3	25.9	27.2
H_3AlNH_3	26.1	27.3
H_3BPH_3	21.1	22.5
H_3AlPH_3	14.0	14.7

Table 3. Calculated Heats of Formation (kcal/mol) at 0K and 298K

Molecule	$\Delta H_f(0K)_{theory}$	$\Delta H_f(298K)_{theory}$
BH_2	77.3	77.5
AlH_2	63.7	63.0
PH_2	32.7	31.8
BH_2NH_2 (rot)	12.9	10.0
BH_2NH_2 (rot-planar)	16.8	13.9
BH_2PH_2 (rot)	32.5	29.6
BH_2PH_2 (rot-planar)	65.6	62.7
AlH_2NH_2 (rot)	10.2	7.1

AlH_2NH_2 (rot-planar)	10.6	7.2
AlH_2PH_2 (rot)	28.1	24.8
AlH_2PH_2 (rot-planar)	49.6	46.2
BH_2NH_2 (G.S. C_{2v})	-17.0	-19.7
AlH_2NH_2 (G.S. C_{2v})	-0.3	-3.3
BH_2PH_2 (G.S. C_s)	23.3	20.7
BH_2PH_2 (planar C_{2v})	29.9	27.1
AlH_2PH_2 (G.S. C_s)	25.4	22.6
AlH_2PH_2 (planar C_{2v})	35.4	32.2

The adiabatic π-bond energy is defined as the rotation barrier between the equilibrium ground state configuration and the C_s symmetry transition state for torsion about the A-X bond. We calculated instrinsic π-bond energies corresponding to the adiabatic rotation barrier corrected for the inversion barrier at N or P. The adiabatic σ-bond energy is defined as the dissociation energy of AH_2XH_2 to AH_2 + XH_2 in their ground states minus the adiabatic π-bond energy. The adiabatic σ-bond strengths for the molecules BH_2NH_2, BH_2PH_2, AlH_2NH_2, and AlH_2PH_2 are 109.8, 98.9, 77.6, and 68.4 kcal/mol, respectively, and the corresponding adiabatic π-bond strengths are 29.9, 10.4, 9.4, and 2.6 kcal/mol, respectively.

Table 4. Rotation Barriers (π-bond energies) and Inversion Barriers at N or P in kcal/mol.

Molecule	**Rotation (G.S→C_s)**	**Rotation (C_{2v}→C_{2v})**	**Inversion (rotated)**
	Adiabatic	**Inherent**	
$H_2B{=}NH_2$	29.9	33.8	3.9
$H_2Al{=}NH_2$	10.5	10.9	0.4
$H_2B{=}PH_2$	9.2	35.7	33.1
$H_2Al{=}PH_2$	2.7	14.2	21.5

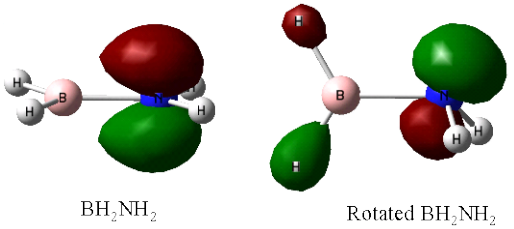

Figure 1. HOMO for the ground state and rotated structures of BH_2NH_2.

The adiabatic σ-bond strengths are substantial consistent with the formation of an sp^2-sp^2 bond and the π-bond strengths are weak consistent with them being a dative π-bond. This shows that the driving force in the H_2 elimination reactions in AH_3XH_3 (A = Group IIIA and X = Group VA) compounds is the strength of the σ-bond that is formed in AH_2XH_2 as compared to the weak donor σ-bond in AH_3XH_3. The dative π-bond orbitals are shown in Figure 1.

Table 5. AH_2-H and XH_2-H σ-Bond Energies in kcal/mol

Molecule	**Adiabatic σ-Bond Energy**
BH_3	103.7
NH_3	106.5
AlH_3	83.4
PH_3	81.0

Comparison of the AH_3 and XH_3 bond energies with the A-B adiabatic σ-bond energies incicate that the X-H bond energies track the A-B bond energies. The σ-bond energy in BH_2NH_2 is larger than the N-H bond energy in NH_3 by only 3 kcal/mol. The σ-bond energy in AlH_2NH_2 is 8 kcal/mol less than the N-H bond energy in NH_3. For $BH_2{=}PH_2$ and $AlH_2{=}PH_2$, the σ-bond

energies are 3 and 13 kcal/mol less than the P-H bond energy in PH_3, essentially the same trend found in comparing the σ-bond energies in BH_2=NH_2 and AlH_2=NH_2 with the N-H bond energy in NH_3. The bonding in these compounds is much closer to that in a normal NH_2R or PH_2R compound with a dative π-bond from N or P.

The bond energies for the H_2AXH_2 compounds provide us with some useful insights into the differences in the donor-acceptor chemistry and covalent bond carbon-based chemistry. The elimination reaction (4) for loss of H_2 from BH_3NH_3 in the gas phase is exothermic (reaction (1) whereas the comparable organic reaction (4) is substantially endothermic. This difference in energetic requirements for H_2 release is due to the fact that a weak B-N dative σ-bond is broken in BH_3NH_3 and a strong sp^2-sp^2 σ-bond is formed in BH_2NH_2 whereas a strong σ-bond is broken in C_2H_6 and a σ-bond of comparable strength to that in BH_2NH_2 is formed in C_2H_4. Even though the adiabatic π-bond energy of BH_2NH_2 is only 30 kcal/mol as compared to the value of 65 kcal/mol in C_2H_4, the difference of 35 kcal/mol is much smaller than the difference of 63 kcal/mol for the σ-bond strengths in BH_3NH_3 and C_2H_6. Thus, the difference in the reactant σ-bond strengths is more important than the differences in the product π-bond strengths because of the strength of the σ-bonds in the product are comparable.

The Lowest Energy States of the Group IIIA–Group VA Heteronuclear Diatomics: BN, BP, AlN, and AlP from Full Configuration Interaction Calculations

In addition, the bonding and lowest energy states in the Group IIIA-Group VA diatomic molecules BN, BP, AlN, and AlP have been studied to benchmark computational methods. Full configuration interaction (CI) calculations on these diatomics been performed with the cc-pVTZ correlation-consistent basis set and compared to CCSD(T) calculations with the same basis set.

Table 6. State Energy Differences (kcal/mol) at the CCSD(T) and Full CI levels with the cc-pVTZ Basis Set.

Molecule	**ΔE(CCSD(T))**	**ΔE(Full CI)**	**T_1(CCSD(T))**
BN($^3\Pi$)	0.0	0.0	0.0368
BN($^3\Sigma^-$)	26.23	26.68	0.0158
BN($^1\Sigma^+$)	-0.50	0.94	0.0762
BP($^3\Pi$)	0.0	0.0	0.0311
BP($^3\Sigma^-$)	19.18	19.50	0.0198
BP($^1\Sigma^+$)	7.97	7.74	0.0402
AlN($^3\Pi$)	0.0	0.0	0.0689
AlN($^3\Sigma^-$)	-1.07	0.11	0.0154
AlN($^1\Sigma^+$)	10.36	12.10	0.1227
AlP($^3\Pi$)	1.64	1.09	0.0312
AlP($^3\Sigma^-$)	0.0	0.0	0.0147
AlP($^1\Sigma^+$)	14.05	13.06	0.0472

The CCSD(T) calculations are good to better than 1 kcal/mol in comparison with the full CI results if the T_1 diagnostic is small and to within about 2 kcal/mol if the T_1 diagnostic is large. Inspection of the T_2 amplitudes shows that the simple T_1 diagnostic is providing useful insight into the quality of the starting wavefunction. The ground state of BN, BP, and AlN is predicted

to be the $^3\Pi$ and for AlP, the ground state is predicted to be the $^3\Sigma^-$. For all molecules except BP, there is an excited state within 1.1 kcal/mol of the ground state. The ordering of the state energies can be explained in terms of simple orbital and bonding models. The results provide little evidence for placing the π orbital below the σ orbital for the ground state of these heteronuclear diatomic molecules.

Table 7. Electronic Dissociation Energies D_e in kcal/mol

Molecule	**D_e(CCSD(T))**	**D_e(Full CI)**
BN($^3\Pi$)	97.14	97.81
BP($^3\Pi$)	71.01	71.63
AlN($^3\Pi$)	51.29	52.59
AlP($^3\Sigma^-$)	46.90	46.96

The valence electronic dissociation energies with the cc-pVTZ basis set for the diatomic ground state at the full CI level are given in Table 7. The CCSD(T) values are always lower than the full CI values and with this basis set, the electronic contribution to the dissociation energy is still 5 to 6 kcal/mol away from the CBS limit, indicating the importance of the extrapolation..

Fundamental Thermochemical Properties of Ammonia Borane and Dehydrogenated Derivatives (BNH_n, n = 0 – 6)

One of our goals is to probe further the reaction thermodynamics of the H_2-release from BNH_n materials. Apart from a literature G2 prediction of the proton affinity of BH_3NH_3, other basic thermochemical parameters of BNH_n compounds such as the ionization energies, electron affinities, basicities and acidities are not available. We have performed high accuracy electronic structure calculations at the CCSD(T)/CBS level plus additional core-valence, scalar relativistic, and atomic spin orbit corrections to evaluate the missing quantities. The calculated heats of formation are given in Table 8.

Table 8. Heats of Formation at 0 and 298 K (in kcal/mol) of BNH_x (x = 0-7) Ionic Species.

Structure	**ΔH_{0K}**	**ΔH_{298K}**
BN^+ ($^4\Sigma$)	407.4	408.2
BN ($^3\Pi$)[a]	145.3	
BN^- ($^2\Sigma$)	72.2	72.9
NBH^+ ($^1\Sigma^+$)	381.5	381.4
BNH^+ ($^1\Sigma^+$)	344.9	345.0
BNH^- ($^1\Sigma$)	30.0	30.4
NBH^- ($^1\Sigma^+$)	19.3	19.3
$BHNH^+$ ($^2\Pi$)	355.4	354.8
BHNH ($^1\Sigma$)[a]	12.5	11.7
$BHNH^-$ ($^2A'$)	41.3	40.5
$BHNH_2^+$ ($^1A_1$)	196.0	194.3
$BHNH_2^-$ ($^1A'$)	38.4	36.6
BH_2NH^- ($^1A'$)	-3.7	-5.6
$BH_2NH_2^+$ ($^2B_1$)	227.8	225.5
BH_2NH_2 ($^1A_1$)[a]	-17.0	-19.7

$BH_2NH_2^-$ ($^2A_1$)	-7.6	-10.4
$BH_2NH_3^+$ ($^1A'$)	168.9	165.6
$BH_3NH_2^-$ ($^1A'$)	-19.8	-23.2
$BH_3NH_3^+$ ($^2A''$)	204.0	199.7
BH_3NH_3 ($^1A_1$)[a]	-10.2	-14.6
$BH_3NH_3^-$ ($^2A_1$)	-9.4	-13.8
$BH_4NH_3^+$ ($^1A'$)	164.3	159.0

[a] Obtained from ΣD_0 values and the new value for the heat of formation of B, 135.1 ± 0.02 kcal/mol.

Table 9. Calculated EA in eV at 0 K for the BNH_n (n = 0 – 6) Species.

Molecule	**EA**
BN	3.17
BNH	1.82
NBH	3.14
HBNH	-1.25
$HBNH_2$	-0.10/-0.07[a]
H_2BNH	2.03
H_2BNH_2	-0.41
H_3BNH_2	2.25
H_2BNH_3	-0.05/0.07[a]
H_3BNH_3	-0.03/0.08[a]

[a] Calculated with double diffuse functions on B and N.

The BN diatomic as well as the radical species of the closed shell molecules for breaking B-H and N-H bonds have a positive electron affinity; the other molecules will not bind an electron. The closed shell BNH_n molecules, except for H_3BNH_3 (double diffuse functions on B and N required), do not bind an electron and behave as nitrogen acids and bases.

Table 10. Calculated Hydride Affinities in kcal/mol at 0 K for the BNH_n (n = 0 – 6) Species.

Reaction	**(0 K)**
$BN + H^- \rightarrow NBH^-$	160.3
$BN + H^- \rightarrow BNH^-$	149.5
$BNH + H^- \rightarrow HBNH + e^-$	93.6
$NBH + H^- \rightarrow HBNH + e^-$	113.4
$HBNH + H^- \rightarrow H_2BNH^-$	50.4
$HBNH + H^- \rightarrow HBNH_2 + e^-$	10.7
$HBNH_2 + H^- \rightarrow H_2BNH_2 + e^-$	87.2
$H_2BNH + H^- \rightarrow H_2BNH_2 + e^-$	94.4
$H_2BNH_2 + H^- \rightarrow H_3BNH_2^-$	37.0
$H_2BNH_2 + H^- \rightarrow H_2BNH_3^-$	-20.2
$H_2BNH_3 + H^- \rightarrow H_3BNH_3^-$	84.9
$H_3BNH_2 + H^- \rightarrow H_3BNH_3^-$	78.4

We also calculated the various hydride affinities of the molecules defined as –ΔH of the reaction for addition of the hydride anion. In some cases, the addition of the hydride anion produces

anions that do not bind an electron and we estimate the hydride affinity as leading to the neutral product plus an electron.

Table 11. Calculated Adiabatic Ionization Potentials in eV at 0 K for the BNH_n (n = 0 – 6) Species.

Molecule	IE	Expt.
BN	11.37	
BNH	11.85	
NBH	12.56	
HBNH	11.27	
$HBNH_2$	6.94	
H_2BNH	6.63	
H_2BNH_2	10.62	11.0 ± 0.1[a]
H_2BNH_3	5.65	
H_3BNH_3	9.29	9.44 ± 0.02[b]

[a] Kwon, C. T.; McGee, H. A., Jr., *Inorg. Chem.*, **1970**, *9*, 2458.
[b] Lloyd, D. R.; Lynaugh, N., *J. Chem. Soc. Faraday Trans. 2*, **1972**, *68*, 947.

The IP of BH_3NH_3 is almost 1 eV lower than IP(NH_3) = 10.17 eV and in good agreement with the experimental values as well. The IP of BH_2NH_2 also shows good agreement with the reported experimental value. The closed shell BNH_n species exhibit ionization energies similar or smaller than those of hydrocarbons, and for the H_2BNH radical, its ionization energy is close to that of the alkali elements.

Table 12. Calculated Proton Affinities in kcal/mol at 298 K for the BNH_n (n = 0 – 6) Species.

Reaction	(298K)
$BN + H^+ \rightarrow NBH^+$	130.4
$BN + H^+ \rightarrow BNH^+$	166.5
$BNH + H^+ \rightarrow HBNH^+$	165.8
$NBH + H^+ \rightarrow HBNH^+$	185.4
$HBNH + H^+ \rightarrow HBNH_2^+$	183.1
$HBNH_2 + H^+ \rightarrow H_2BNH_2^+$	174.5
$H_2BNH + H^+ \rightarrow H_2BNH_2^+$	182.3
$H_2BNH_2 + H^+ \rightarrow H_2BNH_3^+$	180.4
$H_2BNH_3 + H^+ \rightarrow H_3BNH_3^+$	201.3
$H_3BNH_2 + H^+ \rightarrow H_3BNH_3^+$	194.8
$H_3BNH_3 + H^+ \rightarrow H_4BNH_3^+$	192.1

The proton affinities of HBNH, BH_2NH_2, and BH_3NH_3 are modest but higher than that of PA(H_2O) = 165.1 kcal/mol and below the value of 203.5 kcal/mol for PA(NH_3).

Table 13. Calculated Adiabatic Bond Dissociation Energies in kcal/mol at 0 and 298 K for the BNH_n (n = 0 – 6) Species.

Reaction	0 K	298 K
$HBN \rightarrow BN + H$	105.2	106.5
$BNH \rightarrow BN + H$	125.0	126.1

$HBNH \rightarrow BNH + H$	111.0	112.4
$HBNH \rightarrow HBN + H$	130.8	132.0
$H_2BNH \rightarrow HBNH + H$	20.9	21.7
$HBNH_2 \rightarrow HBNH + H$	28.1	29.5
$H_2BNH_2 \rightarrow HBNH_2 + H$	104.6	106.1
$H_2BNH_2 \rightarrow H_2BNH + H$	111.8	113.9
$H_3BNH_2 \rightarrow H_2BNH_2 + H$	2.4	3.6
$H_2BNH_3 \rightarrow H_2BNH_2 + H$	-4.1	-2.9
$H_3BNH_3 \rightarrow H_2BNH_3 + H$	100.5	102.0
$H_3BNH_3 \rightarrow H_3BNH_2 + H$	94.0	95.5

Except for H_3BNH_3, the NH bonds are systematically stronger than the BH bonds, and the BDE(NH) values tend to increase with the increasing multiple character of the BN bonds. Trends and comparisons between properties obtained through reactions on the N and B atoms are given. Comparisons with properties of hydrocarbons show similarities and differences between the two isoelectronic series.

Table 14. Calculated Acidities in kcal/mol at 0 and 298 K for the BNH_n (n = 0 – 6) Species.

Reaction	**(0 K)**	**(298 K)**
$HBN \rightarrow BN^- + H^+$	345.6	346.9
$BNH \rightarrow BN^- + H^+$	365.4	366.5
$HBNH \rightarrow BNH^- + H^+$	382.7	384.4
$HBNH \rightarrow NBH^- + H^+$	371.9	373.2
$H_2BNH \rightarrow HBNH + H^+ + e^-$	334.5	335.3
$HBNH_2 \rightarrow HBNH + H^+ + e^-$	341.7	343.1
$H_2BNH_2 \rightarrow HBNH_2 + H^+ + e^-$	418.2	419.7
$H_2BNH_2 \rightarrow H_2BNH^- + H^+$	378.5	379.8
$H_3BNH_2 \rightarrow H_2BNH_2 + H^+ + e^-$	316.0	317.2
$H_2BNH_3 \rightarrow H_2BNH_2 + H^+ + e^-$	309.5	310.7
$H_3BNH_3 \rightarrow H_2BNH_3^- + H^+$	412.7	414.1
$H_3BNH_3 \rightarrow H_3BNH_2^- + H^+$	355.5	357.0

The acidities (energy to remove a H^+) at N are surprisingly low, especially for BH_3NH_3 as compared to a value of 403.4 kcal/mol for NH_3. Thus BH_3NH_3 is a modest gas phase acid in contrast to NH_3 being a very weak acid. Protonation of H_3BNH_3 leads to nearly spontaneous H_2 release.

Heats of Formation of the $B_xN_xH_y$ Compounds and Reaction Thermodynamic Predictions

In collaboration with D. Camaioni, PNNL, the heats of formation of B-N compounds with two or three B and N atoms were calculated at a high level (CCSD(T)). G3MP2 calculations were also performed for comparison. The heats of formation (kcal/mol) are given in the Table 15. The G3(MP2) values are clearly not as accurate as the CCSD(T)/CBS values.

Table 15. Gas phase Heats of Formation at 0 K and 298 K (kcal/mol) and Entropies at 298 K (cal/mol·K).

Molecule	ΔH_f(0 K) CCSD(T)	ΔH_f(298 K) CCSD(T)	ΔH_f(0 K) G3MP2	ΔH_f(298 K) G3MP2[a]	S (298 K)[b,c]
1	-10.2	-14.6	-7.4	-11.7	57.15
2a	-88.6	-99.9	-82.6	-93.5 (-102.2)	79.31
2b	-87.6	-98.8	-81.4	-92.4 (-101.9)	76.71
3	-112.6	-118.8	-106.5	-112.4 (-122.4)	68.73
4	-48.6	-55.8	-43.9	-50.9 (-57.4)	67.16
5	-83.1	-90.8	-77.3	-84.8	75.77
6	-67.4	-75.1	-61.8	-69.2 (-77.7)	75.61
7	-79.2	-88.6	-73.3	-82.5	78.58
8a	-29.6	-37.5	-24.0	-31.7	77.52
8b	-41.4	-49.8	-35.6	-43.7	74.19
9a	-51.8	-63.2	-43.8	-54.9	97.97
9b	-75.4	-87.6	-67.0	-78.7	87.16
10	-39.4	-46.1	-36.0	-42.1	70.48
11	-55.9	-66.1	-47.9	-57.8	88.79
12	-34.4	-43.5	-28.6	-37.2	83.38[d]
13	22.1	17.1	27.7	23.3	81.35
14	-87.9	-94.5	-81.1	-87.5	84.11
BH_2NH_2	-17.0	-19.7	-15.1	-17.8 (-20.8)	55.92

[a] G3B3 values in parentheses. [b] MP2/cc-pVTZ values. [c] $S(H_2)$ = 31.13 cal/mol·K. [d] From MP2/aVTZ calculation.

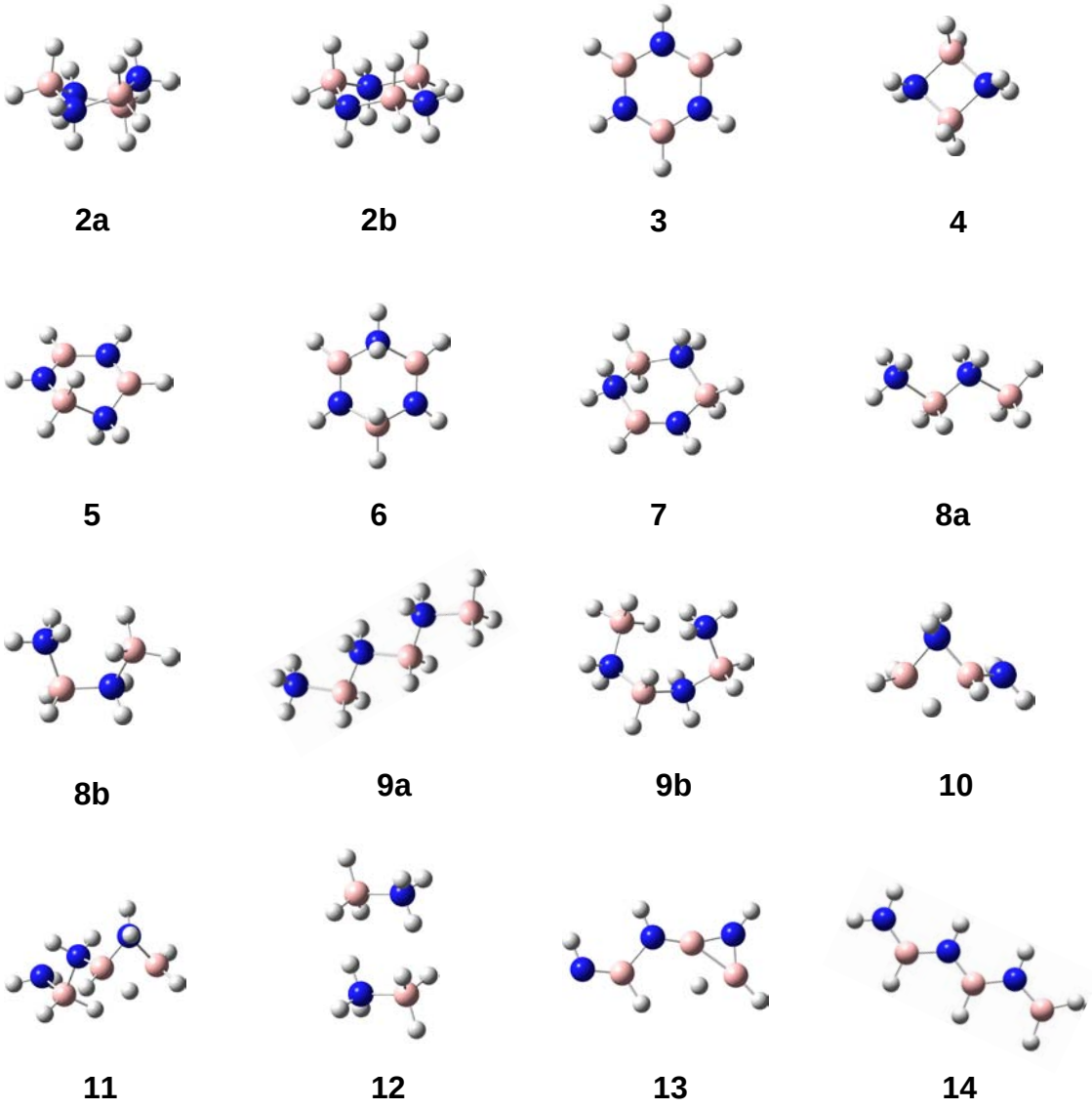

From high accuracy heats of formation, we calculated the heats of reaction for the hydrogen elimination of a number of BN compounds. We show here all the favorable results, as well as the bond energies for some BN cyclic compounds.

Table 16. Hydrogen Elimination Reaction Energetics (kcal/mol)

Reaction	**Δ*H*(298 K)**	**Δ*G*(298 K)**
$2BH_3NH_3 \rightarrow c\text{-}B_2N_2H_8 + 2H_2$	-22.8	-31.1
$3BH_3NH_3 \rightarrow c\text{-}B_3N_3H_{12}$ (twist-boat) + $3H_2$	-50.5	-50.8
$c\text{-}B_3N_3H_{12}$ (twist-boat) $\rightarrow c\text{-}B_3N_3H_6 + 3H_2$	-18.7	-43.3
$2BH_3NH_3 \rightarrow BH_3NH_2BH_2NH_3$ (twist) + H_2	-16.9	-14.2
$3BH_3NH_3 \rightarrow BH_3(NH_2BH_2)_2NH_3$ (twist) + $2H_2$	-38.2	-31.7
$BH_2(NHBH)_2NH_2 \rightarrow c\text{-}B_3N_3H_6 + H_2$	-24.2	-28.9
$BH_3(NH_2BH_2)_2NH_3$ (twist) $\rightarrow c\text{-}B_3N_3H_{12}$ (twist-boat)+ H_2	-12.2	-19.2
$BH_3NH_2BH_2NH_3$ (twist) $\rightarrow c\text{-}B_2N_2H_8 + H_2$	-5.9	-13.1

$3BH_2NH_2 \rightarrow c\text{-}B_3N_3H_6 + 3H_2$	-59.5	-57.8
$3BH_2NH_2 \rightarrow BH_2(NHBH)_2NH_2 + 2H_2$	-35.2	-28.9
$3BH_2NH_2 \rightarrow c\text{-}5,6\text{-}B_3N_3H_8 + 2H_2$	-31.5	-22.7
$BH_3NH_3 \rightarrow BH_2NH_2 + H_2$	-3.2	-12.1
$c\text{-}5,6\text{-}B_3N_3H_8 \rightarrow c\text{-}B_3N_3H_6 + H_2$	-27.9	-35.1
$c\text{-}1,4\text{-}B_3N_3H_8 \rightarrow c\text{-}B_3N_3H_6 + H_2$	-43.6	-50.9
$c\text{-}B_3N_3H_{10} \rightarrow c\text{-}B_3N_3H_6 + 2H_2$	-30.0	-45.7
$c\text{-}B_3N_3H_{10} \rightarrow c\text{-}5,6\text{-}B_3N_3H_8 + H_2$	-2.1	-10.6
$(BH_3NH_3)_2$ (dimer) $\rightarrow c\text{-}B_2N_2H_8 + 2H_2$	-12.1	-25.9
$(BH_3NH_3)_2$ (dimer) $\rightarrow BH_3NH_2BH_2NH_3$ (twist) + H_2	-6.2	-12.8

We have calculated for the first time critical B-N bond energies in kcal/mol as shown below.

BN Dissociation for Cyclotriborazane

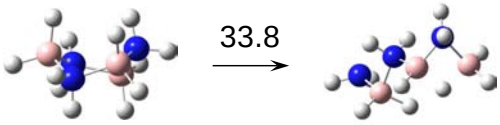

BN Dissociation for 1,2-dihydroborazine

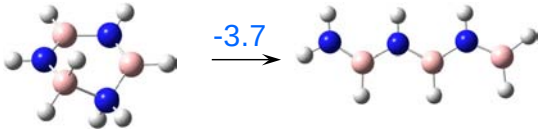

BN Dissociation for Cyclodiborazane

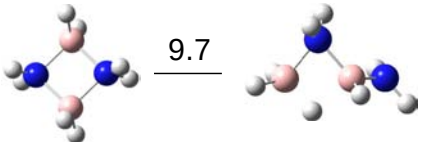

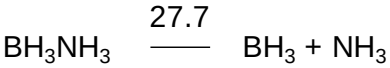

BN Dissociation for Borazine

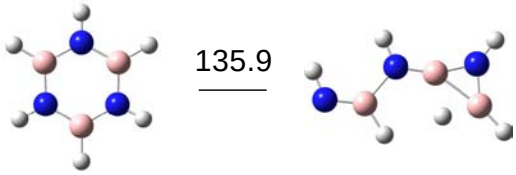

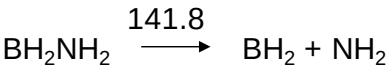

The G3MP2 heats of formation for the isoelectronic cyclic molecules $(BHPH)_3$, $(BH_2PH_2)_3$, $(AlHNH)_3$, $(AlH_2NH_2)_3$, $(AlHPH)_3$, and $(AlH_2PH_2)_3$ as well as for BH_3NH_3, BH_3PH_3, AlH_3NH_3, and AlH_3PH_3. The following reaction energies at 298K in kcal/mol were obtained:

$3BH_3NH_3 \rightarrow c\text{-}(BH_2NH_2)_3 + 3H_2$	ΔH= -49.5	(20)
$c\text{-}(BH_2NH_2)_3 \rightarrow c\text{-}(BHNH)_3 + 3H_2$	ΔH= -20.9	(21)
$3BH_3PH_3 \rightarrow c\text{-}(BH_2PH_2)_3 + 3H_2$	ΔH= -36.4	(22)
$c\text{-}(BH_2PH_2)_3 \rightarrow c\text{-}(BHPH)_3 + 3H_2$	ΔH= 60.6	(23)
$3AlH_3NH_3 \rightarrow c\text{-}(AlH_2NH_2)_3 + 3H_2$	ΔH= -47.2	(24)
$c\text{-}(AlH_2NH_2)_3 \rightarrow c\text{-}(AlHNH)_3 + 3H_2$	ΔH= 20.8	(25)
$3AlH_3PH_3 \rightarrow c\text{-}(AlH_2PH_2)_3 + 3H_2$	ΔH= -80.3	(26)
$c\text{-}(AlH_2PH_2)_3 \rightarrow c\text{-}(AlHPH)_3 + 3H_2$	ΔH= 28.7	(27)

Thus the heteroatom chemistry can clearly be different from the ammonia borane chemistry, especially in the second step.

Hydrogen Release Mechanisms

We have performed computational studies of the mechanism of dehydrogenation of ammonia borane based on forming polymers rather than ring structures in collaboration with the experimental efforts of the LANL group. We focused on the reaction thermodynamics at the B3LYP/DGDZVP2 level; MP2/cc-pVDZ and cc-pVTZ calculations have been obtained to benchmark the DFT results. The reaction energies are shown below. The reaction proceeds by abstraction of an H^- from BH_2NH_3 to form the cation. The reaction then proceeds to form a cluster where a hydrogen atom from a BH3 from a new BH_3NH_3 is shared to with the cation to form a B--H--B bond. All energies given below are in kcal/mol. The first ΔH value is the DFT value; if there is a 2nd value it is the MP2/cc-pVTZ value.

$BH_2NH_3^+ + BH_3NH_3 \rightarrow NH_3BH_2\text{---}H\text{---}BH_2NH_3^+$ ΔH = -45.6, -47.7 (28)

The cluster loses H_2 and rearranges to form a species with a BHB and a $B(NH_2)^+B$ bridging 3-center bonds.

$NH_3BH_2\text{---}H\text{---}BH_2NH_3^+ \rightarrow H_2B\text{-}NH_2\text{-}BHNH_3^+ + H_2$ ΔH = 0.2, -2.1 (29)

H

At this point, two different reaction paths were followed and path (31) is more exothermic:

$H_2B\text{-}NH_2\text{-}BHNH_3^+ + BH_3NH_3 \rightarrow BH_3NH_2BHNH_2$ ΔH = -9.2 (30)

H $NH_3BH_2\text{---}H$

$H_2B\text{-}NH_2\text{-}BHNH_3^+ + BH_3NH_3 \rightarrow BH_2NH_2BH_2NH_3$ ΔH = -23.4 (31)

H $H\text{---}BH_2NH_3$

Both paths involve opening up the bridge bond and forming the B-H-B cluster bridge bond. From paths (30) and (31) we can proceed through different intermediates with BHB and $B(NH_2)^+B$ three center bonds as above. Only the second sets of reactions are exothermic, and thus the most exothermic path proceeds through (2.1).

$BH_3NH_2BHNH_2 \rightarrow BH_3NH_2BH\text{-}NH_2\text{-}BHNH_3^+ + H_2$ ΔH = 10.6 (30.1)

$NH_3BH_2\text{---}H$ H

$BH_3NH_2BHNH_2 \rightarrow BH_3NH_2BH\text{-}NH_2\text{-}BH_2^+ + H_2$ ΔH = 4.8 (30.2)

$NH_3BH_2\text{---}H$ H_3N H

$BH_2NH_2BH_2NH_3 \rightarrow NH_3BH_2NH_2BH\text{-}NH_2\text{-}BH_2^+ + H_2$ ΔH = -6.0 (31.1)

$H\text{---}BH_2NH_3$ H

$BH_2NH_2BH_2NH_3 \rightarrow NH_3BH\text{-}NHBH_2NH_3^+ + H_2$ ΔH = -1.8 (31.2)

$H\text{---}BH_2NH_3$ $H\text{----}BH_2$

The amineborane products of reactions (30.1), (30.2), (31.1) and (31.2) have BHB and $B(NH_2)^+B$ bridging 3-center bonds. Geometries starting from linear structures relaxed to the ones shown and no linear structures were found.

^{11}B nmr chemical shifts were calculated and used to explain the observed values. The values are consistent with the predicted structures with bridging 3-center, 2-electron bonds as found in B_2H_6. The ^{1}H, ^{11}B, and ^{15}N NMR shifts of the following aminoborane polymers and alkoxy boron compounds were calculated at the B3LYP level relatve to the standards boron trifluoride etherate ($BF_3O(CH_2CH_3)_2$) , nitromethane (CH_3NO_2), and tetramethylsilane ($Si(CH_3)_4$) for B, N, and H respectively. The compounds studied are: $BH_2NH_2CH_2^+$, $CH_3NHBH_2BH_2NH_2CH_3^+$, $CH_3NHBH_2BH_2NHCH_3BH_2CH_3^+$, B_2H_6, $H_3B(OCH_3)^-$. $H_2B(OCH_3)_2^-$, $HB(OCH3)_3$, $B(OCH_3)_4^-$, $NH_3BH_2O(CH_2CH_3)_2^+$, $NH_3BH_2NH_2BH_2O(CH_2CH_3)_2^+$, $HSi(CH_3)_3$, and $(OCH_3)Si(CH_3)_3$. In terms of the ^{11}B NMR shifts in the aminoborane polymers, there was a decrease in shift from δ = 70.6 in $BH_2NH_2CH_2^+$ to δ = -21 and -19 in the dimer $CH_3NHBH_2BH_2NH_2CH_3^+$.

The LANL group has developed a simple, unique chemical process for releasing hydrogen from ammonia-borane, where small amounts of an acid initiate the formation of non-volatile oligomeric products. Reaction of strong Lewis or Brønsted acids with ammonia-borane resulted in evolution of H_2 by a dehydropolymerization mechanism. We have used computations based on density functional theory to develop a mechanism as shown below. We predict that metastable linear oligomers are preferentially formed instead of cyclic or branched products. This is consistent with the experimental results. We have also shown that the growing cations form a bridge bond and that the resulting predicted chemical shift is in agreement with the observed value confirming the assignments. The high energy of the initial step is dramatically lowered when the energy of the interaction with the anion is included. The ^{11}B chemical shifts are predicted to be -19.0 and -22.1 ppm for the 1st compound shown below and -22.0, -19.1 and -9.7 ppm for the 2nd compound with the last value for the non-bridging boron.

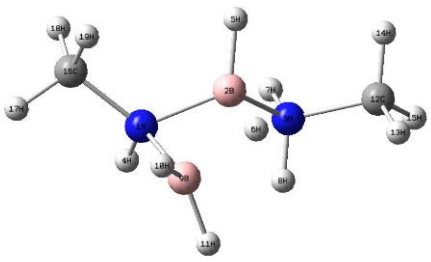

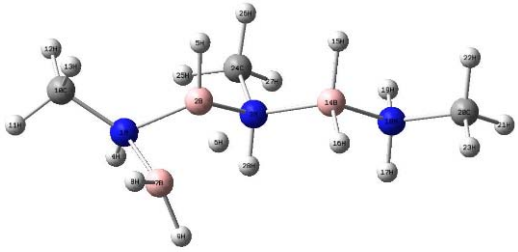

The energies in kcal/mol to abstract a hydride in the gas phase for a number of Lewis acids are shown below.

$BH_3NH_3 + BH_3 \rightarrow BH_2NH_3^+ + BH_4^-$	$\Delta E = 139.3$	(32)
$BH_3NH_3 + H_2SO_4 \rightarrow BH_2NH_3^+ + H_2SO_3^-$	$\Delta E = 124.0$	(33)
$BH_3NH_3 + CF_3SO_3H \rightarrow BH_2NH_3^+ + CF_3SO_3^-$	$\Delta E = 115.4$	(34)
$BH_3NH_3 + B(Ph)_3 \rightarrow BH_2NH_3^+ + B(Ph)_3H^-$	$\Delta E = 139.3$	(35)
$BH_3NH_3 + B(PhF_5)_3 \rightarrow BH_2NH_3^+ + B(PhF_5)_3H^-$	$\Delta E = 100.4$	(36)

Including the lattice energy leads to the formation of a salt, which is equivalent to an ion-pairing interaction, we obtain the following reaction energies in kcal/mol:

$BH_3NH_3 + BH_3 \rightarrow BH_2NH_3^+/BH_4^-$	$\Delta H = 0.5$	(37)

$BH_3NH_3 + B(Ph)_3 \rightarrow BH_2NH_3^+/B(Ph)_3H^-$ $\Delta H = 38.1$ (38)
$BH_3NH_3 + B(PhF_5)_3 \rightarrow BH_2NH_3^+/B(PhF_5)_3H^-$ $\Delta H = 1.6$ (39)
$BH_3NH_3 + H_2SO_4 \rightarrow BH_2NH_3^+/H_2SO_3^-$ $\Delta H = -7.0$ (40)
$BH_3NH_3 + CF_3SO_3H \rightarrow BH_2NH_3^+/CF_3SO_3^-$ $\Delta H = -9.6$ (41)

Clearly, the $B(C_6F_5))_3$ used experimentally is a good choice as they are potentially strong acids.

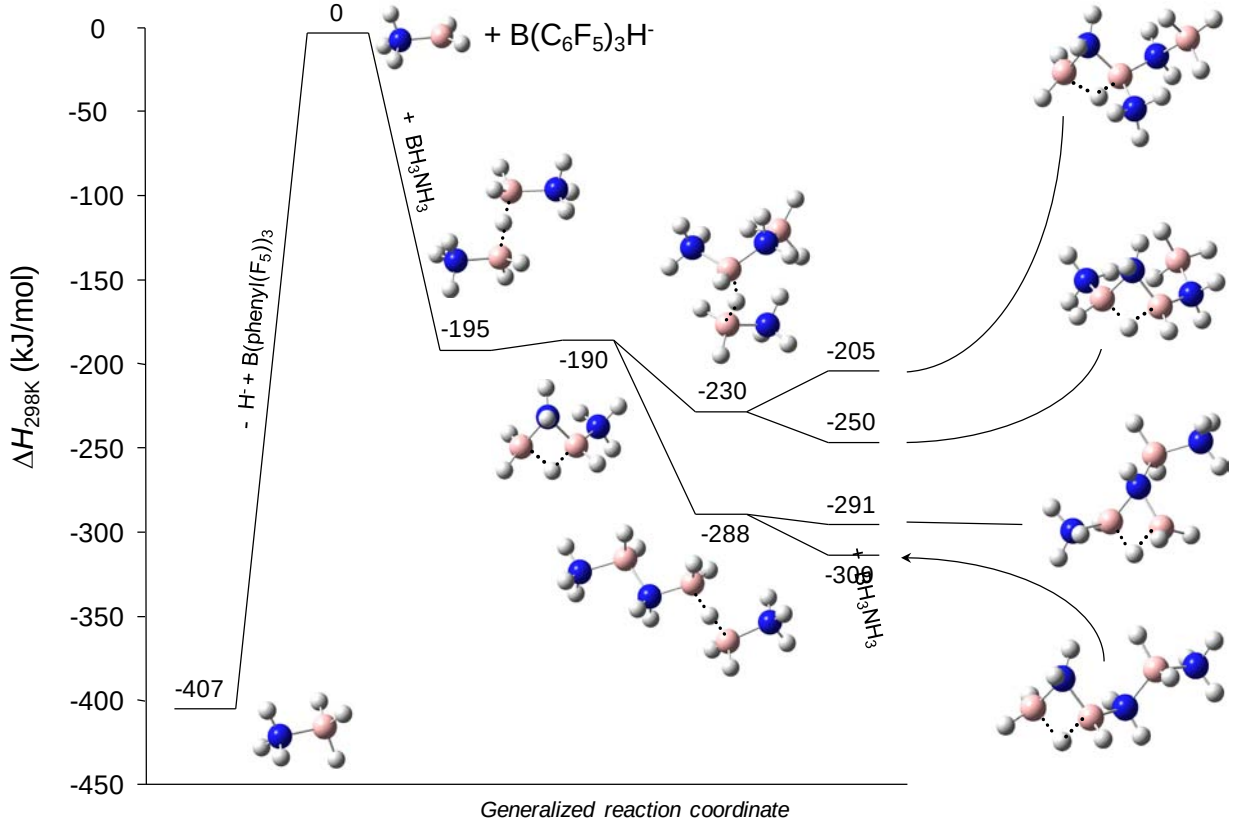

Figure 2. Energy level diagram. Calculated relative energies (kJ/mol) of the B-N species: **1** (-412); **a** (0); **b** (-191); **c** (-190); **d1** (-229); **d2** (-288); **e1** (-185); **e2** (-209); **e3** (-295);

We have calculated the energies of several B-N chains at the G3MP2 level at 0K, and obtain the enthalpies (kcal/mol) for the following reactions:

$BH_3NH_2BH_2NH_2BH_2NH_3 \rightarrow BH_2NH_2BH_2NH_2BH_2NH_2$ (bridge) + H_2 $\Delta E = -5.3$ (42)
$BH_3NH_2BH_2NH_2BH_2NH_3 \rightarrow BH_2NHBHNHBHNH_2 + 3H_2$ $\Delta E = -40.8$ (43)
$BH_3NH_2BH_2NH_2BH_2NH_3 \rightarrow BHNHBHNHBHNH + 4H_2$ $\Delta E = 66.8$ (44)
$BH_2NH_2BH_2NH_2BH_2NH_2$ (bridge) $\rightarrow BH_2NHBHNHBHNH_2 + 2H_2$ $\Delta E = -35.5$ (45)
$BH_2NH_2BH_2NH_2BH_2NH_2$ (bridge) $\rightarrow BHNHBHNHBHNH + 3H_2$ $\Delta E = 72.1$ (46)
$BH_2NHBHNHBHNH_2 \rightarrow BHNHBHNHBHNH$ (bridge) + H_2 $\Delta E = 107.6$ (47)

$BH_2NH_2BH_2NH_2BH_2NH_2$ without a bridging hydrogen, i.e., a linear structure, is a transition state with one imaginary frequency (87i), and is 17 kcal/mol above the bridge structure.

In addition, we predicted the energy differences between cyclic and non-cyclic B-N compounds at the B3LYP/DZVP2 level at 0K:

$BH_2NH_2BH_2NH_2$ (bridge) → c-$(BH_2NH_2)_2$	ΔE = -9.7	(48)
$BH_2NH_2BH_2NH_2BH_2NH_2$ (bridge) → c-$(BH_2NH_2)_3$	ΔE = -32.8 [-33.5]	(49)
$BH_2NH_2BH_2NH_2BH_2NH_2$ → c-$(BH_2NH_2)_3$	ΔE = -49.8	(50)

Boron-nitrogen cycles, $(BH_2NH_2)_n$, where n = 2 to 7, 9 and 13, were calculated by B3LYP/DZVP2 at 0K to obtain enthalpies for the following reactions (kcal/mol). The values in brackets correspond to the normalized values and the third value is the difference between that reaction and the next:

$2BH_3NH_3$ → c-$(BH_2NH_2)_2 + 2H_2$	ΔE = -26.9 [-13.4], 25.5	(51)
$3BH_3NH_3$ → c-$(BH_2NH_2)_3 + 3H_2$	ΔE = -52.3 [-14.5], 12.3	(52)
$4BH_3NH_3$ → c-$(BH_2NH_2)_4 + 4H_2$	ΔE = -64.6 [-16.2], 13.6	(53)
$5BH_3NH_3$ → c-$(BH_2NH_2)_5 + 5H_2$	ΔE = -78.2 [-15.6], 15.9	(54)
$6BH_3NH_3$ → c-$(BH_2NH_2)_6 + 6H_2$	ΔE = -94.1 [-15.7], 19.8	(55)
$7BH_3NH_3$ → c-$(BH_2NH_2)_7 + 7H_2$	ΔE = -113.9 [-16.3], 30.12	(56)
$9BH_3NH_3$ → c-$(BH_2NH_2)_9 + 9H_2$	ΔE = -144.0 [-16.0], 73.7	(57)
$13BH_3NH_3$ → c-$(BH_2NH_2)_{13} + 13H_2$	ΔE = -217.7 [-16.8]	(58)

Coordination of Aminoborane, NH_2BH_2, Dictates Selectivity and Extent of H_2 Release in Metal-catalysed Ammonia Borane Dehydrogenation

While aminodiborane, $B_2H_5(NH_2)$, has been observed as a minor by-product of metal-catalysed BH_3NH_3 (AB) dehydrogenations, discussion of product selectivity has focused on formation of borazine, PB, and the cyclic pentamer, $(BH_2NH_2)_5$. If AB dehydrogenation follows similar pathways as those observed for alkylamine-boranes, is monomeric aminoborane, NH_2BH_2, formed? Calculations at the B3LYP/DZVP2 level were performed to map out possible reaction pathways to address this question. A reaction scheme is shown in Figure 3. Previous work in our groups has shown that this level of calculation provides a semi-quantitative potential energy surface.

In complementary results to those found for BH_3 and AB, the initial reaction of NH_2BH_2 with AB can either weakly catalyze the unimolecular loss of H_2 from AB or the BH_2 of NH_2BH_2 interacts with AB in a complex transition state leading to loss of H_2 (TS-Hbond and TS-Hbond2. In both cases, two NH_2BH_2 molecules are formed and the chain structure $BH_3NH_2BHNH_2$ can only be formed by an unfavorable high-energy pathway (TSlew-NH2c). (There is a slightly higher energy structure where the BH_3 forms a bridging H to the BH group). The $BH_3NH_2BHNH_2$ chain can be generated in a slightly exothermic reaction by the dimerization of the two weakly interacting NH_2BH_2 with a low barrier of 10.5 kcal/mol. We found no evidence for formation of the other chain isomer $NH_3BH_2NHBH_2$ in the dimerization process even though it is only 2.3 kcal/mol higher in energy at the G3MP2 level. The $BH_3NH_2BHNH_2$ chain can then catalyze H_2 loss from AB leading to formation of NH_2BH_2 which subsequently adds to the chain $BH_3NH_2BHNH_2$ to form an NH_2BH_2 trimer with a BHB terminal bond with a low barrier of 5.0 kcal/mol. Finally, this trimer chain can rearrange in an exothermic process with a small barrier

(<6 kcal/mol) to form the ring compound $B_2N_2H_7NH_2BH_3$ (NH_2BH_3 side chain bonded to B) as observed. The other ring compound $B_2N_2H_7BH_2NH_3$ which is higher in energy (G3MP2 calculations: $\Delta\Delta H_{298}$ = 2.3 kcal/mol, $\Delta\Delta G_{298}$ = 2.7 kcal/mol) was never formed in any of our simulations. The H_2 elimination barriers that have been found so far for the isolated molecules are comparable to the B-N bond energy in BH_3NH_3 suggesting a potential role for solvent or coordination to the catalyst. These results are consistent with the DFT B3LYP/6-311+G(2d,p) calculations of Nutt and McKee. Further work is in progress to understand the detailed thermochemistry and reaction pathways of the final intermediate as well as more details on its generation. Reaction energies at the C3(MP2) level are summarized in Table 17.

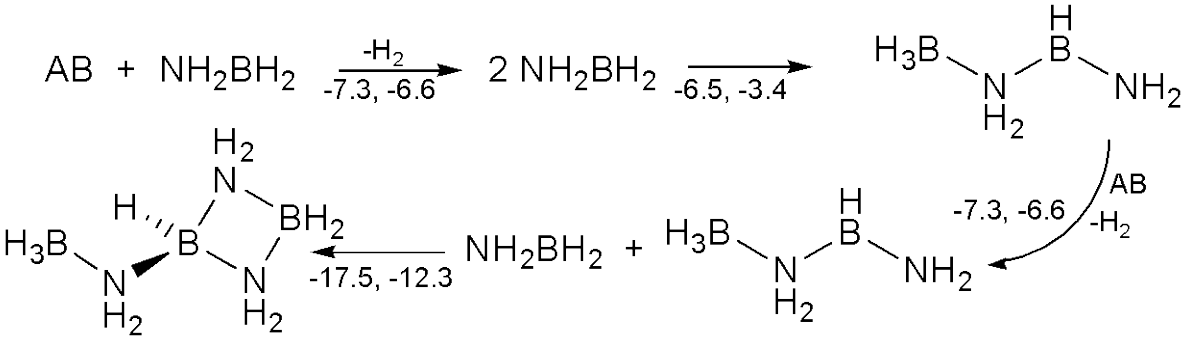

Figure 3. Trapping of NH_2BH_2 by AB. G3MP2, B3LYP/DZVP2 gas phase enthalpies at 298 K. The highly accurate CCSD(T)/CBS (complete basis set) result for the first step is -5.1 kcal/mol

Table 17. Reaction Enthalpies and Free Energies (298K) at the G3(MP2) Level in kcal/mol

	Reaction	**ΔH**	**ΔG**
1	$BH_3NH_3 + BH_2NH_2 \rightarrow NH_3BH_2NHBH_2 + H_2$	-11.5	-9.3
2	$BH_3NH_3 + BH_2NH_2 \rightarrow BH_3NH_2BHNH_2 + H_2$	-13.8	-11.5
3	$BH_3NH_2BHNH_2 \rightarrow BH_2H_bNH_2BHNH_2$	0.0	0.0
4	$NH_3BH_2NHBH_2 \rightarrow c\text{-}B_2N_2H_8$	-11.1	-8.4
5	$BH_3NH_2BHNH_2 \rightarrow c\text{-}B_2N_2H_8$	-8.8	-6.2
6	$BH_3NH_3 + c\text{-}B_2N_2H_8 \rightarrow c\text{-}B_2N_2H_7\text{-}NH_2BH_3 + H_2$	-16.0	-14.0
7	$BH_3NH_3 + c\text{-}B_2N_2H_8 \rightarrow c\text{-}B_2N_2H_7\text{-}BH_2NH_3 + H_2$	-13.6	-11.2

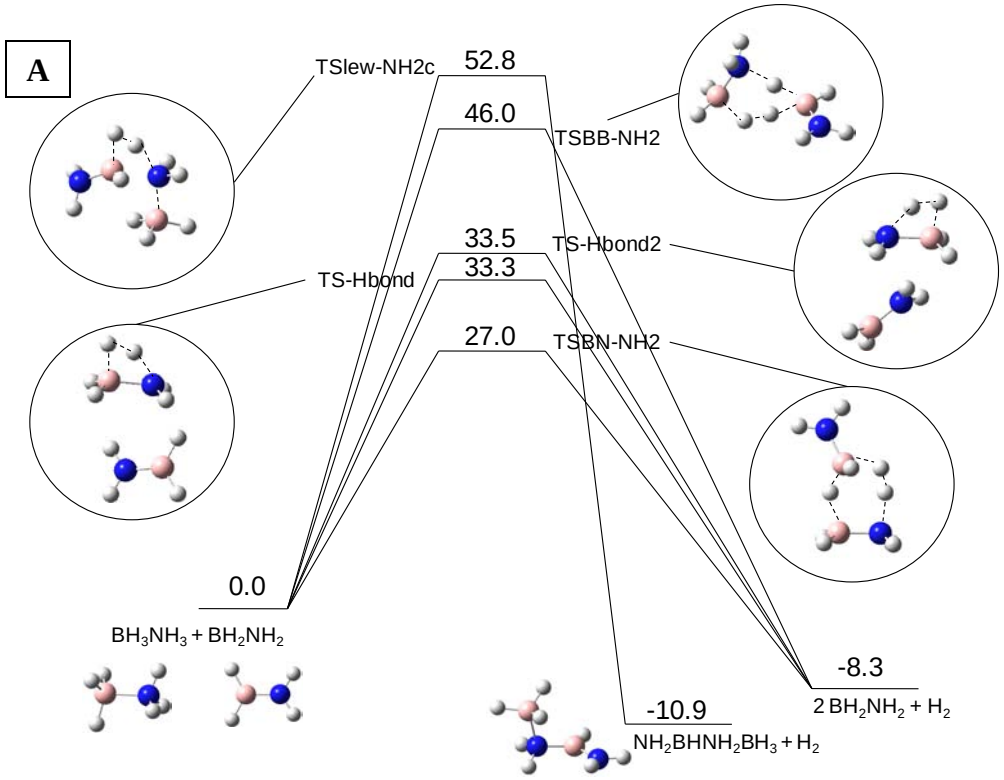
A
TSlew-NH2c
52.8
46.0
TSBB-NH2
33.5
TS-Hbond2
TS-Hbond
33.3
27.0
TSBN-NH2
0.0
BH3NH3 + BH2NH2
-8.3
2 BH2NH2 + H2
-10.9
NH2BHNH2BH3 + H2

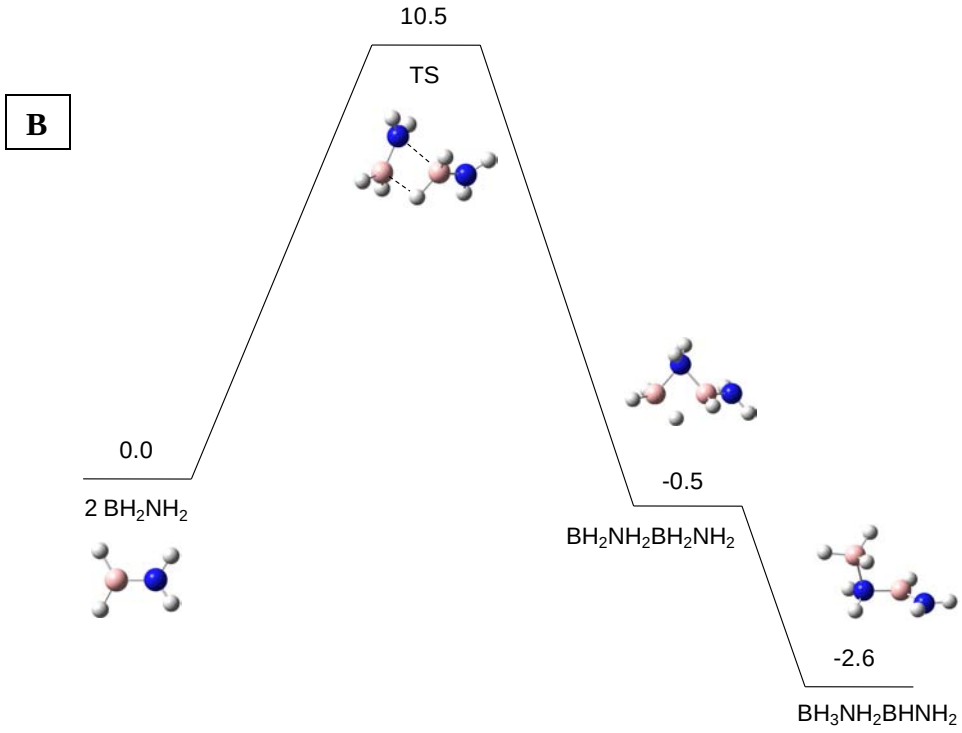
B
10.5
TS
0.0
2 BH2NH2
-0.5
BH2NH2BH2NH2
-2.6
BH3NH2BHNH2

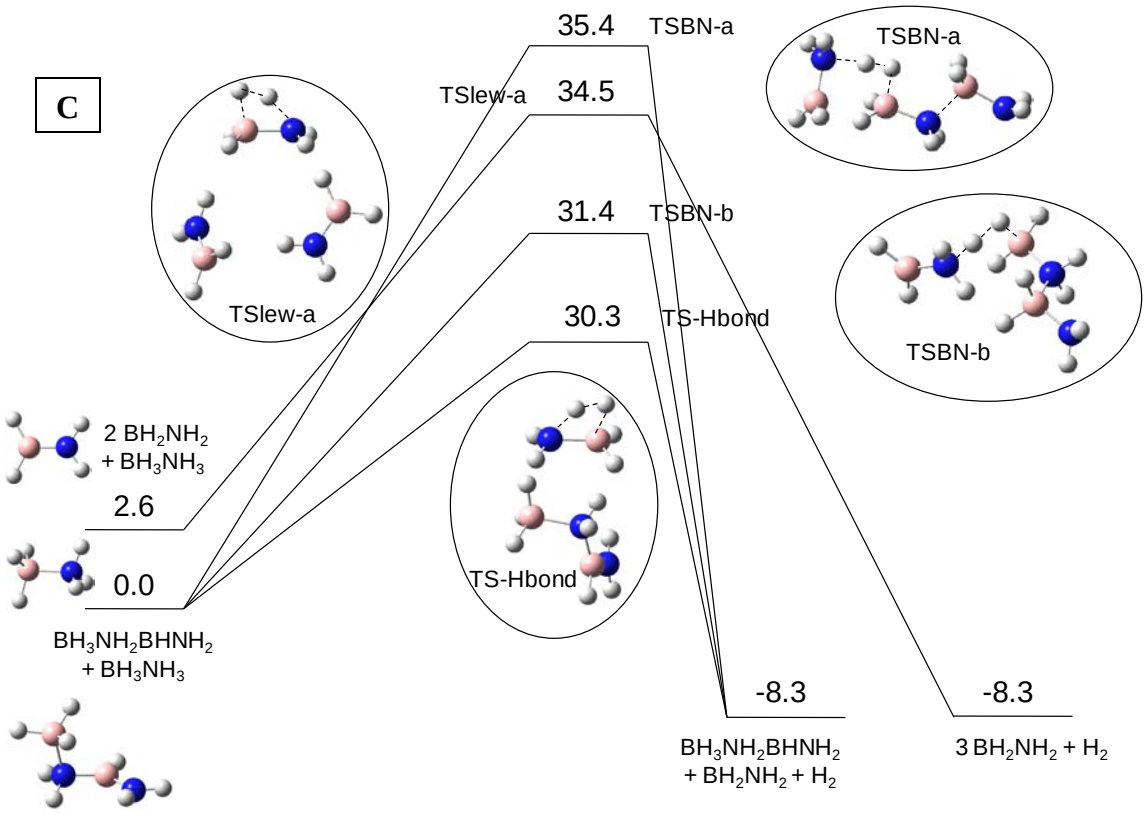
C
35.4
TSBN-a
TSlew-a
34.5
TSBN-a
31.4
TSBN-b
TSlew-a
30.3
TS-Hbond
TSBN-b
2 BH2NH2
+ BH3NH3
2.6
TS-Hbond
0.0
BH3NH2BHNH2
+ BH3NH3
-8.3
-8.3
BH3NH2BHNH2
+ BH2NH2 + H2
3 BH2NH2 + H2

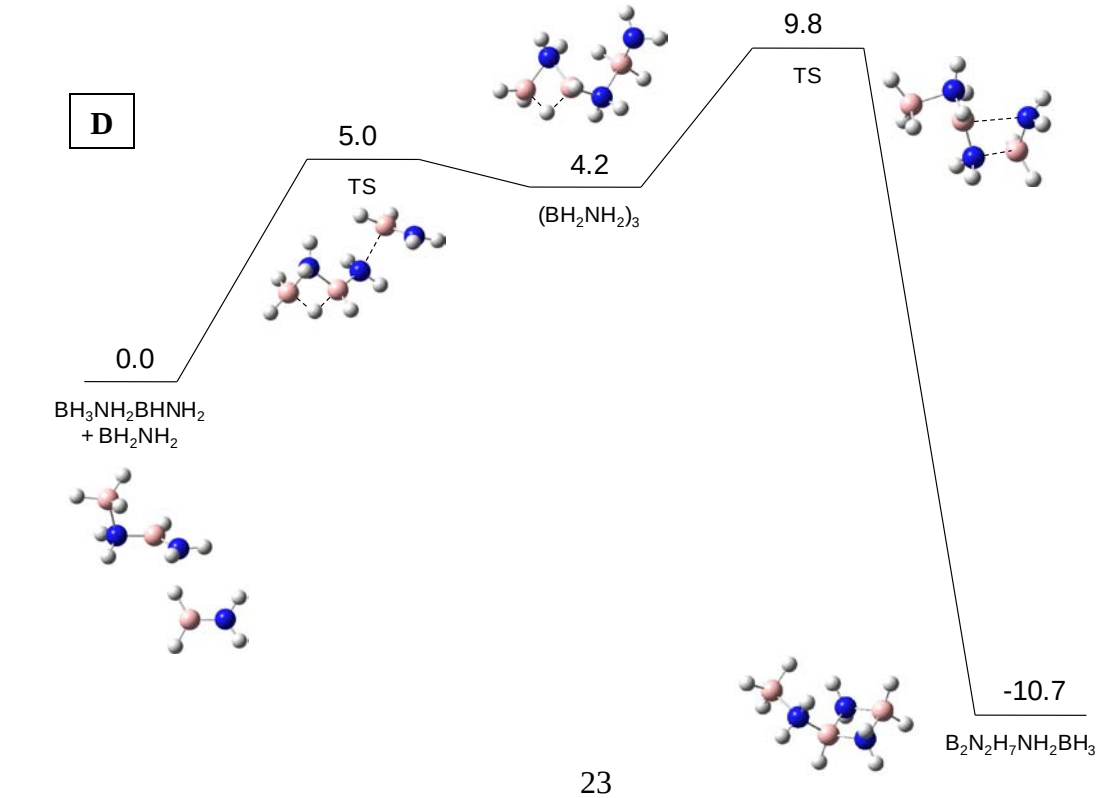
D
9.8
TS
5.0
TS
4.2
(BH2NH2)3
0.0
BH3NH2BHNH2
+ BH2NH2
-10.7
B2N2H7NH2BH3

Figure 4. Potential energy surfaces calculated at the B3LYP/DZVP2 level (Energies in kcal/mol include ZPE). **A.** H_2 elimination from AB catalyzed by NH_2BH_2. Note the lowest energy paths lead to formation of two weakly interacting NH_2BH_2 molecules. **B.** Reaction of two NH_2BH_2 molecules to form the $BH_3NH_2BHNH_2$ chain. **C.** H_2 elimination from AB catalyzed by the $BH_3NH_2BHNH_2$ chain. **D.** Chain elongation and cyclization to form the ring compound $B_2N_2H_7NH_2BH_3$ (NH_2BH_3 side chain bonded to B) resulting from addition of NH_2BH_2 to $BH_3NH_2BHNH_2$.

BH_3 as a Bifunctional Acid-Base Catalyst in H_2-Elimination

Electronic structure calculations using various high level methods, up to the coupled-cluster CCSD(T) level, in conjunction with the aug-cc-pV*n*Z basis sets with *n* = D, T and Q, extrapolated to the complete basis set limit, show that the borane molecule (BH_3) can act as an efficient bifunctional acid-base catalyst in the H_2-elimination reactions of XH_nYH_n systems (X, Y = C, B, N). The kinetics of these processes was analyzed using both transition state and RRKM theory. We have located reaction pathways using state-of-the-art quantum chemical methods, and analyzed the electronic reorganization during the H_2-release in ethane and borane amine. We have identified the role of BH_3 and NH_3 fragments produced by decomposition of the B-N bond in BH_3NH_3, in particular BH_3, as an active bifunctional acid-base catalyst for H_2-formation. For ethane, the barrier height for H_2-production is reduced by more than 50 kcal/mol with BH_3 in the supermolecule. For borane amine, we were able to locate six different transition structures for the H_2 dissociation with the additional BH_3 and NH_3 present. Along with a more conventional pathway, where BH_3 unit behaves as a Lewis acid catalyst, we find an energetically lower-lying reaction channel involving a participation of BH_3 as a catalyst, which actively participates in the hydrogen transfer through a six-member cyclic transtition structure involving a B-H-H-N interaction. NH_3 shows a similar behavior, but with a less pronounced ability to reduce the barrier height. Stabilizing electrostatic interactions are likely the main reason for the beneficial catalytic effect. The barrier height in the catalytic pathway for H_2-release from borane amine with an active participation of BH_3, amounts to 6.1 kcal/mol with respect to the separated reactants and 23.9 kcal/mol from the complex. This corresponds to a reduction of 30 kcal/mol, relative to that of the monomer, and is consistent with the experimental finding that the H_2-release from borane amine proceeds under mild conditions, under the melting temperature of 385

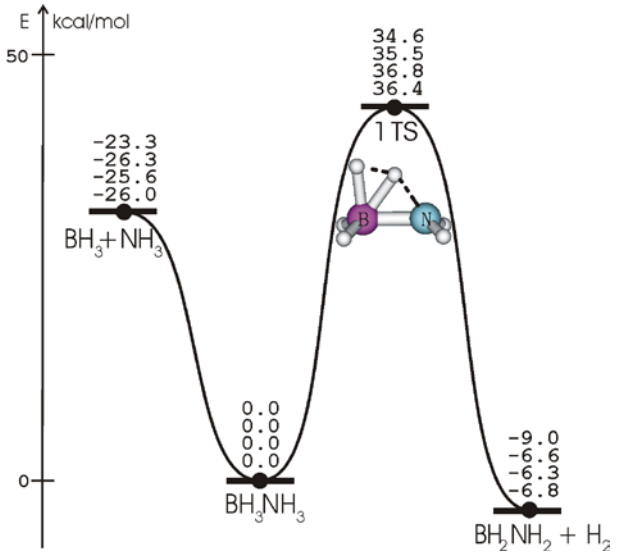

Figure 5. Schematic energy profiles showing the reaction pathways for H_2-release from BH_3NH_3. Relative energy in kcal/mol were obtained from: *upper*: B3LYP/aVTZ; *middle upper*: MP2/aVTZ; *middle lower*: CCSD(T)/aVTZ, and *lower*: CSD(T)/CBS. ZPE's were derived from B3LYP for the first entry and from MP2 for the others.

K. In summary, our present calculations demonstrate that in either ethane or borane amine, the 1,2-H_2-release is greatly accelerated by an active participation of a BH_3 molecule. The latter acts thus as a bifunctional (acid-base) catalyst facilitating the H-transfer and H_2 bond formation. The catalytic effect of BH_3 has also been probed by an analysis of the electronic densities of the transition structures using the atom-in-molecule (AIM) and electron localization function (ELF) approaches.

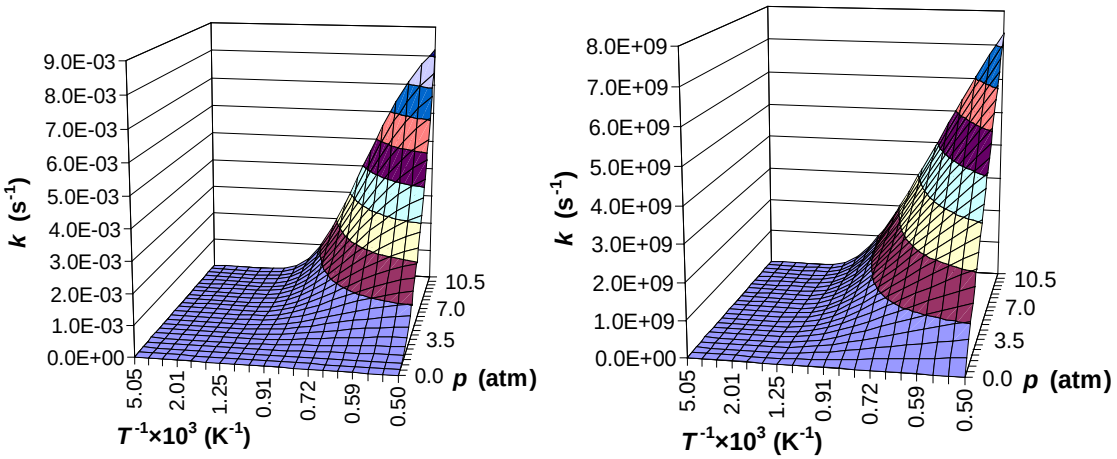

Figure 6. 3-D plots of the rate coefficients $k(T, p)$ of the for **(a)** H_2-release, and **(b)** B–N bond cleavage in borane amine, using the RRKM method with N_2 as the bath gas in the temperature range (T) from 200 to 2000 K and pressure range (p) from 0.1 to 8360 Torr.

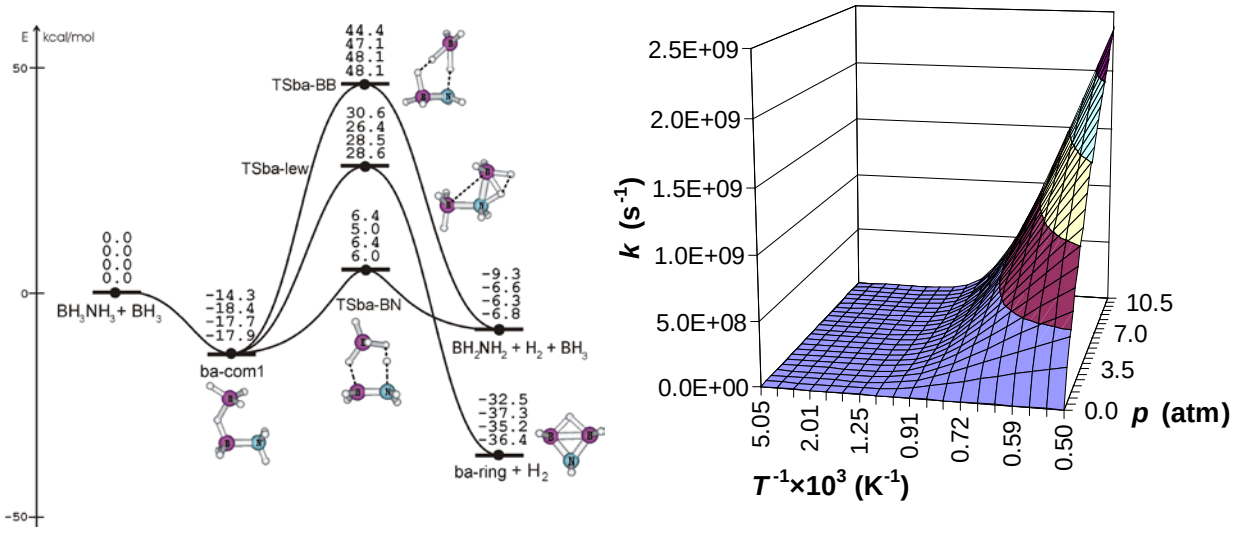

Figure 7. (A, left) Schematic energy profiles illustrating the H_2-release from BH_3NH_3 in the presence of BH_3. Relative energies given in kcal/mol, were obtained, from upper to lower: B3LYP/aVTZ, MP2/aVTZ, CCSD(T)/aVTZ and CCSD(T)/CBS. (B, right) 3D plot of the rate coefficients $k(T, p)$ of the H_2-release from borane amine with the presence of BH_3 via **TSba-BN**, using the RRKM method with N_2 as the bath gas in the temperature range (T) from 200 to 2000 K and pressure range (p) from 0.1 to 8360 Torr.

H_2 Elimination from $(AB)_2$ and BH_3NH_3 Dimer Salts

Ammonia borane (**ab**), which is promising materials for chemical hydrogen storage for the transportation sector, is known to yield H_2 at mild temperatures ($T \leq 80\ ^0C$). However, without a catalyst, the rate of H_2-release from the **ab** monomer was found to be very low. Therefore, a dimer or a small oligomer, $(BH_3NH_3)_n$ with $n \geq 2$, could involve in the process. It has been experimentally found that a "seeding" of **ab** results in significantly faster H_2-production. The seed compound has been proposed to be the diammoniate of diborane $[(BH_4^-)(NH_3BH_2NH_3)^+]$, which is a zwitterionic form of the **ab** dimer, and could also be formed from another starting $(B_2H_6 + 2NH_3)$ reactants. To probe the H_2-release of **ab** from its dimeric and isomeric systems, electronic structure calculations were applied to map out the relevant portion of the potential energy surface. Geometries of stationary points were optimized at the second-order perturbation MP2 level using the correlation consistent aug-cc-pVTZ basis set, whereas relative energies were computed using the coupled-cluster CCSD(T) theory whose energies were extrapolated at the complete basis set limit. Calculated results reveal that there are a large number of possible AB dimers involving different types of H-bonded interactions. The most stable gaseous phase **ab** dimer results from a head-to-tail cyclic interaction, and is stabilized by about 14 kcal/mol, with respect to the two monomers. The neutral dimer **dim** could generate one or two H_2 molecules through direct pathways having energy barriers ranging from 43 to 48 kcal/mol. The two H_2 pathway is less favored. Successive additions of two NH_3 molecules to B_2H_6 leads to a low-lying complex, which connects with the $[BH_4^-/NH_3BH_2NH_3^+]$ zwitterion via an energetically high-lying ts. The latter zwitterions is only 2.2 kcal/mol less stable than the neutral dimer. In addition, the pathway for H_2-elimination from the zwitterion is characterized by a smaller energy barrier of about 20 kcal/mol. The second zwitterion $[BH_4^-/NH_3BH_2NH_3^+]$ is about 6 kcal/mol less stable than the neutral and characterized by a larger energy barrier for H_2-elimination. We were not able to identify unimolecular rearrangement connecting the zwitterions with the most stable neutral $(BH_3NH_3)_2$ dimer.

dim (C_{2h})

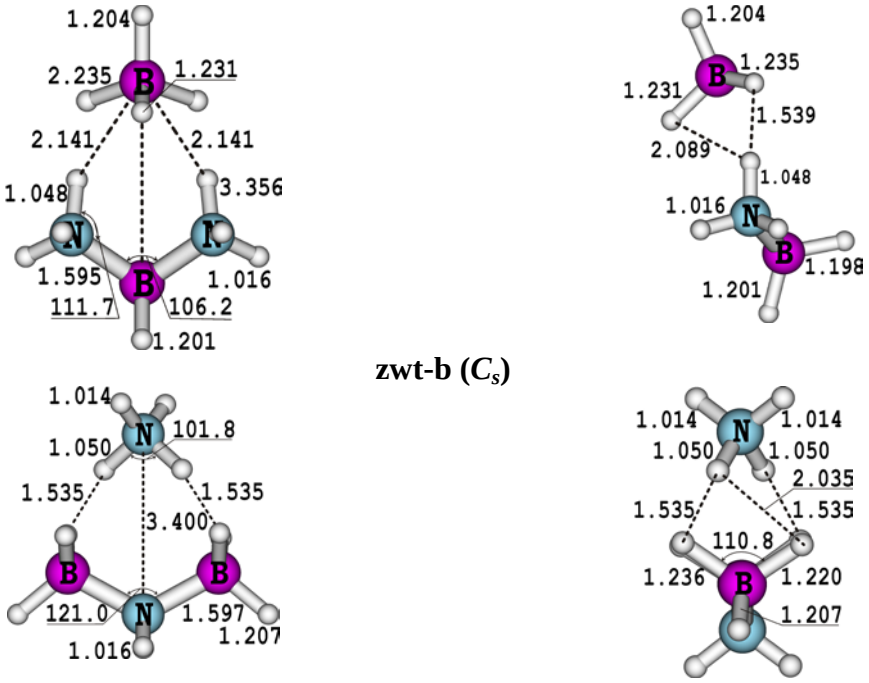

Figure 8. Selected MP2/aVTZ geometrical parameters of ammonia borane dimer **dim** and its zwitterionic isomers **zwt-b** and **zwt-n**. Each structure is projected in two different plans. Bond lengths are given in angstrom and bond angles in degree.

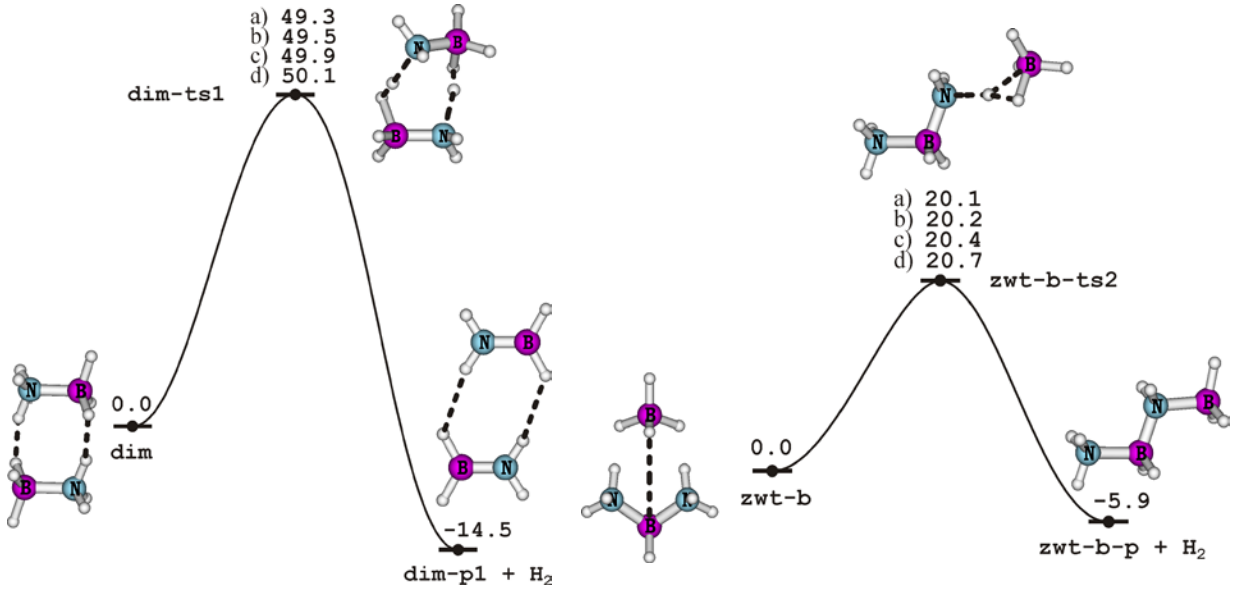

Figure 9. Schematic energy profiles showing the reaction pathways for H_2-release from **dim** and **zwt-b** calculated with the CCSD(T) method using four basis sets including zero-point corrections. The entries are: a) CBS, b) aVQZ, c) aVTZ, and d) aVDZ.

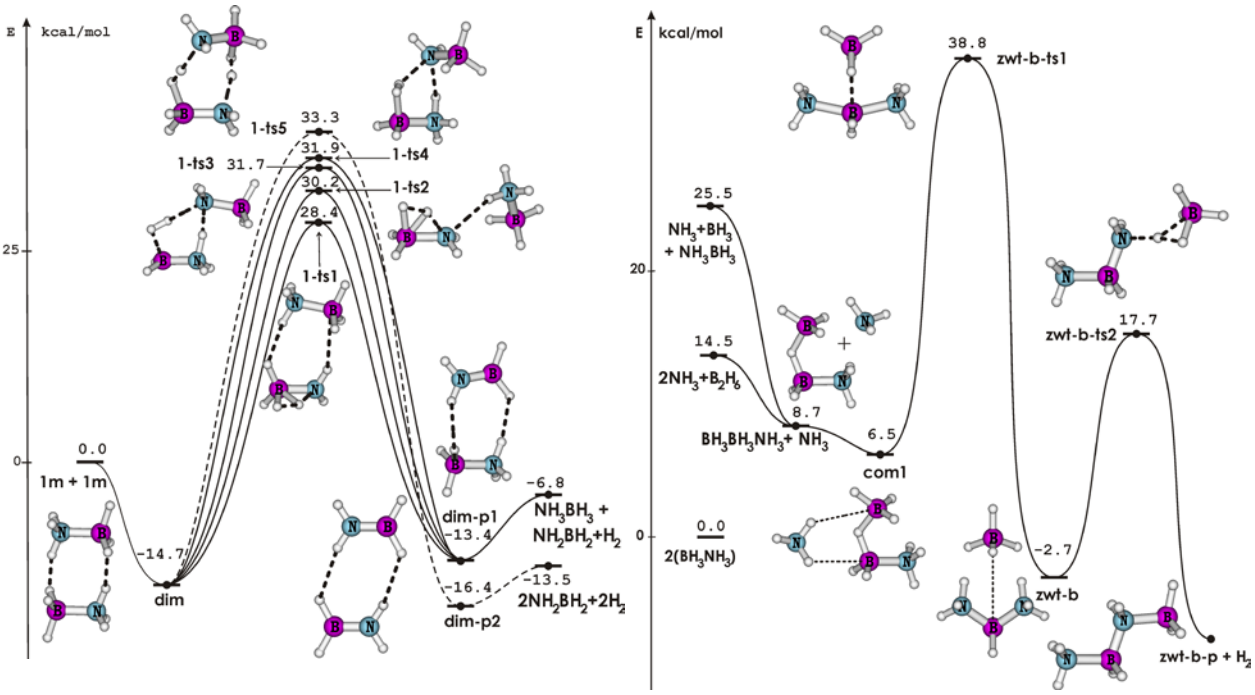

Figure 10. Schematic energy profiles illustrating five different reaction pathways for H_2-release from **dim.** Relative energies given in kcal/mol were obtained from CCSD(T)/aVTZ + ZPE calculations.

We have also calculated the heats of formation of $[NH_3BH_2NH_3^+][BH_4^-]$ and $[BH_3NH_2BH_3^-][NH_4^+]$ both at 0K and 298K on the basis of CCSD(T)/CBS values in combination with an empirical expression to estimate the lattice energy of the salt.

Molecule	**ΔH_f (0K)**	**ΔH_f (298K)**
$NH_3BH_2NH_3^+$	104.8	99.2
$BH_3NH_2BH_3^-$	-51.6	-57.5
$[NH_3BH_2NH_3^+][BH_4^-]$	-39.4	-50.4
$[BH_3NH_2BH_3^-][NH_4^+]$	-62.8	-73.7

Based on these values together with the heats of formation of BH_3NH_3, we can calculate the following reaction energies in kcal/mol at 298 K:

$2BH_3NH_3 \rightarrow NH_3BH_2NH_3^+ + BH_4^-$ $\Delta H = 113.5$ (59)

$2BH_3NH_3 \rightarrow [NH_3BH_2NH_3^+][BH_4^-]$ $\Delta H = -20.4$ (60)

$2BH_3NH_3 \rightarrow BH_3NH_2BH_3^- + NH_4^+$ $\Delta H = 123.8$ (61)

$2BH_3NH_3 \rightarrow [BH_3NH_2BH_3^-][NH_4^+]$ $\Delta H = -13.4$ (62)

Release of H_2 Ammonia Triborane

Yoon and Sneddon recently reported that the long known ammonia triborane has properties which also make it a promising candidate for amine borane-based chemical hydrogen storage, and presented an efficient, convenient, and safe method for its preparation. They report that

oxidative-hydrolysis of $B_3H_7NH_3$ in aqueous solution leads to the release of up to eight equivalents of H_2, upon addition of either acids or metal catalysts (such as $RhCl_3$). As part of our efforts in predicting the thermodynamic properties of H_2 storage materials using high level molecular orbital theory, we have studied the thermodynamic properties of ammonia triborane. High level electronic structure calculations have been used to predict the thermodynamic stability of $B_3H_7NH_3$ and the molecular mechanism of H_2 elimination from various isomeric forms in the gas phase. Geometries of stationary points were optimized at the second-order perturbation theory MP2 level and relative energies were computed at the coupled-cluster CCSD(T) theory with the aug-cc-pVnZ (n = D, T, Q) basis sets and extrapolated to the complete basis set limit. The molecular hydrogen release reaction at 298 K is endothermic by 7.5 kcal/mol (5.7 kcal/mol at 0 K) giving an amino-triborane ring. Starting from its most stable from in the gas phase, ammonia triborane can release one H_2 molecule by a direct 1,3-H_2-elimination pathway characterized by an energy barrier of 28.9 kcal/mol. 1,2-H_2-elimination is found to be a less favored process. In contrast to the parent homologue BH_3NH_3, the barrier height for H_2-release from $B_3H_7NH_3$ is slightly smaller than the B-N bond cleavage energy of 32.1 kcal/mol at 298 K (30.7 kcal/mol at 0 K) yielding the fragments B_3H_7 + NH_3.

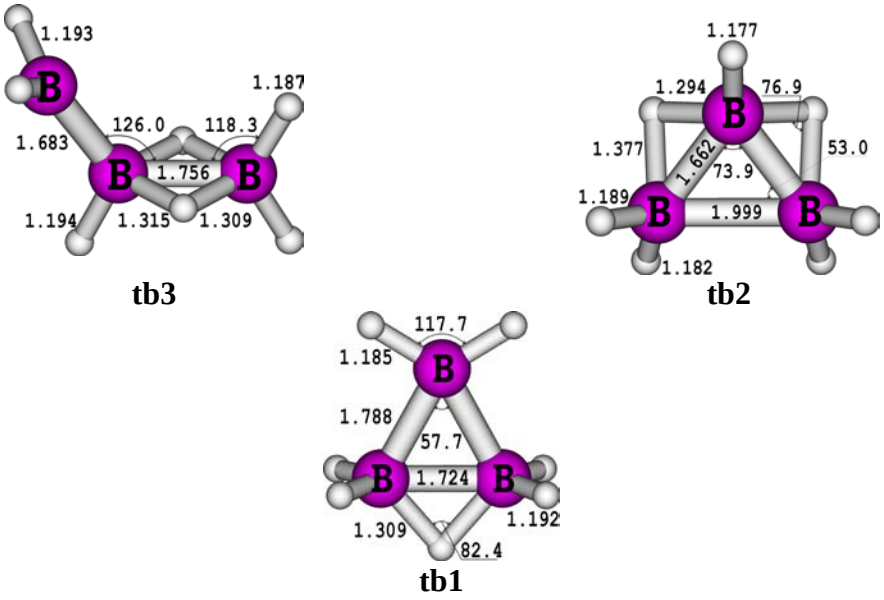

Figure 11. Selected MP2/aVTZ geometrical parameters of three triborane isomeric forms.

Table 18. Relative Energies of B_3H_7 Isomers Calculated with the CCSD(T) Method.

Basis Set	tb3	tb2	tb1
aVDZ	6.72	0.0	2.63
aVTZ	8.16	0.0	3.32
aVQZ	8.48	0.0	3.47
CBS	8.64	0.0	3.54

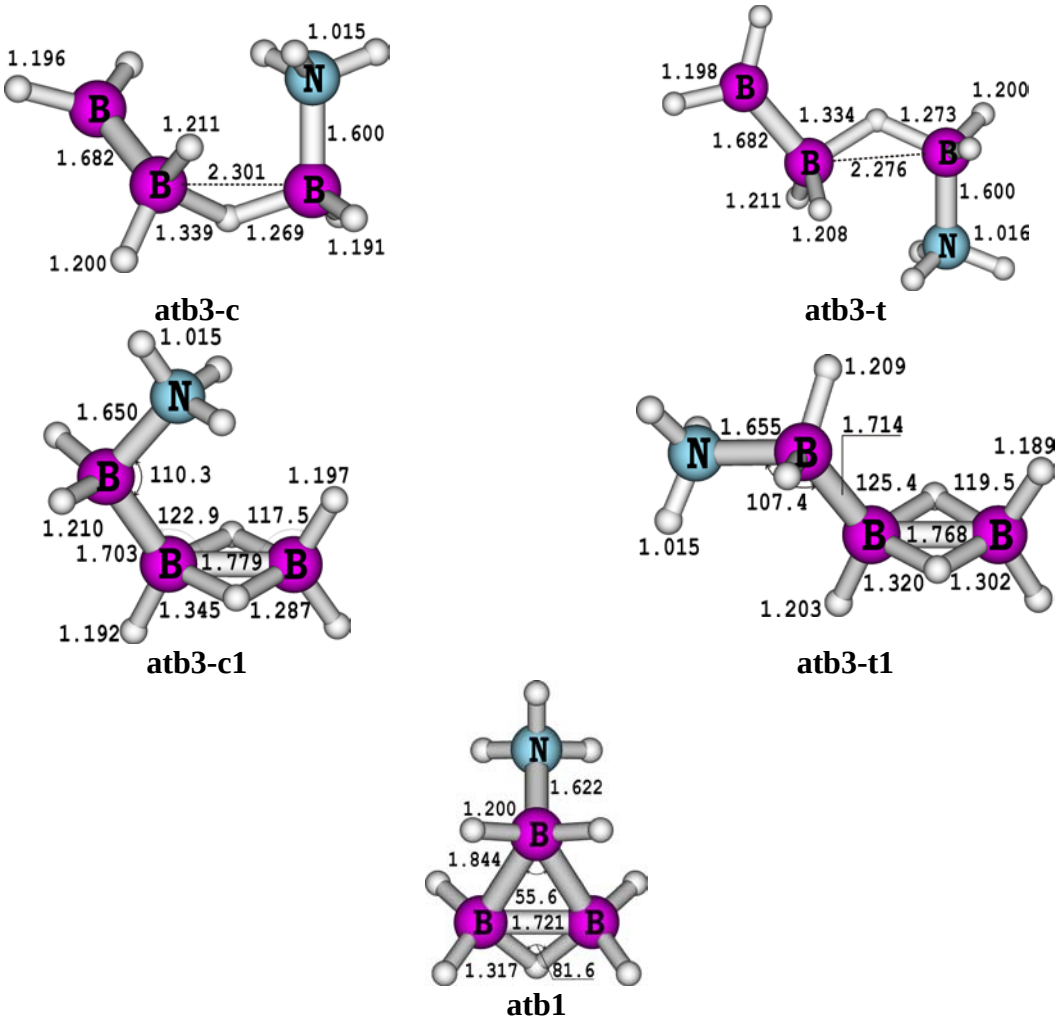

Figure 12. Selected MP2/aVTZ geometrical parameters of ammonia triborane $B_3H_7NH_3$ isomers.

Table 19. Relative CCSD(T) Energies of the $B_3H_7NH_3$ Isomers.

Isomer	aVDZ	aVTZ	aVQZ	CBS
atb3-c	27.50	29.27	31.64	31.83
atb3-t	27.02	28.76	31.12	31.32
atb3-c1	9.84	10.50	10.71	10.77
atb3-t1	11.64	12.22	12.56	12.61
atb1	0.0	0.0	0.0	0.0

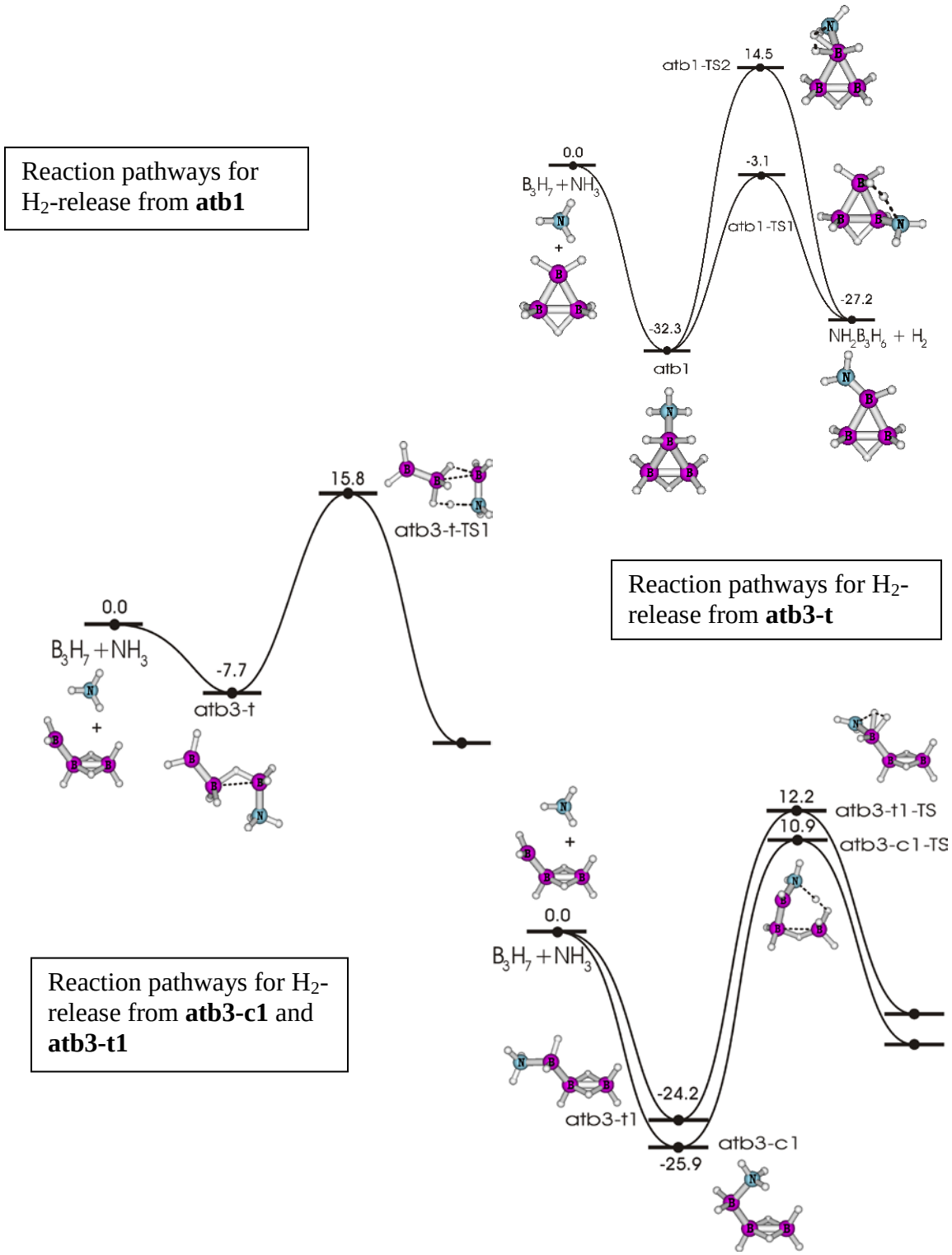

Figure 13. Schematic energy profiles illustrating the different reaction pathways for H_2-release from different ammonia triborane $B_3H_7NH_3$. Relative energies, given in kcal/mol, were obtained from CCSD(T)/CBS calculations.

AlH_3 as a Bifunctional Acid-Base Catalyst

We studied hydrogen release from BH_3NH_3 and P_2H_4 molecules with and without BH_3 as a catalyst. We studied hydrogen release with AlH_3 as a catalyst. Geometries were optimized up to MP2/aVTZ and energies were calculated up to CCSSD(T)/aVTZ. The Al-N bond energy for AlH_3NH_3 is comparable to that for BH_3NH_3, however, the transition state (TS) for H_2 release is about 5 kcal/mol lower in energy for the AlH_3NH_3 compound. A complete potential energy surface (PES) was analyzed for the different reactants: BH_3NH_3 + AlH_3, AlH_3NH_3 + BH_3, and AlH_3BH_3 + NH_3. We found that the reaction starting from BH_3NH_3 + AlH_3 as reactants leading to stable complex formation is energetically comparable to that of BH_3NH_3 + BH_3, about a complexation energy of ~ -18.0 kcal/mol. The TS and the products for the AlH_3 catalyzed reaction are about 4.0 lower in energy than those for the BH_3 catalyzed reaction.

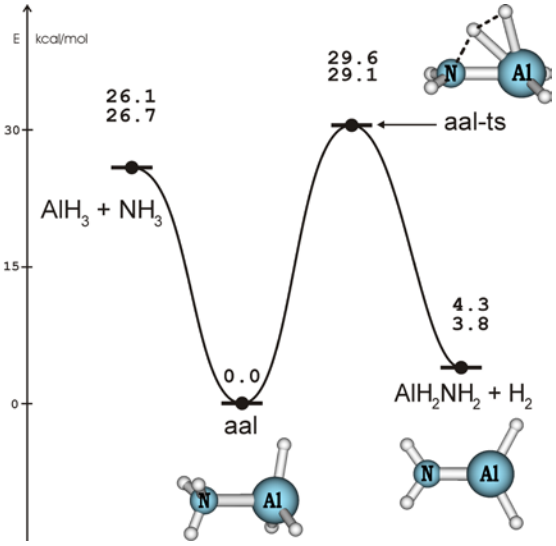

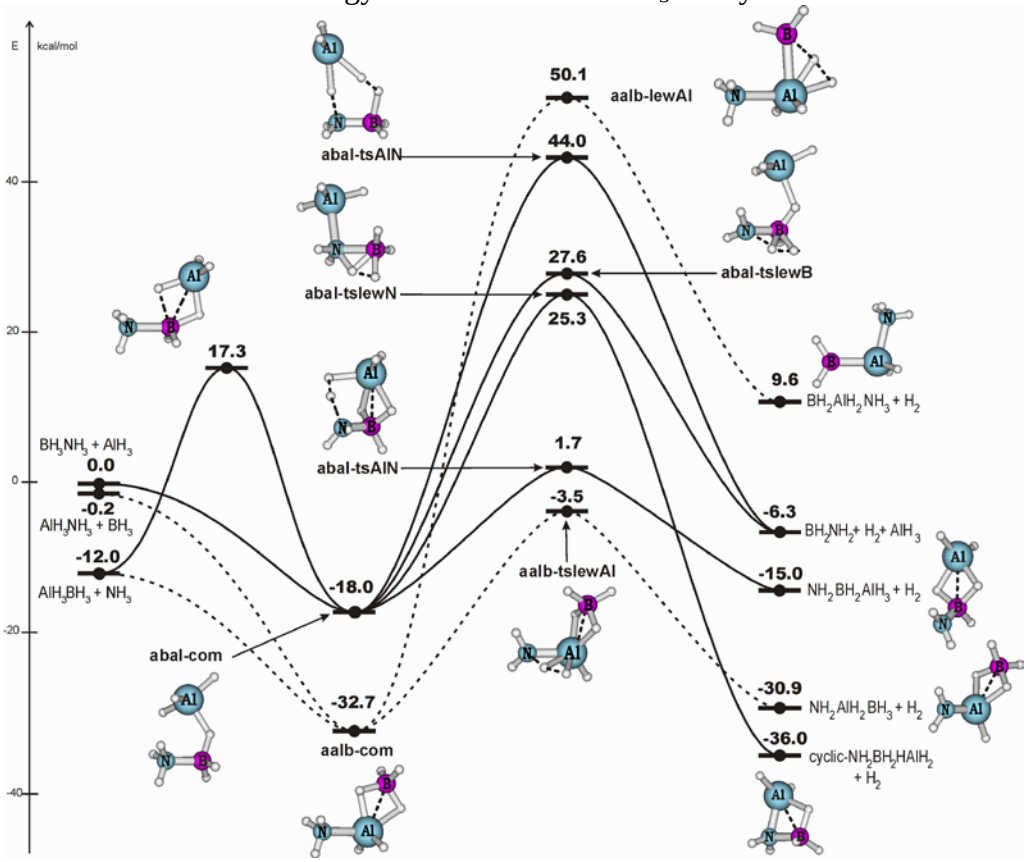

Figure 14. Complete Potential Energy Surface for ($AlH_3BH_3NH_3$)

Our electronic structure calculations demonstrate that AlH_3 can play the role of an efficient bifunctional acid-base catalyst, not only for a H_2 release from ammonia borane but it could also be useful for the regeneration process.

We have analyzed the potential energy surfaces for the hydrogen release from a series of reactions involving AlH_3. The reaction pathway (energies in kcal/mol):

$AlH_3NH_3 + AlH_3$ (0.0) → $AlH_3NH_3\cdots AlH_3$ (complex) (-23.0) → $AlH_3BH_3\cdots AlH_3$ (TS) (-4.3) → $NH_2AlH_2AlH_3 + H_2$ (-23.3) → $AlH_2NH_2 + AlH_3 + H_2$ (2.7)

is the lowest energy channel. The overall reaction is marginally endothermic by ~3 kcal/mol. The transition state is 4.3 kcal/mol below reactants and is 18.7 kcal/mol above the adduct. The adducts of both reactants and products are of similar energy with an energy difference of ~0.3 kcal/mol. We have used TST and RRKM to study the kinetics of the lowest energy reaction paths:

$AlH_3NH_3 \rightarrow AlH_3 + NH_3$ (63)
$AlH_3NH_3 \rightarrow AlH_2NH_2\cdots H_2$ (TS) → $AlH_2NH_2 + H_2$ (64)
$AlH_3NH_3\cdots AlH_3$ (complex) → $AlH_3NH_3\cdots AlH_3$ (TS) → $NH_2AlH_2AlH_3 + H_2$ (65)
$AlH_3BH_3\cdots AlH_3$ (complex) → $AlH_3BH_3\cdots AlH_3$ (TS) → $NH_2BH_2AlH_3 + H_2$ (66)

Table 20. Rate Constants $k(T)$ Obtained by TST and RRKM Theory (in s^{-1}) at Different Temperatures (in Kelvin) Including Skodje & Truhlar Tunneling Corrections (Q_{ST}).[a)]

Rxn	T	$Q_{ST}(T)$	TST	RRKM
63[b)]			$k_\infty(T) = 5.012 \times 10^{21}\, T^{-1.85}$ exp (-29.1/RT) s^{-1}	$k(T, p) = 8.128 \times 10^{9}\, p^{0.913}$ exp (-22.7/RT) s^{-1}
	298.15	-	5.02×10^{-5}	2.25×10^{-4}
	400	-	8.19	1.70×10^{1}
64			$k_\infty(T) = 1.995 \times 10^{11}\, T^{0.585}$ exp (-28.4/RT) s^{-1}	$k(T, p) = 3.981 \times 10^{10}\, p^{0.477}$ exp (-27.5/RT) s^{-1}
	298.15	2.29×10^{2}	1.95×10^{-6}	2.28×10^{-6}
	400	4.21	8.92×10^{-3}	1.01×10^{-2}
65			$k_\infty(T) = 1.995 \times 10^{10}\, T^{0.641}$ exp (-18.5/RT) s^{-1}	$k(T, p) = 7.943 \times 10^{9}\, p^{0.501}$ exp (-17.9/RT) s^{-1}
	298.15	1.13	2.58×10^{-2}	2.60×10^{-2}
	400	1.07	8.38×10^{1}	8.40×10^{1}
66			$k_\infty(T) = 7.943 \times 10^{10}\, T^{0.284}$ exp (-19.4/RT) s^{-1}	$k(T, p) = 5.754 \times 10^{9}\, p^{0.45}$ exp (-18.9/RT) s^{-1}
	298.15	1.69	3.72×10^{-3}	4.36×10^{-3}
	400	1.32	1.36×10^{1}	1.54×10^{1}

[a] RRKM results are at 1 atm of p. The rate constants at 298.15 and 400 K include the tunneling correction.
[b] Barrierless reaction.

Reaction (65) is predicted to have a faster rate constant than the corresponding Boron reaction, where BH_3 is the catalyst for H_2 elimination from BH_3NH_3:

$BH_3NH_3\cdots BH_3$ (complex) → $BH_2NH_2 + H_2 + BH_3$ (67)

with k_∞(298 K) = 6.1 × 10^{-5} s^{-1} and k_∞(400 K) = 1.06 s^{-1}, including tunneling. The kinetic predictions show that AlH_3 can be produced by dissociation of the Al-N bond in AlH_3NH_3. The alane can then serve as an efficient bifunctional catalyst for H_2 release from ammonia alane. In addition, AlH_3 is a better catalyst for elimination of H_2 from BH_3NH_3 than is BH_3.

B_2H_6 Reactions

We have analyzed the PES for the hydrogen elimination from the following reactions:

$B_2H_6 + NH_3$ (68)
$B_2H_6 + NH_3 + BH_3$ (69)
$B_2H_6 + BH_3NH_3$ (70)

We show an updated PES for reaction (68) as well as a comparison with the PES for $BH_3NH_3 + BH_3$ in Figure 15.

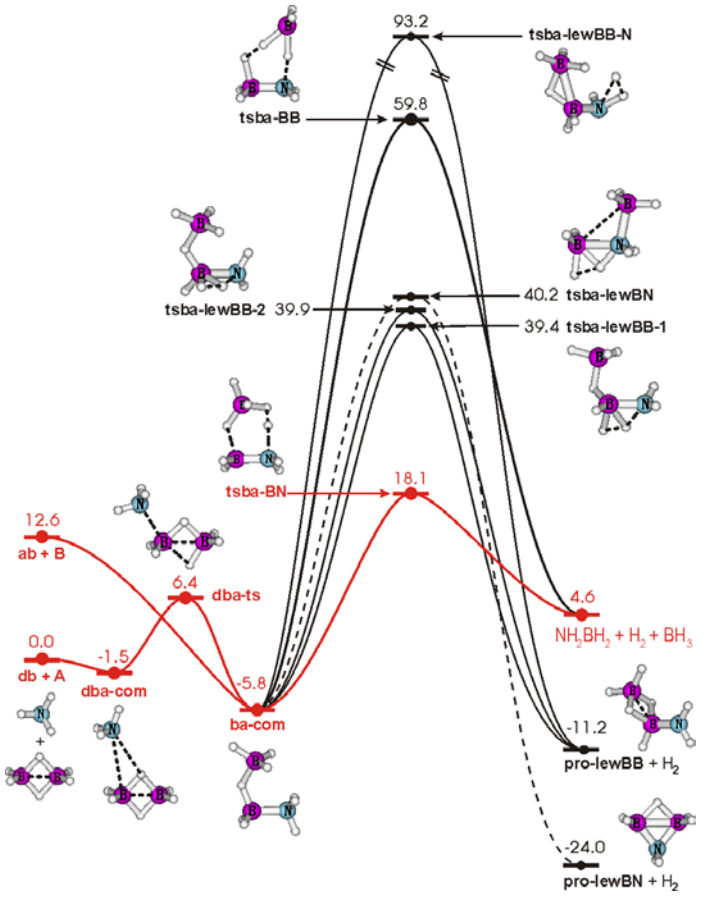

Figure 15. Schematic energy profiles illustrating different reaction pathways for H_2-release from diborane + ammonia (**db** + **A**). Relative energies given in kcal/mol were obtained from CCSD(T)/aVTZ + ZPE calculations.

The initial steps lead to a stable $H_3BHBH_2NH_3$ adduct **ba-com,** which is also formed from condensation of ammonia borane with borane ($BH_3NH_3 + BH_3$). From this common intermediate, six transition states for H_2 loss have been located with energy barriers ranging from 14 to 90 kcal/mol relative to the reactants. The lowest-lying TS (**tsba-BN**) is characterized a six-member cycle in which BH_3 exerts a bifunctional catalytic effect favoring the H_2 generation. We have completed the PES for reactions (69) and (70) as shown in Figure 15. The lowest energy reaction path is that for (70). This includes two transition states with activation energies of 11.2 (**dbab-c1-tscom**) and 23.8 kcal/mol (**comB1-s3-taBN1**), with respect to the reactant complex in the pathway.

db + **ab** (0.0) → **dbab-c1** (-0.3) → **dbab-c1-tscom** (10.9) → **comB1-s3** (8.9) → **comB1-s3-tsBN1** (32.7) → $B_2H_6 + NH_2BH_2 + H_2$ (-6.6)

Thus, this pathway is similar to that from reaction (68), which also has two transition states with activation energies of 7.9 and 23.9 kcal/mol, respectively. However, the overall reaction for (68) is endothermic (4.6 kcal/mol), whereas reaction (70) is exothermic (-6.6 kcal/mol).

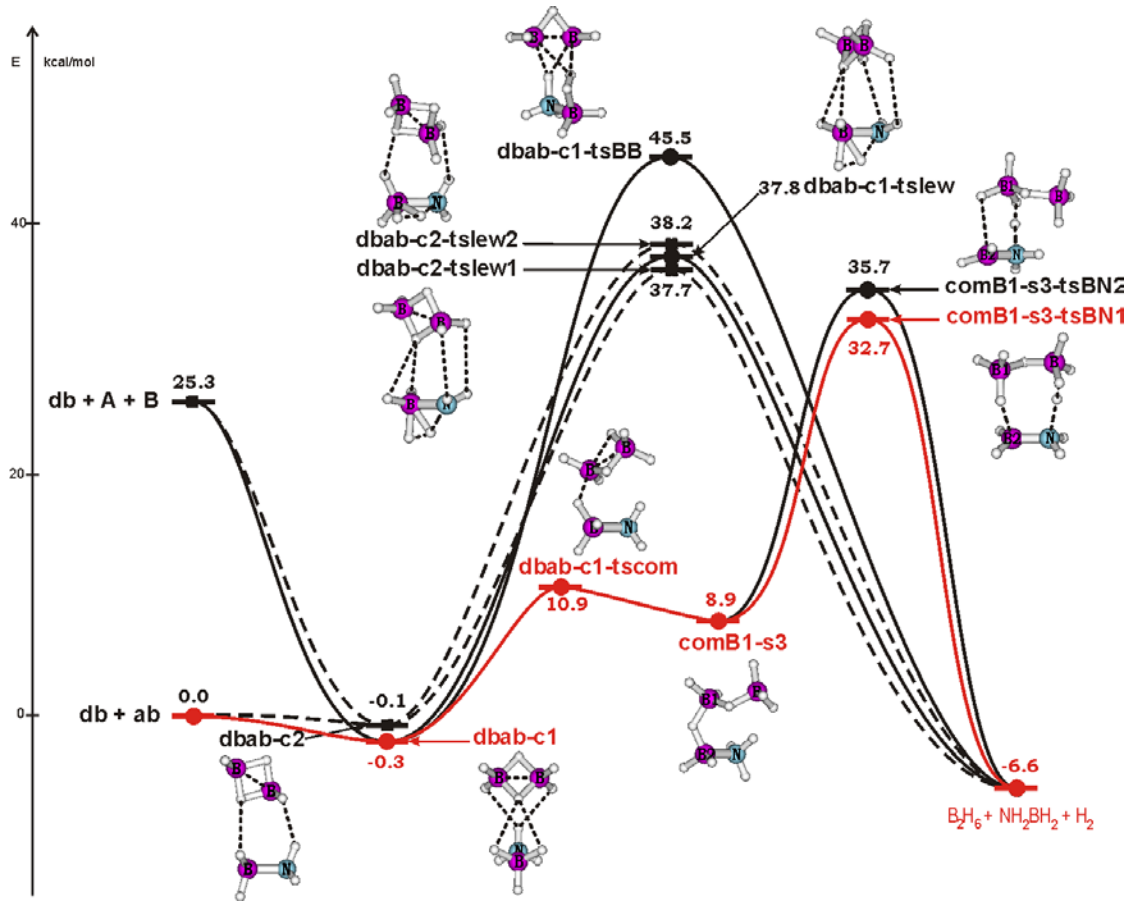

Figure 16. Schematic energy profiles illustrating pathways for rearrangement and H_2 release from two complexes between diborane plus ammonia borane **db** + **ab**. Relative energies given in kcal/mol were obtained from CCSD(T)/aVTZ + ZPE calculations.

In both Figures 15 and 16, the profiles colored in red correspond to the lowest-energy pathways.

N_2H_4 as an Alternative for NH_3

Potential energy surfaces for H_2 release from hydrazine in interaction with borane, alane, diborane, dialane and borane-alane were constructed at the CCSD(T) level with the aug-cc-pVTZ basis set (reactions 71-75):

$BH_3 + N_2H_4$ (71)

$B_2H_6 + N_2H_4$ (72)

$AlH_3 + N_2H_4$ (73)

$Al_2H_6 + N_2H_4$ (74)

$BH_3AlH_3 + N_2H_4$ (75)

Relative energies at the CCSD(T)/aug-cc-pVTZ level including ZPE (MP2/aug-cc-pVTZ) are shown in Table 21.

Table 21. Energetics for H_2-Release for Reactions (70) to (74) in kcal/mol.

Reaction	$\Delta H_{reaction}$(0 K)	TS	$\Delta H_{reactant}^{\ddagger a}$	$\Delta H_{complex}^{\ddagger b}$
71	-35.5	TS4-1	7.4	38.2
72	0.9	TS5-1	2.7	5.3
		TS5-2	12.7	23.5
73	-20.4	TS6-1	2.6	30.4
74	-31.7	TS7-1	3.4	20.4
75	-5.0	TS8-1	11.2	[c]
		TS8-2	7.9	17.7

[a] Activation energy from the TS to the initial reactants in the corresponding reaction. [b] Activation energy from the TS to the corresponding complex. [c] No complex was formed previous to this TS.

With one borane or alane molecule, the energy barrier for H_2-loss of ~38 or 30 kcal/mol does not compete with the B–N or Al-N bond cleavage (~30 or ~28 kcal/mol). The second borane or alane molecule can play the role of a bifunctional catalyst. The barrier energy for H_2 elimination is reduced from 38 to 23 kcal/mol or 30 to 21 kcal/mol with the presence of diborane or dialane, respectively. A more attractive feature is that the presence of the mixed borane-alane dimer reduces the barrier energy for H_2 release from hydrazine to ~17 kcal/mol. A systematic comparison with the reaction pathways from ammonia borane (BH_3NH_3) shows that hydrazine could be regarded as an interesting alternative for ammonia in producing a borane amine derivative.

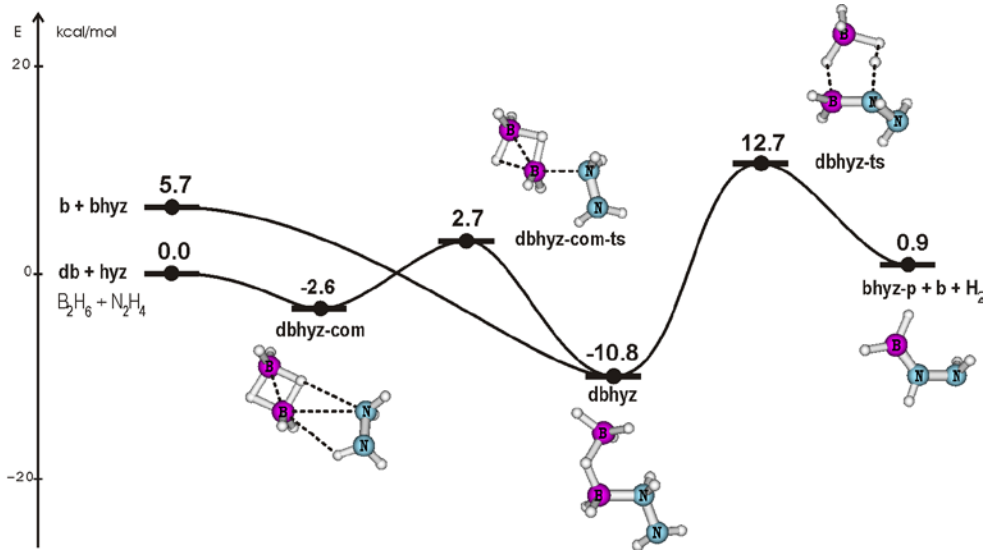

Figure 17. Schematic energy profiles illustrating the H_2-release from $B_2H_6 + N_2H_4$.

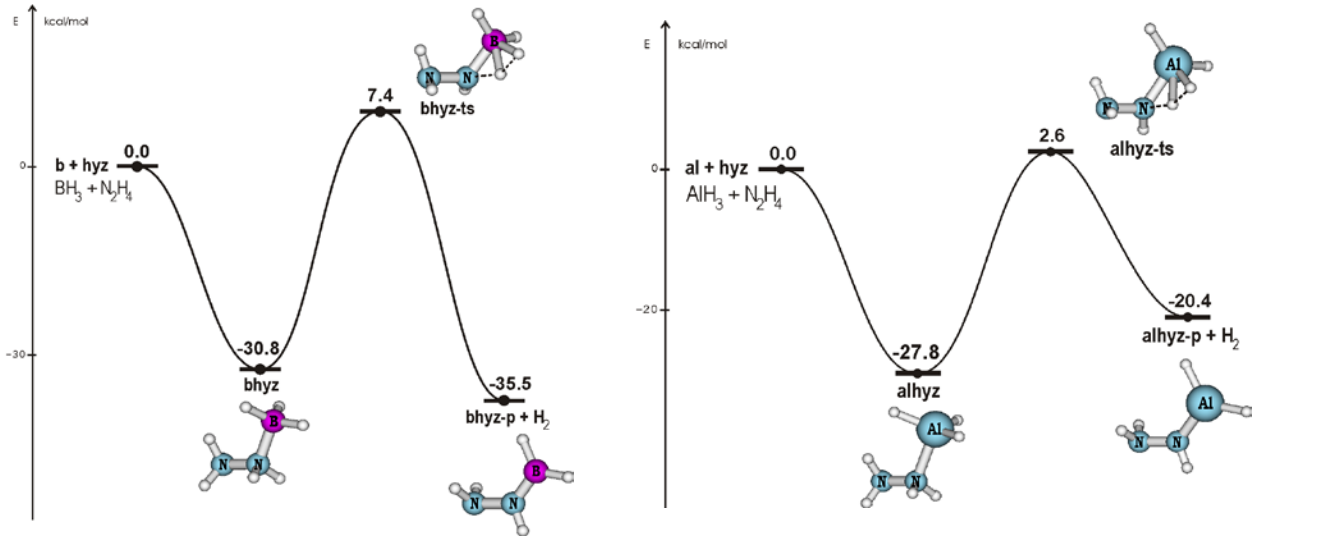

Figure 18. (Left) Schematic minimum energy pathways for H_2-release from BH_3 + N_2H_4. (Right) Pathways for H_2-release from AlH_3 + N_2H_4.

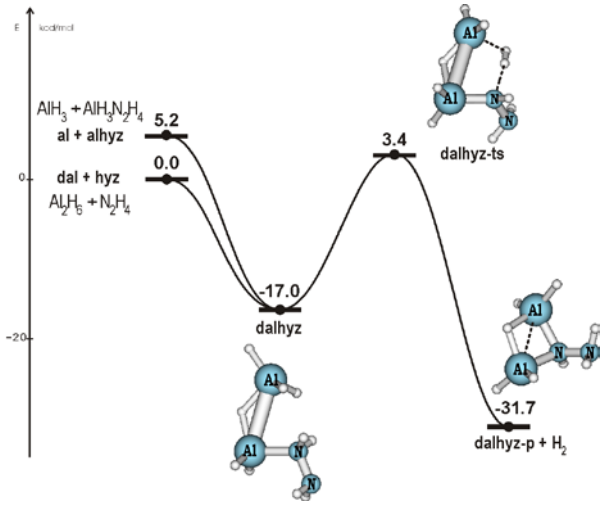

Figure 19. Pathways for H_2-release from Al_2H_6 + N_2H_4.

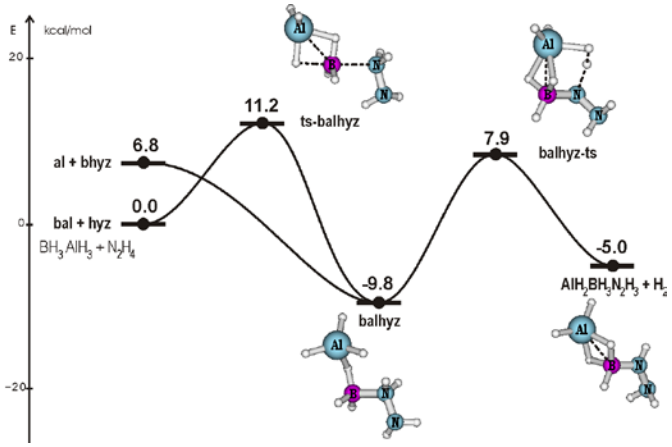

Figure 20. Energy profiles showing the pathways for H_2-release from AlH_3 + BH_3 + N_2H_4.

Computational Study of Molecular Complexes Based on Ammonia Alane

We have continued our studies of alane complexes for H_2 storage as well as for regeneration efforts in the Metal Hydride Center of Excellence. Electronic structure calculations at the CCSD(T) level with the aug-cc-pV*n*Z and aug-cc-pV(*n*+d)Z basis sets (*n* = D, T and Q) were employed to construct the potential energy surfaces for H_2 release from a series of derivatives of ammonia alane. H_2 production from AlH_3NH_3 is facilitated by the addition of alane, which plays the role of a Lewis acid bifunctional catalyst. The effect of methyl and amino substituents on the amine moiety is not large and leads to a decrease in the energy barrier for H_2 release relative to Al-N bond dissociation. As in the case of ammonia borane, H_2 release is not competitive from the combination of two AlH_3NH_3 monomers in the form of a stable dimer.

An alternative route involves the reactions of one AlH_3NH_3 monomer with two separated molecules of AlH_3 and NH_3, in two successive steps: i) an initial condensation of AlH_3NH_3 with NH_3 leads to a stable linear $NH_3AlH_3NH_3$ species, and ii) a subsequent combination of the latter with AlH_3 gives rise to a bicycle framed by dihydrogen bonds. From the new bicyclic form, H_2 production becomes a facile process. Condensation of dialane (Al_2H_6) with two separated ammonia molecules ($2NH_3$) is also a potential route for H_2 release. These results provide further insights into the chemistry of alane complexes and the ability of ammonia to promote dehydrogenation as well as rehydrogenation of spent fuel. Examples of the various potential energy surfaces constructed are given in Figures 21 to 23.

Hydrogen Elimination from Borane Phosphine BH_3PH_3 with the Presence of AlH_3.

Figure 24 illustrates the different reaction pathways for H_2 release from the three reactant systems including AlH_3, BH_3 and PH_3. The most favored pathway involves BH_3-PH_3 + AlH_3 as reactants, in which H_2 is formed from borane phosphine and catalyzed by alane. An initial adduct **pbal-com** is formed, which undergoes a H_2 release via TS **pbal-tsAlP**, which is ~20 kcal/mol above the adduct, but only 7 kcal/mol above the reactants. The reaction is exothermic by 15 kcal/mol, but slightly endothermic by 3 kcal/mol with respect to the adduct.

As the previous case, this could be of interest for the H_2 regeneration process. Our calculated results show that (i) the alane molecule (AlH_3) behaves as a strong bifunctional catalyst reducing considerable the barrier heights for H_2 release, and (ii) borane phosphine can be considered as potentially interesting starting materials for H_2 production.

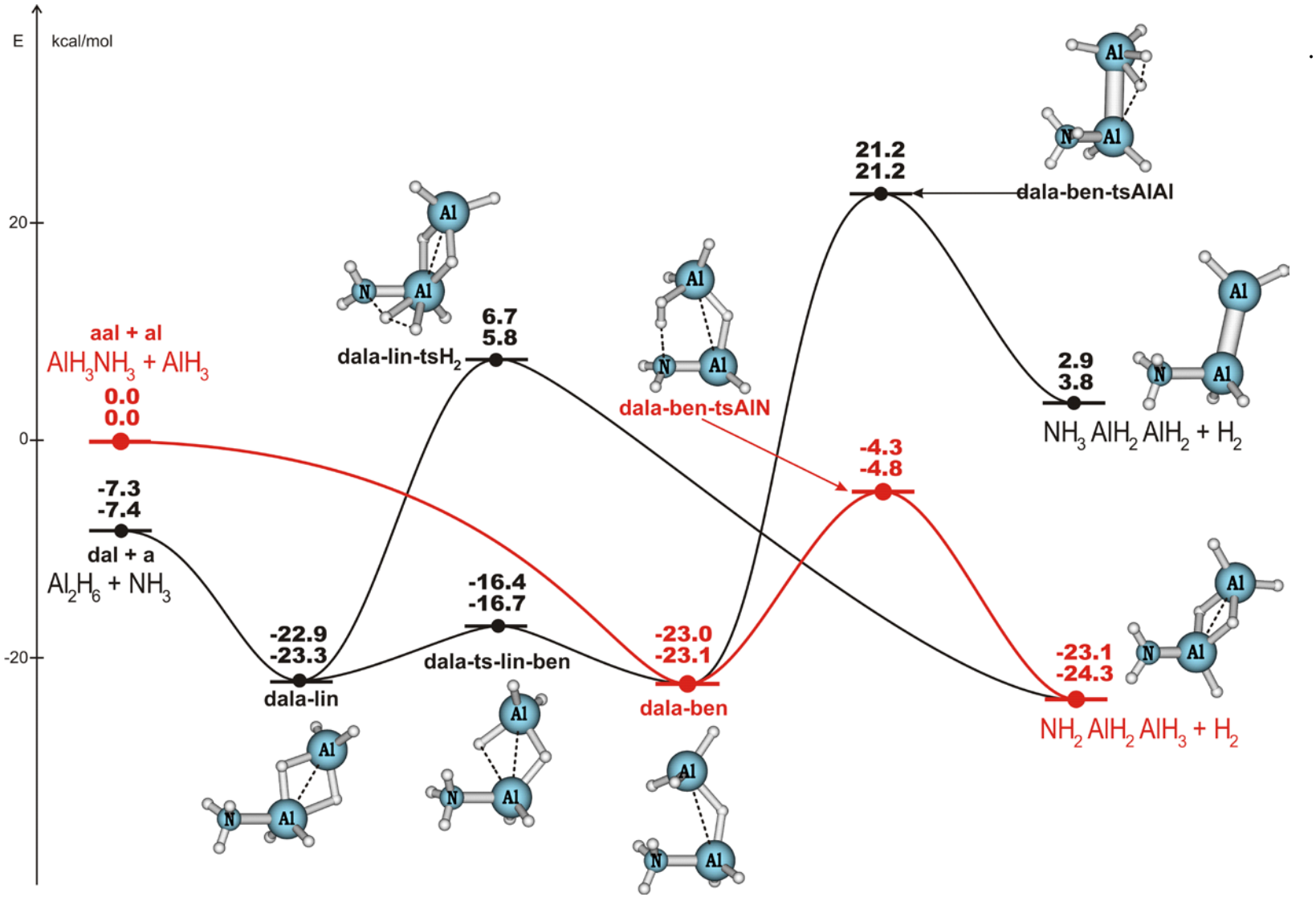

Figure 21. Schematic energy profiles showing the pathways for H_2-release from two adducts **dala-ben** and **dala-lin**. Relative energies in kcal/mol from calculations at the levels: *upper* CCSD(T)/aVTZ and *lower* CCSD(T)/CBS-aV*n*Z

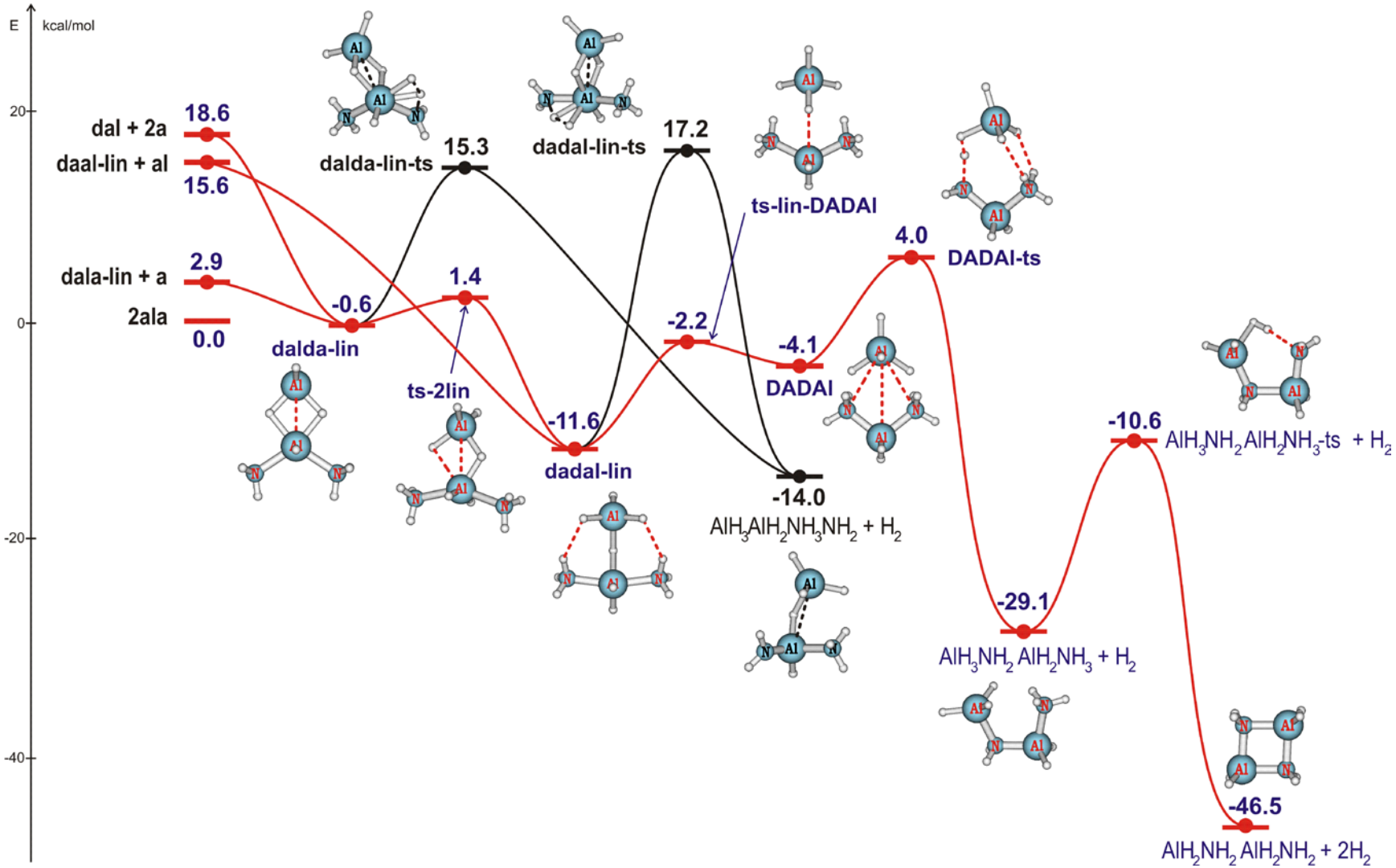

Figure 22. Schematic reaction pathways illustrating the H_2-release from $NH_3AlH_3NH_3$ + AlH_3, $Al_2H_6NH_3$ + NH_3, and Al_2H_6 + $2NH_3$. Relative energies given in kcal/mol at the CCSD(T)/aVTZ + ZPE level.

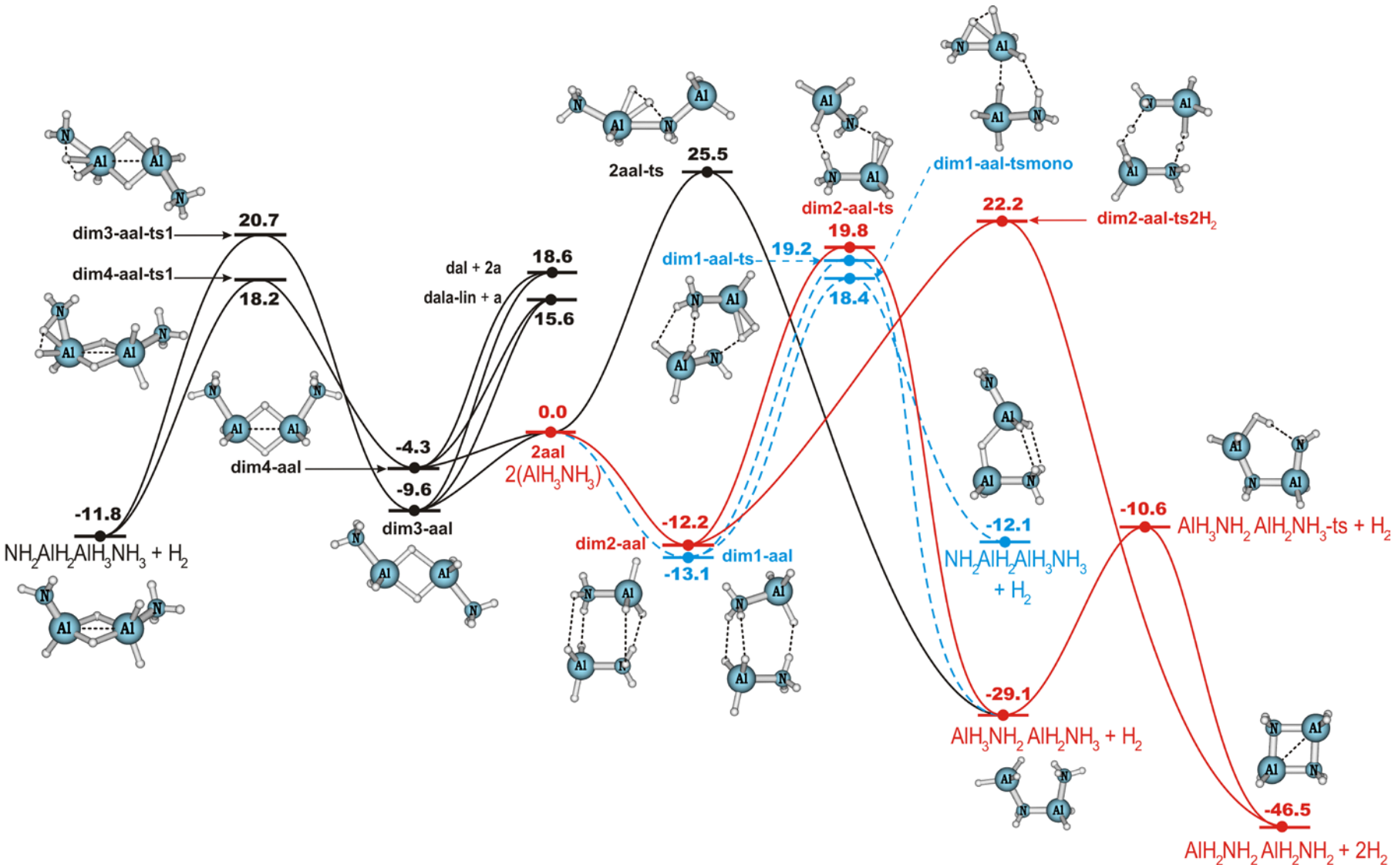

Figure 23. Schematic reaction pathways illustrating the H_2-release from dimers of ammonia alane. Relative energies in kcal/mol at the CCSD(T)/aVTZ + ZPE level.

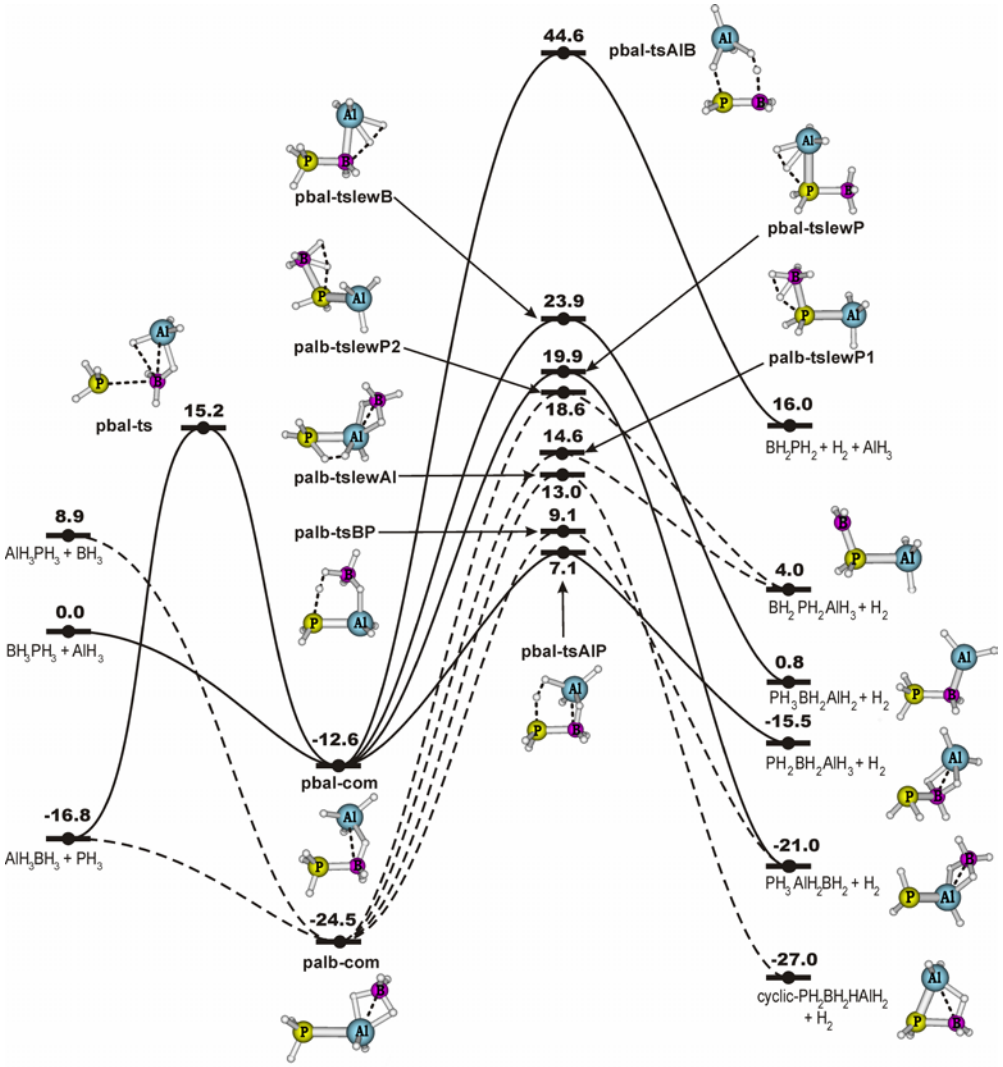

Figure 24. Schematic energy profiles illustrating reaction pathways for H_2-release from BH_3-PH_3 + AlH_3. Relative energies, in kcal/mol, were obtained from CCSD(T)/aug-cc-pVTZ + ZPE calculations

Transition States of the XH_3ZH_3 Dehydrogenation Reactions

We calculated the energy barriers (kcal/mol) at 0 K by B3LYP/DZVP2, obtaining the transition states (TS) for the $XH_3ZH_3 \rightarrow XH_2ZH_2 + H_2$ reaction, where X = Al or B and Z = N or P.

$AlH_3NH_3 \rightarrow AlH_2NH_2\cdots H_2$ (TS)	$\Delta E‡ = 27.6$	(76)
$AlH_3PH_3 \rightarrow AlH_2PH_2\cdots H_2$ (TS)	$\Delta E‡ = 34.4$	(77)
$BH_3PH_3 \rightarrow BH_2PH_2\cdots H_2$ (TS)	$\Delta E‡ = 34.5$	(78)
$BH_3NH_3 \rightarrow BH_2NH_2\cdots H_2$ (TS)	$\Delta E‡ = 30.4$	(79)

The barrier heights are comparable can be compared to the D-A donor-acceptor bond energies. The barrier heights tend to above the D-A bond dissociation energies.

Thermochemistry of Methyl Substitution

Thermochemistry for the Dehydrogenation of Alkyl Substituted Ammonia Boranes

It has recently been found that borane amine can be solubilized in methyl substituted borane amine enabling the generation of a liquid fuel and make refueling much easier and enabling the use of the current infrastructure. As the methyl substituted compounds are also hydrogen carriers, we have investigated the thermochemistry for the dehydrogenation of methyl substituted ammonia boranes from high level electronic structure coupled cluster theory (CCSD(T)) calculations to see if these would improve the weight issues. Heats of formation at 0 K and 298 K were predicted for $(CH_3)H_2N\text{-}BH_3$, $(CH_3)HN{=}BH_2$, $(BH_3)HN{=}CH_2$, $(CH_3)H_2B\text{-}NH_3$, $(CH_3)HB{=}NH_2$, and $(NH_3)HB{=}CH_2$, as well as various molecules involved in the different bond breaking processes, from CCSD(T) calculations plus additional corrections. The heats of formation were also predicted for the respective dimethyl- and trimethyl- substituted ammonia boranes, as well as their dehydrogenated derivatives and the various molecules involved in the different bond breaking processes, based on isodesmic reaction schemes calculated at the G3(MP2) level of theory.

Table 22. Calculated Heats of Formation in kcal/mol. Experimental Values at 298 K in Parentheses.

Molecule	**CCSD(T)**		**G3(MP2)**	
	Theory (0K)	**Theory (298K)**	**Theory (0K)**	**Theory (298K)**
$HBCH_2$ (C_{2v} - $^1A_1$)	53.2	52.4	54.1	53.2
$HBNH_2$ (C_s - $^2A'$)	36.2	34.4	37.8	36.1
$HNBH_2$ (C_1 - ^2A)	43.3	42.1	44.8	43.5
$HNCH_2$ (C_s - $^1A'$)	23.6	21.7	23.2	21.3
$HBCH_3$ (C_1 - ^2A)	61.4	59.8	62.3	60.9
$HBNH_3$ (C_1 - ^1A)	82.7	80.4	83.1	81.2
$HBNH_3$ (C_s - $^3A''$)	90.3	87.9	92.1	89.7
$HNBH_3$ (C_1 - ^3A)	83.4	81.3	85.0	82.7
$HNCH_3$ (C_s - $^2A''$)	45.9	43.3	45.9	43.3
H_2BCH_3 (C_s - $^1A'$)	10.3	7.7	11.6	9.1
H_2NCH_3 (C_s - $^1A'$)	-1.4	-4.7 (-5.6 ± 0.2)	-0.5	-4.1
$H_2B{=}NH_2$ (C_{2v} - $^1A_1$)	-17.0[c]	-19.7[c]	-15.1	-17.8
$(CH_3)HB{=}NH_2$ (C_s - $^1A'$)	-30.5	-34.7	-29.2	-33.3
$(NH_3)HB{=}CH_2$ (C_s - $^1A'$)	17.2	13.0	18.1	14.0
$(CH_3)HN{=}BH_2$ (C_s - $^1A'$)	-12.8	-17.1	-11.4	-15.7
$(BH_3)HN{=}CH_2$ (C_s - $^1A'$)	18.7	14.4	20.1	15.9
$H_3B\text{-}NH_3$ (C_{3v} - $^1A_1$)	-10.2[c]	-14.6[c]	-7.4	-11.7
$(CH_3)H_2B\text{-}NH_3$ (C_s - $^1A'$)	-19.4	-25.3	-17.8	-23.5
$(CH_3)H_2N\text{-}BH_3$ (C_s - $^1A'$)	-7.6	-13.7	-5.7	-11.6
$B(CH_3)_2$ (C_2 - ^2A)	45.8	42.6	46.4	43.5
$HB(CH_3)_2$ (C_2 - ^1A)	-5.2	-9.2	-4.3	-8.1
$N(CH_3)_2$ (C_{2v} - $^1A_1$)	43.6	39.9	43.1	39.1
$HN(CH_3)_2$ (C_s - $^1A'$)	1.8	-2.8 (-4.5 ± 0.4)	2.3	-2.9
$(CH_3)_2B{=}NH_2$ (C_{2v} - $^1A_1$)	-44.4	-49.8	-43.4	-48.6

$(CH_3)_2HB\text{-}NH_3$ (C_s - $^1A'$)	-30.9	-38.1	-29.5	-36.5
$(CH_3)_2N{=}BH_2$ (C_{2v} - $^1A_1$)	-11.3	-16.9	-10.4	-16.2
$(CH_3)_2HN\text{-}BH_3$ (C_s - $^1A'$)	-7.8	-15.1	-6.3	-13.8
$B(CH_3)_3$ (C_1 - ^1A)	-20.6	-25.7 (-29.7, -29.2 ± 3.0)	-20.0	-24.8
$N(CH_3)_3$ (C_{3v} - $^1A_1$)	1.5	-4.4 (-5.6 ± 0.3)	1.5	-5.2
$(CH_3)_3B\text{-}NH_3$ (C_{3v} - $^1A_1$)	-43.0	-51.5 (-54.1)	-42.0	-50.2
$(CH_3)_3N\text{-}BH_3$ (C_{3v} - $^1A_1$)	-9.2	-17.8 (-20.3, -20.4 ± 0.6)	-8.0	-17.2

Given the accurately calculated heats of formation, we have considered the possibility of several dehydrogenation pathways in the monomethyl substituted molecules, and predict that the dehydrogenation process across the B-N bond is more favorable as opposed to dehydrogenation across the B-C and N-C bonds for the compounds studied. The heat of reaction for the dehydrogenation of *N*-methylaminoborane, across the B-N bond, was predicted to be -3.7 kcal/mol at the CCSD(T) level at 298 K and -5.2 kcal/mol at the G3(MP2) level also at 298 K. The equivalent reaction for *B*-methylaminoborane was predicted to be -9.6 kcal/mol at the CCSD(T) level at 298 K and -11.0 kcal/mol at the G3(MP2) level also at 298 K. Considering the identical pathway for dehydrogenation in *N*-dimethylaminoborane and *B*-dimethylaminoborane, the reaction energies were predicted to be -2.0 and -11.9 kcal/mol at the CCSD(T) level at 298 K and -3.6 and -13.3 kcal/mol at the G3(MP2) level also at 298 K respectively.

Table 23. Dehydrogenation Reactions at 0 K and 298 K (kcal/mol).

Reaction	**CCSD(T)**		**G3(MP2)**	
	(0 K)	**(298 K)**	**(0 K)**	**(298 K)**
$H_3B\text{-}NH_3 \rightarrow H_2B{=}NH_2 + H_2$	-6.8	-5.1	-8.9	-7.3
$(CH_3)H_2N\text{-}BH_3 \rightarrow (CH_3)HN{=}BH_2 + H_2$	-5.4	-3.7	-6.9	-5.2
$(CH_3)H_2N\text{-}BH_3 \rightarrow (BH_3)HN{=}CH_2 + H_2$	26.0	27.7	24.5	26.3
$(CH_3)H_2B\text{-}NH_3 \rightarrow (CH_3)HB{=}NH_2 + H_2$	-11.3	-9.6	-12.6	-11.0
$(CH_3)H_2B\text{-}NH_3 \rightarrow (NH_3)HB{=}CH_2 + H_2$	36.6	38.2	34.7	36.3
$(CH_3)_2HN\text{-}BH_3 \rightarrow (CH_3)_2N{=}BH_2 + H_2$	-3.8	-2.0	-5.3	-3.6
$(CH_3)_2HB\text{-}NH_3 \rightarrow (CH_3)_2B{=}NH_2 + H_2$	-13.7	-11.9	-15.1	-13.3

In order to further understand their chemistry in terms of reactivity and stability, we estimate the π- and σ-bond energies of the various "double" bonds following the procedures we recently used for the Group IIIA–Group VA $H_2A{=}XH_2$ compounds based on rotation barriers. For the B=N bond, the transition state lies on the singlet surface as a dative π-bond is being broken. For the C=N and B=C bonds, a covalent π-bond is broken so we estimate the rotation barrier by calculating the energy of the triplet rotated transition state.

Table 24. Adiabatic Rotation Barriers (π-Bond Energies) at 0 K at the MP2/VTZ level (kcal/mol).

Molecule	**Rotation (G.S. → C_s)**
$H_2B{=}NH_2$[a]	29.7 (29.9)
$(CH_3)HN{=}BH_2$	36.8
$(BH_3)HN{=}CH_2$	71.3

$(CH_3)HB=NH_2$	26.3
$(NH_3)HB=CH_2$	63.0
$(CH_3)_2N=BH_2$	32.8
$(CH_3)_2B=NH_2$	25.3

[a] Value in parenthesis was calculated at the CCSD(T)/CBS level.

The adiabatic BDEs corresponds to dissociation to the ground states of the separated product species and are equal to the σ-bond energies in the singly bonded compounds or to the sum of the σ- and π-bond energies (binding energy) of the doubly bonded compounds, where the strength of the σ-bond energy of the doubly bonded compound is obtained by the difference in the binding energy and the π-bond energy (rotational energy barrier).

Table 25. Adiabatic (σ + π) Total Dissociation Energies and Adiabatic σ-Bond Energies 0 K at the CCSD(T) level (kcal/mol).

Reaction	**Bond Type**	**Total Dissociation Energy**	**σ-Bond Energy**
$H_2B=NH_2\ (^1A_1) \rightarrow BH_2\ (^2A_1) + \cdot NH_2\ (^2B_1)$	B=N	139.7	109.8
$(CH_3)HN=BH_2\ (^1A') \rightarrow BH_2\ (^2A_1) + H\cdot N\text{-}CH_3\ (^2A'')$	B=N	136.1	99.3
$(BH_3)HN=CH_2\ (^1A') \rightarrow CH_2\ (^3B_1) + HN\text{-}BH_3\ (^3A)$	N=C	158.2	86.9
$(CH_3)HB=NH_2\ (^1A') \rightarrow NH_2\ (^2B_1) + H\cdot B\text{-}CH_3\ (^2A)$	B=N	137.2	110.9
$(NH_3)HB=CH_2\ (^1A') \rightarrow CH_2\ (^3B_1) + HB\text{-}NH_3\ (^1A)$	B=C	158.9	95.9
$(CH_3)_2N=BH_2\ (^1A_1) \rightarrow BH_2\ (^2A_1) + N(CH_3)_2\ (^2A_1)$	B=N	132.3	99.5
$(CH_3)_2B=NH_2\ (^1A_1) \rightarrow NH_2\ (^2B_1) + B(CH_3)_2\ (^2A)$	B=N	135.4	110.1

As we have shown by the thermodynamic properties of the monomer analagues, the G3(MP2) method predicts reasonable heats of formation, BDEs, and dehydrogenation energies so we can use this method for larger B-C-N compounds, which would be too computationally expensive to calculate at the CCSD(T) level. Thus, we have used the G3(MP2) method to predict the heats of formation and dehydrogenation energies of the methlyated cyclodi-, cyclotri- and cyclotetraborazanes.

Table 26. Adiabatic σ-Bond Energies (B.E.) in kcal/mol.

Reaction	Bond Type	B.E. Calc (0K)	B.E. Calc (298 K)	B.E. Expt (298 K)	B. E. Calc (0 or 298 K)[b]
$H_3B\text{-}NH_3$ ($^1A_1$) → BH_3 ($^1A_1'$) + NH_3 ($^1A_1$)	B-N dative	25.9	27.7	31.1 ± 1.0	26.0 G2(MP2) 28.3 MP2/TZ2P (28.5) MP4 27.9 MP2 26.5 MP2 29.6 MP2
$(CH_3)HN{=}BH_2$ ($^1A'$) → $\cdot CH_3$ ($^2A_2''$) + $H\cdot N{=}BH_2$ (^2A)	C-N covalent	91.7	94.2		
$(BH_3)HN{=}CH_2$ ($^1A'$) → BH_3 ($^1A_1'$) + H $N{=}CH_2$ ($^1A'$)	B-N dative	30.2	31.7		
$(CH_3)HB{=}NH_2$ ($^1A'$) → $\cdot CH_3$ ($^2A_2''$) + $H\cdot B{=}NH_2$ ($^2A'$)	B-C covalent	102.4	104.1		
$(NH_3)HB{=}CH_2$ ($^1A'$) → NH_3 ($^1A_1$) + $HB{=}CH_2$ ($^1A_1$)	B-N dative	26.4	28.1		
$(CH_3)H_2N\text{-}BH_3$ ($^1A'$) → BH_3 ($^1A_1'$) + $NH_2(CH_3)$ ($^1A'$)	B-N dative	31.5	33.4	35.0 ± 0.8	31.9 G2(MP2) (31.3) HF/6-31G* 33.1 MP2 32.3 MP2 34.7 MP2
$(CH_3)H_2B\text{-}NH_3$ ($^1A'$) → $BH_2(CH_3)$ ($^1A'$) + NH_3 ($^1A_1$)	B-N dative	20.1	21.7		(23.5) HF/6-31G*
$(CH_3)_2HN\text{-}BH_3$ ($^1A'$) → BH_3 ($^1A_1'$) + $HN(CH_3)_2$ ($^1A'$)	B-N dative	34.9	36.7	36.4 ± 1.0	35.2 G2(MP2) (31.8) HF/6-31G* 35.9 MP2 35.6 MP2 37.3 MP2
$(CH_3)_2HB\text{-}NH_3$ ($^1A'$) → $HB(CH_3)_2$ (^1A) + NH_3 ($^1A_1$)	B-N dative	16.0	17.6		(19.0) HF/6-31G*
$(CH_3)_3N\text{-}BH_3$ ($^1A_1$) → BH_3 ($^1A_1'$) + $N(CH_3)_3$ ($^1A_1$)	B-N dative	36.0	37.8	34.8 ± 0.5 39.2 31.5	36.2 G2(MP2) 38.7 MP2/TZ2P (30.6) HF/6-31G* 36.6 MP2 36.8 MP2
$(CH_3)_3B\text{-}NH_3$ ($^1A_1$) → $B(CH_3)_3$ ($^1A_1'$) + NH_3 ($^1A_1$)	B-N dative	12.8	14.5	13.8 ± 0.3	(14.9) HF/6-31G* 15.4 MP2

Table 27. Calculated G3(MP2) Heats of Formation (kcal/mol).

Molecule	Theory (0 K)	Theory (298 K)
c-$B_2N_2H_4$ (D_{2h})	-23.6	-27.1
c-$B_2N_2H_8$ (D_{2h})[a]	-43.9	-50.9
c-$B_3N_3H_6$ (D_{3h})[a]	-106.5	-112.4
c-$B_3N_3H_{12}$ twist boat (C_3)[a]	-82.6	-93.5
c-$B_4N_4H_8$ (D_{4h})	-123.3	-131.0
c-$B_4N_4H_{16}$ (C_{4v})	-95.2	-110.0
c-$B_2N_2H_2(CH_3)_2$ *trans* (C_i)	-16.1	-21.6
c-$B_2N_2H_6(CH_3)_2$ *trans* (C_{2h})	-40.2	-50.0
c-$B_3N_3H_3(CH_3)_3$ (C_{3h})	-94.2	-103.5
c-$B_3N_3H_9(CH_3)_3$ (C_{3v})	-78.4	-93.6
c-$B_4N_4H_4(CH_3)_4$ (S_4)	-99.4	-111.8
c-$B_4N_4H_{12}(CH_3)_4$ (C_1)	-99.2	-119.6
$(H_3BH_2N)H_2C\text{-}CH_2(NH_2BH_3)$ (C_s)	0.3	-10.5
$(H_2B{=}NH)H_2C\text{-}CH_2(NH_2BH_3)$ (C_1)	-7.6	-16.8
$(H_3B)HN{=}CH\text{-}CH_2(NH_2BH_3)$ (C_1)	24.3	17.4
$(H_3BH_2N)HC{=}CH(NH_2BH_3)$ (C_i)	30.4	21.5
$(H_2B{=}NH)H_2C\text{-}CH_2(HN{=}BH_2)$ (C_i)	-14.8	-22.4
$(H_3B)HN{=}CHHC{=}NH(BH_3)$ (C_{2h})	47.2	40.0
$(H_3BH_2N)C{\equiv}C(NH_2BH_3)$ (C_2)	88.2	81.4
$(H_2B{=}NH)HC{=}CH(NH_2BH_3)$ (C_1)	20.6	13.2
$(H_2B{=}NH)HC{=}CH(HN{=}BH_2)$ (C_{2h})	7.3	1.4
$(H_3NH_2B)H_2C\text{-}CH_2(BH_2NH_3)$ (C_s)	-19.0	-29.3
$(H_2N{=}BH)H_2C\text{-}CH_2(BH_2NH_3)$ (C_1)	-30.8	-39.6
$(H_3N)HB{=}CH\text{-}CH_2(BH_2NH_3)$ (C_1)	16.6	7.9
$(H_3NH_2B)HC{=}CH(BH_2NH_3)$ (C_i)	2.0	-6.6
$(H_2N{=}BH)H_2C\text{-}CH_2(HB{=}NH_2)$ (C_i)	-41.4	-48.6
$(H_3N)HB{=}CH\text{-}HC{=}BH(NH_3)$ (C_{2h})	47.8	40.7
$(H_3NH_2B)C{\equiv}C(BH_2NH_3)$ (C_2)	19.5	12.7
$(H_2N{=}BH)HC{=}CH(BH_2NH_3)$ (C_1)	-8.5	-15.7
$(H_2N{=}BH)HC{=}CH(HB{=}NH_2)$ (C_{2h})	-21.0	-26.6

Methyl substitution at N in the cycloborazane rings increases the endothermicity of the dehydrogenation reactions and for *c*-$B_4N_4H_{12}(CH_3)_4$, the thermodynamics for dehydrogenation reaction become favorable as it is near thermoneutral. Dehydrogenation of *c*-$B_2N_2H_6(CH_3)_2$, *c*-$B_3N_3H_9(CH_3)_3$, and *c*-$B_4N_4H_{12}(CH_3)_4$ producing two, three, and four molecules of H_2 are 26.2, -13.0, and 3.4 kcal/mol at the G3(MP2) level at 298 K, respectively. Besides predicting the thermodynamics of the dehydrogenation of *N*-methylammonia borane and *B*-methylammonia borane as models for hydrogen release from the BCN compounds, we have also predicted the thermodynamics for dehydrogenation from $(H_3BH_2N)H_2C\text{-}CH_2(NH_2BH_3)$ and $(H_3NH_2B)H_2C\text{-}CH_2(BH_2NH_3)$, which are obtained from substituting NH_2BH_3 and BH_2NH_3 for H in C_2H_6, as two step processes at the G3MP2 level as shown in Table 28.

Table 28. Dehydrogenation Reactions at the G3(MP2) level (kcal/mol).

1st Dehydrogenation Step	**(0 K)**	**(298 K)**
c-$B_2N_2H_8 \rightarrow$ *c*-$B_2N_2H_4 + 2H_2$	17.9	21.6
c-$B_3N_3H_{12}$ twist boat $\rightarrow$ *c*-$B_3N_3H_6 + 3H_2$	-27.5[a]	-22.2[a]
c-$B_4N_4H_{16} \rightarrow$ *c*-$B_4N_4H_8 + 4H_2$	-33.0	-25.4
c-$B_2N_2H_6(CH_3)_2 \rightarrow$ *c*-$B_2N_2H_2(CH_3)_2 + 2H_2$	21.6	26.2
c-$B_3N_3H_9(CH_3)_3 \rightarrow$ *c*-$B_3N_3H_3(CH_3)_3 + 3H_2$	-19.4	-13.0
c-$B_4N_4H_{12}(CH_3)_4 \rightarrow$ *c*-$B_4N_4H_4(CH_3)_4 + 4H_2$	-7.3	3.4
$(H_3BH_2N)H_2C\text{-}CH_2(NH_2BH_3) \rightarrow (H_2B{=}NH)H_2C\text{-}CH_2(NH_2BH_3) + H_2$	-9.0	-7.4
$(H_3BH_2N)H_2C\text{-}CH_2(NH_2BH_3) \rightarrow (H_3B)HN{=}CH\text{-}CH_2(NH_2BH_3) + H_2$	22.9	26.7
$(H_3BH_2N)H_2C\text{-}CH_2(NH_2BH_3) \rightarrow (H_3BH_2N)HC{=}CH(NH_2BH_3) + H_2$	29.0	30.8
$(H_3NH_2B)H_2C\text{-}CH_2(BH_2NH_3) \rightarrow (H_2N{=}BH)H_2C\text{-}CH_2(BH_2NH_3) + H_2$	-13.0	-11.4
$(H_3NH_2B)H_2C\text{-}CH_2(BH_2NH_3) \rightarrow (H_3N)HB{=}CHC\text{-}H_2(BH_2NH_3) + H_2$	34.4	36.1
$(H_3NH_2B)H_2C\text{-}CH_2(BH_2NH_3) \rightarrow (H_3NH_2B)HC{=}CH(BH_2NH_3) + H_2$	19.8	21.6
2nd Dehydrogenation Step		
$(H_2B{=}NH)H_2C\text{-}CH_2(NH_2BH_3) \rightarrow (H_2B{=}NH)H_2CCH_2(HN{=}BH_2) + H_2$	-8.4	-6.8
$(H_3B)HN{=}CH\text{-}CH_2(NH_2BH_3) \rightarrow (H_3B)HN{=}CHHC{=}NH(BH_3) + H_2$	21.7	21.5
$(H_3BH_2N)HC{=}CH(NH_2BH_3) \rightarrow (H_3BH_2N)C{\equiv}C(NH_2BH_3) + H_2$	56.6	58.8
$(H_2B{=}NH)H_2C\text{-}CH_2(NH_2BH_3) \rightarrow (H_2B{=}NH)HC{=}CH(NH_2BH_3) + H_2$	27.0	28.9
$(H_2N{=}BH)H_2C\text{-}CH_2(BH_2NH_3) \rightarrow (H_2N{=}BH)H_2C\text{-}CH_2(HB{=}NH_2) + H_2$	-11.8	-10.2
$(H_3N)HB{=}CH\text{-}CH_2(BH_2NH_3) \rightarrow (H_3N)HB{=}CH\text{-}HC{=}BH(NH_3) + H_2$	30.0	31.6
$(H_3NH_2B)HC{=}CH(BH_2NH_3) \rightarrow (H_3NH_2B)C{\equiv}C(BH_2NH_3) + H_2$	16.3	18.2
$(H_2N{=}BH)H_2C\text{-}CH_2(BH_2NH_3) \rightarrow (H_2N{=}BH)HC{=}CH(BH_2NH_3) + H_2$	21.0	22.7
3rd Dehydrogenation Step		
$(H_2B{=}NH)H_2C\text{-}CH_2(HN{=}BH_2) \rightarrow (H_2B{=}NH)HC{=}CH(HN{=}BH_2) + H_2$	19.2	20.9
$(H_2N{=}BH)H_2C\text{-}CH_2(BH{=}NH_2) \rightarrow (H_2N{=}BH)HC{=}CH(HB{=}NH_2) + H_2$	20.9	22.6

As for the monomers, dehydrogenation to form B=N bonds are exothermic whereas dehydrogenation to form C=C or N=C bonds are substantially endothermic, following the differences found in dehydrogenation of ethane as compared to borane amine. Considering the third dehydrogenation step occurring across the C-C bond with the consequent energies for $(H_2B{=}NH)H_2C\text{-}CH_2(HN{=}BH_2)$ and $(H_2N{=}BH)H_2C\text{-}CH_2(HB{=}NH_2)$ predicted to be endothermic indicates that dehydrogenation is not likely unless one can couple the exothermicity of the loss of H_2 across the B-N bonds with that of the endothermicity of elimination across the C-C bond.

Thermochemistry of Methylated BN Cycles

There is substantial interest in the Center in improving solvation of ammonia-borane by using methylated derivatives. We calculated the heats of formation of the lowest energy conformers for the methylated BN-cycles at different computational levels (Table 29).

Table 29. Heats of Formation of Methylated BN-Cyles in kcal/mol.

Molecule	ΔH_f^o DFT isodesmic	ΔH_f^o G3MP2 isodesmic	ΔH_f^o G3MP2
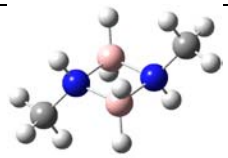	-48.6	-53.5	-47.8
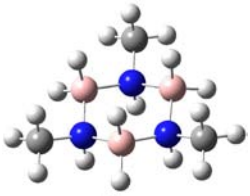	-87.1	-98.1	-90.5
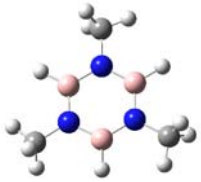	-102.4	-107.8	-100.2

Energies for hydrogen elimination from methylated and non-methylated BN cycles have been calculated in kcal/mol. Based on the calculated dehydrogenation energies, we note that methylation reduces the exothermicity of the reaction and draws it closer to thermoneutral.

Dehydrogenation Reaction		ΔH(298K) from ΔH_f high accuracy	ΔH(298K) from ΔH_f G3MP2
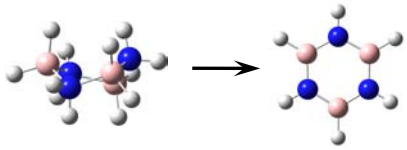	+ $3H_2$	-18.7	-22.2
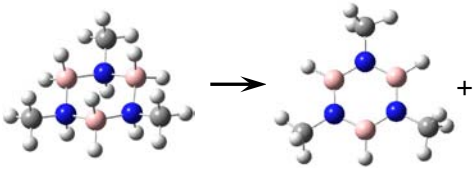	+ $3H_2$		-13.0

The energies of methylated BN cyclic compounds *N*-*N*'-$B_2N_2H_6(CH_3)_2$, *N*-*N*'-*N*''-$B_3N_3H_9(CH_3)_3$ and *N*-*N*'-*N*''-*N*'''-$B_4N_4H_{12}(CH_3)_4$, on every *N*-axial and/or *N*-equatorial Me substitution, have been calculated with B3LYP/DZVP2. The following reaction energies have been calculated (Table 30).

Table 30. Energies for CH_4/H_2 exchange reactions for amin-borane rings in kcal/mol

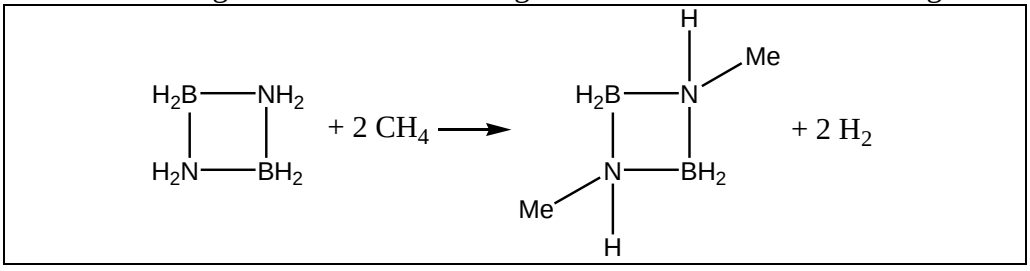

Me axial on N	Me equatorial on N	ΔH(298 K)	ΔG(298 K)
0	2	42.7[a]	45.8[a]
1	1	42.7	45.5
2	0	42.7[a]	45.8[a]

From $B_3N_3H_{12}$, chair conformation

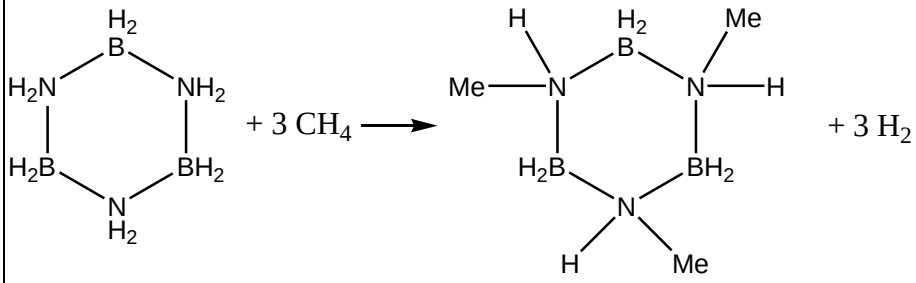

Me axial on N	Me equatorial on N	ΔH(298 K)	ΔG(298 K)
0	3	65.0	70.6
1	2	65.8	71.3
2	1	67.8	73.3
3	0	70.7	76.9

From $B_3N_3H_{12}$, twist-boat conformation

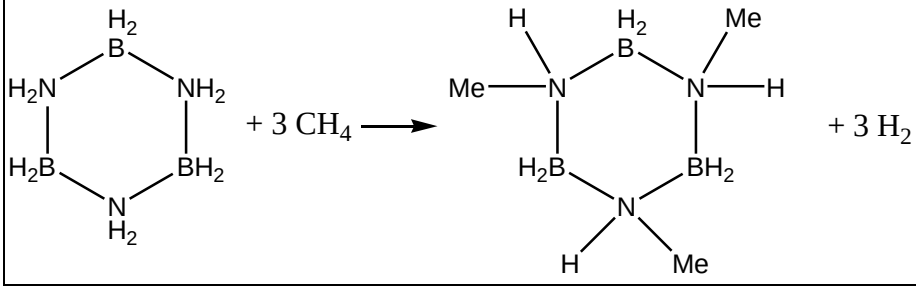

Me axial on N	Me equatorial on N	ΔH(298 K)	ΔG(298 K)
0	3	65.60[b]	71.46[b]
1	2	65.60[b]	71.46[b]
2	1	69.28[c]	75.43[c]
3	0	69.28[c]	75.43[c]

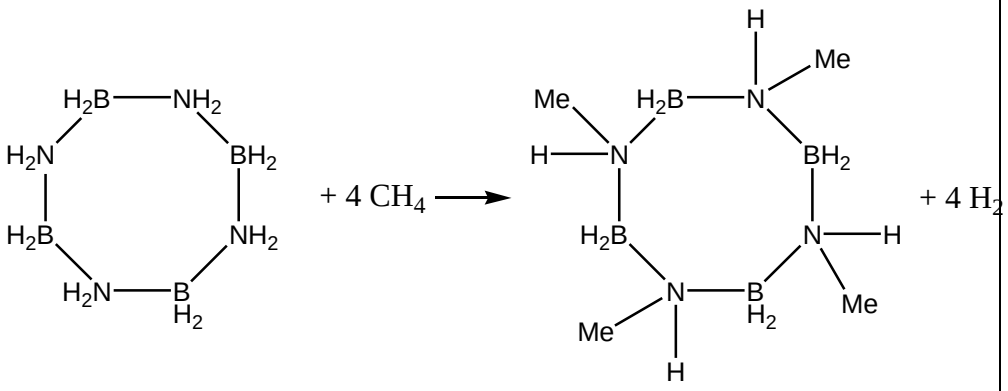

Me axial on N[d]	Me equatorial on N[d]	ΔH(298 K)	ΔG(298 K)
0	4	92.8	101.0
1a	3a	92.3	100.2

1b	3b	101.1	109.4
1c	3c	95.5	103.9
1d	3d	91.1	99.9
2a	2a	95.1	103.6
2b	2b	99.4	108.2
2c	2c	92.0	101.0
2d	2d	95.5	103.7
2e	2e	103.4	111.8
2f	2f	96.0	105.0
3a	1a	96.9	106.0
3b	1b	99.1	107.8
3c	1c	101.6[e]	111.1[e]
3d	1d	100.6	109.2
4	0	101.0	109.7

[a,b,c] The axial-equatorial arrangement leads to the same conformer. [d] $B_4N_4H_{16}$ is not symmetric as $B_3N_3H_{12}$ or $B_2N_2H_8$, therefore, a, b, c, d, e, and f stand for the different obtained conformations. [e] This is a conformer with one of the highest energies and the only one showing an imaginary vibrational mode, although this is very small (-8.23*i*).

Our results show that the release of hydrogen from the methylation on N of $B_xN_xH_{4x}$ (x = 2, 3, and 4) cycles are very endothermic processes.

Thermodynamics for B-N containing heterocyles

Complete Dehydrogenation of $B_2N_2C_2H_{12}$ to $B_2N_2C_2H_6$

We calculated all possible combinations for the $B_2N_2C_2H_6$ compound, in order to find the isomer with the lowest energy. We used B3LYP/DZVP2 and G3MP2 and obtained similar results with both methods. The isomers were then hydrogenated to form the compounds with 12 H atoms, in their boat, chair and twist-boat conformations. This enabled us to calculate the thermodynamics for the dehydrogenation process of these compounds. Initially, we calculated the complete dehydrogenation pathways for the $B_2N_2C_2H_{12}$ of the lowest energy isomer (C-C-N-B-N-B sequence), the second lowest energy isomer for $B_2N_2C_2H_{12}$ (C-B-N-C-B-N sequence) and the second lowest energy isomer for $B_2N_2C_2H_6$ (C-B-N-C-N-B sequence). We calculated the dehydrogenation energies for the different conformers (Table 31) with B3LYP/DZVP2 and G3MP2 (and with G3B3 in selected cases due to issues with ring vs. chain structures for the higher energy isomers).

Table 31. G3(MP2), B3LYP/DZVP2, and Selected G3B3 Relative Energies (ΔE_{rel}) at 298 K for the Different $B_2N_2C_2H_6$ and Their Corresponding $B_2N_2C_2H_{12}$ Isomers with Respect to the Lowest Energy Isomer. Dehydrogenation Energies ($\Delta H_{dehydro}$) at 298 K for the Reaction: $B_2N_2C_2H_{12} \rightarrow B_2N_2C_2H_6 + 3H_2$. All Energies are in kcal/mol.[a]

$B_2N_2C_2H_6$ Isomer	$\Delta E_{rel,G3(MP2)}$ [$\Delta E_{rel,B3LYP}$] ($\Delta E_{rel,B3G3}$)	$B_2N_2C_2H_{12}$ Isomer	$\Delta E_{rel,G3(MP2)}$ [$\Delta E_{rel,B3LYP}$] ($\Delta E_{rel,B3G3}$)	$\Delta H_{dehydro,G3(MP2)}$ [$\Delta H_{dehydro,B3LYP}$] ($\Delta H_{dehydro,G3B3}$)
 **1-H_6**	0.0 [0.0] (0.0)	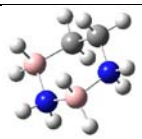 **1-H_{12}**	0.0 [0.0] (0.0)	-0.6 [-0.7] (2.5)
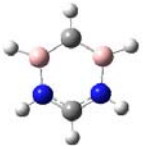 **2-H_6**	34.6 [34.3]	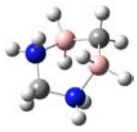 **2-H_{12}**	37.7 [38.9]	-3.7 [-5.3]
 **3-H_6**	37.6 [35.9]	 **3-H_{12}**	20.1 [19.9]	16.9 [15.3]
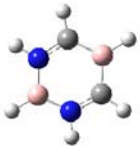 **4-H_6**	39.6 [38.0]	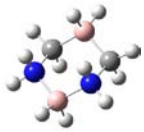 **4-H_{12}**	19.9 [20.1]	19.1 [17.1]
 **5-H_6**	42.4 [40.3]	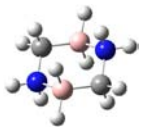 **5-H_{12}**	13.4 [13.1]	28.4 [26.5]
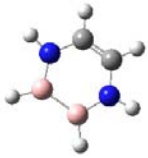 **6-H_6**	43.8 [43.2]	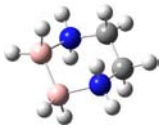 **6-H_{12}**	50.0 [50.7]	-6.8 [-8.2]
 **7-H_6**	51.2 [50.3]	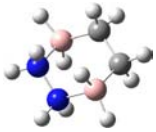 **7-H_{12}**	56.8 [56.4]	-6.2 [-6.8]
	78.1 [76.6] (77.9)	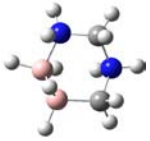	[94.6][b] (93.5)	[-18.8][b] (-13.1)

8-H_6		**8-H_{12}**		
		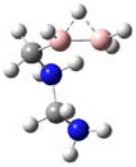	83.6 [81.7] (84.1)	-6.2 [-5.9] (-3.7)
		non cyclic 8-H_{12}		
	86.9 [84.9] (86.7)		102.1[c]	-15.8[c]
9-H_6		**chair 9-H_{12}**		
			[100.1][d] (100.4)	[-16.0][d] (-11.2)
		boat 9-H_{12}		
		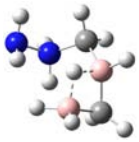	87.1 [87.1] (88.1)	-0.8 [-2.9] (1.2)
		non cyclic 9-H_{12}		
	93.4 [91.2] (92.7)	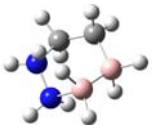	[129.7][b] (129.1)	[-39.2][b] (-33.9)
10-H_6		**10-H_{12}**		
		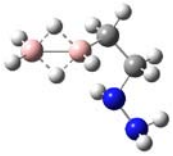	76.2 [73.3] (77.0)	16.6 [17.2] (18.2)
		non cyclic 10-H_{12}		
	131.4 [128.6]	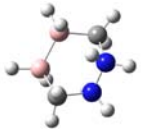	168.0 [168.3]	-37.2 [-40.3]
11-H_6		**11-H_{12}**		

[a] Color code: Pink = Boron; Blue = Nitrogen; Gray = Carbon; White = Hydrogen. [b] Only DFT and G3B3 results. G3MP2 optimization of this cyclic structure yields a non cyclic structure. [c] $\mathbf{\Delta E_{rel}}$ = [102.6] and (102.5) and $\mathbf{\Delta H_{dehydro}}$ = [-18.5] and (-13.2). [DFT] and (G3B3). [d] G3MP2 optimization of the boat structure yield a non cyclic structure, however the boat structure is the lowest energy structure for the cyclic isomer when calculated with B3LYP/DZVP2 and G3B3.

The C-C-B-N-B-N sequence gives the lowest energy isomers, either with 6 H or with 12 H. The dehydrogenation of the 12 H cycle with the C-C-B-N-B-N sequence to give the 6 H cycle also shows a process close to thermoneutral at 298 K. Due to the formation of three H_2 molecules in the gas phase, the free energies are more negative by about 25 kcal/mol as compared to the enthalpies.

From the lowest energy 12 H isomer we calculated the thermodynamics for the step–by-step dehydrogenation sequence for all possible dehydrogenated compounds with 10 H and 8 H. Figure 25 shows the different dehydrogenation processes. Overall exothermic schemes (Table 32) were found.

Table 32. All Possible $B_2N_2C_2H_{10} \rightarrow B_2N_2C_2H_8 + H_2$ Reactions for the Cycles with the C-C-B-N-B-N Sequence (see Figure 25 for further details).

Reaction	*ΔH (298 K)*	*[ΔG (298 K)]*	Reaction	*ΔH (298 K)*	*[ΔG (298 K)]*
1	-10.5	[-19.2]	**10**	13.4	[-2.8]
2	-19.2	[9.5]	**11**	33.9	[1.7]
3	18.9	[19.1]	**12**	24.8	[-12.3]
4	9.5	[-21.8]	**13**	1.3	[14.7]
5	27.9	[13.4]	**14**	-7.3	[13.4]
6	19.1	[24.8]	**15**	-1.8	[0.3]
7	-13.2	[-7.3]	**16**	-10.5	[-4.5]
8	-21.8	[-10.5]	**17**	15.8	[3.9]
9	22.1	[6.8]	**18**	6.8	[4.7]

We calculated the different dehydrogenation pathways for the **3-H_{12}** (Figure 26) and **6-H_{12}** (Figure 27) isomers since both of them have relatively low enthalpies for the loss of $3H_2$ molecules, ΔH = 16.9 kcal/mol and -6.8 kcal/mol, respectively, at the G3MP2 level of calculation. In Figure 26, the lowest energy pathway is the one with the initial H_2 loss coming from one of the B-N groups in the structure (ΔH = 10.1 kcal/mol at the G3MP2 level), the second H_2 loss is from opposite C-N (ΔH = 8.2 kcal/mol at the G3MP2 level) leaving a structure with hydrogens on a B and C that are in the 1,4 orientation. The final H_2 loss has ΔH = -1.5 kcal/mol at the G3MP2 level. It is interesting to note that the free energy for each step (1.2, -0.8, -8.8 kcal/mol, respectively) is almost 0, making this pathway very feasible. In Figure 26, the overall energy is small and exothermic (ΔH = -6.9 kcal/mol at G3MP2) in comparison with the previous isomer. Loss of the first and the second H_2 from the B-N groups in the structure yields slightly exothermic steps (ΔH = -13.8 and -5.1 kcal/mol at the G3MP2 level, respectively). The third H_2 is lost from the C-C group with a slightly endothermic energy (ΔH = 12.0 kcal/mol at the G3MP2 level).

Computational Predictions of Thermodynamics for Hydrogen Release from Alkyl-Substituted Boron-Nitrogen Heterocyles

Substituted C_4BNR (R = H, CH_3, t-butyl) heterocycles have been investigated as hydrogen storage materials that are readily reversible in collaboration with the University of Oregon. Initially, geometry optimizations and vibrational frequencies were calculated with the DFT method at the B3LYP/DZVP2 level. In order to improve our predicted energies, we further

performed calculations at the G3(MP2) level of theory starting from the DFT-B3LYP geometries. By combining our computed G3MP2 total atomization energies with the known heats of formation at 0 K for the elements, we derived $\Delta H_{f,0K}$ values for the molecules under study in the gas phase from which the various dehydrogenation pathways were predicted as indicated in Figure 28. The results show that both the methyl- and t-butyl substituents have similar effects on the overall energetics of the various hydrogenation reactions to within 1 kcal/mol. Methylation reduces the endothermicity of the overall hydrogenation reaction, adding 3 molecules of hydrogen to the fully depleted material, and makes it more thermoneutral. On the basis of the free energies, initial hydrogenation of a C-C bond is slightly endothermic by ~5 kcal/mol, in contrast to the second hydrogen addition which is exothermic by ~16 kcal/mol. The final hydrogenation of the B-N bond is endothermic by ~14 kcal/mol based on the free energy values.

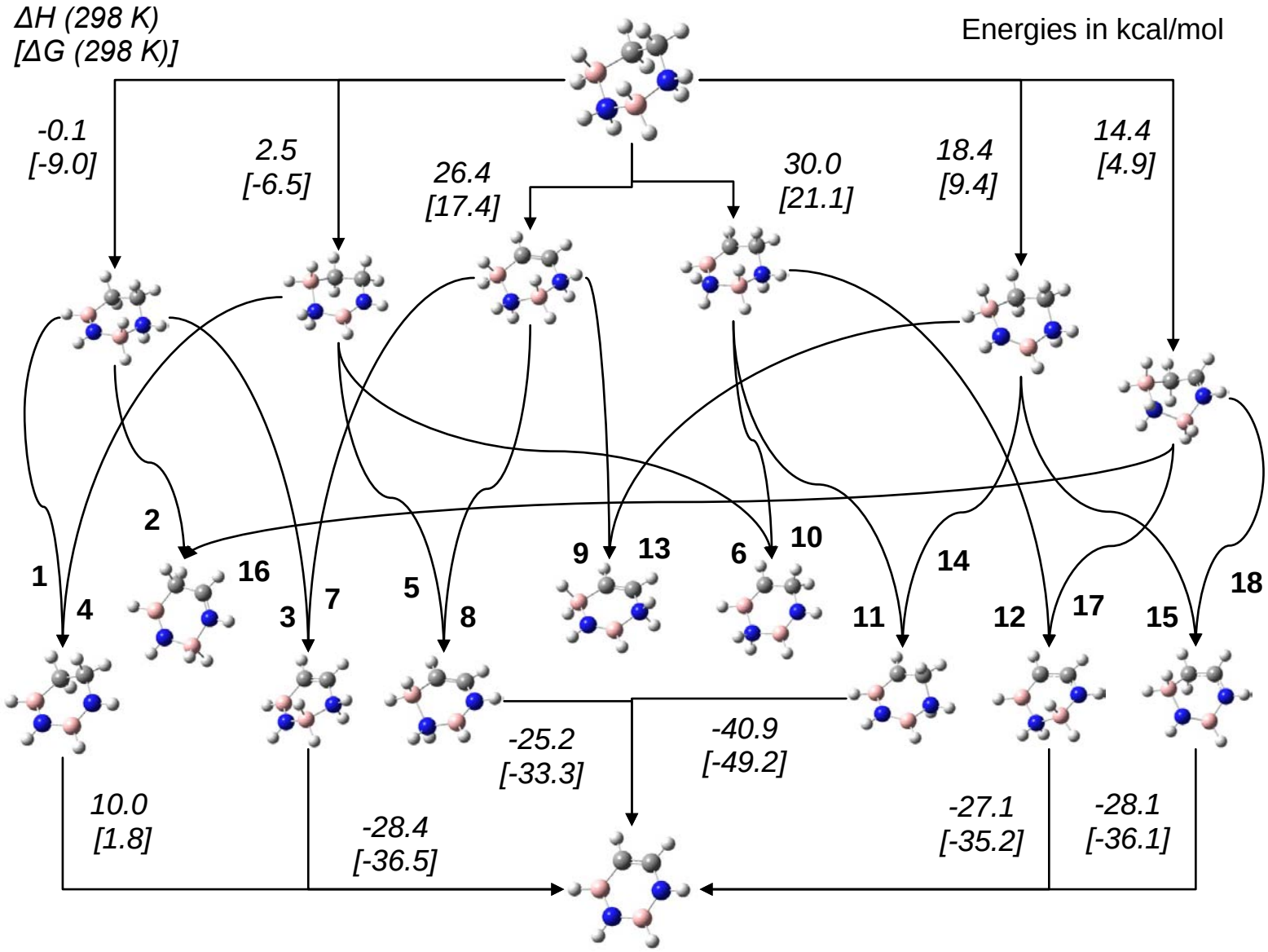

Figure 25. Step by step dehydrogenation process from $B_2N_2C_2H_{12}$ to $B_2N_2C_2H_6$ (lowest energy isomers).

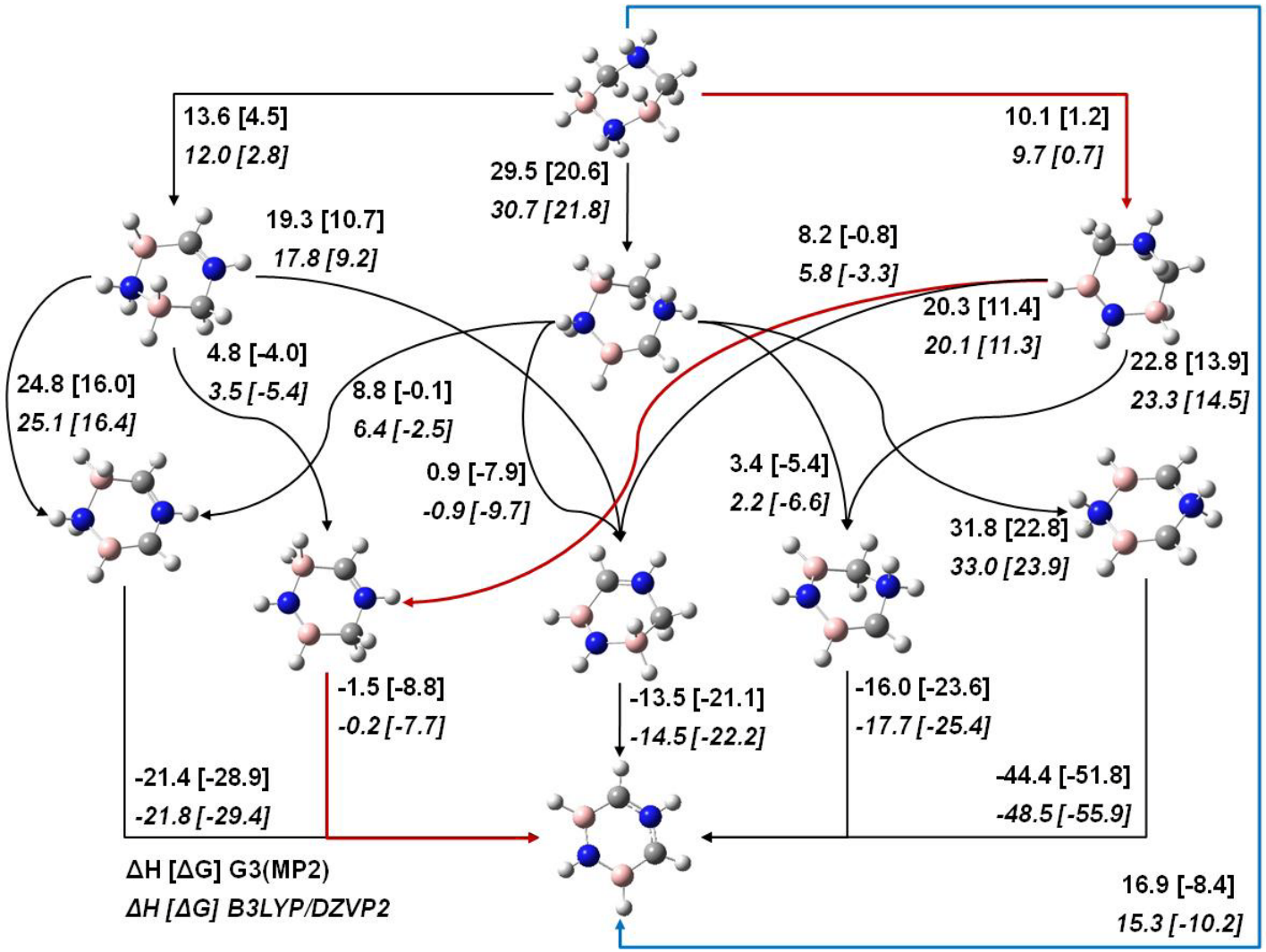

Figure 26. Step by step dehydrogenation process from $B_2N_2C_2H_{12}$ to $B_2N_2C_2H_6$ (third lowest energy isomer for 6 H, C-N-C-B-N-B sequence). Red lines show the most feasible pathways. Blue line shows the energy for the reaction: $B_2N_2C_2H_{12} \rightarrow B_2N_2C_2H_6 + 3H_2$. All energies are in kcal/mol.

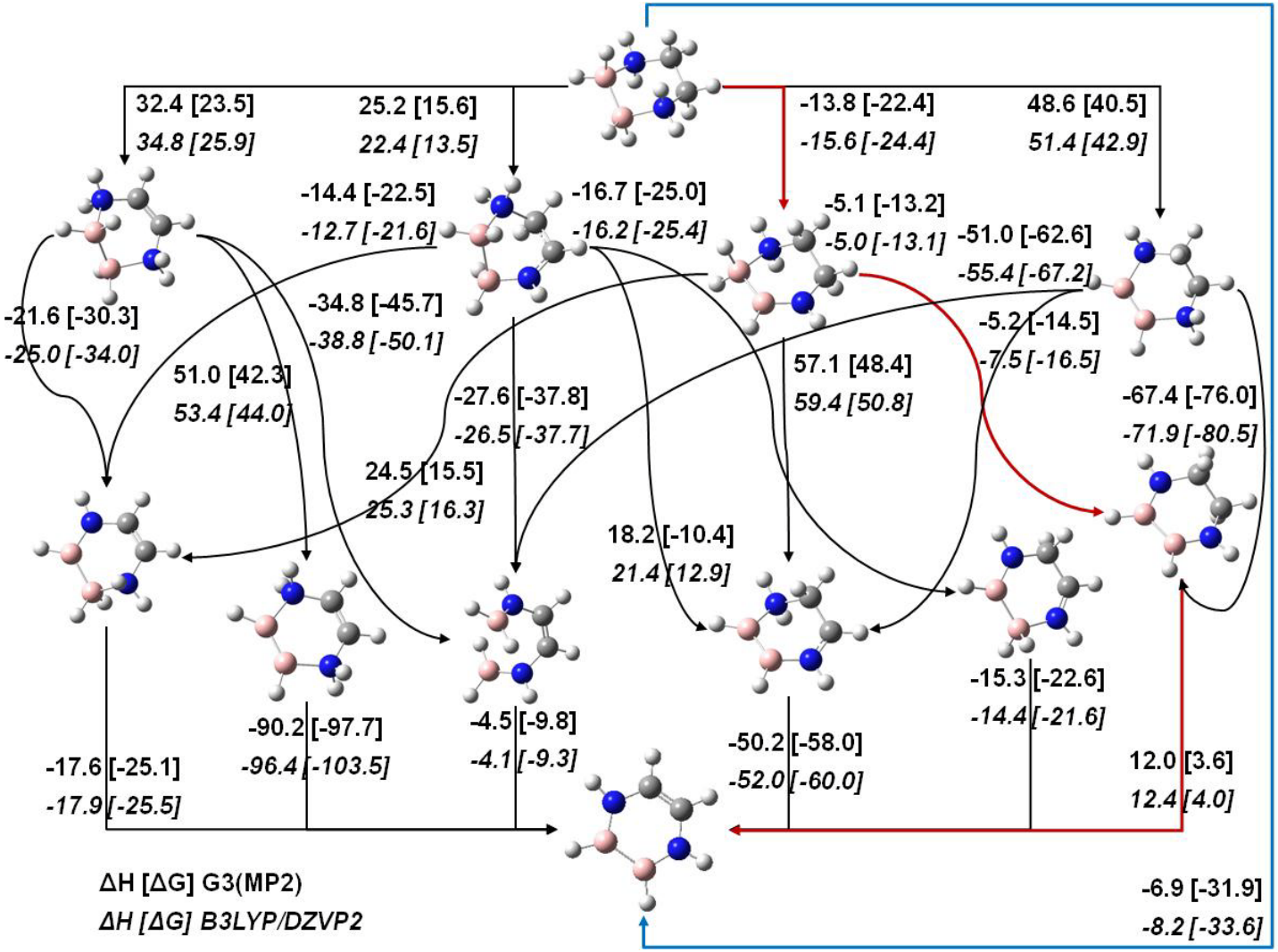

Figure 27. Step by step dehydrogenation process from $B_2N_2C_2H_{12}$ to $B_2N_2C_2H_6$ (C-C-N-B-B-N sequence). Red lines show the most feasible pathways. Blue line shows the energy for the reaction: $B_2N_2C_2H_{12} \rightarrow B_2N_2C_2H_6 + 3H_2$. All energies are in kcal/mol.

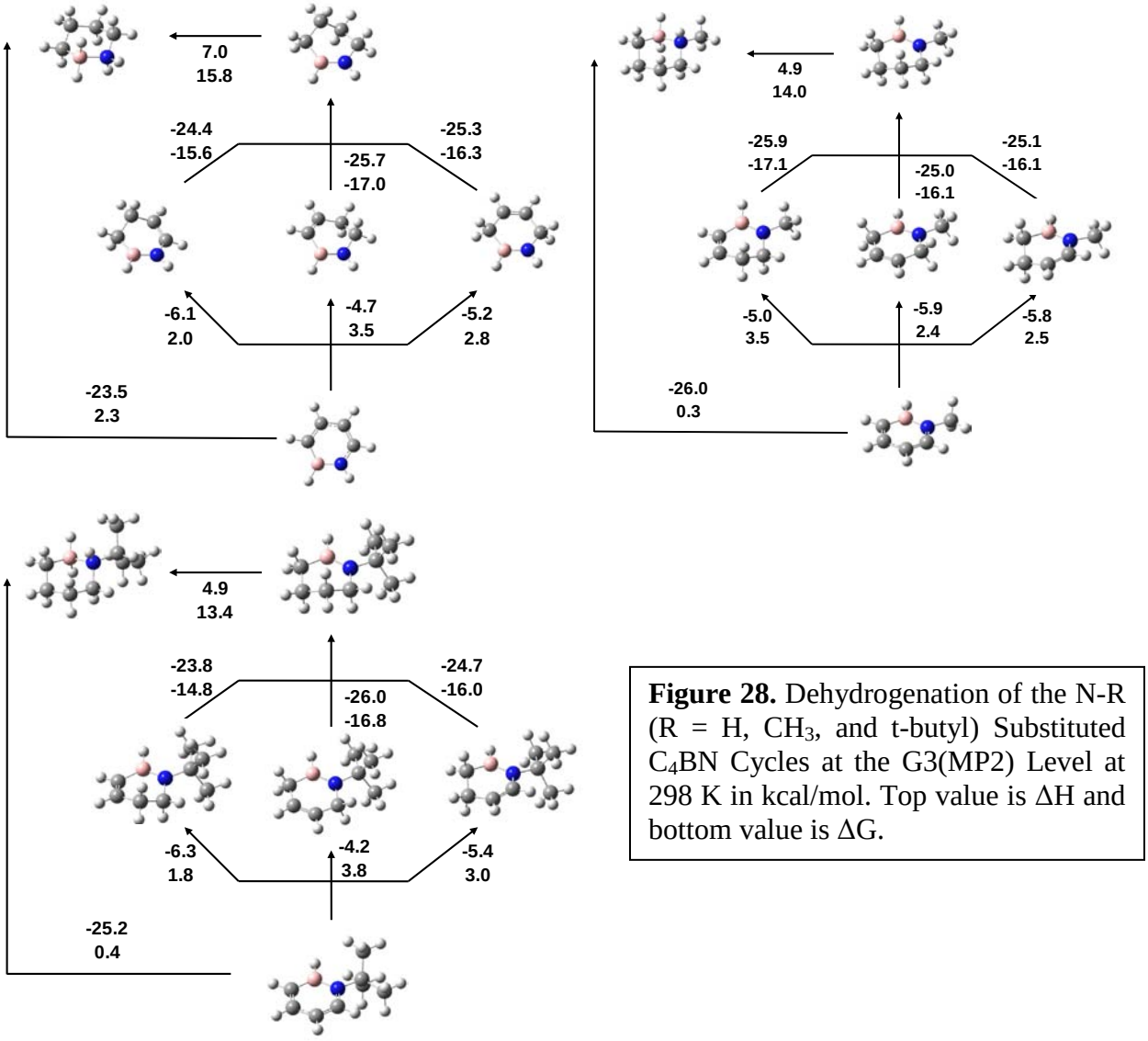

Figure 28. Dehydrogenation of the N-R (R = H, CH_3, and t-butyl) Substituted C_4BN Cycles at the G3(MP2) Level at 298 K in kcal/mol. Top value is ΔH and bottom value is ΔG.

Heats of Formation and Thermochemistry of Condensed Rings Containing the B-N Bond

We have calculated the dehydrogenation energies of various rings containing C, B, N, H for the Center especially the groups at UW, Oregon, PNNL, and LANL, on the basis of heats of formation calculated at the G3MP2 level. The calculated heats of formation at 298 K are given in Table 33. We have analyzed the various pathways for hydrogen release across different available bonds and find that dehydrogenation across the B-N is more favorable as opposed to dehydrogenation across a C-C bond as expected. In addition, we have shown that the size of the alkyl substituent (methyl as opposed to isopropyl) essentially has no effect on the heat of reaction for hydrogen release to within 1 kcal/mol. We have also looked at dehydrogenation in the "indole-type" and "naphthalene-type" heterocycles and find that hydrogen release from the "indole-type" molecules as well as the "naphthalene-type" molecules across the C-C bonds are largely endothermic, whereas for the "naphthalene-type" molecules, the dehydrogenation process occurring across the single available B-N bond was the most favorable.

Table 33. Calculated G3(MP2) Feats of Formation at 298 K in kcal/mol.

Molecular Structure	ΔH_f^0	Molecular Structure	ΔH_f^0
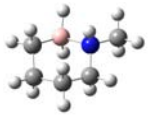	-26.1		8.6
	-29.8		0.3
	-2.8	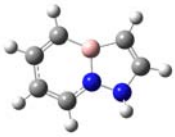	49.1
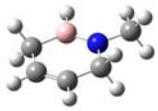	-3.6		-18.3
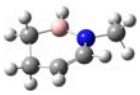	-3.6		32.7
	-44.9	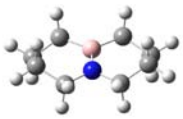	-43.5
	-48.7		25.5
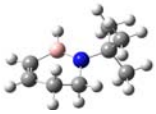	-22.9	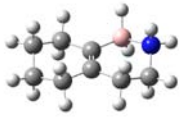	-12.1
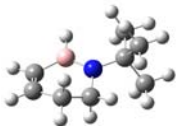	-21.6	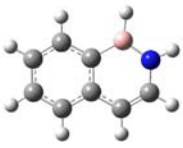	13.0

	-23.8	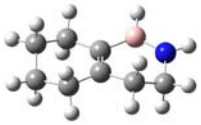	-17.9
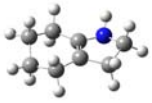	6.7	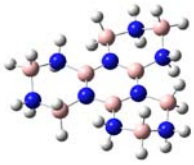	-315.5
	37.9		-384.8
	-39.6	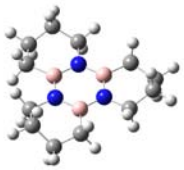	-146.1
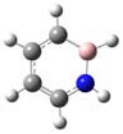	3.7		-37.0

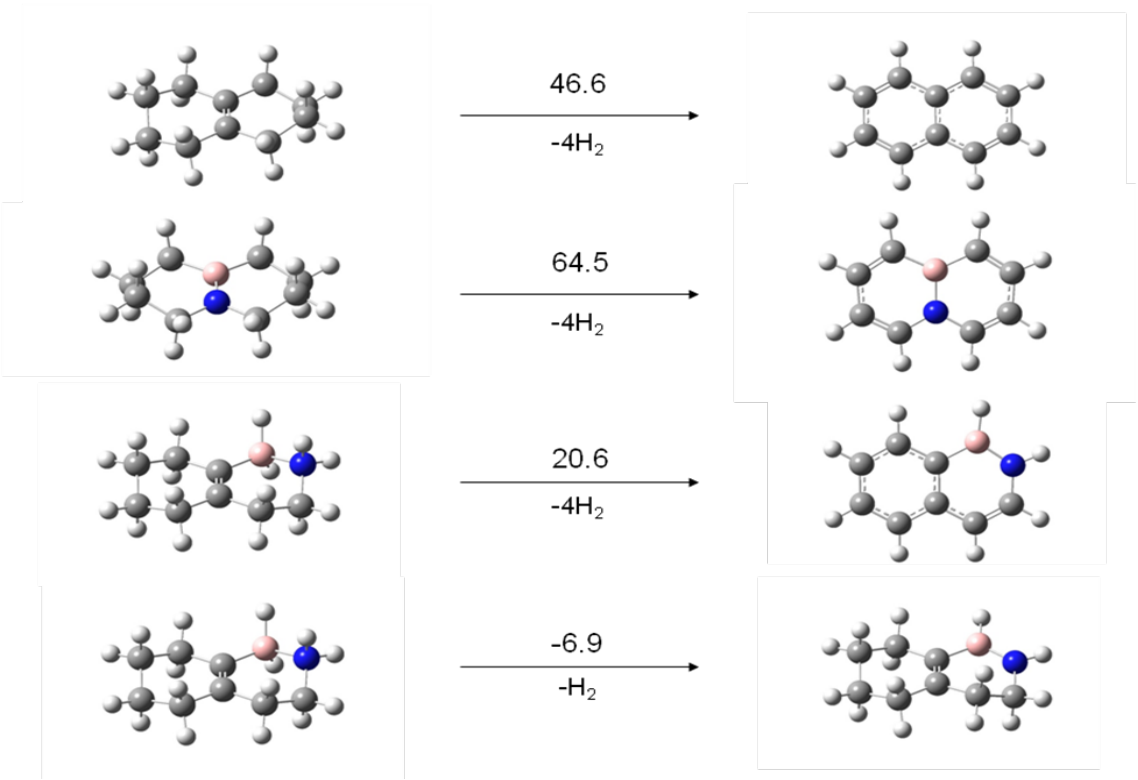

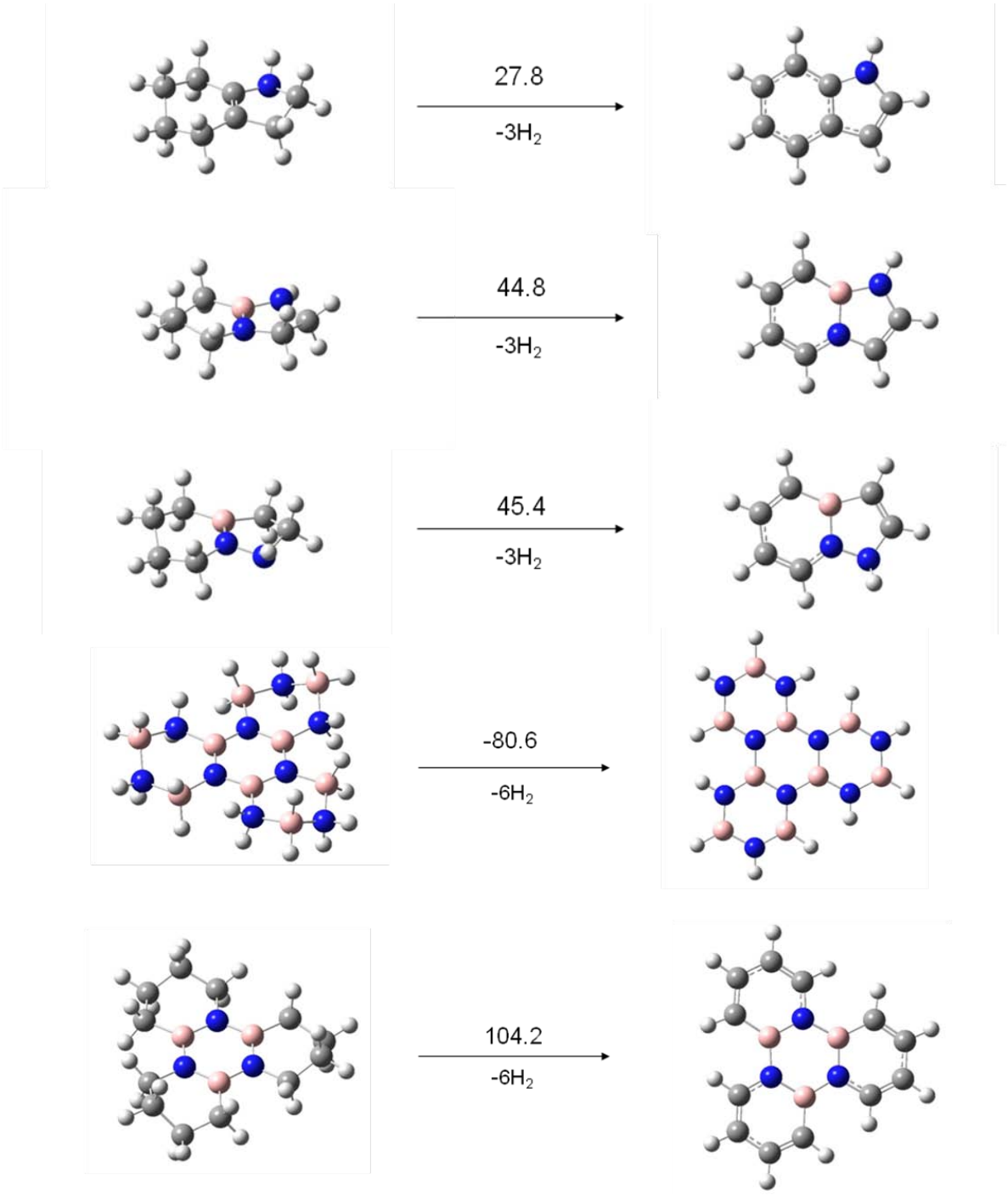

Figure 29. Dehydrogenation energies at the G3MP2 level at 298 K in kcal/mol.

We calculated the dehydrogenation energies of various rings containing C, B, N, H for the Center especially the groups at UW, Oregon, PNNL, and LANL, such as various substituted C_4BN rings and various "indole type" rings on the basis of heats of formation calculated at the G3MP2 level. Examples of the work done for the Liu group at Oregon are shown in the Figures 30 and 31 below.

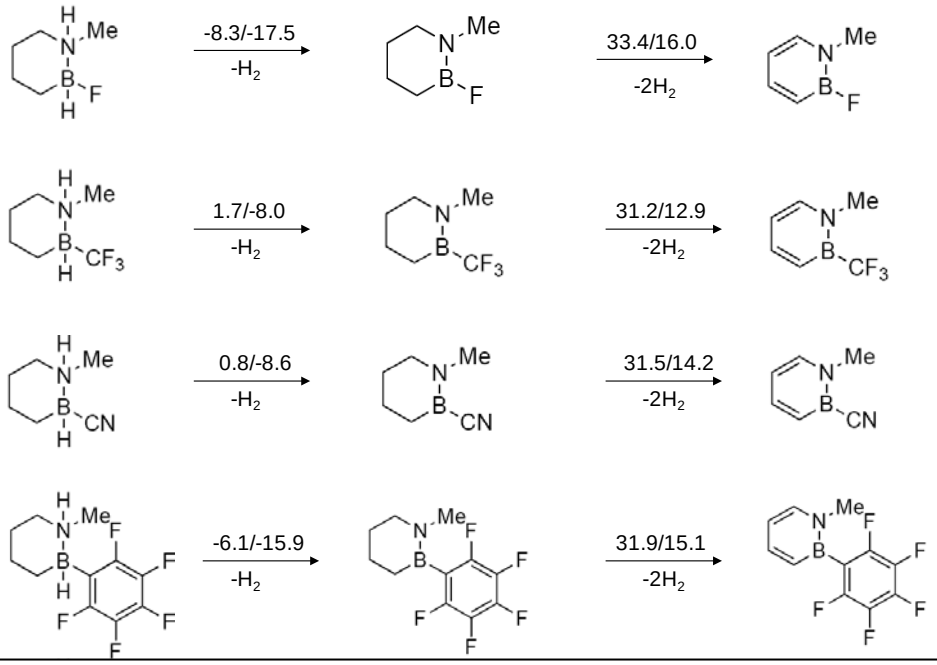

Figure 30. Reaction energies in kcal/mol at 298 K at the G3MP2 level. The values are given as ΔH/ΔG.

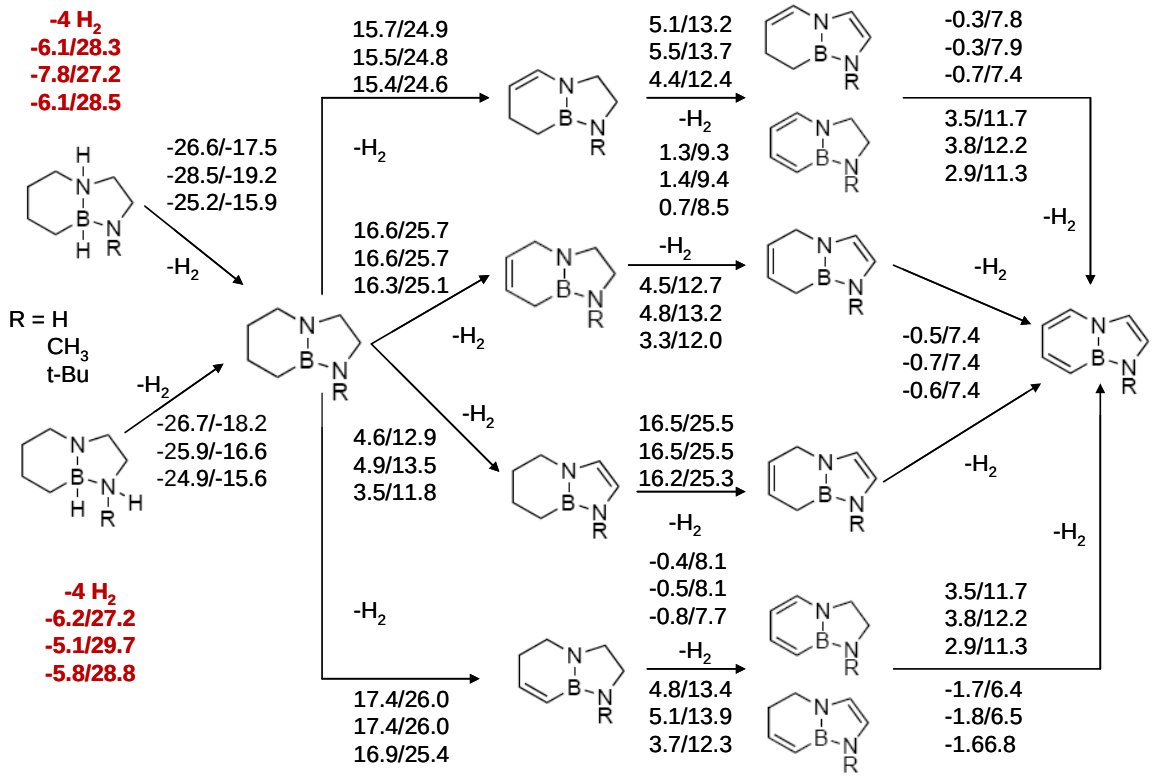

Figure 31. Dehydrogenation reaction energies in kcal/mol at 298 K at the G3MP2 level. The values are given as ΔG/ΔH.

Thermodynamics of Novel Storage Materials: $B_xH_y^{z-}$

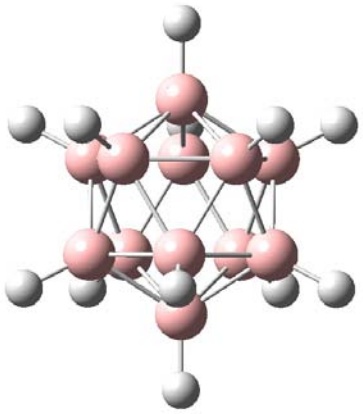

Thermochemical parameters of the *closo* boron hydride $B_nH_n^{2-}$ dianions, with n = 5 to 12, the $B_3H_8^-$ and $B_{11}H_{14}^-$ anions, and the B_5H_9 and $B_{10}H_{14}$ neutral species were predicted by high level ab initio electronic structure calculations. Total atomization energies obtained from coupled-cluster CCSD(T)/complete basis set (CBS) extrapolated energies, plus additional corrections were used to predict the heats of formation of the simplest $B_nH_m^{y-}$ species in the gas phase in kcal/mol at 298 K: $\Delta H_f(B_3H_8^-)$ = -26.4 ± 1.0; $\Delta H_f(B_5H_5^{2-})$ = 113.9 ± 1.5; $\Delta H_f(B_6H_6^{2-})$ = 57.5 ± 1.5; and $\Delta H_f(B_5H_9)$ = 18.6 ± 1.5. At the composite coupled-cluster CCSD(T)/CBS level, the calculated heat of formation for B_5H_9, is 6.6 kcal/mol above the experimental heat of formation. The lack of substantial multireference character in B_5H_9 suggests that our calculated values are reasonable and that the experimental value needs to be redetermined. The heats of formation of the larger species were evaluated by the G3 method from hydrogenation reactions (values at 298 K, in kcal/mol with estimated error bars of ± 3 kcal/mol): $\Delta H_f(B_7H_7^{2-})$ = 47.1; $\Delta H_f(B_8H_8^{2-})$ = 40.7; $\Delta H_f(B_9H_9^{2-})$ = 18.3; $\Delta H_f(B_{10}H_{10}^{2-})$ = -19.1; $\Delta H_f(B_{11}H_{11}^{2-})$ = -19.2; $\Delta H_f(B_{12}H_{12}^{2-})$ = -94.3; $\Delta H_f(B_{11}H_{14}^-)$ = -65.4; and, $\Delta H_f(B_{10}H_{14})$ = 11.1. A linear correlation between atomization energies of the dianions and energies of the BH units was found. The heats of formation of the ammonium salts of the anions and dianions were predicted using lattice energies (U_L) calculated from an empirical expression based on ionic volumes. The U_L values (0 K) of the $B_nH_n^{2-}$ dianions range from 319 to 372 kcal/mol. The values of U_L for the $B_3H_8^-$ and $B_{11}H_{14}^-$ anions are 113 and 135 kcal/mol, respectively. The calculated lattice energies and gas phase heats of formation of the constituent ions were used to predict the heats of formation of the ammonium crystal salts $[B_nH_m^{y-}][NH_4^+]_y$ (y = 1-2). These results were used to evaluate the thermodynamics of the H_2 release reactions from the ammonium hydro-borate salts. As expected, $B_{12}H_{12}^{2-}$ has a special stability and reaction (80):

$$[B_{12}H_{12}^{2-}][NH_4^+]_2\ (s) \rightarrow 10H_2 + 2BN\ (s) + 10B\ (s) \qquad (80)$$

differs by only 10 to 12 kcal/mol from being thermoneutral at 298 K.

Table 34. Calculated Heats of Reaction for the H_2 Release from the Salts at 298 K in kcal/mol.[a]

H_2 Release Reactions	**G3**	**G3B3**
$[B_3H_8^-][NH_4^+]\ (s) \rightarrow 6H_2 + BN\ (s) + 2B\ (s)$ [b]	-50.4	-50.9
$[B_{11}H_{14}^-][NH_4^+]\ (s) \rightarrow 8H_2 + BN\ (s) + 10B\ (s)$	-37.9	-36.5
$[B_5H_5^{2-}][NH_4^+]_2\ (s) \rightarrow {}^{13}/_2H_2 + 2BN\ (s) + 3B\ (s)$ [c]	-163.3	-162.5
$[B_6H_6^{2-}][NH_4^+]_2\ (s) \rightarrow 7H_2 + 2BN\ (s) + 4B\ (s)$ [d]	-112.8	-111.5
$[B_7H_7^{2-}][NH_4^+]_2\ (s) \rightarrow {}^{15}/_2H_2 + 2BN\ (s) + 5B\ (s)$	-115.2	-114.0
$[B_8H_8^{2-}][NH_4^+]_2\ (s) \rightarrow 8H_2 + 2BN\ (s) + 6B\ (s)$	-120.0	-118.9
$[B_9H_9^{2-}][NH_4^+]_2\ (s) \rightarrow {}^{17}/_2H_2 + 2BN\ (s) + 7B\ (s)$	-104.8	-103.5
$[B_{10}H_{10}^{2-}][NH_4^+]_2\ (s) \rightarrow 9H_2 + 2BN\ (s) + 8B\ (s)$	-76.0	-74.6
$[B_{11}H_{11}^{2-}][NH_4^+]_2\ (s) \rightarrow {}^{19}/_2H_2 + 2BN\ (s) + 9B\ (s)$	-83.5	-81.8
$[B_{12}H_{12}^{2-}][NH_4^+]_2\ (s) \rightarrow 10H_2 + 2BN\ (s) + 10B\ (s)$	-12.1	-10.3

$[B_3H_8^-][NH_4^+]$ (s) → $3H_2$ + 2B (s) + H_3BNH_3 (s) [e]	-27.0	-27.5
$[B_{11}H_{14}^-][NH_4^+]$ (s) → $6H_2$ + 10B (s)+ H_3BNH_3 (s)	-14.5	-13.2
$[B_5H_5^{2-}][NH_4^+]_2$ (s) → $^1/_2H_2$ + 3B (s) + $2H_3BNH_3$ (s) [f]	-116.5	-115.8
$[B_6H_6^{2-}][NH_4^+]_2$ (s) → H_2 + 4B (s) + $2H_3BNH_3$ (s) [g]	-66.1	-64.8
$[B_7H_7^{2-}][NH_4^+]_2$ (s) → $^3/_2H_2$ + 5B (s) + $2H_3BNH_3$ (s)	-68.5	-67.3
$[B_8H_8^{2-}][NH_4^+]_2$ (s) → $2H_2$ + 6B (s) + $2H_3BNH_3$ (s)	-73.3	-72.2
$[B_9H_9^{2-}][NH_4^+]_2$ (s) → $^5/_2H_2$ + 7B (s) + $2H_3BNH_3$ (s)	-58.1	-56.8
$[B_{10}H_{10}^{2-}][NH_4^+]_2$ (s) → $3H_2$ + 8B (s) + $2H_3BNH_3$ (s)	-29.2	-27.9
$[B_{11}H_{11}^{2-}][NH_4^+]_2$ (s) → $^7/_2H_2$ + 9B (s) + $2H_3BNH_3$ (s)	-36.8	-35.1
$[B_{12}H_{12}^{2-}][NH_4^+]_2$ (s) → $4H_2$ + 10B (s) + $2H_3BNH_3$ (s)	34.7	36.4
$[B_3H_8^-][NH_4^+]$ (s) → $5H_2$ + 2B (s) + $^1/_3B_3N_3H_6$ (l) [h]	-31.3	-31.8
$[B_{11}H_{14}^-][NH_4^+]$ (s) → $8H_2$ + 10B (s)+ $^1/_3B_3N_3H_6$ (l)	-18.8	-17.4
$[B_5H_5^{2-}][NH_4^+]_2$ (s) → $^9/_2H_2$ + 3B (s) + $^2/_3B_3N_3H_6$ (l) [i]	-125.1	-124.3
$[B_6H_6^{2-}][NH_4^+]_2$ (s) → $5H_2$ + 4B (s) + $^2/_3B_3N_3H_6$ (l) [j]	-74.6	-73.3
$[B_7H_7^{2-}][NH_4^+]_2$ (s) → $^{11}/_2H_2$ + 5B (s) + $^2/_3B_3N_3H_6$ (l)	-77.0	-75.8
$[B_8H_8^{2-}][NH_4^+]_2$ (s) → $6H_2$ + 6B (s) + $^2/_3B_3N_3H_6$ (l)	-81.8	-80.7
$[B_9H_9^{2-}][NH_4^+]_2$ (s) → $^{13}/_2H_2$ + 7B (s) + $^2/_3B_3N_3H_6$ (l)	-66.6	-65.3
$[B_{10}H_{10}^{2-}][NH_4^+]_2$ (s) → $7H_2$ + 8B (s) + $^2/_3B_3N_3H_6$ (l)	-37.8	-36.4
$[B_{11}H_{11}^{2-}][NH_4^+]_2$ (s) → $^{15}/_2H_2$ + 9B (s) + $^2/_3B_3N_3H_6$ (l)	-45.3	-43.6
$[B_{12}H_{12}^{2-}][NH_4^+]_2$ (s) → $8H_2$ + 10B (s) + $^2/_3B_3N_3H_6$ (l)	26.1	27.9

[a] The heats of formation of H_2 and B are 0 kcal/mol as they are the form of the element. The heat of formation of BN (crystal) was taken from Chase, M. W. Jr. *NIST-JANAF Tables*, 4th ed., *J. Phys. Chem. Ref. Data* **1998**, Monograph 9 (Suppl. 1): -59.97 ± 0.4 kcal/mol at 298 K. The heats of formation at 298 K of BH_3NH_3 (s) and $B_3N_3H_6$ (l) are -36.6 and -122.6 kcal/mol, respectively (Matus, M. H.; Anderson, K. D.; Camaioni, D. M.; Autrey, S. T.; Dixon, D. A. *J. Phys. Chem. A* **2007**, 111, 4411). [b] Value obtained using the CCSD(T)/CBS heat of formation of the anion is -50.4 kcal/mol at 298 K. [c] Value obtained using the CCSD(T)/CBS heat of formation of the dianion is -165.2 kcal/mol at 298 K. [d] Value obtained using the CCSD(T)/CBS heat of formation of the dianion is -114.2 kcal/mol at 298 K. [e] Value obtained using the CCSD(T)/CBS heat of formation of the anion is -27.0 kcal/mol at 298 K. [f] Value obtained using the CCSD(T)/CBS heat of formation of the dianion is -118.4 kcal/mol at 298 K. [g] Value obtained using the CCSD(T)/CBS heat of formation of the dianion is -67.5 kcal/mol at 298 K. [h] Value obtained using the CCSD(T)/CBS heat of formation of the anion is -31.3 at 298 K. [i] Value obtained using the CCSD(T)/CBS heat of formation of the dianion is -127.0 kcal/mol at 298 K. [j] Value obtained using the CCSD(T)/CBS heat of formation of the dianion is -76.0 kcal/mol at 298 K.

Boron Cluster Chemistry

Boron clusters have a wide range of properties and have been characterized by a number of experimental techniques including mass spectrometry. Similar to carbon–based materials, boron nanotubes (and fullerenes, if synthesized) have been considered as potential materials for hydrogen storage. Recent findings on novel properties of boron-based nanotubular materials are stimulating further studies on the small-sized gas phase clusters to determine their fundamental properties and growth patterns. Thermochemical parameters of a set of small-sized neutral (B_n) and anionic (B_n^-) boron clusters, with n = 5 – 13, were determined using coupled-cluster theory CCSD(T) calculations with the aug-cc-pVnZ (n = D, T and Q) basis sets extrapolated to the complete basis set limit (CBS) plus addition corrections and/or G3B3 calculations.

Enthalpies of formation, adiabatic electron affinities (EA), vertical (VDE) and adiabatic (ADE) detachment energies were evaluated. Our calculated EAs are in good agreement with recent experiments (values in eV): B_5 (CBS, 2.29; G3B3, 2.48; exptl., 2.33 ± 0.02), B_6 (CBS, 2.59; G3B3, 3.23; exptl., 3.01 ± 0.04), B_7 (CBS, 2.62; G3B3, 2.67; exptl., 2.55 ± 0.05), B_8 (CBS, 3.02; G3B3, 3.11; exptl., 3.02 ± 0.02), B_9 (G3B3, 3.03; exptl., 3.39 ± 0.06), B_{10} (G3B3, 2.85; exptl., 2.88 ± 0.09), B_{11} (G3B4, 3.48;, exptl., 3.43 ± 0.01), B_{12} (G3B3, 2.33; exptl., 2.21 ± 0.04) and B_{13} (G3B3, 3.62; exptl., 3.78 ± 0.02).

The difference between the calculated adiabatic electron affinity and the adiabatic detachment energy for B_6 is due to the fact that the geometry of the anion is not that of the ground state neutral. The calculated adiabatic detachment energies to the ^3A_u, C_{2h} and ^1A_g, D_{2h} excited states of B_6, which have geometries similar to the ^1A_g, D_{2h} state of B_6^-, are 2.93 and 3.06 eV in excellent agreement with experiment. The VDE's were also well reproduced by calculations. Calculated heats of formation are given in Table 35.

Table 35. Calculated Heats of Formation (ΔH_f at 298 K, kcal/mol) of the Neutral B_n and Anionic B_n^- Boron Clusters (n = 5 – 13) Using CCSD(T)/CBS and G3B3 Approaches.

Structure (State)	Symmetry	G3B3	CBS	Structure (State)	Symmetry	G3B3
B_2 ($^3\Sigma_g^-$)	$D_{\infty h}$	206.0	207.4	B_{10} (^1A_g)	**XVI** C_{2h}	314.8
B_2^- ($^4\Sigma_g^-$)	$D_{\infty h}$	160.6	162.4	B_{10}^- ($^2A''$)	**XVII** C_s	249.3
B_3 ($^2A_1'$)	D_{3h}	211.5	211.7	B_{11} ($^2B_2$)	**XVIII** C_{2v}	336.0
B_3^- ($^1A_1'$)	D_{3h}	144.3	145.3	B_{11} ($^2B_2$)	**XIX** C_{2v}	346.4
B_4 (^1A_g)	D_{2h}	228.5	226.4	B_{11}^- ($^1A_1$)	**XX** C_{2v}	255.7
B_4^- ($^2B_{1u}$)	D_{2h}	189.8	187.5	B_{11}^- ($^1A_1$)	**XXI** C_{2v}	255.6
B_5 ($^2B_2$)	**I** C_{2v}	256.8	253.5	B_{12} ($^1A_1$)	**XXII** C_{3v}	335.7
B_5^- ($^1A_1$)	**II** C_{2v}	199.6	200.7	B_{12}^- ($^2A'$)	**XXIII** C_s	282.6
B_5^- (^3B)	**II-t** C_2		211.9	B_{13} ($^2A_2$)	**XXIV** C_{2v}	373.1
B_6 ($^1A_1$)	**III** C_{5v}	286.9	280.9	B_{13} ($^2B_1$)	**XXV** C_{2v}	372.4
B_6 (^3A_u)	**IV-t** C_{2h}	293.1	289.5	B_{13} ($^2B_{3u}$)	**XXVI** D_{2h}	376.7
B_6 (^1A_g)	**IV-d** D_{2h}		291.8	B_{13}^- ($^3B_2$)	**XXVII** C_{2v}	311.8
B_6 (^1A)	**IV-s** C_2		292.8	B_{13}^- ($^3B_2$)	**XXVIII** C_{2v}	312.3
B_6^- ($^2B_{2g}$)	**V** D_{2h}	213.0	220.8	B_{13}^- (^1A_g)	**XXIX** D_{2h}	288.3
B_6^- ($^2B_{1u}$)	**V-u** D_{2h}		236.5			
B_6^- (^2B_u)	**VI** C_{2h}	237.1	228.2			
B_6^- (^2A_u)	**V-c** C_{2h}		246.6			
B_6^- ($^2A''$)	**V-s** C_s		236.7			
B_7 ($^2B_2$)	**VII** C_{2v}	288.3	284.0			
B_7 ($^2B_2$)	**VIII** C_{2v}	315.1				
B_7^- ($^1A_1$)	**IX** C_{2v}	225.6	223.5			
B_7^- ($^1A_1$)	**IX-a** C_{2v}		232.9			
B_7^- ($^3A_1$)	**X** C_{6v}	226.4	224.5			
B_8 ($^3A_2'$)	**XI** D_{7h}	287.5	284.8			
B_8^- ($^2B_1$)	**XII** C_{2v}	216.0	215.3			
B_9 ($^2A_1$)	**XIII** C_{2v}	315.0				
B_9 ($^2B_{1g}$)	**XIV** C_{2v}	327.0				

B_9^- ($^1A_{1g}$)	**XV** D_{8h}	245.3	244.3
B_9^- ($^3A'$)	**XV-t** C_s		275.6

To probe further the thermodynamic stability of the boron clusters, we now examine the binding energy (D_e) and average binding energy (E_b) defined as follows:

$$D_e(B_n) = \Delta H_f(B_{n-1}) + \Delta H_f(B) - \Delta H_f(B_n) \quad (81a)$$
$$D_e(B_n^-) = \Delta H_f(B_{n-1}^-) + \Delta H_f(B) - \Delta H_f(B_n^-) \quad (81b)$$
$$E_b(B_n) = [n\Delta H_f(B) - \Delta H_f(B_n)]/n = TAE/n \quad (82a)$$
$$E_b(B_n^-) = [(n)\Delta H_f(B) + \Delta H_f(e) - \Delta H_f(B_n^-)]/n \quad (82b)$$

where ΔH_f (e) is set equal to zero. The D_e corresponds to a dissociation energy, which is the energy required to remove one B atom from a cluster, and the E_b is the average energy of stabilization per atom in the cluster. The evolution of the quantities D_e and E_b with respect to *n* is shown in Figures 32 and 33. The experimental D_e is the heat of atomization of B which is 5.86 eV at 0 K. E_b essentially increases as a function of *n*. The evolution of E_b is nearly parallel for both neutral and anionic forms (Figure 32). It grows rapidly in small-sized clusters (*n* from 2 to 6), but the rate becomes smaller from *n* = 7, and then the quantity varies more smoothly and tends to approach the asymptote limit value of the D_e slowly (for *n* = 13, E_b being ~4.6 eV for the neutral and ~5 eV for the anion). Note that in the series of $B_nH_n^{2-}$ dianions with *n* = 5 – 12, the energy per BH-group was also found to linearly increase with respect to *n*.

The D_e is size-dependent and exhibits irregular oscillations for the smaller compounds (Figure 32). B_3^- is thus the most stable and B_4 the least stable cluster with respect to bond cleavage. Up to *n* = 10, there is a nearly parallel evolution of BEs in both neutral and anionic systems, where within each of the pairs B_8/B_8^-, B_9/B_9^- and B_{10}/B_{10}^-, the neutral and anionic forms have nearly the same BE values. An odd-even alternation begins at *n* = 11, where a closed-shell species is more stable than an open-shell counterpart. The clusters B_{11}^-, B_{12} and B_{13}^-, having each an even number of electrons, are thus more stable and expected to be associated with higher abundance in, for example, a mass spectrum recording their formation.

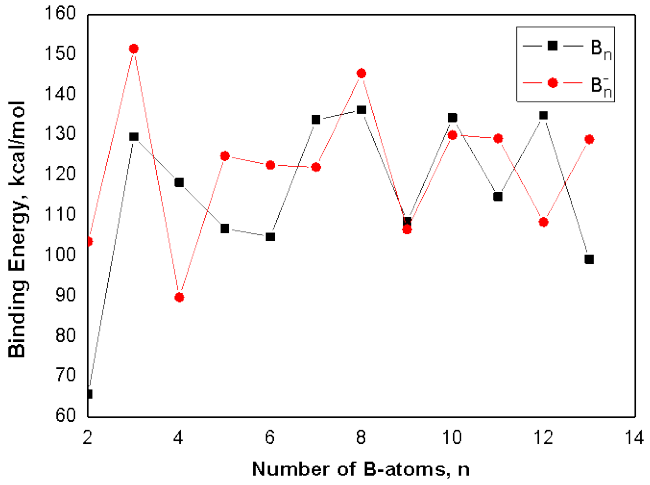

Figure 32. Size dependence of the binding energies (D_e in kcal/mol) of B_n and B_n^- clusters. Values obtained from G3B3 heats of formation at 0K.

The resonance energy (RE) is defined by equations (83):

$$RE(B_n) = \Delta E(B_n \rightarrow nB) - m\Delta E(B_2 \rightarrow nB) = TAE(B_n) - mTAE(B_2) \quad (83a)$$
$$RE(B_n^-) = \Delta E(B_n \rightarrow nB) - (m\text{-}1)\Delta E(B_2 \rightarrow nB) - \Delta E(B_2^- \rightarrow 2B + e) \quad (83b)$$

in which the diatomic B_2 can be in either the $^1\Sigma_g^+$ or the $^3\Sigma_g^-$ state, and *m* is the number of BB bonds in B_n. The evolution of the REs is in Figure 34. Taking the singlet state for B_2 and assuming *m* = 3, 5, 7 for B_3^-, B_4 and B_5^-, the RE's amount to 111, 62 and 146 kcal/mol, respectively.

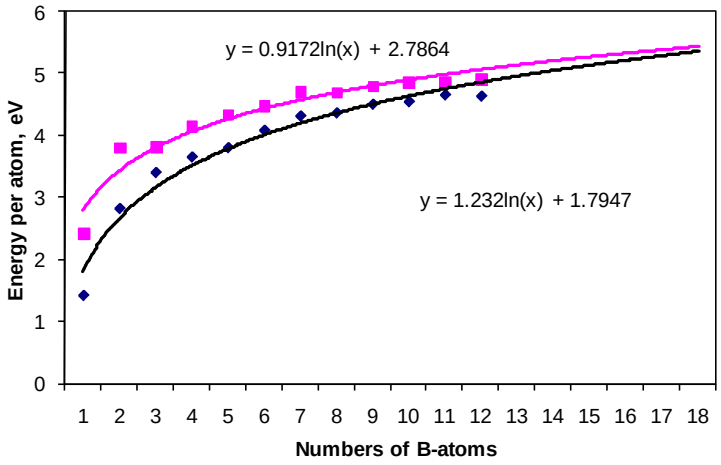

Figure 33. Size dependence of the average energy per atom (E_b in eV) of B_n (black line) and B_n^- (violet line) clusters. Values obtained from G3B3 heats of formation at 0K

For larger clusters, the determination of the number of effective BB bonds becomes more difficult. For B_6, there are arguments as to whether to assign *m* being either 8 or 9. For B_{12}, *m* could be taken as 21 (each additional B bringing in two bonds), or 24 (number of BB bonds being counted from structure **XXII** ($^1A_1$)). This leads to the RE values of 230 (*m* = 21) and 78 (*m* = 24) kcal/mol. The merit of this parameter is that its emphasizes the enormous excess energy brought about following a clustering of elements, with respect to a simple combination of BB bond energies.

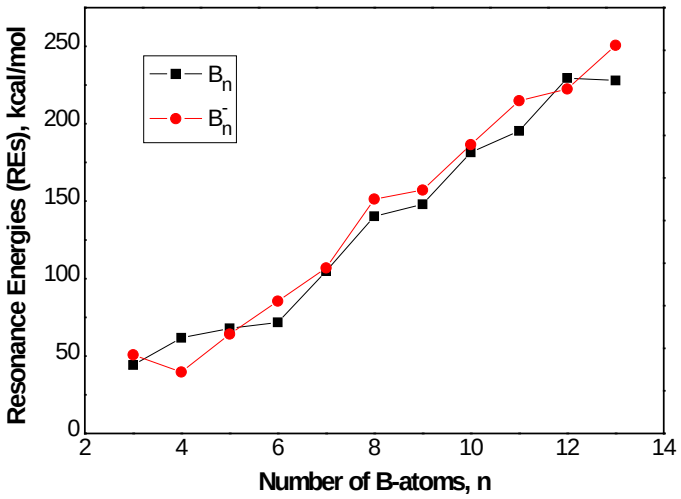

Figure 34. Size dependence of the resonance energies (RE in kcal/mol) of B_n and B_n^- clusters. Values obtained from G3B3 heats of formation at 0K

The normalized resonance energy is defined as NRE = RE/*n*, and thus describes the amount of resonance energy per atom, which may be a more convenient index to quantify the electron delocalization. The variation of the calculated values are illustrated in Figure 35. For the boron clusters, the NRE values range from 9 to 20 kcal/mol; the larger the NRE, the more stabilized is the cluster. For example, B_3^- is more stabilized than B_3, B_4 more stabilized than B_4^-, and B_3^- more stabilized than B_4. A species having an even number of electrons (such as B_6, B_8, B_{10}) does not necessarily possess a larger NRE than its odd number counterpart. The clusters B_8^-, B_9^-, B_{10}^-, B_{11}^-, B_{12} and B_{13}^- have comparable NRE values.

Partition of the electron localization functions into π and σ components allows probing of the partial and local delocalization in global non-aromatic systems. The larger clusters appear to exhibit multiple aromaticity. The binding energies per atom vary in a parallel manner for both neutral and anionic series, and approach the experimental value for the heat of atomization of B.

The resonance energies and the normalized resonance energies are convenient indices to quantify the stabilization of a cluster of elements.

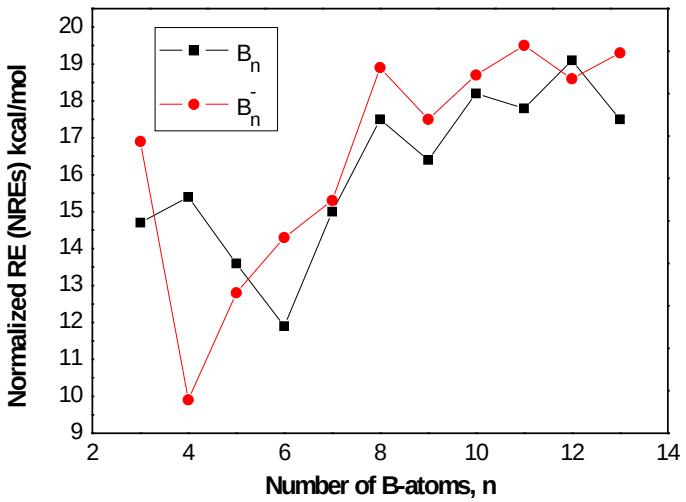

Figure 35. Size dependence of the normalized resonance energies (NRE in kcal/mol) of B_n and B_n^- clusters. Values obtained from G3B3 heats of formation at 0K

Boron Cluster Oxidation Chemistry

The molecular and electronic structures of a series of small boron monoxide and dioxide clusters B_nO_m (n = 5-10, m = 1,2) plus their anions were predicted. The enthalpies of formation (ΔH_fs), electron affinities (EAs), vertical detachment energies and energies of different fragmentation processes are predicted using the G3B3 method. The G3B3 results were benchmarked with respect to more accurate CCSD(T)/CBS values for n = 1 to 4 with average deviations of ± 1.5 kcal/mol for ΔH_fs and ± 0.03 eV for EAs. We have continued our analysis of the properties of the boron clusters by looking at their oxidation. Table 36 shows the benchmarking of the G3B3 method vs. the more accurate coupled cluster-complete basis set results previously obtained for up through 4 boron atoms in the cluster.

Table 36. Calculated Heats of Formation (ΔH_f, kcal/mol) for the Boron Oxides B_nO_m (n = 1-4, m = 1-2) at the G3B3 and CCSD(T)/CBS levels.

Structure	Symmetry, State	ΔH_f(298K)	
		G3B3	CBS
BO	$C_{\infty h}$ $^2\Sigma^+$	2.9	2.4
BO^-	$C_{\infty h}$ $^1\Sigma^+$	-56.4	-55.3
OBO	$D_{\infty h}$ $^2\Pi_g$	-66.6	-65.9
BO_2^-	$D_{\infty h}$ $^1\Sigma_g^+$	-170.0	-169.5
BOB	$D_{\infty h}$ $^1\Sigma_g^+$	42.1	41.7
BOB^-	$D_{\infty h}$ $^2\Sigma_g^+$	39.6	40.5
BBO	$C_{\infty h}$ $^1\Sigma^+$	57.6	58.4
BBO^-	$C_{\infty h}$ $^2\Pi$	23.6	25.1[b]
OBBO	$D_{\infty h}$ $^1\Sigma_g^+$	-109.5	-109.4
$OBBO^-$	$D_{\infty h}$ ^2B_u	-118.0	-117.6
B_3O	$C_{\infty h}$ $^4\Sigma^-$	99.2	99.3
B_3O^-	C_{2v} $^3A_1$	47.8	51.8
B_3O_2	$D_{\infty h}$ $^2\Pi_g$	-38.0	-38.4
$B_3O_2^-$	$D_{\infty h}$ $^3\Sigma_u^-$	-106.6	-105.5
B_4O	C_{2v} $^1A_1$	112.8	114.2
B_4O^-	C_{2v} $^2A_1$	49.8	54.7
B_4O_2	$D_{\infty h}$ $^3\Sigma_g^-$	-8.0	-6.6

$B_4O_2^-$ $D_{\infty h}$ $^2\Pi$ -81.2 -79.0

A wide range of isomers were studied. The calculated heats of formation of the most stable isomers for the larger clusters are given in Table 37. Excited states were also studied

Table 37. G3B3 Calculated Heats of Formation (ΔH_f, kcal/mol) for the Boron Oxides B_nO_m (n = 5-10, m = 1-2).

Structure	Symmetry, State	ΔH_f(298K)	Structure	Symmetry, State	ΔH_f(298K)
B_5O-A	C_{2v}, $^2A_1$	144.1	B_7O_2-A$^-$	C_{2v}, $^1A_1$	5.1
B_5O-B	C_s, $^2A'$	141.4	B_7O_2-B$^-$	D_{2h}, ^1A_g	-10.7
B_5O-D	C_s, $^2A'$	150.7	B_7O_2-C$^-$	C_{2v}, $^1A_1$	-24.3
B_5O-A$^-$	C_{2v}, $^1A_1$	62.6	B_8O-A	C_{2v}, $^1A_1$	169.9
B_5O_2-A	C_s, $^2A'$	30.2	B_8O-A$^-$	C_{2v}, $^2B_1$	114.7
B_5O_2-B	C_{2v}, $^2B_2$	36.6	B_8O-B$^-$	C_s, $^2A'$	111.4
B_5O_2-C	C_s, $^2A'$	44.5	B_8O_2-A	C_{2v}, $^1A_1$	57.5
B_5O_2-D	C_{2v}, $^2B_2$	34.8	B_8O_2-B	C_{2h}, ^1A_g	80.1
B_5O_2-E	$D_{\infty h}$, $^2\Pi_u$	35.4	B_8O_2-A$^-$	C_{2v}, $^2A_2$	16.8
B_5O_2-A$^-$	C_s, $^1A'$	-49.2	B_8O_2-B$^-$	C_{2h}, ^2B_g	-15.3
B_5O_2-D$^-$	C_{2v}, $^1A_1$	-69.5	B_9O-A	C_s, $^2A'$	217.2
B_5O_2-D$^-$	C_{2v}, $^3A_1$	-43.1	B_9O-B	C_{2v}, $^2B_1$	224.8
B_5O_2-E$^-$	$D_{\infty h}$, $^1\Sigma_g^+$	-53.7	B_9O-C	C_{2v}, $^2B_2$	230.2
B_6O-A	C_s, $^1A'$	147.1	B_9O-A$^-$	C_s, $^1A'$	131.9
B_6O-A$^-$	C_s, $^2A''$	84.7	B_9O-B$^-$	C_{2v}, $^1A_1$	157.0
B_6O_2-A	C_s, $^1A'$	26.5	B_9O-C$^-$	C_{2v}, $^1A_1$	133.9
B_6O_2-B	D_{2h}, ^1A_g	33.8	B_9O_2-A	C_{2v}, $^2A_2$	97.0
B_6O_2-C	C_s, $^1A'$	36.7	B_9O_2-B	C_s, $^2A'$	106.3
B_6O_2-E	C_{2h}, ^1A_g	48.5	B_9O_2-A$^-$	C_{2v}, $^1A_1$	-11.4
B_6O_2-A$^-$	C_s, $^2A'$	-6.1	$B_{10}O$-A	C_s, $^1A'$	212.5
B_6O_2-B$^-$	D_{2h}, ^2A_g	-49.3	$B_{10}O$-B	C_{2v}, $^1A_1$	234.3
B_6O_2-C$^-$	C_s, $^2A'$	-19.4	$B_{10}O$-C	C_s, $^1A'$	237.3
B_7O-A	C_{2v}, $^2A_2$	171.7	$B_{10}O$-A$^-$	C_s, $^2A'$	151.4
B_7O-B	C_s, $^2A''$	183.0	$B_{10}O$-B$^-$	C_{2v}, $^2A_2$	136.3
B_7O-C	C_{2v}, $^2B_1$	191.8	$B_{10}O$-C$^-$	C_s, $^2A''$	164.7
B_7O-A$^-$	C_{2v}, $^1A_1$	104.0	$B_{10}O_2$-A	C_{2h}, ^1A_g	105.0
B_7O-B$^-$	C_s, $^1A'$	103.4	$B_{10}O_2$-B	C_{2v}, $^1A_1$	114.0
B_7O-C$^-$	C_{2v}, $^1A_1$	112.4	$B_{10}O_2$-C	C_{2v}, $^1A_1$	107.3
B_7O-D$^-$	C_s, $^1A'$	103.4	$B_{10}O_2$-A$^-$	C_{2h}, ^2B_u	23.3
B_7O_2-A	C_{2v}, $^2A_2$	57.8	$B_{10}O_2$-B$^-$	C_{2v}, $^2A_1$	37.5
B_7O_2-B	D_{2h}, $^2B_{1g}$	59.9	$B_{10}O_2$-C$^-$	C_{2v}, $^2B_2$	52.8
B_7O_2-C	C_{2v}, $^2B_1$	62.0			

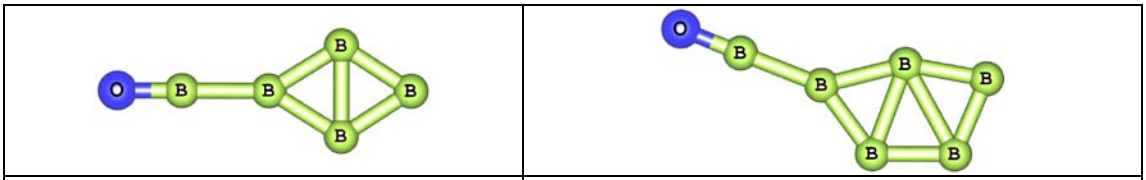

B_5O-A	**B_6O-A**

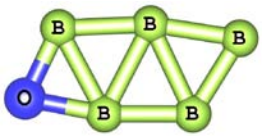	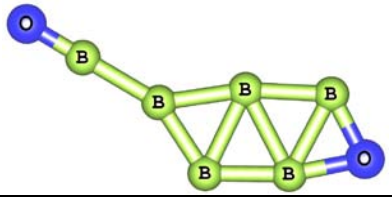
B_5O-B	**B_6O_2-A**
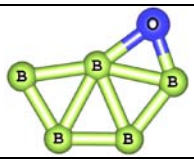	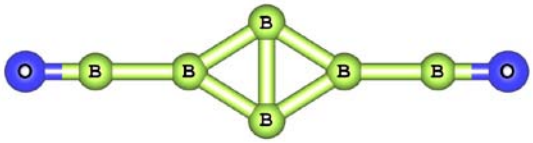
B_5O-D	**B_6O_2-B**
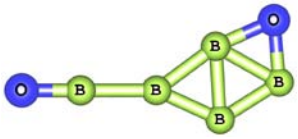	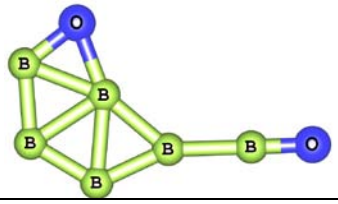
B_5O_2-A	**B_6O_2-C**
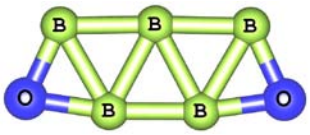	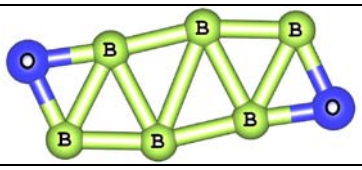
B_5O_2-B	**B_6O_2-E**
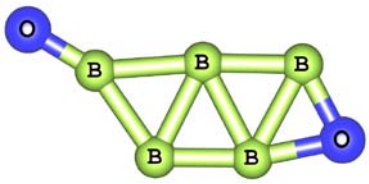	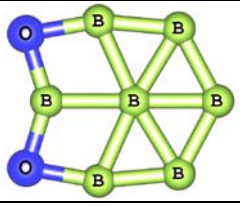
B_5O_2-C	**B_7O_2-A**
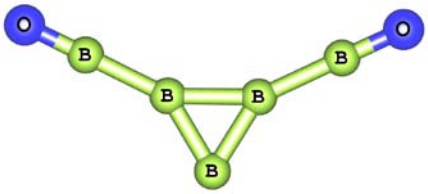	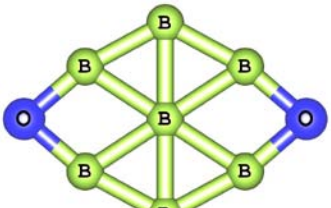
B_5O_2-D	**B_7O_2-B**
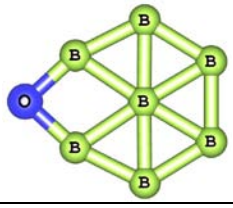	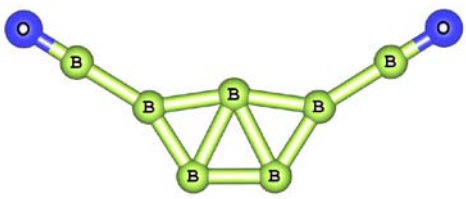
B_7O-A	**B_7O_2-C**

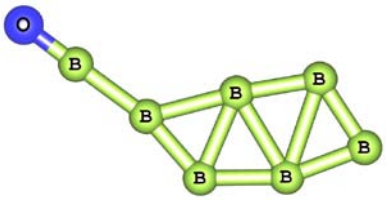	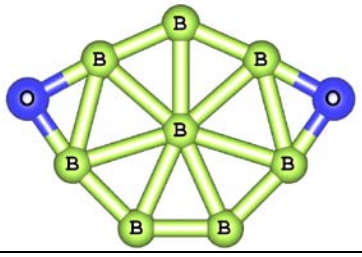
B_7O-B	**B_8O_2-A**
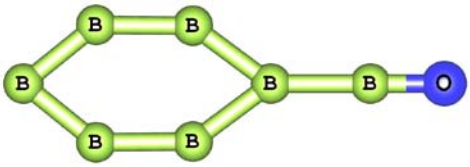	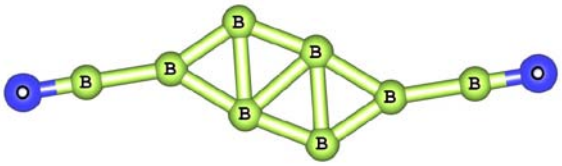
B_7O-C	**B_8O_2-B**
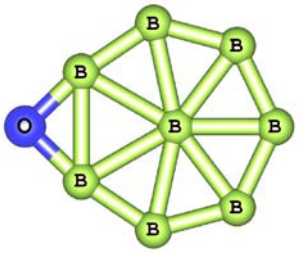	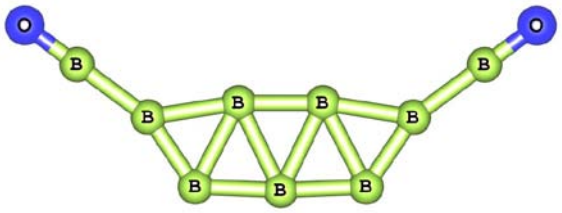
B_8O-A	**B_9O_2-A**
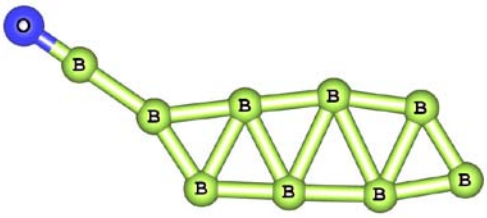	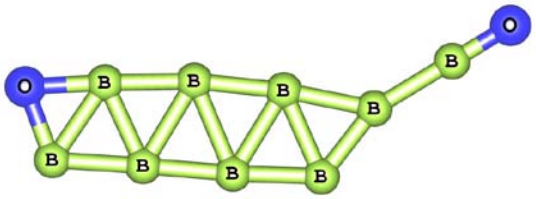
B_9O-A	**B_9O_2-B**
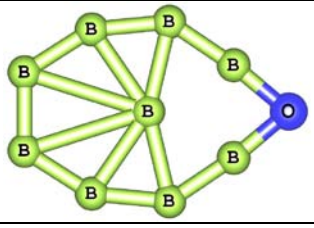	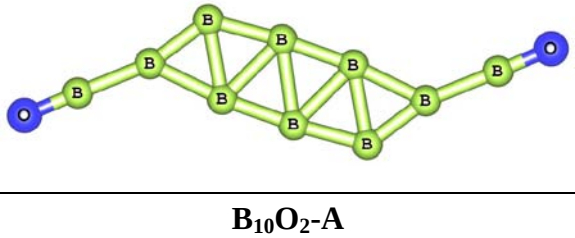
B_9O-B	**$B_{10}O_2$-A**
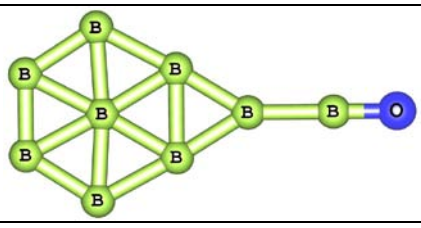	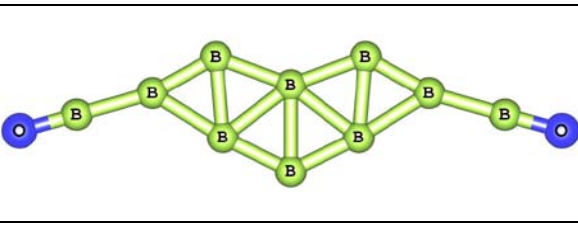
B_9O-C	**$B_{10}O_2$-B**

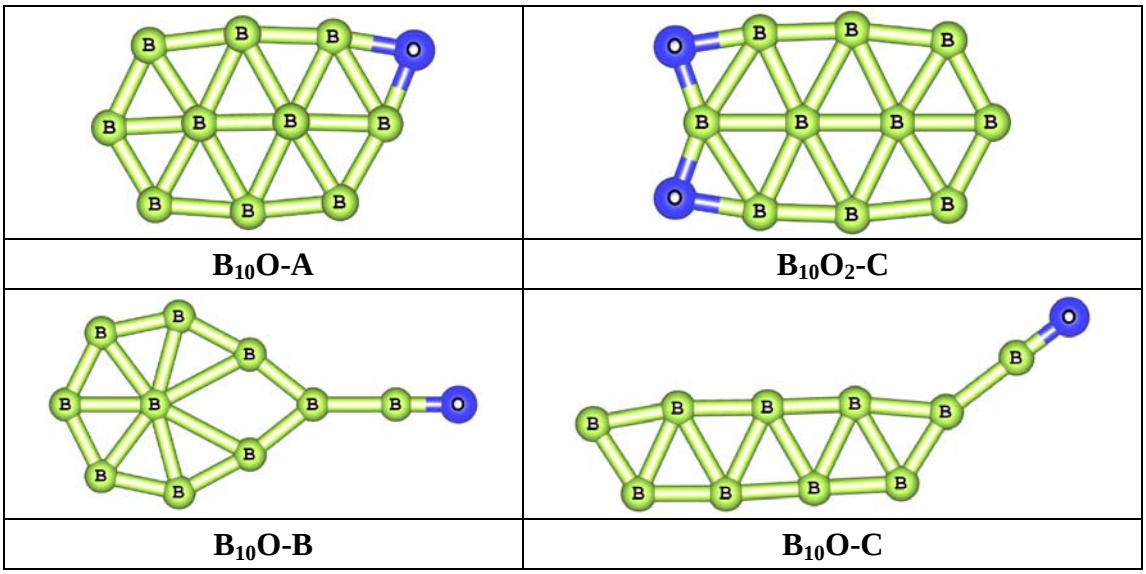

Figure 36. Low energy structures for B_nO and B_nO_2 complexes

The adiabatic electronic affinities (EA, eV) at 0K of the boron oxides B_nO_m for n = 1-10, m = 1-2 are given in Table 38.

Table 38. Adiabatic Electronic Affinities (EA, eV) at 0K of the Boron Oxides B_nO_m for n = 1-10, m = 1-2.

Neutral	**Anion**	**EA (G3B3)**
BO ($^2\Sigma^+$)	BO^- ($^1\Sigma^+$)	2.57
OBO ($^2\Pi_g$)	BO_2^- ($^1\Sigma_g^+$)	4.47
BOB ($^1\Sigma_g^+$)	BOB^- ($^2\Sigma_g^+$)	0.10
BBO ($^1\Sigma_g^+$)	BBO^- ($^2\Pi$)	1.47
OBBO ($^1\Sigma_g^+$)	$OBBO^-$ (^2B_u)	0.37
BBBO ($^4\Sigma^-$)	B_3O^- ($^3A_1$)	2.05
OB_3O ($^2\Pi_g$)	$B_3O_2^-$ ($^3\Sigma_u^-$)	2.97
B_4O ($^1A_1$)	B_4O^- ($^2A_1$)	2.73
B_4O_2 ($^3\Sigma_g^-$)	$B_4O_2^-$ ($^2\Pi$)	3.17
B_5O-B ($^2A'$)	B_5O-A ($^1A_1$)	3.44
B_5O_2-A ($^2A'$)	B_5O_2-D ($^1A_1$)	4.34
B_6O-A ($^1A'$)	B_6O-A ($^2A''$)	2.69
B_6O_2-A ($^1A'$)	B_6O_2-B (^2A_g)	3.31
B_7O-A ($^2A_2$)	B_7O-B ($^1A'$)	3.00
B_7O_2-A ($^2A_2$)	B_7O_2-B ($^1A_1$)	3.62
B_8O-A ($^1A_1$)	B_8O-B ($^2A'$)	2.56
B_8O_2-A ($^1A_1$)	B_8O_2-C (^2B_g)	3.19
B_9O-A ($^2A'$)	B_9O-A ($^1A'$)	3.70
B_9O_2-A ($^2A_2$)	B_9O_2-A ($^1A_1$)	4.69
$B_{10}O$-A (^1A)	$B_{10}O$-B ($^2A_2$)	3.36
$B_{10}O_2$-A (^1A_g)	$B_{10}O_2$-A (^2B_u)	3.54

The energies for various decomposition reactions are given in Table 39.

Table 39. Energies (ΔH_r in kcal/mol) of the Decomposition Reactions of the Boron Oxides.

Decomposition Reaction	**ΔH_r (298K)**
B_5O-A ($^2A_1$) → B_4 (^1A_g) + BO ($^2\Sigma^+$)	87.3
B_5O-A ($^2A_1$) → B_5 ($^2B_2$) + O (^3P)	172.7
B_5O-B ($^2A'$) → B_4 (^1A_g) + BO ($^2\Sigma^+$)	90.0
B_5O-B ($^2A'$) → B_5 ($^2B_2$) + O (^3P)	175.4
B_5O-A ($^1A_1$)$^-$ → B_4 (^1A_g) + BO^- ($^1\Sigma^+$)	109.5
B_5O-A ($^1A_1$)$^-$ → B_4^- ($^2B_{1u}$) + BO ($^2\Sigma^+$)	130.1
B_5O_2-A ($^2A'$) → B_5O-A ($^2A_1$) + O (^3P)	173.9
B_5O_2-D ($^1A_1$)$^-$ → B_3 ($^2A_1'$) + BO ($^2\Sigma^+$) + BO^- ($^1\Sigma^+$)	227.5
B_5O_2-D ($^1A_1$)$^-$ → B_3^- ($^1A_1'$) + 2BO ($^2\Sigma^+$)	219.6
B_6O-A ($^1A'$) → B_5 ($^2B_2$) + BO ($^2\Sigma^+$)	112.6
B_6O-A ($^2A''$)$^-$ → B_5 ($^2B_2$) + BO^- ($^1\Sigma^+$)	115.7
B_6O-A ($^2A''$)$^-$ → B_5^- ($^1A_1$) + BO ($^2\Sigma^+$)	117.8
B_6O_2-A ($^1A'$) → B_6O-A ($^1A'$) + O (^3P)	180.6
B_6O_2-A ($^1A'$) → B_5O-B ($^2A'$) + BO ($^2\Sigma^+$)	117.8
B_6O_2-B (^2A_g)$^-$ → B_4 (^1A_g) + BO ($^2\Sigma^+$) + BO^- ($^1\Sigma^+$)	224.3
B_6O_2-B (^2A_g)$^-$ → B_4^- ($^2B_{1u}$) + 2BO ($^2\Sigma^+$)	244.9
B_7O-A ($^2A_2$) → B_7 ($^2B_2$) + O (^3P)	176.6
B_7O-A ($^2A_2$) → B_6 ($^1A_1$) + BO ($^2\Sigma^+$)	118.1
B_7O-B ($^1A'$)$^-$ → B_6 ($^1A_1$) + BO^- ($^1\Sigma^+$)	127.1
B_7O-B ($^1A'$)$^-$ → B_6^- ($^2B_{2g}$) + BO ($^2\Sigma^+$)	112.5
B_7O_2-A ($^2A_2$) → B_7O-A ($^2A_2$) + O (^3P)	173.9
B_7O_2-B ($^1A_1$)$^-$ → B_5 ($^2B_2$) + BO^- ($^1\Sigma^+$) + BO ($^2\Sigma^+$)	227.6
B_7O_2-B ($^1A_1$)$^-$ → B_5^- ($^1A_1$) + 2BO ($^2\Sigma^+$)	229.7
B_7O_2-B ($^1A_1$)$^-$ → B_6O-A ($^1A'$) + BO^- ($^1\Sigma^+$)	115.0
B_7O_2-B ($^1A_1$)$^-$ → B_6O-A$^-$ ($^2A''$) + BO ($^2\Sigma^+$)	111.9
B_8O-A ($^1A_1$) → B_8 ($^3A'_2$) + O (^3P)	177.6
B_8O-B ($^2A''$) → B_7 ($^2B_2$) + BO^- ($^1\Sigma^+$)	120.5
B_8O-B ($^2A'$) → B_7^- ($^1A_1$) + BO ($^2\Sigma^+$)	117.7
B_8O_2-A ($^1A_1$) → B_8O-A ($^1A_1$) + O (^3P)	172.4
B_8O_2-C (^2B_g)$^-$ → B_6 ($^1A_1$) + BO^- ($^1\Sigma^+$) + BO ($^2\Sigma^+$)	248.7
B_8O_2-C (^2B_g)$^-$ → B_6^- ($^2B_{2g}$) + 2BO ($^2\Sigma^+$)	234.1
B_9O-A ($^2A'$) → B_8 ($^3A'_2$) + BO ($^2\Sigma^+$)	73.2
B_9O-A ($^1A'$)$^-$ → B_8^- ($^2B_1$) + BO ($^2\Sigma^+$)	87.0
B_9O-A ($^1A'$)$^-$ → B_8 ($^3A'_2$) + BO^- ($^1\Sigma^+$)	99.2
B_9O_2-A ($^2A_2$) → B_7 ($^2B_2$) + 2BO ($^2\Sigma^+$)	197.1
B_9O_2-A ($^1A_1$)$^-$ → B_7 ($^2B_2$) + BO ($^2\Sigma^+$) + BO^- ($^1\Sigma^+$)	246.2
B_9O_2-A ($^1A_1$)$^-$ → B_7^- ($^1A_1$) + 2BO ($^2\Sigma^+$)	242.8
$B_{10}O$-A (^1A) → B_{10} (^1A_g) + O (^3P)	162.3
$B_{10}O$-B ($^2A_2$)$^-$ → B_9^- ($^1A_{1g}$) + BO ($^2\Sigma^+$)	111.9
$B_{10}O$-B ($^2A_2$)$^-$ → B_9 ($^2A_1$) + BO^- ($^1\Sigma^+$)	122.3
$B_{10}O_2$-A (^1A_g) → B_8 ($^3A'_2$) + 2BO ($^2\Sigma^+$)	188.3
$B_{10}O_2$-A (^2B_u)$^-$ → B_8 ($^3A'_2$) + BO ($^2\Sigma^+$) + BO^- ($^1\Sigma^+$)	210.7

$B_{10}O_2$-A $(^2B_u)^- \rightarrow B_8^- (^2B_1) + 2BO (^2\Sigma^+)$ 198.5

A topological analysis of electron densities is performed by the ELF technique, which is a useful approach for the analysis of the bonding, aromaticity, and electron delocalization in a compound. Evaluation of aromaticity can be done using the bifurcation values of the components ELF_σ and ELF_π obtained separately from the total densities; a high bifurcation value of either ELF_σ or ELF_π indicates a good electron delocalization. The total ELF of the boron dioxide anions at their bifurcations are illustrated in Figure 37. The electron distribution around the B-O and the B-BO bonds in all systems are similar to each other. Each of V(B,O) basins contains ~3.4-3.5 e, and the population in each V(B,BO) basin is approximate to 2.4 e. The remaining basins are perfectly delocalized in local rings containing (n-2) B-atoms (i.e. a three-membered ring for $B_5O_2^-$ and a four-membered ring for $B_6O_2^-$, etc…), which is consistent with a high thermodynamic stability for the anions. The electron populations of the total ELF also confirm the presence of multi-center bonds, which are a typical feature in boron compounds. The anion $B_7O_2^-$ possesses three multi-electron-three-center bonds in which each of the V(B,B,B) basins contains ~2.8 e. Similar observations can be made for $B_8O_2^-$, $B_9O_2^-$ and $B_{10}O_2^-$, which have four, five and six multiple bonds, respectively. Overall, the inherent features of pure boron clusters such as planarity, strong electron delocalization, aromaticity, and multi-center bonds remain the essential characteristics of the boron oxide anions.

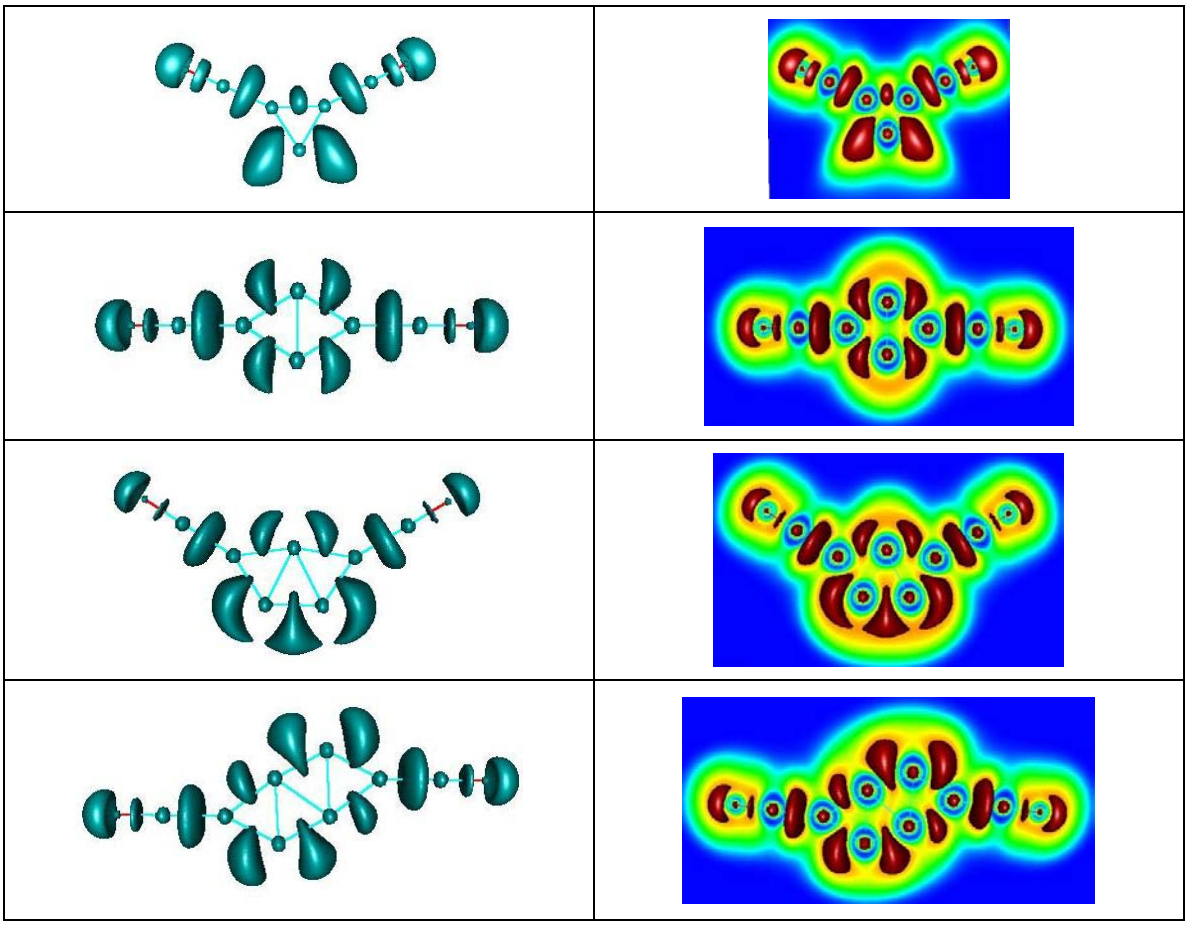

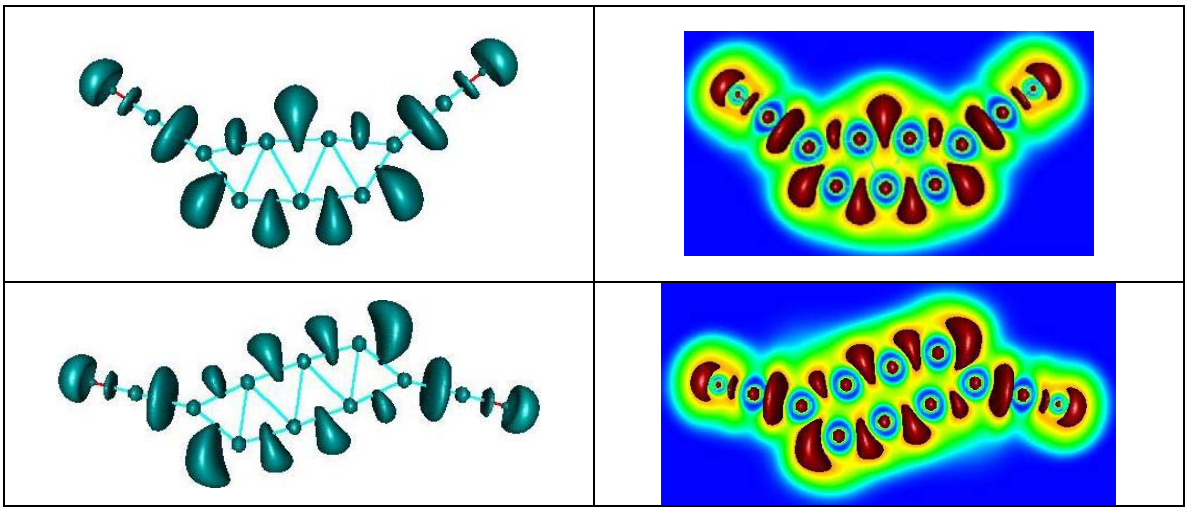

Figure 37. ELF plots for boron dioxide anions $B_nO_m^-$ (n = 5-10 and m = 1-2)

Stability, Binding Energy and Resonance Energy.

The size dependence of the EAs are illustrated in Figure 38. Except for the B_2 species, all of the oxides possess EAs larger than 2 eV with B_5O_2 having the largest EA. Beginning with B_4, there is a moderate odd-even alternation in both monoxide and dioxide series.

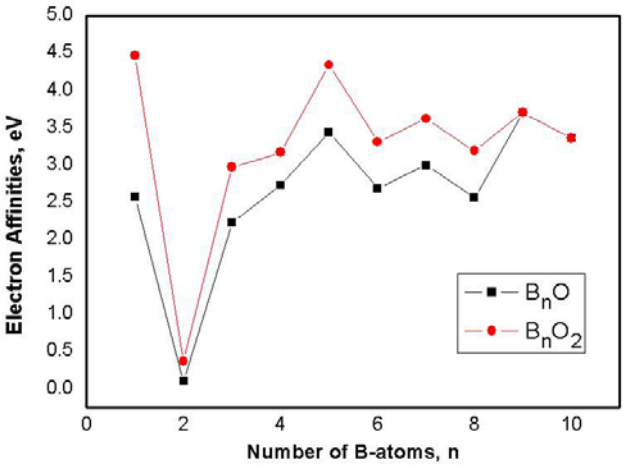

Figure 38. Size-dependence of the adiabatic electron affinities (EAs) of B_nO and B_nO_2 clusters.

The relative stability of the clusters B_nO_m (n = 1-10 and m = 0, 1 and 2) can be evaluated in terms of the average binding energy (E_b defined as the normalized binding energy per atom),

$$E_b = [nE(B) + mE(O) - E(B_nO_m)] / (n+m) \quad (84)$$

and the second difference in the total energy (Δ^2E), defined as follows

$$\Delta^2E(B_nO_m) = [E(B_{n-1}O_m) + E(B_{n+1}O_m) - 2E(B_nO_m)] \quad (85)$$

The average binding energies E_b of the pure B_n and oxide B_nO_m clusters for both neutral and anions are compared in Figures 39 and 40, respectively. The binding energy is increased when oxygen is added to a boron cluster forming BO bonds. For the same total number of atoms, E_b of B_nO_2 is higher than the E_b of B_nO and B_n. The binding energy of B_2O_2 is remarkably high for the neutrals; the additional stability of B_2O_2 is also found in Δ^2E. The plots for the anions show that BO^- and BO_2^- have E_b values > 0.5 eV larger than the values for the other oxides.

In our previous work, we considered the resonance energy (RE) of a boron cluster defined by equation (86):

$$RE(B_n) = \Delta E(B_n \rightarrow nB) - x\Delta E(B_2 \rightarrow nB) \quad (86)$$

in which the diatomic B_2 can be in either the $^1\Sigma_g^+$ or the $^3\Sigma_g^-$ state, and x is the number of BB bonds in B_n. In a similar way, we can define the REs of the neutral and anion boronoxides as expressed in equations (87) and (88), respectively:

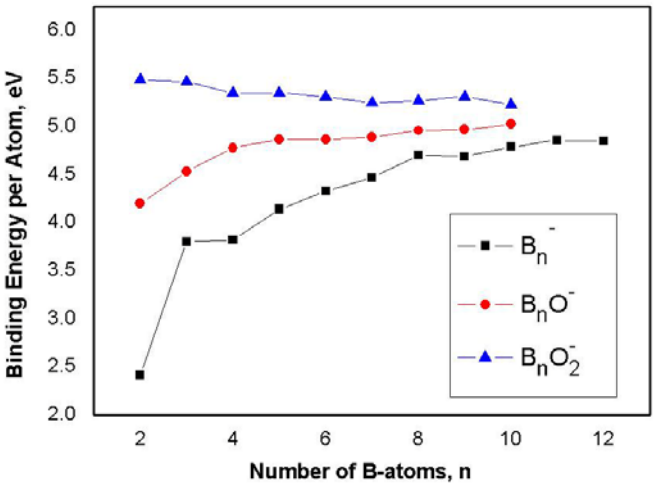

Figure 39. Size-dependence of the binding energy per atom of the neutrals B_n, B_nO and B_nO_2.

$$RE(B_nO_m) = \Delta E(B_nO_m \rightarrow nB + mO) - x\Delta E(B_2(^1\Sigma^+_g) \rightarrow 2B) - m\Delta E(BO(^2\Sigma^+) \rightarrow B + O) \quad (87)$$

$$RE(B_nO_m^-) = \Delta E(B_nO_m^- \rightarrow nB + mO) - (x-1)\Delta E(B_2(^1\Sigma^+_g) \rightarrow 2B) - \Delta E(B_2^-(^4\Sigma_g^-) \rightarrow 2B + e) - m\Delta E(BO(^2\Sigma^+) \rightarrow B + O) \quad (88)$$

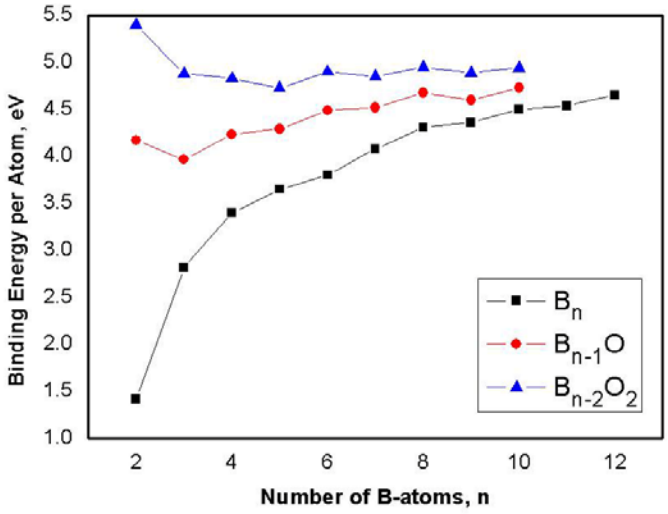

Figure 40. Size-dependence of the binding energy per atom of the anions B_n^-, B_nO^- and $B_nO_2^-$.

where n is the number of B atoms, m = 1 for monoxides, m = 2 for dioxides, and similarly x is the number of BB bonds. The normalized resonance energy (NRE) is defined as RE/(n + m). To facilitate the comparison, we consider the same value of x for each series of n. We initially analyzed the resonance energies of the boron clusters up to n = 4 using the approach employed for analyzing the Al_n clusters for up to n = 4. In this approach, we only counted the number of delocalized pi electrons so for B_4^{2-} we used x = 3. In our study of the larger boron clusters, use of only the delocalized electrons would have led to unreasonably large resonance energies and as discussed previously, it is difficult to determine how many delocalized electrons should be counted. As the r eference model for predicting the resonance energy is somewhat arbitrary, we chose to use the total number of BB bonds in a cluster in our resonance energy estimates for the pure boron clusters. We thus use the singlet state for B_2 ($^1\Sigma_g^+$) as the energy of a bond. For B_3, x = 3, whereas for B_4, x = 5, and for B_5, x = 7, with the values for B_4 and B_5 coming from our analysis of the structures including the electron density analysis. For

example, B_4 is a trapezoid so there is one B-B bond across the center which we include in addition to the four B-B bonds around the perimeter; B_5 has five perimeter BB bonds and two in the center of the cluster giving x = 7. For the larger clusters, a count for effective BB bonds becomes more difficult. For B_6, there are arguments as to whether to assign x to either 8 or 9. The values of x and the calculated values for REs and NREs are given in the ESI. Figures 42 and 43 illustrate the variation of both quantities as a function of n. The REs of the anions tend to be larger than those of the corresponding neutrals. Compared with the B_n counterparts, addition of O atoms decreases the REs. The same trend is also observed for the NREs. Thus, the BO groups act as electron-withdrawing substituents reducing the electron delocalization, and thereby the resonance energies. The reduction of the NRE amounts to 2-8 kcal/mol in going from a B_n to a B_nO_2, in which the larger the cluster (n), the larger the reduction. However, the BO groups that are formed following oxidation of boron clusters contribute in many ways to the stability of the whole system, even though they apparently reduce the resonance energy.

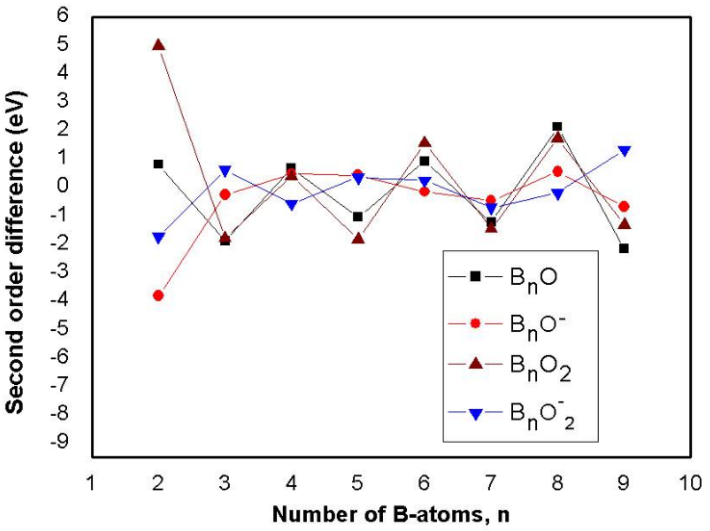

Figure 41. Second-order energy differences of the B_nO_m species

The present results extend the observations we have previously made on the growth mechanism of boron oxide clusters, and can be summarized as follows: (i) in each oxide, the low spin state is consistently favored over the corresponding high spin state; (ii) for neutral clusters, the most stable structure for a boron monoxide B_nO tends to be built up either by condensing the O atom on a BB edge of the B_n cycle (for B_5O, B_7O, B_8O), or by binding one boronyl (BO) group to the B_{n-1} ring (for B_4O, B_6O, B_9O and $B_{10}O$). The balance between the two factors is likely determined by the inherent stability of the boron cycle; (iii) a boron dioxide cluster is formed by incorporating the second O atom to the most stable form of the corresponding monoxide, with one (or two) B atom(s) at the opposite side of the first O atom (except for B_7O_2). The balance between the ring stability and the BO bond strength is again a determining factor; (iv) the anionic $B_nO_m^-$ clusters prefer to form exocyclic BO groups bound to either the B_{n-1} (for boron monoxides) or B_{n-2} (for

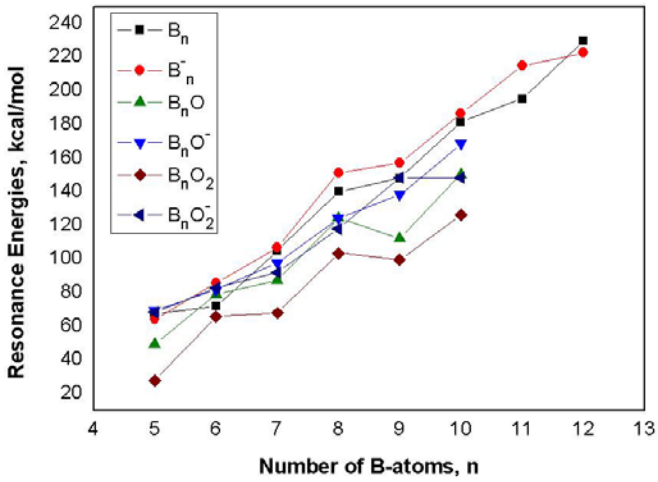

Figure 42. Resonance energies (RE, kcal/mol) of the B_nO_m and $B_nO_m^-$ Clusters (n = 5 - 10, m = 0, 1, 2)

boron dioxides) rings. This motif becomes the preferred geometrical feature of the larger size boron dioxides, even in the neutral state (for B_9O_2 and $B_{10}O_2$), in such a way that a boron oxide anion $B_nO_m^-$ can be described as $B_{n-2}(BO)_2^-$; (v) there is a similarity between boron hydrides B_nH_2 and boron oxides $B_n(BO)_2$. The boronyl group behaves as an electron-withdrawing group; and (vi) the boron oxides possess some of the inherent electronic properties of the parent boron clusters, such as the planar geometries and multiple aromaticity. Nevertheless, the presence of O atoms significantly reduces the average energy per atom and resonance energy of the boron oxides. We also expanded on concepts such as improved definitions of aromaticity for these compounds including the idea of using normalized values.

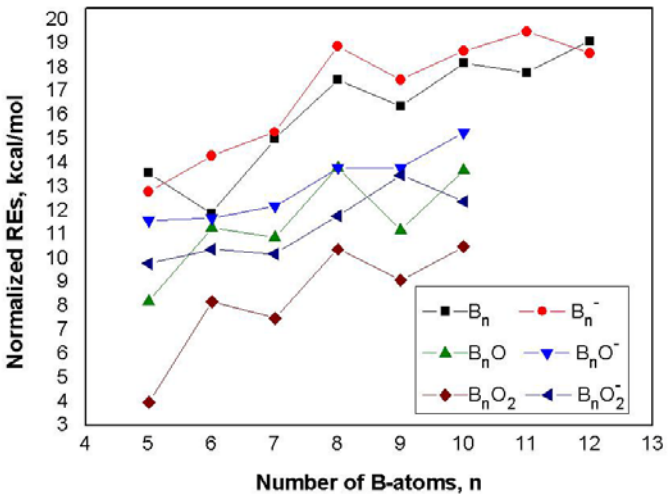

Figure 43. Normalized resonance energies (NRE) of the B_nO_m and $B_nO_m^-$ Clusters (n = 5-10, m = 0, 1, 2)

Thermochemistry of Hydrogen Release and B-N Bond Dissociation Energy (BDE) from Metal Ammonia Borane Compounds

We have extended our computational studies to main group and transition metal complexes of borane amines bonded to main group compounds and transition metals. An important set of main group and transition metal complexes are derived from binding $(NH_2BH_3)^-$ to a cationic center such as Li^+, Ca^{2+}, Al^{3+} or Ti^{4+} to form the respective complexes $Li(NH_2BH_3)$, $Ca(NH_2BH_3)_2$, $Al(NH_2BH_3)_3$, and $Ti(NH_2BH_3)_4$. We have initiated such calculations. We also are doing calculations on the reverse compositions based on $M^-(BH_2NH_3)_n$ Calculations have been done for a number of molecular systems at the density functional theory and molecular orbital theory levels as shown in the following Figures 44-53.

For M = Li, the thermodynamics predict that $Li(NH_2BH_3)$ is stable with regards to hydrogen release and none of the dehydrogenation pathways are favorable, even when considering the free energy values. The B-N BDE is also considerable larger than that found in BH_3NH_3. For $Li(BH_2NH_3)$ however, the first dehydrogenation pathway is predicted to exothermic with the second dehydrogenation enthalpy predicted to be endothermic. There is the possibility of removing two hydrogen molecules coupling the exothermicity of the first reaction. The B-N BDE is less than that found in BH_3NH_3.

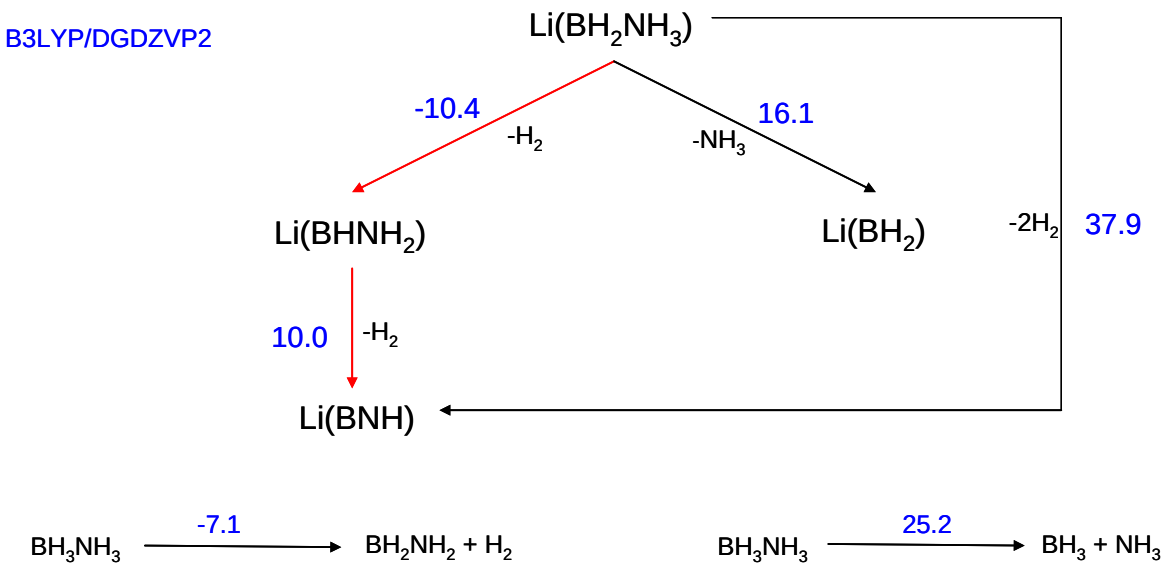

• First number given is ΔH_{rxn} (298 K) followed by ΔG_{rxn} (298 K)

Dehydrogenation Pathways and B-N BDE for the Lithium Borane Amines

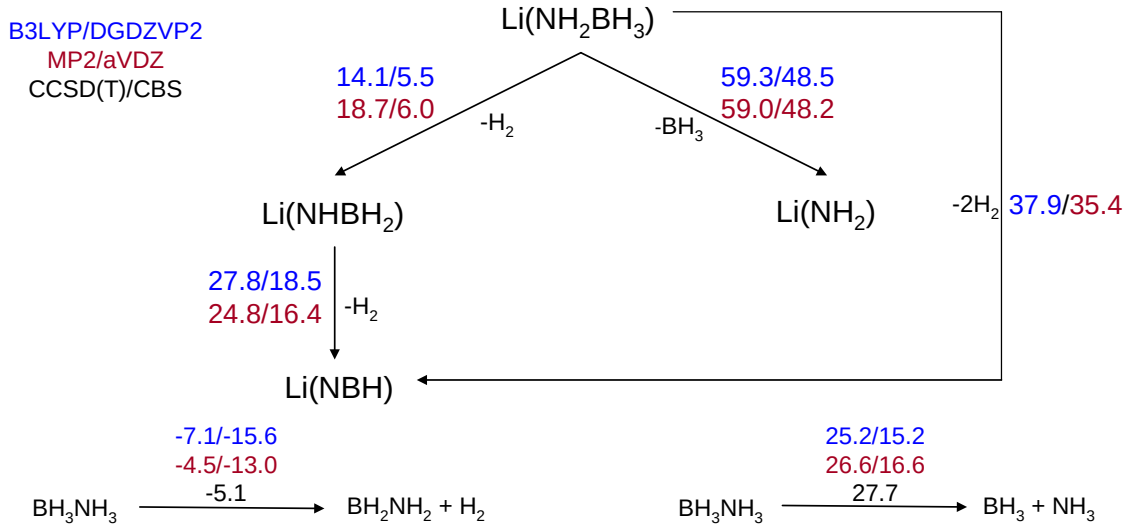

• First number given is ΔH_{rxn} (298 K) followed by ΔG_{rxn} (298 K)

Figure 44. Dehydrogenation pathways and and B-N BDEs for $Li(NH_2BH_3)$ at the B3LYP/DZVP2 and MP2/aVDZ levels and for $Li(BH_2NH_3)$ at the B3LYP/DZVP2 level.

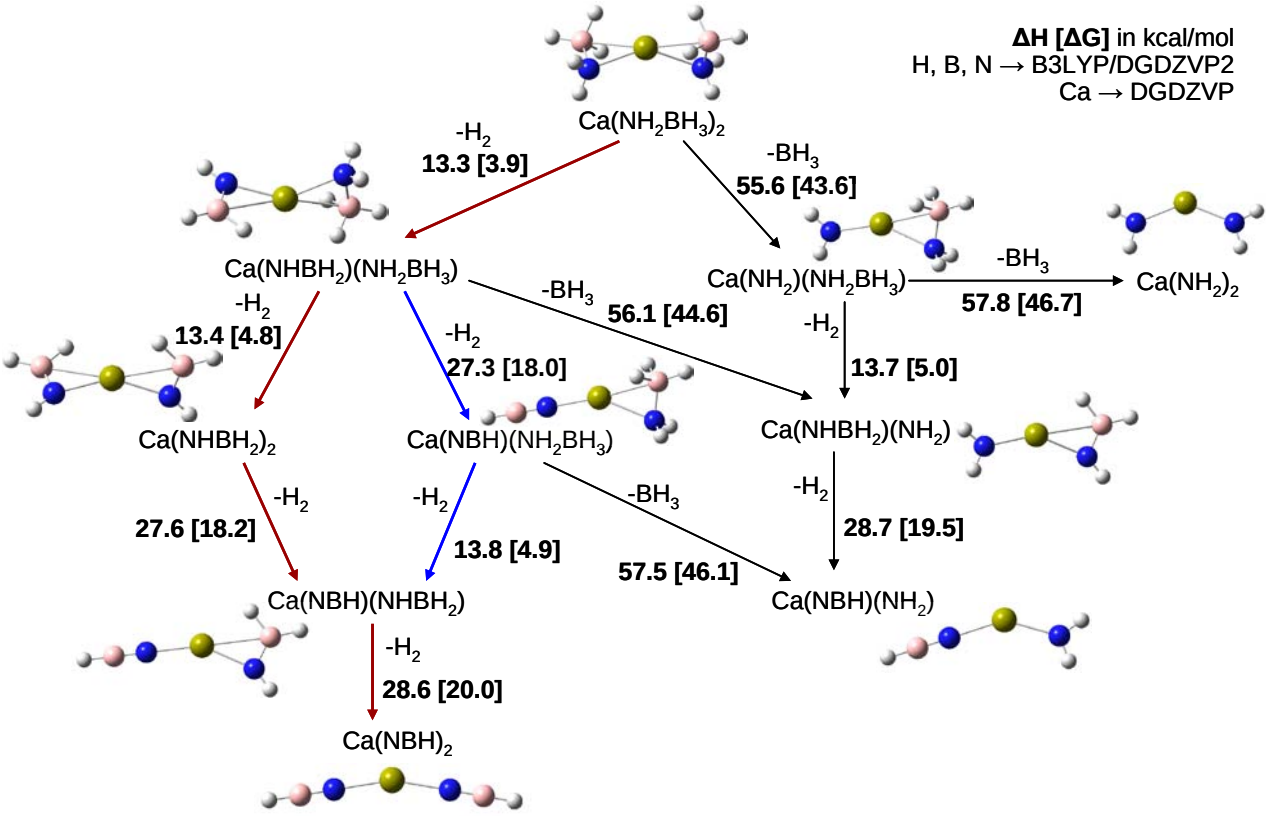

Figure 45. Complete dehydrogenation and B-N BDE pathways for $Ca(NH_2BH_3)_2$ at the B3LYP/DZVP2 (DZVP, Ca) level. The red and blue arrows show the lowest energy pathways.

For Ca, we found that the lowest energy pathway marked in red, is endothermic and energetically similar to that of the next highest pathway shown in blue (see Figure 45). Dehydrogenation from the $–NH_2BH_3$ group is ~13.5 kcal/mol, whereas it is 27 to 29 kcal/mol from the $–NHBH_2$ group. The most endothermic process is the B-N BDE, which is 55 to 58 kcal/mol, due to the strong interaction between the B and the Ca atoms.

We tried to find minima without this type of interaction, but were unable to find any. Therefore, we can conclude that the B-Ca interactions are very important for the stabilization of this kind of Ca compounds. The ΔG values show the predicted non-spontaneity of these processes. For Mg, the reactions are slightly endothermic for the first few steps. For M = Al, DFT and MO (MP2) levels of theory give slightly different results. DFT predicts the first and second dehydrogenation reactions of $Mg(NH_2BH_3)_2$ to be slightly exothermic and favorable pathways for hydrogen release, as indicated by the red arrows. At the G3(MP2) level however, $Mg(NH_2BH_3)_2$ is stable with respect to hydrogen release. There is the possibility for the removal of two hydrogen molecules when consider both molecules with the exothermicity of the dehydrogenation reaction of $Mg(BH_2NH_3)_2$ predicted to be larger.

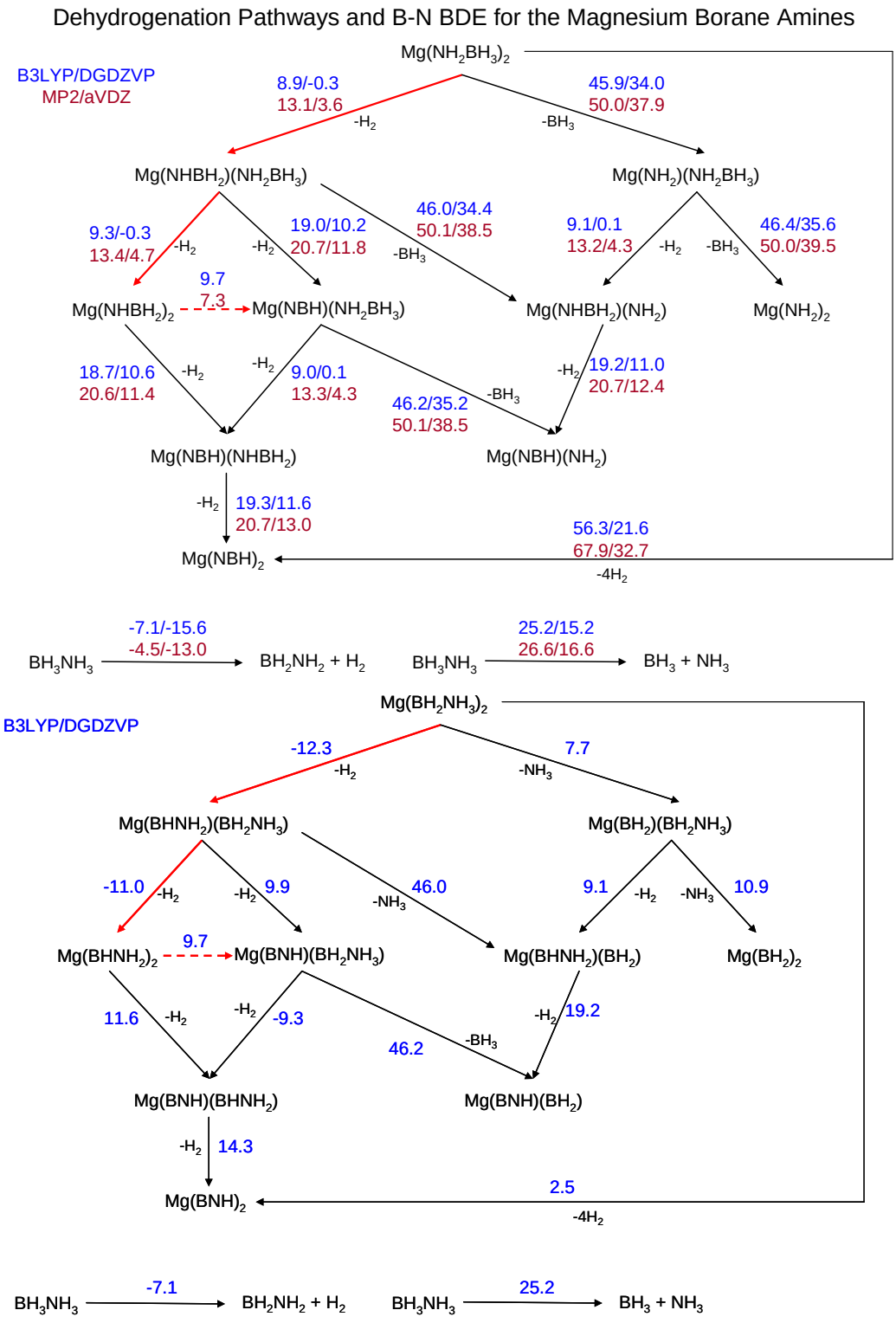

Figure 46. Complete dehydrogenation and B-N BDE pathways for $Mg(NH_2BH_3)_2$ at the B3LYP/DZVP2 and MP2/aVDZ levels. and for $Mg(BH_2NH_3)_2$ at the B3LYP/DZVP2 level. The red arrows show the lowest energy pathways.

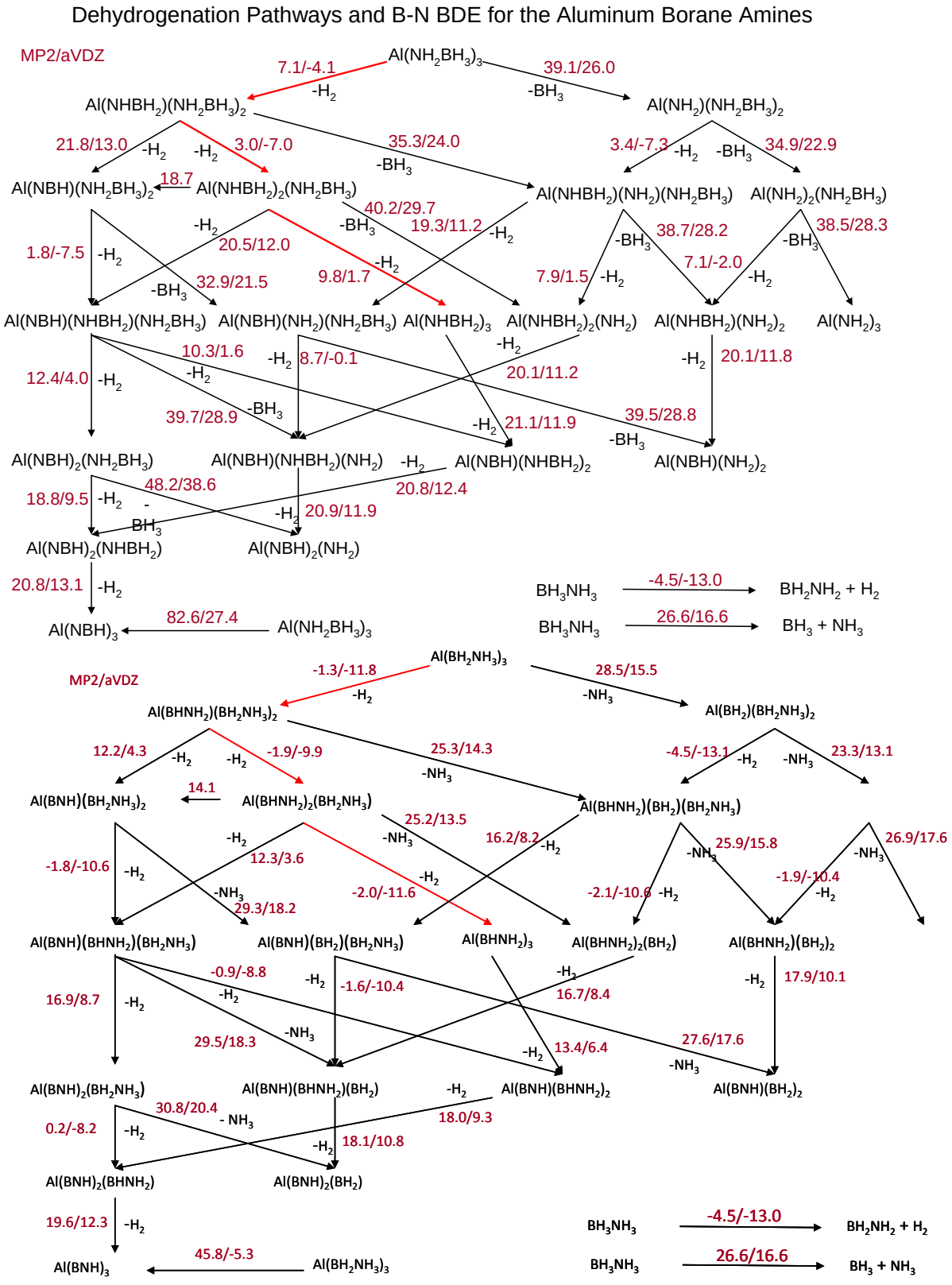

Figure 47. Complete dehydrogenation and B-N bond dissociation energy (BDE) pathways for $Al(NH_2BH_3)_3$ and $Al(BH_2NH_3)_3$. The red arrows show the lowest energy pathways.

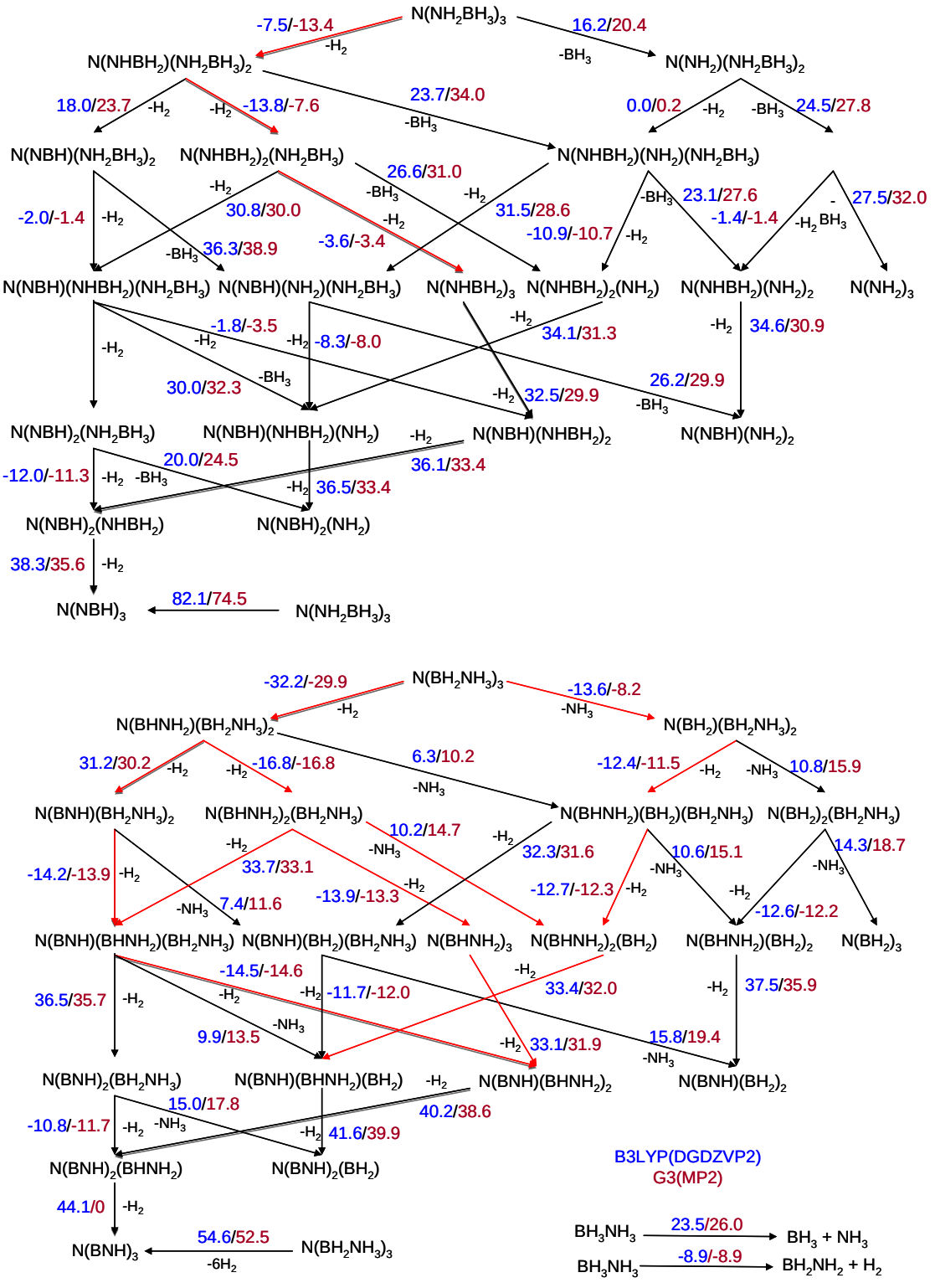

Figure 48. Complete dehydrogenation and B-N bond dissociation energy (BDE) pathways for $N(NH_2BH_3)_3$ and $N(BH_2NH_3)_3$ at the B3LYP/DZVP2 and G3MP2 levels, respectively. The red arrows show the lowest energy pathways.

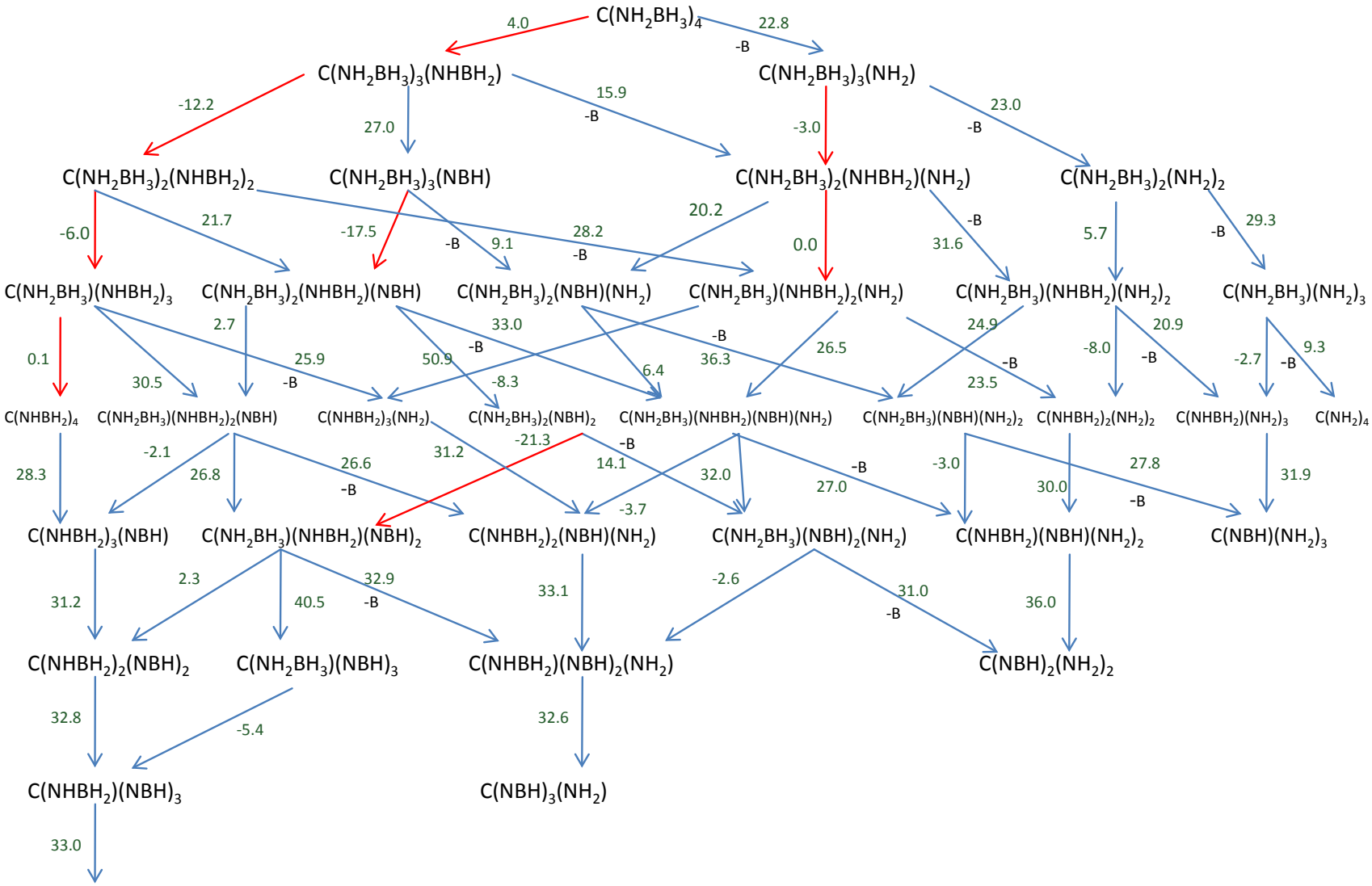

Figure 49. Complete dehydrogenation and B-N bond dissociation energy (BDE) pathways for $C(NH_2BH_3)_4$. The red arrows show the lowest energy pathways. Values are B3LYP enthalpies.

The initial reaction enthalpy for the dehydrogenation reaction of $C(NH_2BH_3)_4$ to release one molecule of H_2 is predicted to be slightly endothermic by 4.0 kcal/mol in terms of the enthalpy but considering the ΔG is negative by ~8 kcal/mol due to releasing H_2.

The results for Ti and V as the central atom for complexation to BH_2NH_3 and NH_2BH_3 as the ligand are shown in Figures 51-54 in kcal/mol at the B3LYP level. In addition, Table 40 shows the number of hydrogens that can be exothermically removed from several of the metal amido borane species.

Table 40. Reaction Energies (kcal/mol) for Release of H_2 from Metal Amido Boranes

Reaction	**#Species**	**ΔH (298 K)**	**#H_2 Exothermically Released**
$V(NH_2BH_3)_5 \rightarrow V(NBH)_5 + 10H_2$	52	149.0	7
$V(BH_2NH_3)_5 \rightarrow V(BNH)_5 + 10H_2$	52	122.7	9
$Ti(NH_2BH_3)_4 \rightarrow Ti(NBH)_4 + 8H_2$	35	112.2	5
$Ti(BH_2NH_3)_4 \rightarrow V(BNH)_4 + 8H_2$	35	75.8	7
$Si(NH_2BH_3)_4 \rightarrow Si(NBH)_4 + 8H_2$	35	62.8	5
$Si(BH_2NH_3)_4 \rightarrow Si(BNH)_4 + 8H_2$	35	90.3	6
$C(NH_2BH_3)_4 \rightarrow C(NBH)_4 + 8H_2$	35	111.2	5
$C(BH_2NH_3)_4 \rightarrow C(BNH)_4 + 8H_2$	35	94.8	6
$Al(NH_2BH_3)_3 \rightarrow Al(NBH)_3 + 6H_2$	20	74.3	4
$Al(BH_2NH_3)_3 \rightarrow Al(BNH)_3 + 6H_2$	20	48.2	5

Transition States for Hydrogen Elmination from Metal Ammonia Boranes

In addition, we have initiated studies on the transition states for H_2 removal from the lithium, magnesium, and aluminium ammona boranes at the B3LYP level with the DZVP2 (Li and Al) and DZVP (Na) basis sets. Figure 55 shows the structures and transition states (Energies at 298 K) for both the $M^{n+}(NH_2BH_3)_n^-$ and $M^{n+}(BH_2NH_3)_n^-$ complexes. The barriers are often higher than that in the parent BH_3NH_3 suggesting that the H_2 elimination reaction needs to proceed through multiple molecules starting with the dimer.

Thermodynamics of 5-membered rings containing N

On the basis of new materials discussions, we are studying hydrogen elimination from azolium borohydrides (polymeric amine borane analogs). We have calculated the energies for 5-membered rings containing N: pyrrole, pyrazole and imidazole, triazoles and tetrazole. Isodesmic reactions (Table 41) were used to predict the various heats of formation at the G3MP2 level of theory. The calculated heats of formation, acidities, which is defined by the negative enthalpy for the following reaction $AH \rightarrow A^- + H^+$, and basicities, also as definited by the negative enthalpy of the following reaction $A + H^+ \rightarrow AH^+$ are given in Table 42.

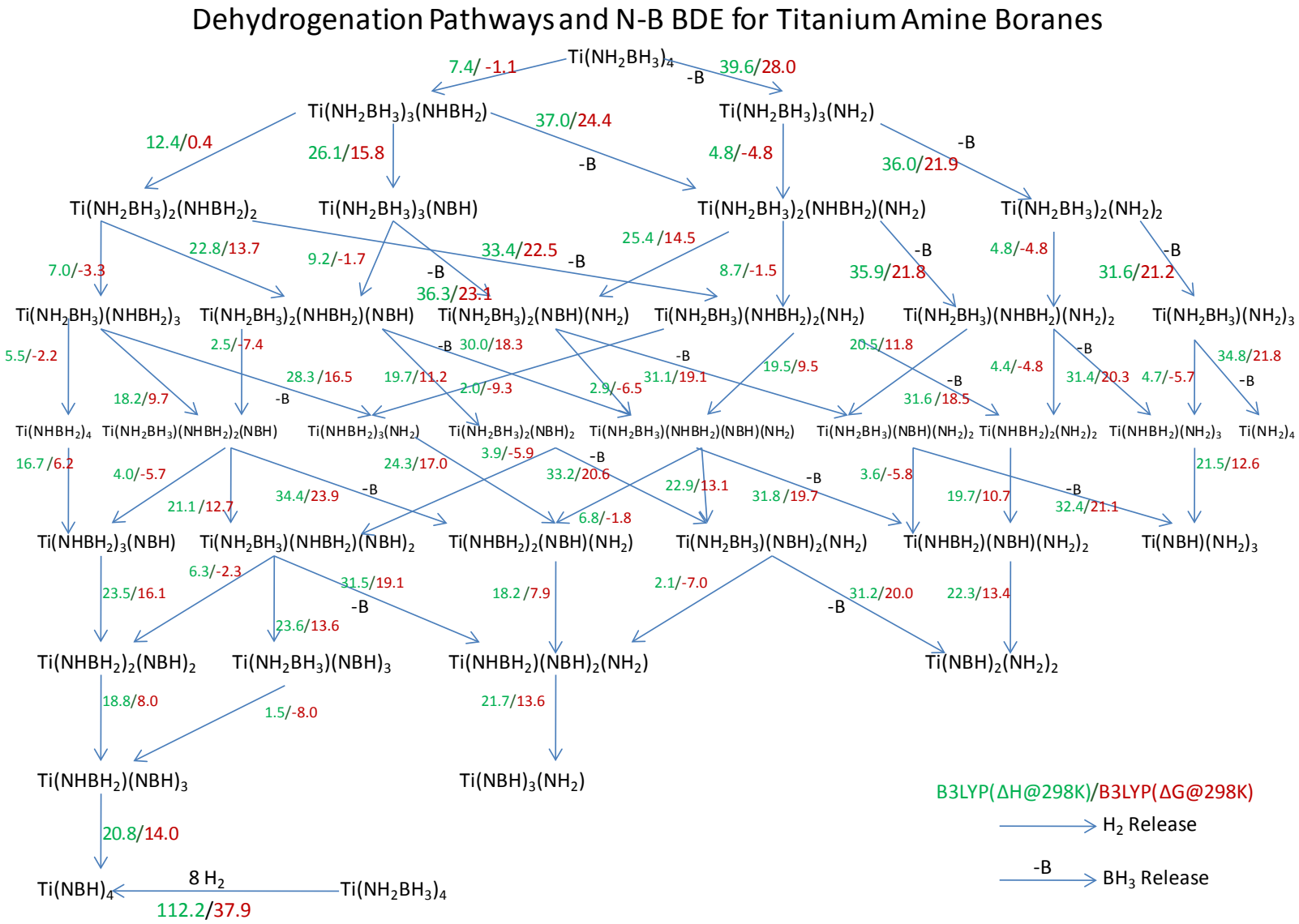

Figure 50. Dehydrogenation pathways and B-N bond dissociation energies for $Ti(NH_2BH_3)_4$ in kcal/mol at the B3LYP level.

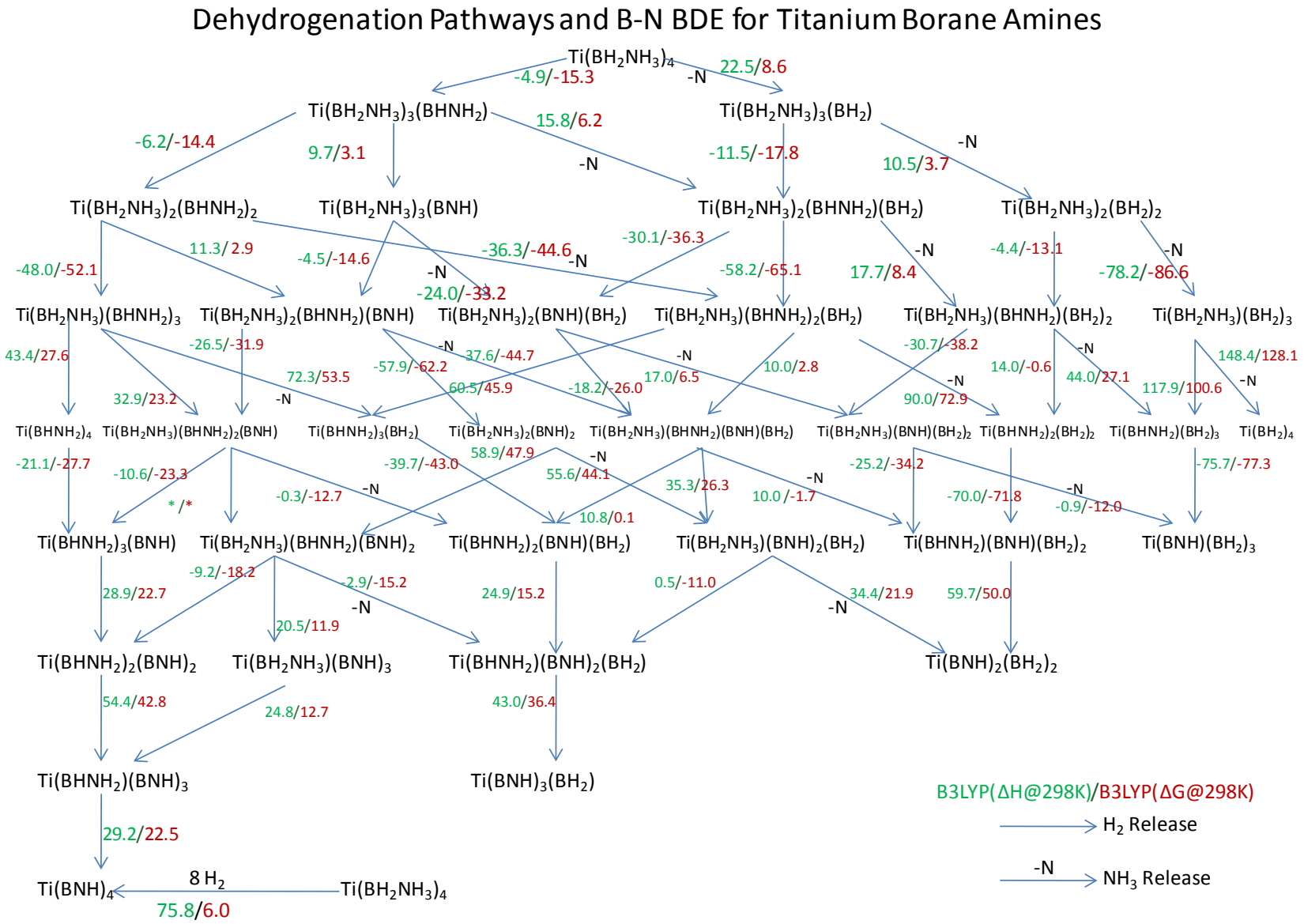

Figure 51. Dehydrogenation pathways and B-N bond dissociation energies for $Ti(BH_2NH_3)_4$ in kcal/mol at the B3LYP level.

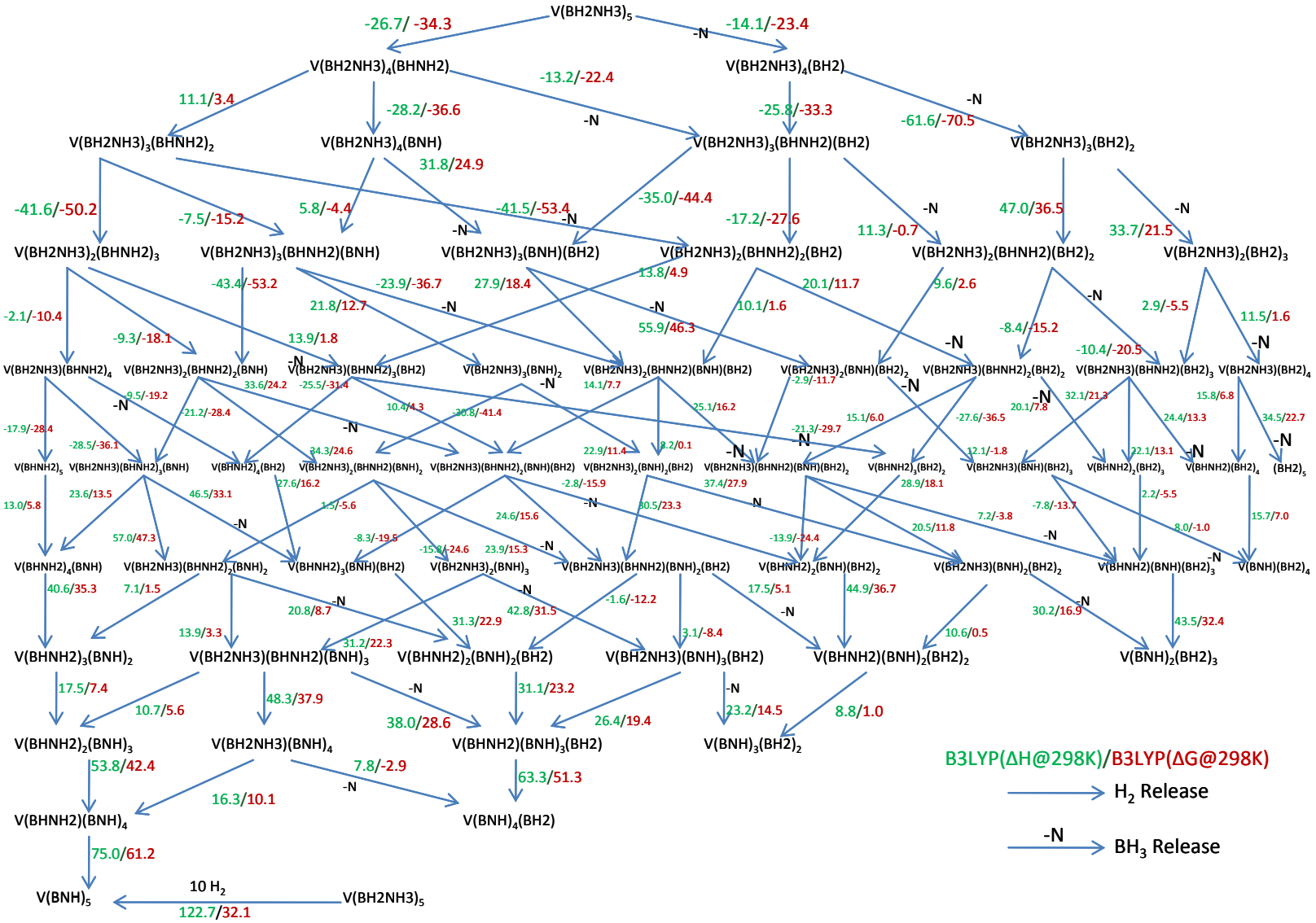

Figure 52. Dehydrogenation pathways and B-N bond dissociation energies for $V(BH_2NH_3)_5$ in kcal/mol at the B3LYP level

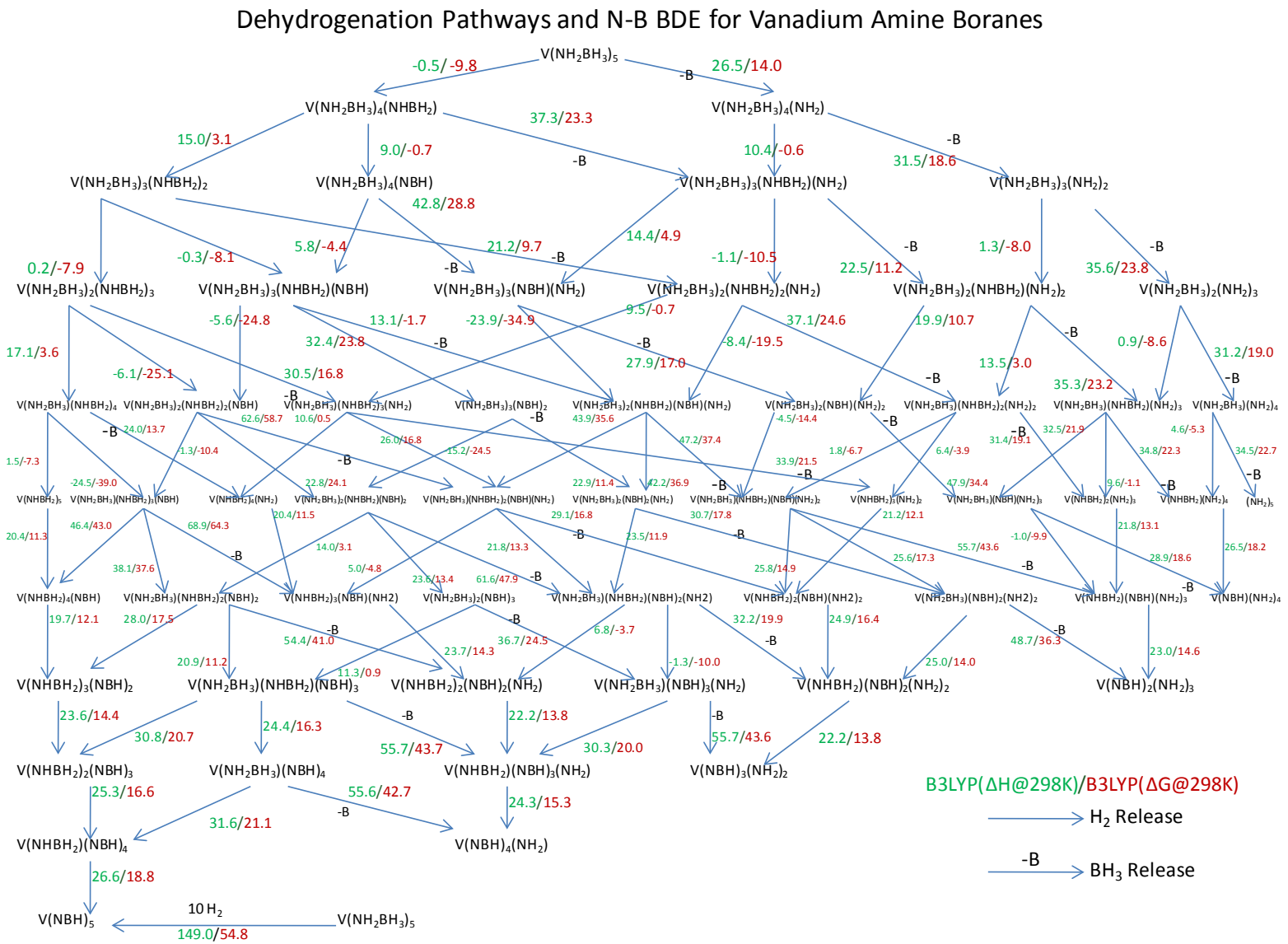

Figure 53. Dehydrogenation pathways and B-N bond dissociation energies for $V(NH_2BH_3)_5$ in kcal/mol at the B3LYP level.

$Li(NH_2BH_3) \rightarrow [Li(NHBH_2)\cdots H_2]^{\ddagger} \rightarrow Li(NHBH_2) + H_2$

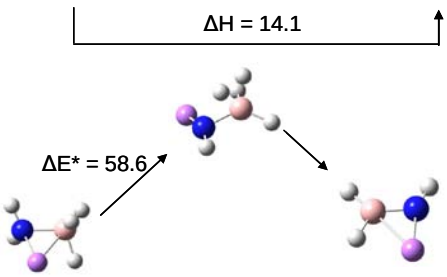

$Li(BH_2NH_3) \rightarrow [Li(BHNH_2)\cdots H_2]^{\ddagger} \rightarrow Li(BH_2NH_2) + H_2$

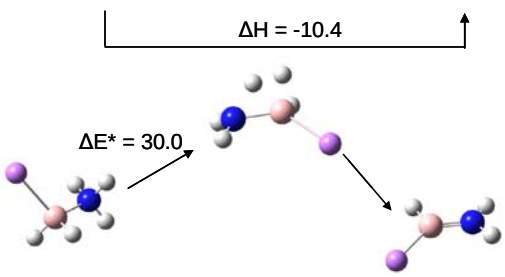

$Na(NH_2BH_3) \rightarrow [Na(NHBH_2)\cdots H_2]^{\ddagger} \rightarrow Na(NHBH_2) + H_2$

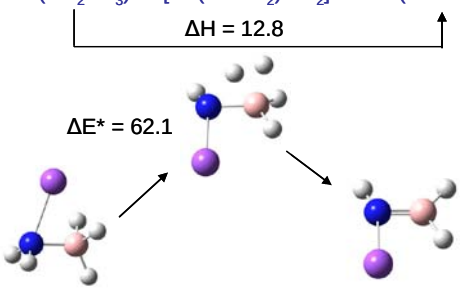

$Na(BH_2NH_3) \rightarrow [Na(BHNH_2)\cdots H_2]^{\ddagger} \rightarrow Na(BH_2NH_2) + H_2$

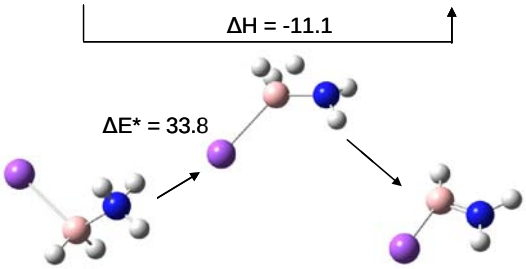

$Al(NH_2BH_3)_3 \rightarrow [Al(NH_2BH_3)_2(NHBH_2)\ldots H_2]^{\ddagger} \rightarrow Al(NH_2BH_3)_2(NH_3BH_2)+H_2$

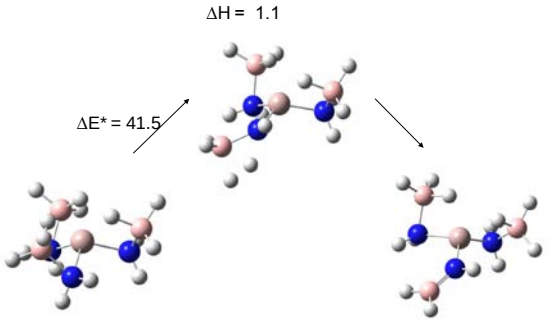

$Al(NH_2BH_3)_2(NHBH_2) \rightarrow [Al(NH_2BH_3)(NHBH_2)_2\ldots H_2]^{\ddagger} \rightarrow Al(NH_2BH_3)(NHBH_2)_2+H_2$

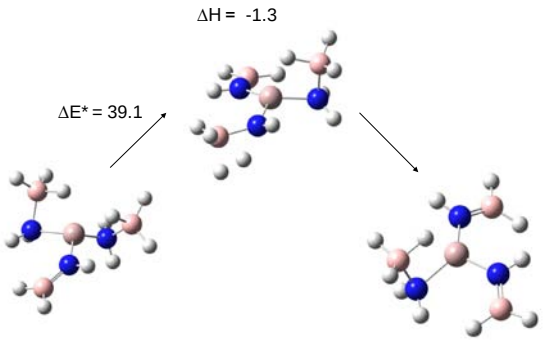

$Al(NH_2BH_3)(NHBH_2)_2 \rightarrow [Al(NHBH_2)_3\ldots H_2]^{\ddagger} \rightarrow Al(NHBH_2)_3+H_2$

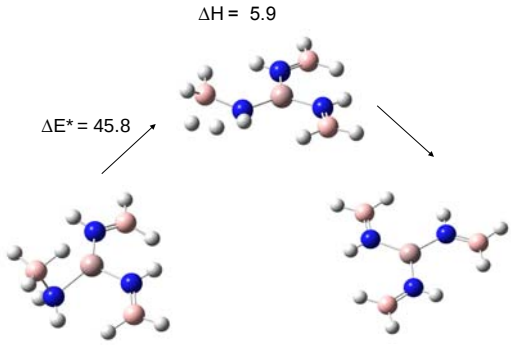

$Al(BH_2NH_3)_3 \rightarrow [Al(BH_2NH_3)_2(BHNH_2)\ldots H_2]^{\ddagger} \rightarrow Al(BH_2NH_3)_2(BH_3NH_2)+H_2$

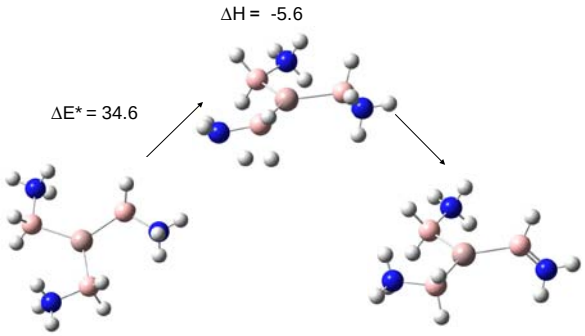

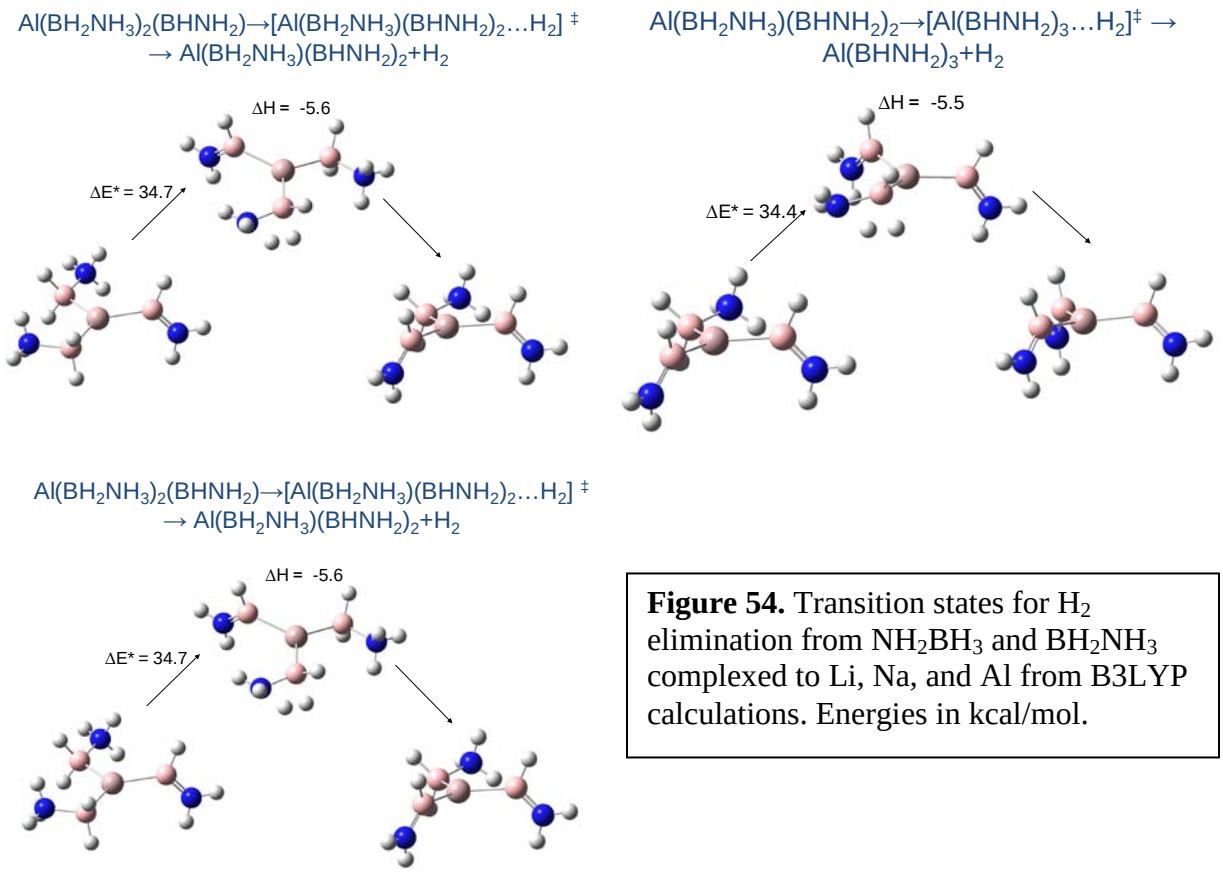

Figure 54. Transition states for H_2 elimination from NH_2BH_3 and BH_2NH_3 complexed to Li, Na, and Al from B3LYP calculations. Energies in kcal/mol.

Our results show that some of the nitrogen 5-membered ring compounds are extremely acidic in the gas phase rivaling the polyoxometallates and the very strong inorganic acids like H_2SO_4, FSO_3H, CF_3SO_3H, $(CF_3SO_2)_2NH$, and $(CF_3SO_2)_3CH$. Addition of a BH_3 group to an NH makes the NH more acidic as does addition of a BH_3 to an N in the ring that is not an NH. As would then be expected, addition of a BH_3 to an N makes the site a very weak base with very low basicities comparable to CO or CH_4.

Table 41. Isodesmic Reaction Energies at 298K in kcal/mol at the G3(MP2) Level.

Reaction	ΔH_{rxn}
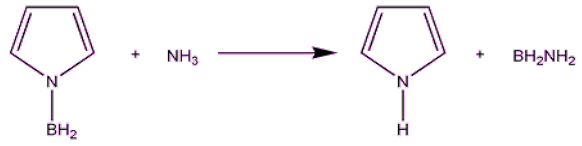	3.4
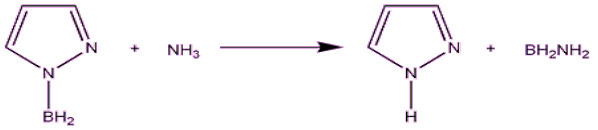	4.2
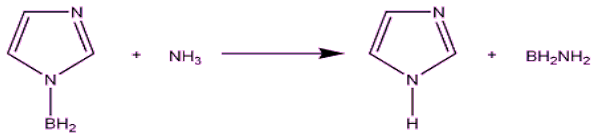	3.9

Reaction	ΔH_{rxn}
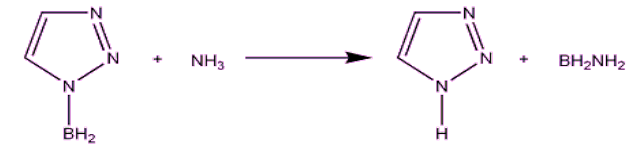	4.9
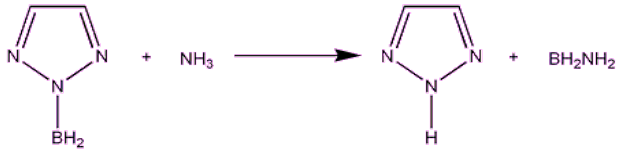	4.9
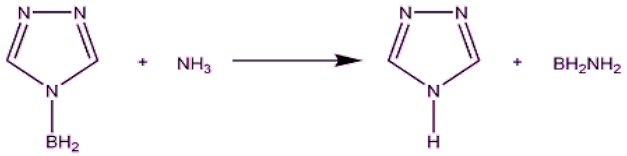	4.7
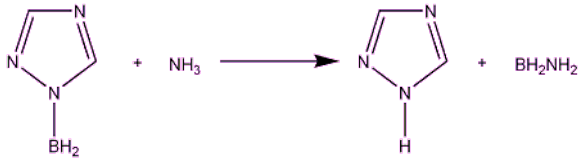	4.9
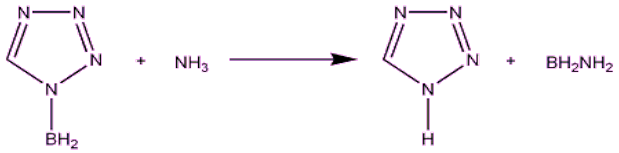	5.8
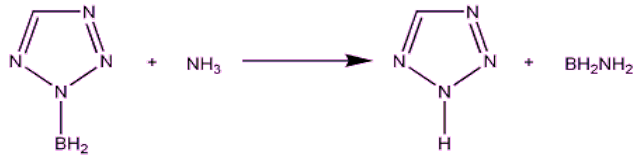	5.8

Table 42. Acidities, Proton Affinities (PA), and Heats of Formation at 298K in kcal/mol using G3(MP2).

Molecule	Structure	Acidity	PA*	ΔH_f^0
pyrrole	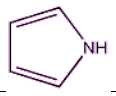	351.5	190.5	26.5
pyrrole.BH_3	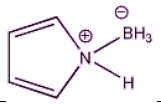	303.7	-	41.2
pyrazole	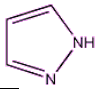	346.8	213.6/182.1	178.9
pyrazole.BH_3(N-H, N-BH_3)	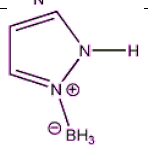	322.5	165.4/186.7	38.9

pyrazole.BH_3(N-H, BH_3)	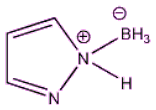	298.0	210.7	62.8
pyrazoleH.2BH_3	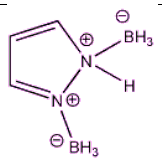	288.8	-	60.9
imidazole	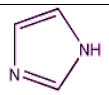	342.1	225.8/177.1	32.8
imidazole.BH_3(N-H, N-BH_3)	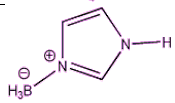	318.6	158.3/196.2	26.1
imidazole.BH_3(N-H, BH_3)	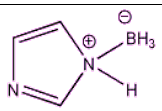	293.7	221.6	51.5
imidazoleH.2BH_3	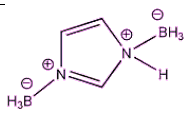	278.5	-	51.3
1(H).2.3.triazole	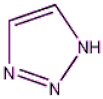	334.6	201.2/213.4/ 187.6	65.1
1(H).2.3(BH_3).triazole	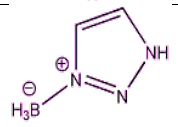	309.6	160.8/178.1	62.8
1(H).2(BH_3).3.triazole	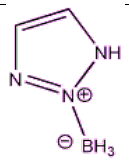	310.0	154.5/163.0	64.9
1(H, BH_3).2.3.triazole	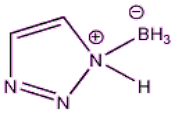	293.2	201.5/212.7	86.6
1(H).2(BH_3).3(BH_3).triazole	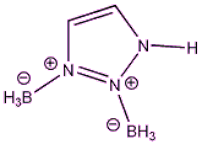	289.6	144.5	70.4

1(H.BH_3).2(BH_3).3.triazole	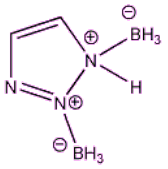	290.3	175	71.3
1(H.BH_3).2.3(BH_3).triazole	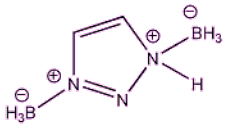	274.5	181.3	88.3
1(H).2.3.triazoleH.3BH_3	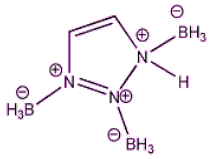	278.9	-	76.7
1.2(H).3.triazole	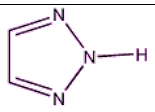	338.0	197.4/172.6	61.3
1(BH_3).2(H).3.triazole	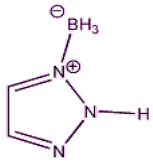	312.2	150.0/175.6	60.3
1.2(H, BH_3).3.triazole	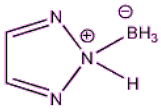	295.8	201.2	86.3
1(BH_3).2(H).3(BH_3).triazole	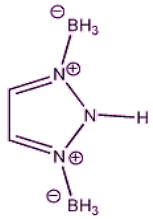	289.0	131.5	63.9
1(BH_3).2(H.BH_3).3.triazole	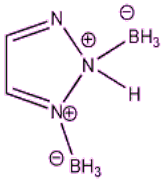	299.9	157.6	64.6

1.2(H).3.triazoleH.3BH_3	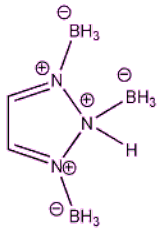	272.7	-	89.5
1.2.4(H).triazole	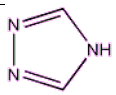	330.5	217.9/162.4	54.0
1(BH_3).2.4(H).triazole	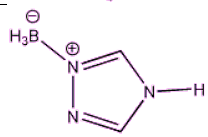	307.3	192.5/144.9	50.0
1.2.4(H, BH_3).triazole	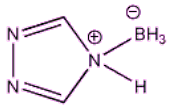	287.5	221.1	79.4
1(BH_3).2(BH_3).4(H).triazole	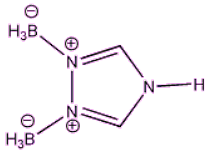	288.7	133.1	54.1
1(BH_3).2.4(H.BH_3).triazole	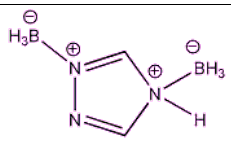	271.1	202.3	75.0
1.2.4(H).triazoleH.3BH_3	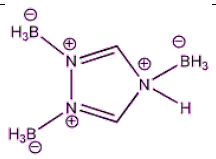	258.2	-	78.0
1(H).2.4.triazole	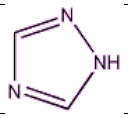	336.7	212.1/201.4/ 167.4	48.2
1(H).2(BH_3).4.triazole	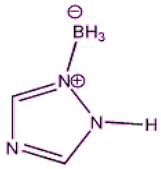	311.4	151.2/188.8	46.4
1(H).2.4(BH_3).triazole	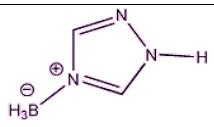	313.8	183.8/150.8	45.2

1(H, BH_3).2.4.triazole	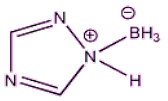	311.4	178.1/188.0	46.4
1(H).2(BH_3).4(BH_3).triazole	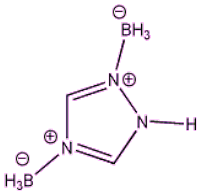	291.8	132.6	47.8
1(H.BH_3).2(BH_3).4.triazole	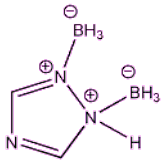	290.8	180.5	53.1
1(H.BH_3).2.4(BH_3).triazole	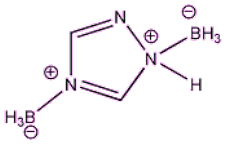	276.3	187.6	70.2
1(H).2.4.triazoleH.3BH_3	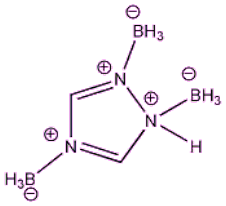	274.2	-	55.5
1(H).2.3.4.tetrazole	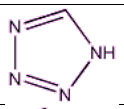	321.9	201.3/200.4/ 184.7/173.6	82.9
1(H).2(BH_3).3.4.tetrazole	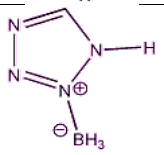	297.1	184.3/184.3/ 135.7	86.6
1(H).2.3(BH_3).4.tetrazole	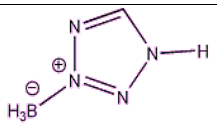	298.4	183.9/167.7/ 136.4	86.3
1(H).2.3.4(BH_3).tetrazole	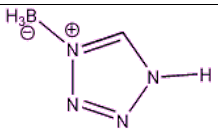	297.6	181.0/164.3/ 50.9	83.9

1(H, BH_3).2.3.4.tetrazole	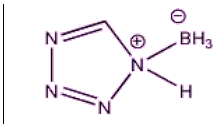	281.7	189.6/204.3/ 205.0	108.2
1(H).2(BH_3).3(BH_3).4. tetrazole	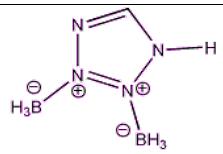	281.2	172.4/121.1	97.1
1(H).2(BH_3).3.4(BH_3). tetrazole	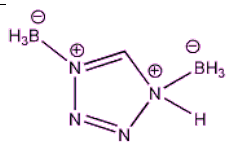	277.4	117.9/203.5	91.3
1(H).2.3(BH_3).4(BH_3). tetrazole	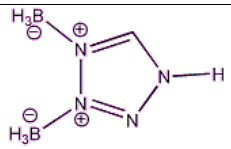	280.9	154.8/122.7	93.7
1(H.BH_3).2(BH_3).3.4. tetrazole	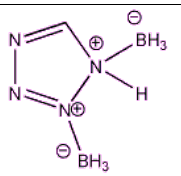	280.8	168.5/206.0	94.2
1(H.BH_3).2.3(BH_3).4. tetrazole	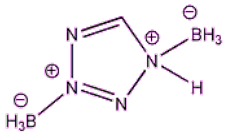	265.3	172.0/186.0	111.0
1(H.BH_3).2.3.4(BH_3). tetrazole	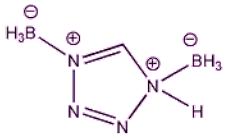	266.1	168.6/183.2	108.2
1(H).2(BH_3).3(BH_3).4(BH_3). tetrazole	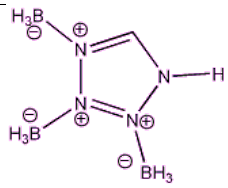	272.4	108.1	106.6
1(H.BH_3).2(BH_3).3(BH_3).4. tetrazole	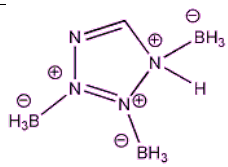	271.6	196.9	103.9

1(H.BH_3).2(BH_3).3.4(BH_3). tetrazole	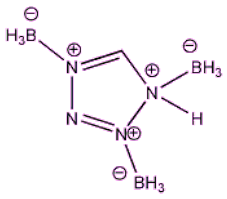	267.5	191.5	99.8
1(H.BH_3).2.3(BH_3).4(BH_3). tetrazole	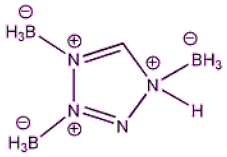	254.9	210.5	117.9
1(H).2.3.4.tetrazoleH.4BH_3	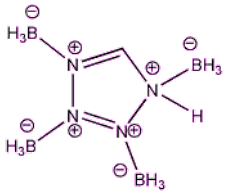	266.2	-	113.2
1.2(H).3.4.tetrazole	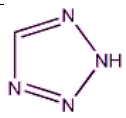	323.9	183.7/182.7/ 198.4/203.8	80.9
1(BH_3).2(H).3.4.tetrazole	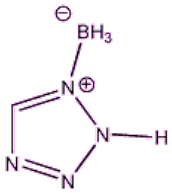	299.2	181.3/167.3/ 184.1	84.3
1.2(H).3(BH_3).4.tetrazole	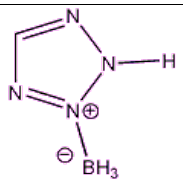	298.7	182.6/166.3/ 184.8	84.9
1.2(H).3.4(BH_3).tetrazole	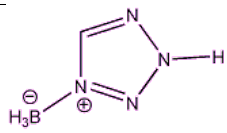	300.4	165.5/162.8/ 190.2	82.5
1.2(H, BH_3).3.4.tetrazole	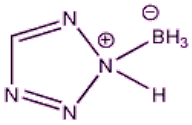	300.2	166.5/167.1/ 181.2	106.4

1(BH_3).2(H).3(BH_3).4. tetrazole	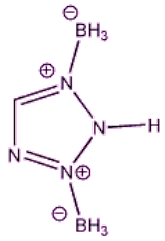	277.6	204.6/168.9	92.3
1(BH_3).2(H).3.4(BH_3). tetrazole	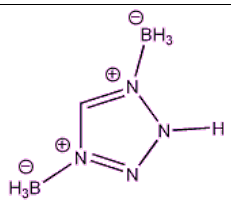	278.0	150.9/164.8	89.4
1.2(H).3(BH_3).4(BH_3). tetrazole	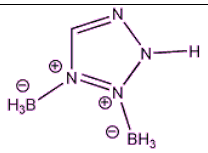	280.7	142.0/154.1	93.1
1(BH_3).2(H.BH_3).3.4. tetrazole	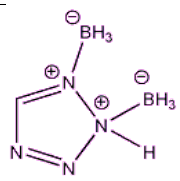	284.0	153.3/221.6	91.9
1.2(H.BH_3).3(BH_3).4. tetrazole	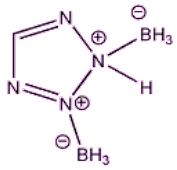	288.3	152.2/205.3	91.9
1.2(H.BH_3).3.4(BH_3). tetrazole	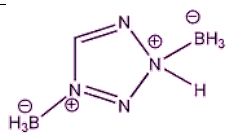	268.4	166.9/168.1	106.6
1(BH_3).2(H).3(BH_3).4(BH_3). tetrazole	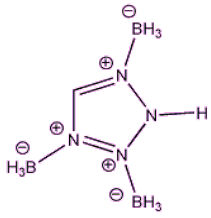	259.5	167.1	109.5

1(BH_3).2(H.BH_3).3(BH_3).4. tetrazole	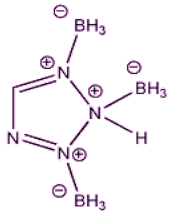	273.9	206.7	101.7
1(BH_3).2(H.BH_3).3.4(BH_3). tetrazole	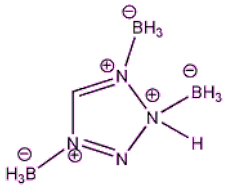	268.8	138.8	98.8
1.2(H.BH_3).3(BH_3).4(BH_3). tetrazole	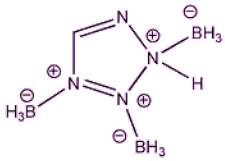	277.7	204.0	100.3
1.2(H).3.4.tetrazoleH.4BH_3	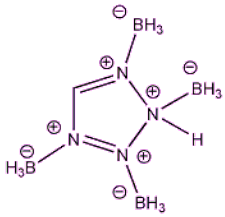	267.2	-	111.4

* Multiple values given due to multiple N-base protonation sites.

Acidities of the N-H Bond in BH_3-5-Member Ring Complexes (loss of H^+ from N)

We have been exploring other amine-borane complexes including the interaction of BH_3 with organic amines based on pyrrole, triazoles, and tetrazoles. We have now calculated the pK_a's of theses compounds. Some of these compounds are predicted to to be among the most acidic compounds in aqueous solution with pK_a's that are more negative than those of CF_3SO_3H with pK_a = -14.2. This provides further insight into the design of new species with highly activated hydrogen. The structures were intiatilly optimized at the B3LYP/DZVP2 level. These geometries were used as input for G3MP2 calculations of the gas phase acidities and COSMO/ B3LYP/DZVP2 calculations of the pK_a's.

Table 43. Predicted pKa's of BH_3-Organic Amine Complexes. Values in Italics are Experimental pK_a's.

Compound	**pK_a**	**Compound**	**pK_a**
pyrrole	22.2/*23.0*	1(H).2.3.4.tetrazole	8.2
pyrrole.BH_3	-4.1	1(H).2(BH_3).3.4.tetrazole	-2.4
pyrazole	17.1/*18.6*	1(H).2.3(BH_3).4.tetrazole	2.5
pyrazole.BH_3(N-H,N-BH_3)	8.6	1(H).2.3.4(BH_3).tetrazole	2.9
pyrazole.BH_3(N-H,BH_3)	-9.8	1(H.BH_3).2.3.4.tetrazole	-18.6

pyrazole.2BH_3	-14.3	1(H).2(BH_3).3(BH_3).4.tetrazole	-5.1
imidazole	19.0/*19.8*	1(H).2(BH_3).3.4(BH_3).tetrazole	-7.5
imidazole.BH_3(N-H,N-BH_3)	13.8	1(H).2.3(BH_3).4(BH_3).tetrazole	-1.7
imidazole.BH_3(N-H,BH_3)	-9.6	1(H.BH_3).2(BH_3).3.4.tetrazole	-15.2
imidazole.2BH_3	-12.4	1(H.BH_3).2.3(BH_3).4.tetrazole	-21.9
1(H).2.3.triazole	12.2/*13.9*	1(H.BH_3).2.3.4(BH_3).tetrazole	-21.1
1(H).2.3(BH_3).triazole	6.6	1(H).2(BH_3).3(BH_3).4(BH_3).tetrazole	-9.0
1(H).2(BH_3).3.triazole	1.6	1(H.BH_3).2(BH_3).3(BH_3).4.tetrazole	-17.0
1(H, BH_3).2.3.triazole	-14.6	1(H.BH_3).2(BH_3).3.4(BH_3).tetrazole	-18.6
1(H).2(BH_3).3(BH_3).triazole	-1.9	1(H.BH_3).2.3(BH_3).4(BH_3).tetrazole	-24.0
1(H.BH_3).2(BH_3).3.triazole	-12.9	1(H).2.3.4.tetrazole.4BH_3	-13.9
1(H.BH_3).2.3(BH_3).triazole	-19.9	1.2(H).3.4.tetrazole	4.8/*8.2*
1(H).2.3.triazole.3BH_3	-14.3	1(BH_3).2(H).3.4.tetrazole	-4.7
1.2(H).3.triazole	10.2	1.2(H).3(BH_3).4.tetrazole	-4.8
1(BH_3).2(H).3.triazole	1.5	1.2(H).3.4(BH_3).tetrazole	-0.8
1.2(H, BH_3).3.triazole	-13.4	1.2(H.BH_3).3.4.tetrazole	-10.8
1(BH_3).2(H).3(BH_3).triazole	-6.1	1(BH_3).2(H).3(BH_3).4.tetrazole	-13.7
1(BH_3).2(H.BH_3).3.triazole	-3.9	1(BH_3).2(H).3.4(BH_3).tetrazole	-9.9
1.2(H).3.triazole.3BH_3	-15.6	1.2(H).3(BH_3).4(BH_3).tetrazole	-9.0
1.2.4(H).triazole	15.1	1(BH_3).2(H.BH_3).3.4.tetrazole	-11.1
1(BH_3).2.4(H).triazole	10.0	1.2(H.BH_3).3(BH_3).4.tetrazole	-9.9
1.2.4(H, BH_3).triazole	-11.7	1.2(H.BH_3).3.4(BH_3).tetrazole	-25.2
1(BH_3).2(BH_3).4(H).triazole	5.7	1(BH_3).2(H).3(BH_3).4(BH_3).tetrazole	-18.4
1(BH_3).2.4(H.BH_3).triazole	-17.1	1(BH_3).2(H.BH_3).3(BH_3).4.tetrazole	-20.0
1.2.4(H).triazole.3BH_3	-20.6	1(BH_3).2(H.BH_3).3.4(BH_3).tetrazole	-20.0
1(H).2.4.triazole	14.1/*14.8*	1.2(H.BH_3).3(BH_3).4(BH_3).tetrazole	-16.9
1(H).2(BH_3).4.triazole	4.5	1.2(H).3.4.tetrazole.4BH_3	-19.6
1(H).2.4(BH_3).triazole	8.2		
1(H,BH_3).2.4.triazole	2.1		
1(H).2(BH_3).4(BH_3).triazole	-1.0		
1(H.BH_3).2(BH_3).4.triazole	-10.5		
1(H.BH_3).2.4(BH_3).triazole	-19.5		
1(H).2.4.triazole.3BH_3	-14.4		

Regeneration of Ammonia Borane

Heats of Formation and Bond Energies of the $H_{(3-n)}BX_n$ compounds for (X = F, Cl, Br, I, NH_2, OH, and SH)

We calculated the heats of formation of HX, HBX, BHX_2, and BX_3 (X = F, Cl, Br, I, NH_2, OH, and SH) at the CCSD(T)/CBS level including additional corrections. We have completed our extensive set of predictions on the bond dissociation energies of substituted boranes. Atomization energies at 0 K and heats of formation at 0 K and 298 K are predicted for the borane compounds $H_{(3-n)}BX_n$ for (X = F, Cl, Br, I, NH_2, OH, and SH) and various radicals from coupled cluster theory (CCSD(T)) calculations with an effective core potential correlation-consistent basis set for I. In order to achieve near chemical accuracy (±1.5 kcal/mol), three corrections were added to the complete basis set binding energies based on frozen core coupled cluster theory

energies: a correction for core-valence effects, a correction for scalar relativistic effects, and a correction for first order atomic spin-orbit effects. Vibrational zero point energies were computed at the MP2 level of theory.

Table 44. Heats of Formation (kcal/mol) at 298 K.[a]

Molecule	**$\Delta H_f(298\ K)_{theory}$**	**$\Delta H_f(298\ K)_{expt}$**
HF ($^1\Sigma$)	-64.8	-65.32 ± 0.17
HCl ($^1\Sigma$)	-22.1	-22.06 ± 0.024
HBr ($^1\Sigma$)	-8.5	-8.674 ± 0.038
HI ($^1\Sigma$)	6.8	6.334 ± 0.024
BH ($^1\Sigma$)[d]	105.9	105.8 ± 2.0
BF ($^1\Sigma$)	-25.6	-27.7 ± 3.3, -25.3, (-26.5)
BCl ($^1\Sigma$)	43.4	33.8 ± 4.0, (36.9), (43.5)
BBr ($^1\Sigma$)	61.1	55.9 ± 10.0, (59.7), (71.0)
BI ($^1\Sigma$)	82.5	72.9 ± 10.0
$B(NH_2)$	51.7	
B(OH)	-11.1	
B(SH)	74.2	
HBF	-20.6	
HBCl	34.4	
HBBr	51.2	
HBI	67.7	
$HB(NH_2)$	34.7	
HB(OH)	-13.6	
HB(SH)	49.7	
H_2B[d]	77.5	48.0 ± 15.1
H_2BF	-73.3	
H_2BCl	-18.5	
H_2BBr	-2.6	
H_2BI	16.3	
$H_2B(NH_2)$	-19.7	
$H_2B(OH)$	-65.6	
$H_2B(SH)$	-2.4	
HBF_2	-175.5	-175.4 ± 0.8
$HBCl_2$	-59.6	-59.3 ± 1.0
$HBBr_2$	-27.2	-25.0 ± 1.2
HBI_2	10.6	
$HB(NH_2)_2$	-49.9	
$HB(OH)_2$	-154.6	
$HB(SH)_2$	-22.5	
BF_2	-118.7	-141.0 ± 3.1, -120.0 ± 4, ≤ -124 ± 9
BCl_2	-6.9	-19.0 ± 3.0

BBr_2	24.2	15.0 ± 3.6
BI_2	59.9	58.1 ± 15.1
$B(NH_2)_2$	5.5	
$B(OH)_2$	-99.3	-114.00 ± 3.6
$B(SH)_2$	29.5	
BH_3	24.4	25.5 ± 2.4
BF_3	-271.4	-271.4 ± 0.4
BCl_3	-96.7	-96.3 ± 0.5
BBr_3	-48.3	-48.8 ± 0.05
BI_3	7.6	17.0 ± 12.0
$B(NH_2)_3$	-74.9	
$B(OH)_3$	-239.8	-237.2 ± 0.6
$B(SH)_3$	-38.4	

The calculated heats of formation are in excellent agreement with the available experimental data for the closed shell molecules, but show a larger discrepancy with the reported experimental values for the BX_2 radicals. The heats of formation of the BX_2 radicals were also calculated at the G3(MP2) level of theory for further verification and the values were in excellent agreement with our more accurate CCSD(T) values, but not with the experimental values. On the basis of extensive comparisons with experiment for a wide range of compounds, our calculated values for these radicals should be good to ±1.5 kcal/mol and thus are to be preferred over the experimental values.

Table 45. B-X and B-H Bond Dissociation Energies (BDE) in kcal/mol at 0 K.

Bond	**BDE calc.**	**BDE expt.**
$BF_3 \rightarrow BF_2 + F$	170.3	150.0, 149.4, 169
$BCl_3 \rightarrow BCl_2 + Cl$	117.9	106.3, 110.0
$BBr_3 \rightarrow BBr_2 + Br$	98.3	89.7
$BI_3 \rightarrow BI_2 + I$	77.3	66.5
$B(NH_2)_3 \rightarrow B(NH_2)_2 + NH_2$	123.8	
$B(OH)_3 \rightarrow B(OH)_2 + OH$	147.8	132.1 ± 7
$B(SH)_3 \rightarrow B(SH)_2 + SH$	99.4	
$HBF_2 \rightarrow HBF + F$	172.5	
$HBCl_2 \rightarrow HBCl + Cl$	121.9	
$HBBr_2 \rightarrow HBBr + Br$	102.1	
$HBI_2 \rightarrow HBI + I$	81.7	
$HB(NH_2)_2 \rightarrow HB(NH_2) + NH_2$	127.6	
$HB(OH)_2 \rightarrow HB(OH) + OH$	148.2	
$HB(SH)_2 \rightarrow HB(SH) + SH$	103.5	
$BF_2 \rightarrow BF + F$	111.0	136, 132.3, 110
$BCl_2 \rightarrow BCl + Cl$	78.4	81.8, 93
$BBr_2 \rightarrow BBr + Br$	62.7	67.7
$BI_2 \rightarrow BI + I$	47.5	40.5

$B(NH_2)_2 \rightarrow B(NH_2) + NH_2$	89.2	
$B(OH)_2 \rightarrow B(OH) + OH$	95.4	121.3 ± 7
$B(SH)_2 \rightarrow B(SH) + SH$	76.1	
$H_2BF \rightarrow BH_2 + F$	168.2	144.4 ± 6
$H_2BCl \rightarrow BH_2 + Cl$	123.6	
$H_2BBr \rightarrow BH_2 + Br$	105.2	
$H_2BI \rightarrow BH_2 + I$	85.4	
$H_2B(NH_2) \rightarrow BH_2 + NH_2$	139.7	
$H_2B(OH) \rightarrow BH_2 + OH$	150.0	
$H_2B(SH) \rightarrow BH_2 + SH$	110.7	
$HBF \rightarrow BH + F$	144.2	145.5 ± 6
$HBCl \rightarrow BH + Cl$	99.3	
$HBBr \rightarrow BH + Br$	81.9	
$HBI \rightarrow BH + I$	62.6	
$HB(NH_2) \rightarrow BH + NH_2$	113.9	
$HB(OH) \rightarrow BH + OH$	126.7	
$HB(SH) \rightarrow BH + SH$	87.3	
$BF \rightarrow B + F$	179.9	181.0, 181.0 ± 0.2
$BCl \rightarrow B + Cl$	121.0	122.2 ± 1.1, 129
$BBr \rightarrow B + Br$	100.9	94.6, 104.6, 93.4 ± 0.1
$BI \rightarrow B + I$	78.5	86.4
$B(NH_2) \rightarrow B + NH_2$	128.0	
$B(OH) \rightarrow B + OH$	155.2	144.3 ± 7
$B(SH) \rightarrow B + SH$	93.7	
$BH \rightarrow B + H$	81.6	83.9, 81.3, 82.5 ± 0.6
$HF \rightarrow F + H$	135.6	135.2 ± 0.2
$HCl \rightarrow Cl + H$	102.3	102.23 ± 0.05
$HBr \rightarrow Br + H$	86.3	86.64 ± 0.04[e]
$HI \rightarrow I + H$	69.9	70.42 ± 0.05[e]
$BH_3 \rightarrow BH_2 + H$	103.7	82.6, 74.6
$NH_3 \rightarrow NH_2 + H$	106.5	
$H_2O \rightarrow OH + H$	117.6	
$H_2S \rightarrow SH + H$	88.5	
$HBF_2 \rightarrow BF_2 + H$	107.4	86.5
$HBCl_2 \rightarrow BCl_2 + H$	103.4	
$HBBr_2 \rightarrow BBr_2 + H$	102.1	
$HBI_2 \rightarrow BI_2 + H$	100.0	
$HB(NH_2)_2 \rightarrow B(NH_2)_2 + H$	105.9	
$HB(OH)_2 \rightarrow B(OH)_2 + H$	105.9	
$HB(SH)_2 \rightarrow B(SH)_2 + H$	102.6	
$H_2BF \rightarrow HBF + H$	103.3	
$H_2BCl \rightarrow HBCl + H$	103.6	
$H_2BBr \rightarrow HBBr + H$	102.7	

$H_2BI \rightarrow HBI + H$	102.1	
$H_2B(NH_2) \rightarrow HB(NH_2) + H$	105.1	
$H_2B(OH) \rightarrow HB(OH) + H$	102.7	
$H_2B(SH) \rightarrow HB(SH) + H$	102.8	
$BH_2 \rightarrow BH + H$	79.3	89.9, 109.9
$HBF \rightarrow BF + H$	45.9	
$HBCl \rightarrow BCl + H$	59.9	
$HBBr \rightarrow BBr + H$	62.6	
$HBI \rightarrow BI + H$	65.8	
$HB(NH_2) \rightarrow BNH_2 + H$	67.5	
$HB(OH) \rightarrow BOH + H$	53.1	
$HB(SH) \rightarrow BSH + H$	75.2	

The accurately calculated heats of formation allow us to predict the B-X and B-H adiabatic bond dissociation energies (BDEs) to within ±1.5 kcal/mol. The B-F BDE in the $H_{3-n}BF_n$ compounds as well as the diatomic BF ($^1\Sigma^+$) is the highest BDE predicted when comparing to the other substituents investigated. The second and third highest B-X BDEs in the $H_{3-n}BX_n$ and BX compounds are predicted for the OH and NH_2 substituents respectively. The substituents have a minimal effect on the B-H BDE in HBX_2 and H_2BX compared to the first B-H BDE of borane. The differences in adiabatic and diabatic BDEs, which are related to the reorganization energy in the product, can be estimated from singlet-triplet splittings in these molecules, and can account for the large fluctuations in adiabatic BDEs observed, specifically for the BX_2 and HBX radicals, during the stepwise loss of the respective substituents.

On the basis of the BDEs, it is unlikely that B-X to B-H conversion will occur for any of the substituted HBX_2, H_2BX and HBX molecules studied. However, the iodine derivatives of the compounds studied were the most favorable for B-X to B-H conversion in that the B-H BDEs in HBI_2, H_2BI and BHI were more stable than the corresponding B-I BDEs respectively, and that the B-I BDE in BI_3 was the least endothermic of the substituents studied.

We can calculate the heats of reaction for the disproportionation step in proposed reprocessing schemes for the regeneration of ammonia borane. The results are in Table 46. The generic disproportionation reaction mechanism is:

$$2HBX_2 \rightarrow H_2BX + BX_3 \quad (89)$$

$$H_2BX + HBX_2 \rightarrow BH_3 + BX_3 \quad (90)$$

$$2H_2BX \rightarrow BH_3 + HBX_2 \quad (91)$$

The sequence of disproportionation reactions involving the halide and hydroxyl derivatives are all relatively close to thermoneutral. The reaction involving the F substituent was the only exothermic reaction with a value of 4.7 kcal/mol at 0 K.

Table 46. Disproportionation Reactions in kcal/mol at 0 K and 298 K.

Disproportionation Reactions	$\Delta H_{rxn}(0\ K)_{theory}$	$\Delta H_{rxn}(298\ K)_{theory}$
$2HBF_2 \rightarrow H_2BF + BF_3$	6.2	6.3
$H_2BF + HBF_2 \rightarrow BH_3 + BF_3$	1.5	2.7
$2H_2BF \rightarrow BH_3 + HBF_2$	-4.7	-3.6

$2HBCl_2 \rightarrow H_2BCl + BCl_3$	3.7	4.0
$H_2BCl + HBCl_2 \rightarrow BH_3 + BCl_3$	5.4	6.7
$2H_2BCl \rightarrow BH_3 + HBCl_2$	1.6	2.8
$2HBBr_2 \rightarrow H_2BBr + BBr_3$	3.3	3.6
$H_2BBr + HBBr_2 \rightarrow BH_3 + BBr_3$	5.3	6.8
$2H_2BBr \rightarrow BH_3 + HBBr_2$	2.0	3.3
$2HBI_2 \rightarrow H_2BI + BI_3$	2.3	2.7
$H_2BI + HBI_2 \rightarrow BH_3 + BI_3$	4.3	6.0
$2H_2BI \rightarrow BH_3 + HBI_2$	2.0	3.3
$2HB(NH_2)_2 \rightarrow H_2B(NH_2) + B(NH_2)_3$	4.6	5.1
$H_2B(NH_2) + HB(NH_2)_2 \rightarrow BH_3 + B(NH_2)_3$	18.0	19.0
$2H_2B(NH_2) \rightarrow BH_3 + HB(NH_2)_2$	13.4	13.9
$2HB(OH)_2 \rightarrow H_2B(OH) + B(OH)_3$	3.6	3.8
$H_2B(OH) + HB(OH)_2 \rightarrow BH_3 + B(OH)_3$	4.3	5.6
$2H_2B(OH) \rightarrow BH_3 + HB(OH)_2$	0.7	1.9
$2HB(SH)_2 \rightarrow H_2B(SH) + B(SH)_3$	3.9	4.2
$H_2B(SH) + HB(SH)_2 \rightarrow BH_3 + B(SH)_3$	10.2	11.9
$2H_2B(SH) \rightarrow BH_3 + HB(SH)_2$	6.3	7.7

We can predict the thermodynamics for the digestion reaction of borazine with the halide acids at 298 K in kcal/mol given the recalculated heat of formation of borazine of -118.8 kcal/mol at 298 K in the gas phase. The reactions with NH_3, H_2O, and SH_2 are also given for comparison.

$c\text{-}(BHNH)_3 + 6HF \rightarrow 3NH_3 + 3HBF_2$	$\Delta H = -56.3$	(92)
$c\text{-}(BHNH)_3 + 6HCl \rightarrow 3NH_3 + 3HBCl_2$	$\Delta H = 35.6$	(93)
$c\text{-}(BHNH)_3 + 6HBr \rightarrow 3NH_3 + 3HBBr_2$	$\Delta H = 51.2$	(94)
$c\text{-}(BHNH)_3 + 6HI \rightarrow 3NH_3 + 3HBI_2$	$\Delta H = 71.7$	(95)
$c\text{-}(BHNH)_3 + 6NH_3 \rightarrow 3NH_3 + 3HB(NH_2)_2$	$\Delta H = -0.2$	(96)
$c\text{-}(BHNH)_3 + 6H_2O \rightarrow 3NH_3 + 3HB(OH)_2$	$\Delta H = -35.4$	(97)
$c\text{-}(BHNH)_3 + 6SH_2 \rightarrow 3NH_3 + 3HB(SH)_2$	$\Delta H = 43.5$	(98)

We predict the reaction of borazine with hydrofluoric acid to be considerably more exothermic as compared to the other halide acids. In order to better understand the digestion chemistry and the energetics for the borazine reactions, we examined the various bond energies for the respective halide acid reactants and the HBX_2 products.

Table 47. H-X and B-X Bond Dissociation Energies in kcal/mol

Reactant	**ΔH_f (0 K)**	**Product**	**ΔH_f (0 K)**
$HF \rightarrow H + F$	135.4	$HBF_2 \rightarrow HBF + F$	172.4
		$HBF \rightarrow BH + F$	144.2
$HCl \rightarrow H + Cl$	103.4	$HBCl_2 \rightarrow HBCl + Cl$	123.0
		$HBCl \rightarrow BH + Cl$	100.4
$HBr \rightarrow H + Br$	86.0	$HBBr_2 \rightarrow HBBr + Br$	100.9
		$HBBr \rightarrow BH + Br$	80.7
$HI \rightarrow H + I$	69.9	$HBI_2 \rightarrow HBI + I$	78.7
		$HBI \rightarrow BH + I$	62.7

The breaking of an HF bond compared to an HCl bond is more endothermic by 33 kcal/mol; however, much of this energy difference in the HF/BF_3 system is gained back on forming HBF_2. More notably, there is a difference of 96 kcal/mol in the cumulative reaction sequence BH + X → HBX + X → HBX_2 between X = F and X = Cl. Similarly, breaking an HBr bond is about 49 kcal/mol less endothermic than breaking an HF bond; however, the cumulative reaction to form $HBBr_2$ (BH + Br → HBBr + Br → $HBBr_2$) is only exothermic by 184 kcal/mol compared to 317 kcal/mol for the analagous fluorine reaction. Although breaking an HI bond is considerably less endothermic than breaking an HF bond by 66 kcal/mol, only a marginal value of 144 kcal/mol is regained in forming HBI_2, considering a similar cumulative reaction and this value is less than half the equivalent reaction for the fluoride derivatives.

Hydride, Fluoride and X^- Affinities of the $H_{(3-n)}BX_n$ compounds for (X = F, Cl, Br, I, NH_2, OH, and SH) from Coupled Cluster Theory.

Atomization energies at 0 K and enthalpies of formation at 0 K and 298 K are predicted for the $BH_{4-n}X_n^-$ and the $BH_{3-n}X_nF^-$ compounds for (X = F, Cl, Br, I, NH_2, OH, and SH) from coupled cluster theory (CCSD(T)) calculations with correlation-consistent basis sets and with an effective core potential on I. In order to achieve near chemical accuracy (±1.0 kcal/mol), additional corrections were added to the complete basis set binding energies. The hydride, fluoride, and X^- affinities of the $BH_{3-n}X_n$ compounds were predicted. Although the hydride and fluoride affinities differ somewhat in their magnitudes, they show very similar trends and are both suitable for judging the Lewis acidities of compounds. The only significant differences in their acidity strength orders are found for the boranes substituted with the strongly electron withdrawing and back donating fluorine and hydroxyl ligands. The highest H^- and F^- affinities are found for BI_3 and the lowest ones for $B(NH_2)_3$. Within the boron trihalide series, the Lewis acidity increases monotonically with increasing atomic weight of the halogen, i.e., BI_3 is a considerably stronger Lewis acid than BF_3. For the X^- affinities in the BX_3, HBX_2 and H_2BX series, the fluorides show the highest values, whereas the amino and mercapto compounds show the lowest ones. Hydride and fluoride affinities of the $BH_{3-n}X_n$ compounds exhibit linear correlations with the proton affinity of X^- for most X ligands. Reasons for the correlation are discussed. A detailed analysis of the individual contributions to the Lewis acidities of these substituted boranes shows that the dominant effect in the magnitude of the acidity is the strength of the BX_3^--F bond. The main contributor to the relative differences in the Lewis acidities of BX_3 for X a halogen is the electron affinity of BX_3 with a secondary contribution from the distortion energy from planar to pyramidal BX_3. The B-F bond dissociation energy of $X_3B\text{-}F^-$ and the distortion energy from pyramidal to tetrahedral BX_3^- are of less importance in determining the relative acidities. Because the electron affinity of BX_3 is strongly influenced by the charge density in the empty p_z LUMO of boron, the amount of π-back donation from the halogen to boron is crucial and explains why the Lewis acidity of BF_3 is significantly lower than those of BX_3 with X = Cl, Br and I.

Table 48. Heats of Formation (kcal/mol) at 0 K and 298 K for the $H_{3-n}BX_nF^-$ compounds.

Molecule	**ΔH_f(0 K)$_{theory}$**	**ΔH_f(298 K)$_{theory}$**
$H_2BF_2^-$	-216.4	-218.1
H_2BClF^-	-155.9	-157.5

H_2BBrF^-	-142.1	-143.9
H_2BIF^-	-130.4	-132.1
$H_2B(NH_2)F^-$	-114.5	-117.8
$H_2B(OH)F^-$	-174.9	-177.3
$H_2B(SH)F^-$	-125.8	-127.9
HBF_3^-	-304.6	-306.0
$HBCl_2F^-$	-208.0	-209.2
$HBBr_2F^-$	-175.9	-176.8
HBI_2F^-	-146.1	-147.7
$HB(NH_2)_2F^-$	-132.9	-137.3
$HB(OH)_2F^-$	-257.6	-260.3
$HB(SH)_2F^-$	-147.8	-149.9
BF_4^-	-410.7	-411.9
BCl_3F^-	-253.9	-254.4
BBr_3F^-	-202.2	-203.5
BI_3F^-	-155.6	-156.5
$B(NH_2)_3F^-$	-155.7	-161.4
$B(OH)_3F^-$	-339.7	-342.6
$B(SH)_3F^-$	-167.9	-170.1

Given the calculated heats of formation of the $H_{3-n}BX_nF^-$ compounds, their neutral derivatives, and the experimental heat of formation for the fluoride anion, we can predict the fluoride anion (FA), hydride anion (HA), and X^- anion affinities of the neutral molecules, which is defined as -ΔH of the FA reaction $H_{3-n}BX_n + F^- \rightarrow H_{3-n}BX_nF^-$.

Table 49. Calculated Hydride (HA) and Fluoride (FA) Affinities in kcal/mol at 0 K and 298 K for the $H_{(3-n)}BX_n$ compounds.

Molecule	**HA**		**FA**	
	(0 K)	**(298 K)**	**(0 K)**	**(298 K)**
H_3B	72.2	72.2	65.2	66.6
H_2BF	61.8	61.7	66.7	67.9
H_2BCl	79.5	79.4	78.3	79.5
H_2BBr	86.0	85.8	83.8	84.9
H_2BI	93.0	92.8	88.9	90.0
H_2BNH_2	36.6	36.3	38.6	39.7
H_2BOH	47.2	46.9	52.3	53.4
H_2BSH	68.8	68.3	66.2	67.1
HBF_2	58.6	58.4	71.0	72.2
$HBCl_2$	86.9	86.6	88.0	88.9
$HBBr_2$	96.0	95.8	95.0	95.8
HBI_2	104.8	104.5	99.0	99.9
$HB(NH_2)_2$	22.6	22.5	28.1	29.0
$HB(OH)_2$	35.6	35.1	46.6	47.3
$HB(SH)_2$	71.7	71.2	68.5	69.0
BF_3	69.2	69.0	81.1	82.1
BCl_3	94.6	94.3	95.2	96.0

BBr_3	103.6	103.4	101.7	102.5
BI_3	111.4	111.1	105.3	106.0
$B(NH_2)_3$	18.0	18.3	26.7	28.1
$B(OH)_3$	31.3	30.3	44.1	44.4
$B(SH)_3$	74.2	73.7	72.7	73.3

Table 50. Calculated X^- Affinities (XA; X = Cl, Br, I, NH_2, OH, and SH) in kcal/mol at 0 K and 298 K for the $H_{(3-n)}BX_n$ compounds.

Molecule	**XA**	**(0 K)**	**(298 K)**
H_3B	Cl	33.4	33.2
H_3B	Br	27.5	27.2
H_3B	I	21.5	21.2
H_3B	NH_2	72.0	73.9
H_3B	OH	69.2	69.3
H_3B	SH	39.7	41.2
H_2BF	Cl	28.8	28.3
H_2BF	Br	21.9	21.4
H_2BF	I	14.1	13.4
H_2BF	NH_2	70.7	72.4
H_2BF	OH	70.9	70.9
H_2BF	SH	33.8	35.0
H_2BCl	Cl	40.2	39.7
H_2BBr	Br	35.5	34.8
H_2BI	I	31.3	30.5
H_2BNH_2	NH_2	15.8	16.0
H_2BOH	OH	56.8	56.6
H_2BSH	SH	17.7	18.3
$HBCl_2$	Cl	44.2	43.4
$HBBr_2$	Br	39.3	38.3
HBI_2	I	35.9	34.7
$HB(NH_2)_2$	NH_2	35.4	36.9
$HB(OH)_2$	OH	48.9	48.0
$HB(SH)_2$	SH	36.1	36.6
BCl_3	Cl	47.5	46.5
BBr_3	Br	42.3	41.1
BI_3	I	36.9	36.2
$B(NH_2)_3$	NH_2	31.4	33.3
$B(OH)_3$	OH	48.5	47.7
$B(SH)_3$	SH	38.3	38.8

For the BX_3 series, the highest hydride and fluoride affinities are predicted for BI_3 at 112.6 and 105.9 kcal/mol, respectively, and the lowest ones for $B(NH_2)_3$ at 19.8 and 28.1 kcal/mol, respectively, at 298 K. The highest X^- affinity within the BX_3 series to form BX_4^- is found for BF_3 at 82.1 kcal/mol and the lowest one for $B(NH_2)_3$ at 33.3 kcal/mol, at 298 K. For the HBX_2 compounds, HBI_2 has the highest hydride and fluoride affinities at 106.0 and 99.9 kcal/mol, respectively, and $HB(NH_2)_2$ has the lowest ones at 24.0 and 29.0 kcal/mol, respectively, at 298

K. The highest X^- affinity is predicted for HBF_2 at 72.1 kcal/mol at 298 K, while HBI_2 is predicted to have the lowest one at 34.4 kcal/mol at 298 K. Similar trends were observed for the H_2BX compounds with the highest H^- and F^- affinities predicted for H_2BI at 94.3 and 89.9 kcal/mol, respectively, and the lowest ones for H_2BNH_2 at 37.8 and 39.7 kcal/mol, respectively, at 298 K, while H_2BF and H_2BNH_2 are predicted to have the highest and lowest X^- affinities at 67.9 and 16.0 kcal/mol, respectively, at 298 K.

We provided a thermodynamic scheme for the AAs with three steps, the ionization of A^- to a A radical and an electron (step 1), the capture of the electron by the Lewis acid (LA) including the reorganization energy resulting from the structural change from LA to LA^- (step 2), and the subsequent formation of the $[LA\text{-}H]^-$ bond (step 3).

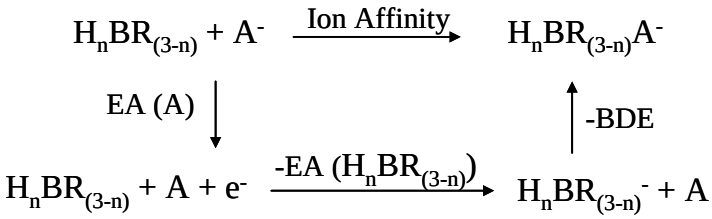

Figure 55. (a) Three step thermodynamic cycle for the A^- ion affinities of $BH_{3-n}X_n$: (1) the first ionization potential of A^-, (2) the electron affinity of $BH_{3-n}X_n$, and (3) the homolytic BDE of the B-A bond in the corresponding $BH_{3-n}X_nA^-$ anion.

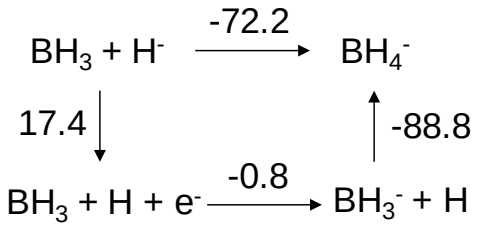

Figure 56. (b) Representative three step thermodynamic cycle for the hydride affinity of BH_3: (1) the electron affinity of the H radical, (2) the electron affinity of BH_3, and (3) the homolytic BDE of the B-H bond in BH_4^-. Energies in kcal/mol.

Table 51. Calculated Electron Affinities at 0 K at the CCSD(T)/CBS and B3LYP/aVTZ levels.

Molecule	CCSD(T) kcal/mol	CCSD(T) eV	B3LYP kcal/mol	B3LYP eV	Expt. eV
BH_3	0.8	0.031	4.5	0.17	0.038 ± 0.015
H_2BF	-11.0	-0.42	-15.9	-0.61	
H_2BCl	1.4	0.05	4.7	0.18	
H_2BBr	6.6	0.26	8.6	0.33	
H_2BI	13.2	0.51	14.7	0.56	
HBF_2	-19.1	-0.73	-13.4	-0.51	
$HBCl_2$	5.8	0.22	9.0	0.35	
$HBBr_2$	14.8	0.57	15.7	0.60	

HBI_2	24.0	0.92	25.0	0.96	
BF_3	-14.7	-0.56	-8.9	-0.34	
BCl_3	12.7	0.49	14.4	0.55	0.33 ± 0.20^b
BBr_3	22.5	0.86	23.2	0.89	0.82 ± 0.20^b
BI_3	32.5	1.25	33.0	1.27	
H_2BNH_2			-8.6	-0.33	
H_2BOH			-8.8	-0.34	
H_2BSH			-4.6	-0.17	
$HB(NH_2)_2$			-7.9	-0.30	
$HB(OH)_2$			-6.2	-0.24	
$HB(SH)_2$			-4.6	-0.18	
$B(NH_2)_3$			-6.1	-0.24	
$B(OH)_3$			-5.3	-0.20	
$B(SH)_3$			1.8	0.07	

For the thermodynamic cycle depicted, we predicted the electron affinities of all of the compounds in our study the B3LYP/aVTZ level, and, for some, at the CCSD(T)/CBS level. We employ the usual convention that a positive EA signifies that a molecule will bind an extra electron and a negative EA that it will not. The DFT values are in good agreement with the CCSD(T)/CBS values for the larger positive EAs and differ somewhat more for negative EAs or weakly positive EAs. Substitution of one to three H atoms by F atoms to form H_2BF, HBF_2 and BF_3 yields negative EAs, so these boranes will not bind a free electron and the appropriate value for use in step 2 is thus 0. The EAs of the BX_3 compounds for X = Cl, Br, and I are all positive so they will bind an electron. The calculated EAs for BCl_3 and BBr_3 are in good agreement with the experimental values

Table 52. Calculated $BH_{3-n}X_n$-A^- Bond Dissociation Energies in kcal/mol at 0 K.[a]

Molecule	**A**	**(0 K)**
H_3B	H	88.8
H_2BF	H	79.2 (90.2)
H_2BCl	H	92.3
H_2BBr	H	96.7
H_2BI	H	97.2
H_2BNH_2	H	53.9
H_2BOH	H	64.6
H_2BSH	H	86.2
HBF_2	H	76.0 (95.1)
$HBCl_2$	H	98.5
$HBBr_2$	H	98.6
HBI_2	H	98.1
$HB(NH_2)_2$	H	40.0
$HB(OH)_2$	H	53.0
$HB(SH)_2$	H	89.1
BF_3	H	86.6 (101.2)
BCl_3	H	99.3
BBr_3	H	98.6

BI_3	H	96.3
$B(NH_2)_3$	H	35.4
$B(OH)_3$	H	48.7
$B(SH)_3$	H	91.6
H_3B	F	142.8
H_2BF	F	145.1 (156.1)
H_2BCl	F	155.4
H_2BBr	F	155.6
H_2BI	F	154.2
H_2BNH_2	F	117.0
H_2BOH	F	130.8
H_2BSH	F	144.6
HBF_2	F	149.5 (168.5)
$HBCl_2$	F	160.6
$HBBr_2$	F	158.6
HBI_2	F	153.4
$HB(NH_2)_2$	F	106.6
$HB(OH)_2$	F	125.1
$HB(SH)_2$	F	146.9
BF_3	F	159.5 (174.2)
BCl_3	F	160.9
BBr_3	F	157.7
BI_3	F	151.3
$B(NH_2)_3$	F	105.1
$B(OH)_3$	F	122.5
$B(SH)_3$	F	151.2
H_3B	Cl	115.9
H_2BF	Cl	112.1 (123.1)
H_2BCl	Cl	121.0
$HBCl_2$	Cl	120.6
BCl_3	Cl	117.0
H_3B	Br	104.2
H_2BF	Br	99.5 (110.5)
H_2BBr	Br	106.4
$HBBr_2$	Br	102.1
BBr_3	Br	97.4
H_3B	I	91.3
H_2BF	I	84.6 (95.7)
H_2BI	I	88.6
HBI_2	I	82.1
BI_3	I	74.9
H_3B	NH_2	89.0
H_2BF	NH_2	88.5 (99.5)
H_2BNH_2	NH_2	33.6
$HB(NH_2)_2$	NH_2	53.1
$B(NH_2)_3$	NH_2	49.1
H_3B	OH	110.5

H_2BF	OH	113.0 (124.1)
H_2BOH	OH	99.0
$HB(OH)_2$	OH	91.1
$B(OH)_3$	OH	90.7
H_3B	SH	92.4
H_2BF	SH	87.2 (98.2)
H_2BSH	SH	70.1
$HB(SH)_2$	SH	88.4
$B(SH)_3$	SH	90.7

[a] Values in parenthesis include calculated negative EA values of the fluoroboranes.

The thermodynamic cycle shows that we can calculate the BDE for the B-A bond in $BH_{3-n}X_n$-A^- by use of the other quantities in the cycle, which we already have. These BDEs are given in Table 52 where we set the EA = 0 if the corresponding Lewis acid repels an electron, i.e., the EA is negative. The dominant component of determining the absolute magnitude of the hydride, fluoride or X- affinities of the boranes is the $BH_{3-n}X_n$-A^- bond dissociation energy.

The H^- and F^- affinities of $BH_{3-n}X_n$, i.e., their Lewis acidities, correlate linearly with the proton affinities of the substituent X^-, i.e., their gas phase Brønsted acidities.

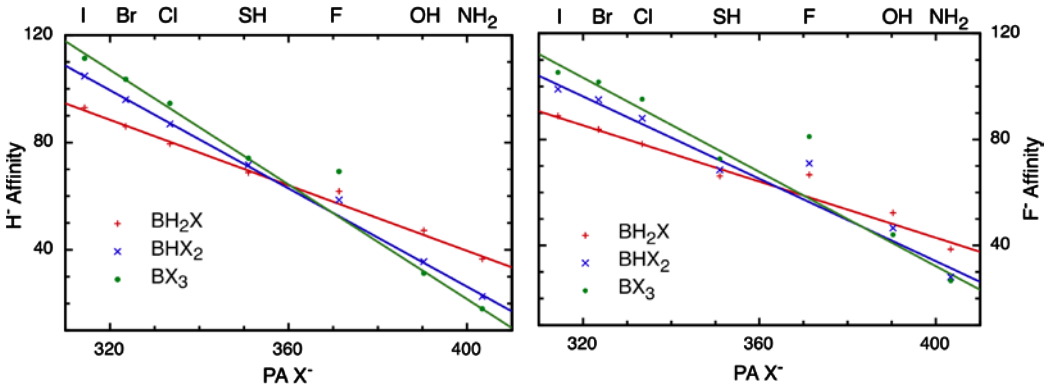

Figure 57. Hydride and fluoride affinities of the $BH_{3-n}X_n$ compounds in kcal/mol at 0 K show a linear correlation with the proton affinity of X^-. Values for X = F deviate from the trend line drawn through the points for I, Br, Cl, SH, OH, and NH_2.

A decreasing proton affinity of the corresponding base, X^-, corresponds to an increase in the Brønsted acidity of HX and in the Lewis acidities of $BH_{3-n}X_n$ although the absolute values go in opposite directions due to their different definitions. This correlation also accounts for the fact that BI_3 is the strongest Lewis acid in our series, in the same way as HI is the strongest gas phase Brønsted acid. The only deviations from this correlation are observed for X being H and F.

These deviations can be attributed to the anomalous values of the electron affinities of the F and H atoms relative to the homolytic bond dissociation energies of the B-F and B-H bonds, respectively, that determine the proton affinities of the corresponding X^- anions.

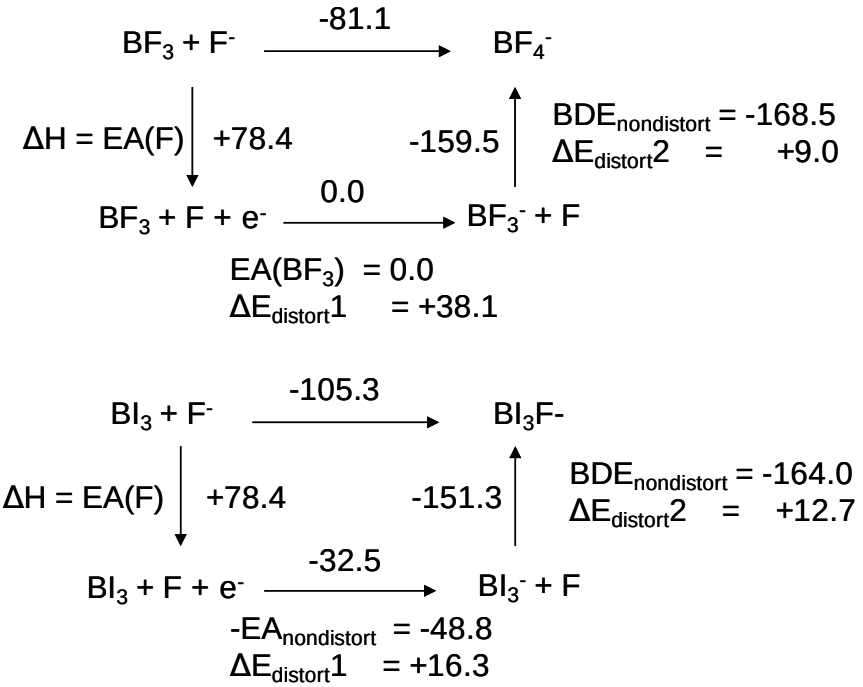

Figure 58. Born-Haber cycles for the FAs of BF_3 and BI_3. For each step, the total energies and the energies of each component are given in kcal/mol. The values for the overall reaction are the sums of steps 1-3 given by the values inside the square defined by the arrows. The values outside the square defined by the arrows are the conceptual values, which include the effect of the distortion energies calculated for BX_3 at the BX_3^- and BX_3F^- geometries. These values are provided as guidelines for understanding the roles of the various terms. The EA of BF_3 is negative so it is set to 0.

The fact that BI_3 is a stronger Lewis acid than BF_3 is primarily due to its higher electron affinity, which is influenced to some extent by the distortion energy from planar to pyramidal BX_3. The roles of the X_3B^-F bond dissociation energy and the concomitant distortion energy from pyramidal to tetrahedral BX_3^- in determining the relative acidities are considerably smaller. Since the electron affinity of BX_3 is strongly influenced by the charge density in the empty p_z LUMO of boron, the π-back donation from the halogen to boron plays a very important role.

The heat of formation for $B(OH)_3$ and $B(OH)_4^-$ were obtained by the CCSD(T)/CBS procedure, giving and solvation reduces the reaction energy from the gas phase value:

$BH_4^- + 4H_2O \leftrightarrow B(OH)_4^- + 4H_2$ $\quad \Delta H(gas) = -78.5$ kcal/mol
$\Delta G(gas) = -70.4$ kcal/mol
ΔG_{solv} (COSMO) = -43.5 kcal/mol

Given the calculated heats of formation, we predict the hydroxide affinity of $B(OH)_3$ is quite low at 47 kcal/mol.

Heats of Formation and Bond Dissociation Energies of the Halosilanes, Methylhalosilanes and Halomethylsilanes

Atomization energies at 0 K and heats of formation at 0 K and 298 K are predicted for SiH_3X, SiH_2XCH_3, and SiH_3CH_2X with X = F, Cl, Br, and I from coupled cluster theory (CCSD(T)) calculations with effective core potential correlation-consistent basis sets for Br and I. In order to achieve near chemical accuracy (±1 kcal/mol), three corrections were added to the complete basis set binding energies based on frozen core coupled cluster theory energies: a correction for core-valence effects, a correction for scalar relativistic effects, and a correction for first order atomic spin-orbit effects. Vibrational zero point energies were computed at the CCSD(T) level of theory and the C-H and Si-H stretches scaled to experiment. The C-H, Si-H, Si-C, C-X, and Si-X (X = F, Cl, Br, and I) bond dissociation energies (BDEs) in the halosilanes, halomethysilanes, and methylhalosilanes were predicted.

Table 53. Calculated Heats of Formation at 0 K and 298 K in kcal/mol.

Molecule	**Theory (0 K)**	**Theory (298 K)**
CH_3 (C_s)	35.8	35.0
CH_2F (C_s)	-6.3	-6.9
CH_2Cl (C_s)	28.1	27.4
CH_2Br (C_s)	43.3	40.8
CH_2I (C_s)	54.7	53.8
SiH_3 (C_{3v})	48.1	46.8
SiH_2F (C_s)	-42.4	-43.7
SiH_2Cl (C_s)	7.6	6.4
SiH_2Br (C_s)	23.3	20.4
SiH_2I (C_s)	37.9	36.3
SiH_3F (C_{3v})	-83.8	-88.8
SiH_3Cl (C_{3v})	-31.6	-33.8
SiH_3Br (C_{3v})	-15.3	-19.2
SiH_3I (C_{3v})	0.7	-1.8
SiH_3CH_3 (C_{3v})	-3.0	-6.9
SiH_3CH_2 (C_s)	45.1	42.5
SiH_2CH_3 (C_s)	36.9	34.0
SiH_2FCH_3 (C_s)	-99.8	-103.4
SiH_2ClCH_3 (C_s)	-46.9	-50.3
SiH_2BrCH_3 (C_s)	-30.4	-35.6
SiH_2ICH_3 (C_s)	-10.2	-14.0
SiH_3CH_2F (C_s)	-39.0	-42.6
SiH_3CH_2Cl (C_s)	-5.0	-8.5
SiH_3CH_2Br (C_s)	7.4	2.1
SiH_3CH_2I (C_s)	17.9	14.0

We can use our calculated heats of formation to predict a wide range of various BDEs in the halosilanes, methylhalosilanes, and halomethylsilanes, and for the BDEs under consideration, the adiabatic BDE is equal to the diabatic BDE.

Table 54. Calculated Bond Dissociation Energies (BDEs) at 0 K (kcal/mol).

BDE	Theory
$SiH_4 \rightarrow SiH_3 + H$	90.2
$SiH_3F \rightarrow SiH_2F + H$	93.1
$SiH_3Cl \rightarrow SiH_2Cl + H$	90.9
$SiH_3Br \rightarrow SiH_2Br + H$	90.3
$SiH_3I \rightarrow SiH_2I + H$	88.8
$SiH_3F \rightarrow SiH_3 + F$	150.5
$SiH_3Cl \rightarrow SiH_3 + Cl$	108.3
$SiH_3Br \rightarrow SiH_3 + Br$	91.6
$SiH_3I \rightarrow SiH_3 + I$	73.0
$CH_3SiH_3 \rightarrow CH_3SiH_2 + H$	91.5
$CH_3SiH_2F \rightarrow CH_3SiH_2 + F$	155.1
$CH_3SiH_2Cl \rightarrow CH_3SiH_2 + Cl$	112.3
$CH_3SiH_2Br \rightarrow CH_3SiH_2 + Br$	95.5
$CH_3SiH_2I \rightarrow CH_3SiH_2 + I$	72.7
$CH_3SiH_3 \rightarrow SiH_3 + CH_3$	86.9
$CH_3SiH_2F \rightarrow SiH_2F + CH_3$	93.0
$CH_3SiH_2Cl \rightarrow SiH_2Cl + CH_3$	90.2
$CH_3SiH_2Br \rightarrow SiH_2Br + CH_3$	89.5
$CH_3SiH_2I \rightarrow SiH_2I + CH_3$	83.7
$CH_3SiH_3 \rightarrow SiH_3CH_2 + H$	99.8
$SiH_3CH_2F \rightarrow SiH_3CH_2 + F$	102.6
$SiH_3CH_2Cl \rightarrow SiH_3CH_2 + Cl$	78.7
$SiH_3CH_2Br \rightarrow SiH_3CH_2 + Br$	65.9
$SiH_3CH_2I \rightarrow SiH_3CH_2 + I$	52.8
$SiH_3CH_2F \rightarrow CH_2F + SiH_3$	80.9
$SiH_3CH_2Cl \rightarrow CH_2Cl + SiH_3$	81.2
$SiH_3CH_2Br \rightarrow CH_2Br + SiH_3$	83.9
$SiH_3CH_2I \rightarrow CH_2I + SiH_3$	84.9

The Si-F BE of SiH_3F is the highest BDE of the halosilanes studied, and only in iodosilane is the Si-H BE more stable than the Si-X BE. The C-H BDE decreases by ~4 kcal/mol as compared to the C-H BDE in methane. Of the halomethylsilanes, the C-F BDE in SiH_3CH_2F is the most stable of the halide substituents at 102.6 kcal/mol. The C-I BDE in SiH_3CH_2I is the least stable of the C-X BDEs in the halomethysilanes ~50 kcal/mol less compared to the C-F BDE in SiH_3CH_2F. There is a direct relation between the decrease in electronegativity of the halide substituent and the decrease in the strength of the C-X BDE down the group.

We can study at the effect of halide substitution at the methyl group on the Si-C BDE. The Si-C BDE in methylsilane is calculated to be 86.9 kcal/mol, and all the SiH_3CH_2X molecules show a decrease in the Si-C BDE. The largest effect of halide substitution was seen for flouromethylsilane in which the Si-C BDE became less stable by ~6 kcal/mol. In general for the halomethylsilanes, the effect of the electronegativity of the halide subsituent was indirectly proportional to the strength of the S-C BDE in methylsilane.

Except for methyliodosilane, methyl substitution leads to an increase in Si-X BDE when compared to the Si-X BDE in the halosilanes. Except for methyliodosilane, halide substitution leads to an increase in the Si-C BDE in comparison to the Si-C BDE in methylsilane of 86.9 kcal/mol at 0 K. Unlike the methylhalosilanes, the halomethylsilanes all show a decrease in the Si-C BDE when compared to the Si-C BDE in methylsilane. The trends correlate with the electronegativity of the substituent.

Silane Compounds as Intermediates in Regeneration Schemes: Diammoniosilane: Computational Prediction of the Thermodynamic Properties of a Potential Chemical Hydrogen Storage System

We have continued the study of diammonia silane as a potential molecule for chemical hydrogen by predicting the thermodynamics for release of hydrogen. Atomization energies at 0 K and heats of formation at 0 K and 298 K were predicted for diammoniosilane, $SiH_4(NH_3)_2$, and its dehydrogenated derivates at the CCSD(T) and G3MP2 levels.

Table 55. Calculated CCSD(T) Heats of Formation (kcal/mol).

Molecule	**CCSD(T)**		**G3(MP2)**	
	Theory (0 K)	**Theory (298 K)**	**Theory (0 K)**	**Theory (298 K)**
NH_3 (C_{3v})	-9.6	-11.3	-8.3	-10.0
SiH_4 (T_d)	9.5	7.2	10.3	8.0
SiH_4 (D_{4h})	98.5	96.1	99.8	97.4
$H_2Si{=}NH$ (C_s)	41.2	39.1	41.5	39.4
$HN{=}Si{=}NH$ (C_2)	66.6	65.2	65.3	64.1
$H_3Si(NH_2)$ (C_s)	-8.1	-11.7	-6.0	-9.6
$H_4Si(NH_3)$ (C_3)	-0.6	-4.4	0.9	-2.8
$HN{=}SiH(NH_2)$ (C_s)	12.9	9.5	14.4	11.1
$H_2Si(NH_2)_2$ (C_{2v})	-31.1	-35.8	-28.3	-32.9
$H_3Si(NH_2)(NH_3)$ (C_s)	-18.6	-23.6	-16.1	-20.9
$H_4Si(NH_3)_2$ (C_i)	17.7	10.0	21.7	13.0

We first discuss the stability of diammoniosilane. The edge inversion of silane (T_d symmetry) is calculated at 0 K and 298 K to be 89.3 and 89.2 kcal/mol at the CCSD(T) and 89.5 and 89.4 kcal/mol at the G3MP2 levels respectively. Complexation with 2 NH_3 molecules recovers a substantial amount of the inversion barrier (-60.9 kcal/mol at 0 K at the CCSD(T) level), but the diammoniasilane complex is still 28.4 kcal/mol above the reactants SiH_4 + 2 NH_3 also at the same level. Therefore, it is a metastable species; it is characterized by all real frequencies at the MP2/aV(T+*d*)Z level so it is a true intermediate. More notably, complexation of the first ammonia group to silane is only a mere 0.2 kcal/mol at 0 K above the reactants SiH_4 + NH_3 at the CCSD(T) level while at the G3MP2 level, the $SiH_4(NH_3)$ complex is actually predicted to be below the reactants by 1.1 kcal/mol at 0K. It is only upon introduction of the second NH_3 group where the inversion barrier is recovered.

The results for the dehydrogenation reactions of diammonia silane and its derivatives are given in Table 56 at the CCSD(T) and G3MP2 levels. After the first two dehydrogenation steps, the dehydrogenation reactions are largely endothermic and it is unlikely that one will be able to

remove hydrogen from these species. However, one will be able to remove two H_2 molecules from $SiH_4(NH_3)_2$ if one can effectively couple the heats of reaction for the loss of H_2, but it will not be possible to remove an additional H_2 as the reaction is too endothermic. In addition, we must consider hydrogen loss from $H_3Si(NH_2)$, the deammoniated product of $H_3Si(NH_2)(NH_3)$. The loss of H_2 from $H_3Si(NH_2)$ to yield $H_2Si{=}NH$ however is predicted to be largely endothermic at 49.0 and 46.3 kcal/mol at the CCSD(T) and G3MP2 levels respectively at 0 K. Therefore, it will be unlikely that H_2 will be removed from the deammoniated product.

Table 56. Dehydrogenation and NH_3 Stabilization Reactions at 0 K and 298 K (kcal/mol).

Reaction	**CCSD(T)**		**G3(MP2)**	
	(0 K)	**(298 K)**	**(0 K)**	**(298 K)**
$H_4Si(NH_3)_2 \rightarrow H_3Si(NH_2)(NH_3) + H_2$	-36.3	-33.6	-38.9	-35.0
$H_3Si(NH_2)(NH_3) \rightarrow H_2Si(NH_2)_2 + H_2$	-12.5	-12.2	-13.5	-13.1
$H_4Si(NH_3)_2 \rightarrow H_2Si(NH_2)_2 + 2H_2$	-48.8	-45.8	-52.4	-48.2
$H_2Si(NH_2)_2 \rightarrow HN{=}SiH(NH_2) + H_2$	44.0	45.3	41.6	42.9
$HN{=}SiH(NH_2) \rightarrow HN{=}Si{=}NH + H_2$	53.7	55.7	49.8	51.9
$H_3Si(NH_2) \rightarrow H_2Si{=}NH + H_2$	49.2	50.7	46.3	47.8
$H_4Si(NH_3)_2 \rightarrow SiH_4$ (T_d) $+ 2NH_3$	-27.4	-25.4	-28.0	-25.0
$H_4Si(NH_3)_2 \rightarrow SiH_4$ (D_{4h}) $+ 2NH_3$	61.6	63.6	61.4	64.4
$H_4Si(NH_3)_2 \rightarrow H_4Si(NH_3) + NH_3$	-27.9	-25.6	-29.1	-25.8
$H_4Si(NH_3) \rightarrow SiH_4$ (T_d) $+ NH_3$	0.5	0.3	1.1	0.8
$H_3Si(NH_2)(NH_3) \rightarrow H_3Si(NH_2) + NH_3$	1.0	0.7	1.7	1.3

In order to aid the search for the hexacoordinate silicon species, we also calculated the nmr chemical shifts for SiH_4(T_d), SiH_4(D_{4h}) and $SiH_4(NH_3)_2$ at the B3LYP/VTZ level. The addition of two amines to produce an octahedral coordination environment at silicon leads to a substantial upfield shift.

Table 57. Calculated Si NMR Chemical Shifts for SiH_4 (T_d), SiH_4 (D_{4h}) and $H_4Si(NH_3)_2$ (C_i) at the B3LYP/Alrichs-VTZ+P level (ppm).[a]

Molecule	**δ**
SiH_4 (T_d)	-107.9
SiH_4 (D_{4h})	323.4
$H_4Si(NH_3)_2$ (C_i)	-234.1

[a] Calculated with respect to tetramethylsilane

Computational Predictions of Thermodynamics for Recycle

In response to requests from Center partners, we have studied different process for regeneration of the spent fuel. We investigated several reactions that could be good for the digestion step of the regeneration scheme. The endothermic reactions are not very high in energy (<10 kcal/mol), and they might be experimentally achieved.

Table 58. $(BN)_3$ Digestion Reactions in kcal/mol

Reaction	ΔH G3MP2	ΔG G3MP2	ΔH B3LYP/ DZVP2	ΔG B3LYP/ DZVP2
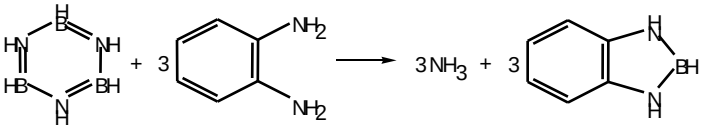	-8.8	-26.0	-7.2	-25.0
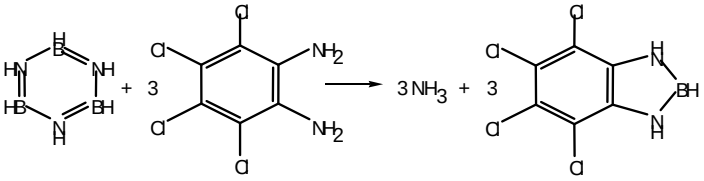	-7.2	-26.1	-5.1	-25.5
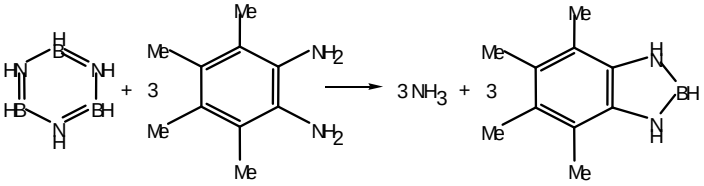	-15.0	-34.2	-16.1	-35.0
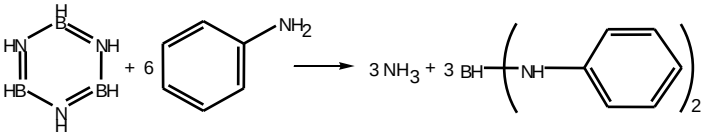	-1.0	11.3	-11.0	11.5
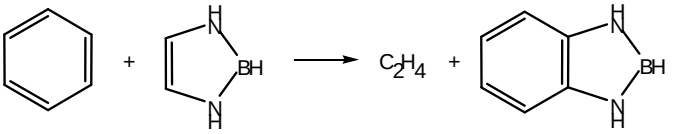	0.2	1.3	-1.0	0.1
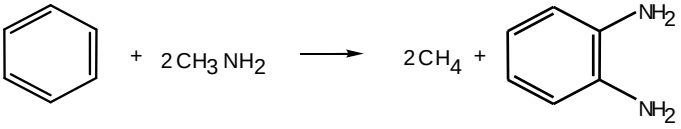	-23.1	-19.0	-24.4	-20.5
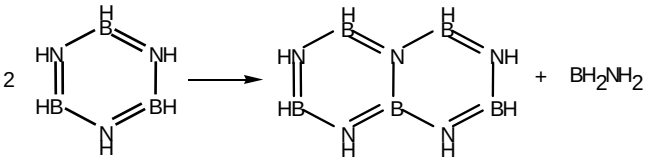	4.8	3.2	6.3	4.8
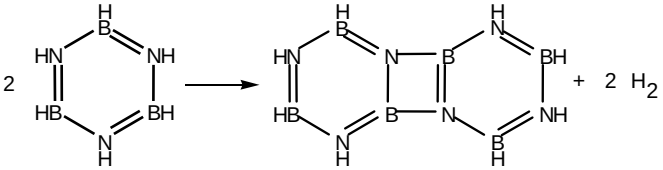	8.8	2.9	15.4	9.5

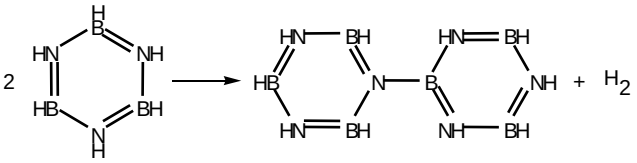

-15.6 -12.2 -9.7 -8.4

We have provided the energetics for the efficiency model developed at LANL.

$$\frac{(\text{Equiv. H}_2\text{ stored})(57.8)}{(\text{Equiv. H}_2\text{ used})(57.8)+\sum(\Delta H_{endo})-(\%\text{ heat recovery})\sum(-\Delta H_{exo})}=efficiency$$

(2 x 58) / (3 x 58 + 133 – (x%)129) = 0.38 for 0% heat recovery

↑ More H_2 release ↑ use less H_2 ↑ Lower endo-thermics ↑ Improve heat recovery ↑ Raise efficiency

Energetics of suggested processes in kcal/mol are shown below.

Reaction	**ΔH**
⅓($B_3N_3H_6$) (s) + 4HBr (g) → NH_4Br (s) + BBr_3 (l) + H_2 (g)	-45.8
BBr_3 (l) + 3 $HSn(nBu)_3$ (l) + NH_3 (g) → BH_3NH_3 (s) + 3$BrSn(nBu)_3$ (l)	-82.8
NH_4Br (s) → HBr (g) + NH_3 (g)	45.1
3$BrSn(nBu)_3$ (l) + 3H_2 (g) →3HBr (g) + 3$HSn(nBu)_3$ (l)	88.2

Efficiency = 38% (zero heat recovery)

Reaction	**ΔH**
⅓($B_3N_3H_6$) (s) + 4HCl (g) → NH_4Cl (s) + BCl_3 (l) + H_2 (g)	-47.8
BCl_3 (l) + 3 $HSi(Et)_3$ (l) + NH_3 (g) → BH_3NH_3 (s) + 3$ClSi(Et)_3$ (l)	-77*
NH_4Cl (s) → HCl (g) + NH_3 (g)	42.1
3$ClSi(Et)_3$ (l) + 3H_2 (g) →3HCl (g) + 3$HSi(Et)_3$ (l)	88*

* Estimated value

Efficiency = 38% (zero heat recovery)

We applied computational chemistry methods to a series of reactions such as the digestion of these materials by thiol reagents and the subsequent reduction by tin hydrides, as suggested by our collaborators at Los Alamos National Laboratory. In order to have a low or non environmental impact, some of the reactions are focused on the recycling of tin compounds. We have calculated a number of these reactions with B3LYP/DZVP2 to help and/or support experimental analysis for the regeneration and digestion processes of hydrogen storage. For those structures with Sn and Zn the cc-pVDZ-PP(ECP) basis set was used.

Table 59. Regeneration Reactions in kcal/mol at the B3LYP/DZVP2 Level.

Reaction	**ΔH (0K)**	**ΔH (298K)**	**ΔG (298K)**
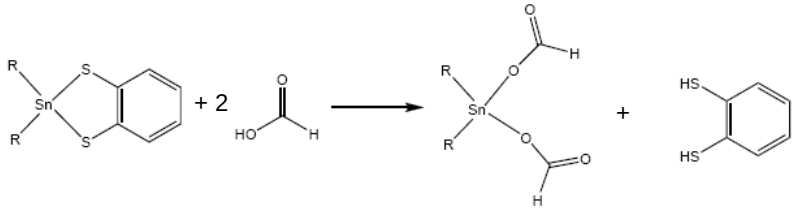			
R = H	1.7	2.1	12.4
R = nBu	-1.8	-1.4	7.7
R = tBu	-0.1	0.1	12.0
R = Ph	1.5	1.8	12.2
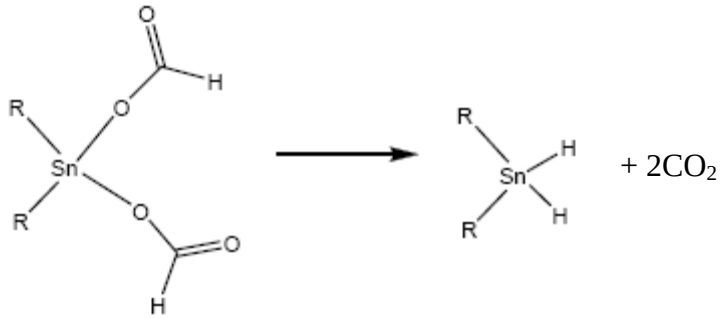			
R = H	13.5	14.6	-4.5
R = nBu	24.4	24.7	5.8
R = tBu	24.1	24.5	3.1
R = Ph	20.0	20.4	-0.6
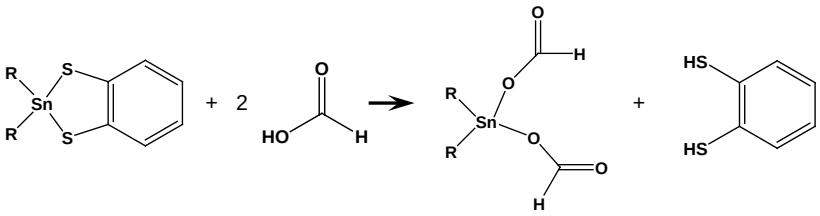			
R = H	1.7	2.1	12.4
R = nBu	-1.8	-1.4	7.7
R = tBu	-0.1	0.1	12.0
R = Ph	1.5	1.8	12.2
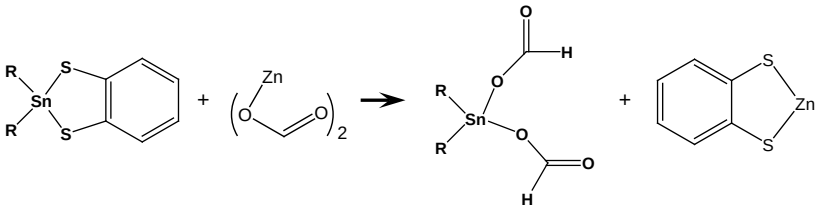			
R = H	24.1	24.1	24.6

R = nBu	20.6	20.6	19.9
R = tBu	22.2	22.1	24.2
R = Ph	23.9	23.8	24.4

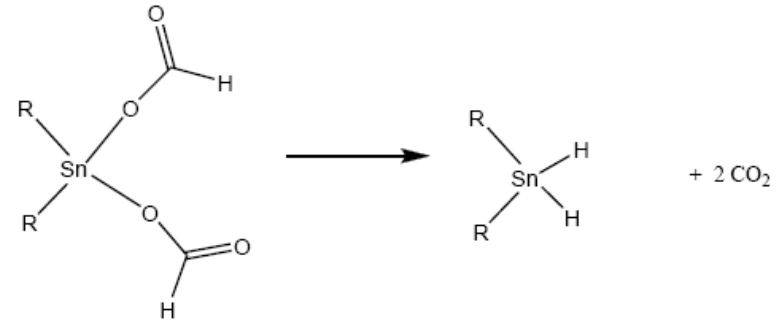

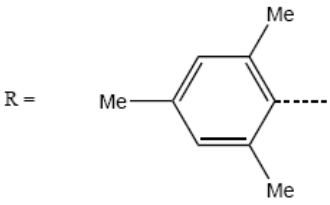

Mes

	17.9	18.2	-2.4

R =

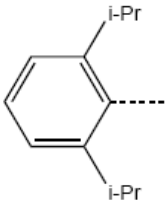

Dipp

	16.8	17.2	-5.7

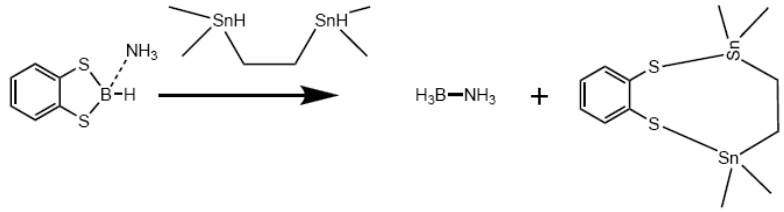

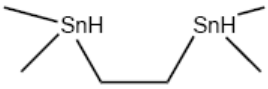

Conformer A

	5.7	6.3	8.9

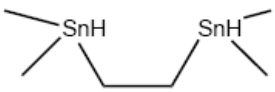

Conformer B

	5.4	6.1	8.4

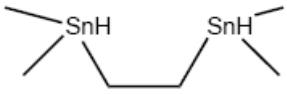

Conformer C | 3.7 | 4.5 | 5.9

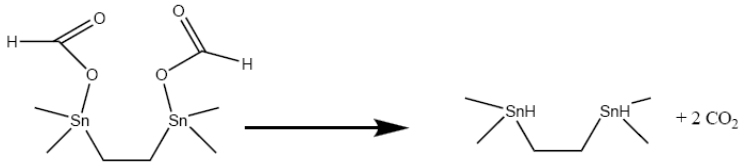

Conformer A	23.3	23.5	3.9
Conformer B	23.3	23.4	4.2
Conformer C	24.2	24.5	3.3

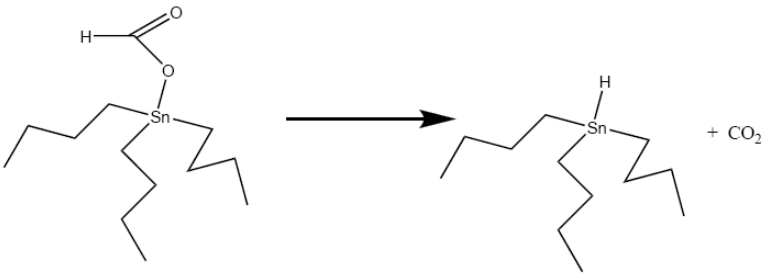

12.8 | 12.9 | 3.9

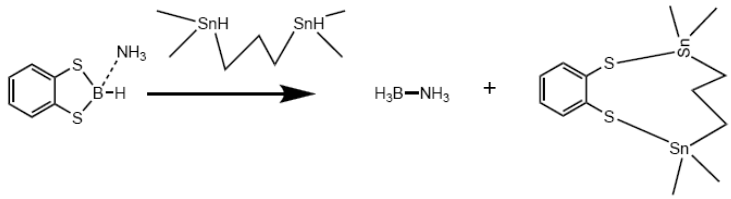

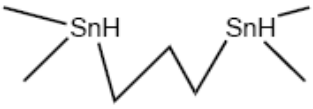

Conformer A’ | 5.5 | 6.1 | 9.8

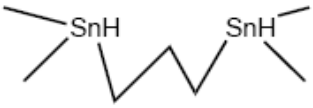

Conformer B’ | 1.3 | 2.1 | 4.1

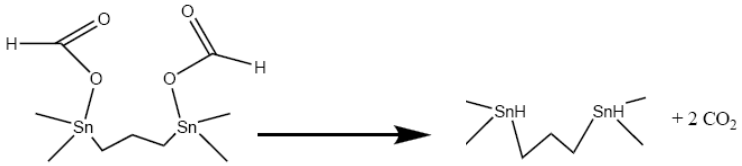

Conformer A’	23.2	23.5	3.2
Conformer B’	26.9	27.1	8.5

Table 60. $(BN)_3$ Digestion Reactions at the B3LYP/DZVP2 Level in kcal/mol

Reaction	ΔH(298K)	ΔG (298 K)
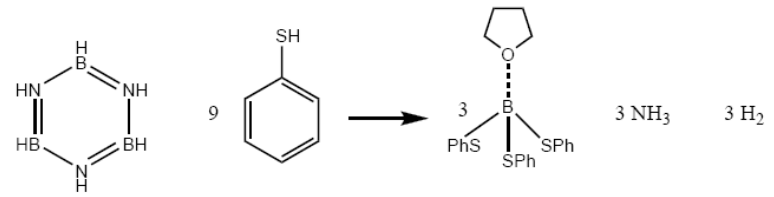	60.0	131.3
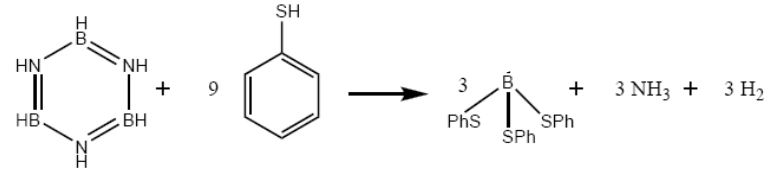	30.4	51.7
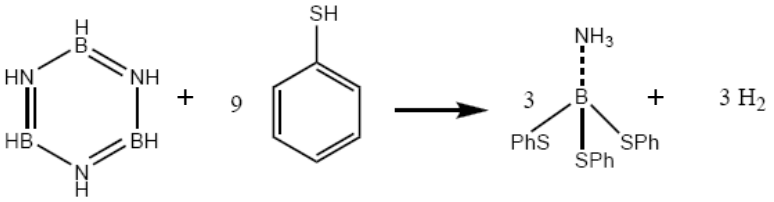	13.1	71.0
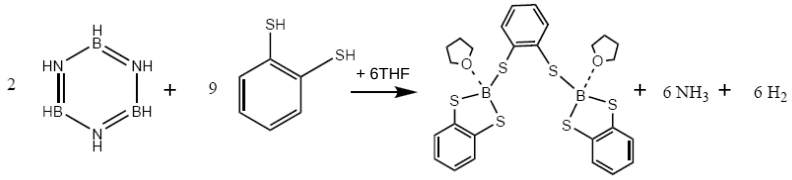	-13.4	21.9
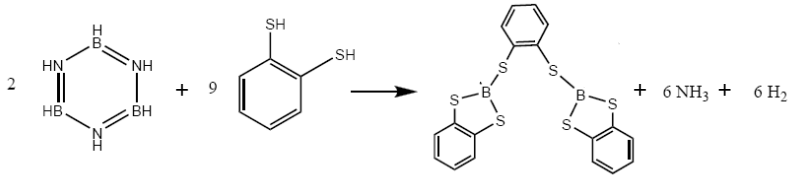	-5.9	-18.0
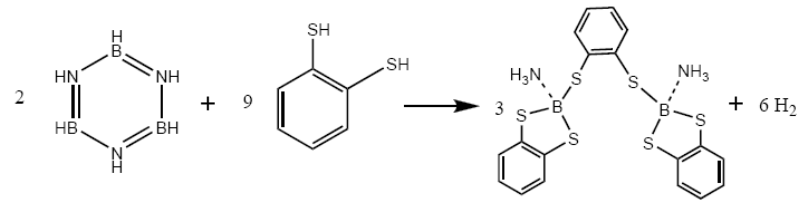	-35.3	20.1
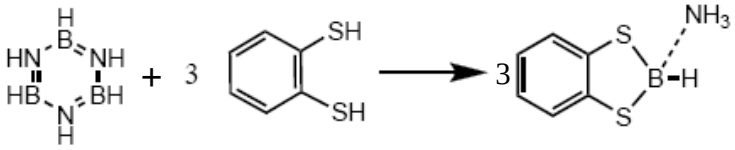	0.5	15.5

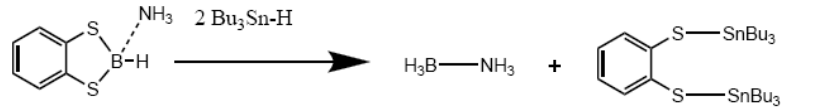	2.8	13.8
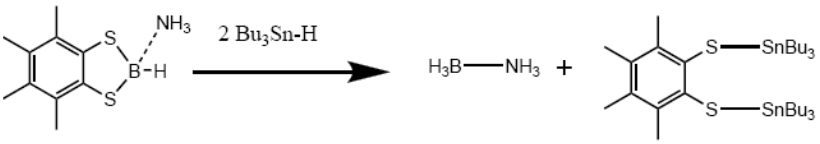	6.2	18.3
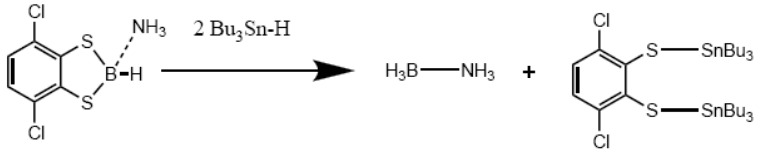	6.9	19.2
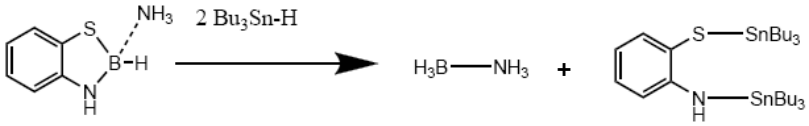	12.0	21.3
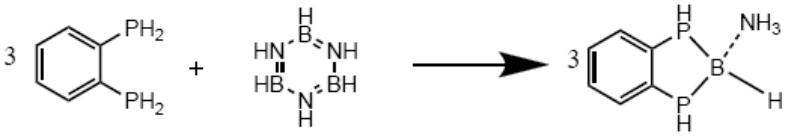	74.0	88.6
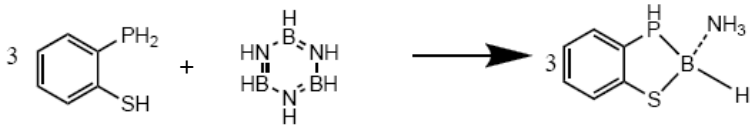	39.0	55.0
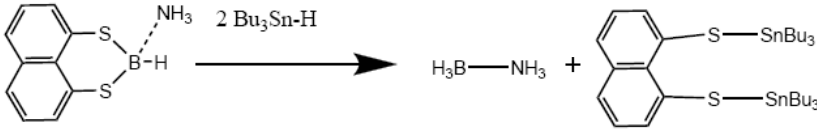	7.9	19.9
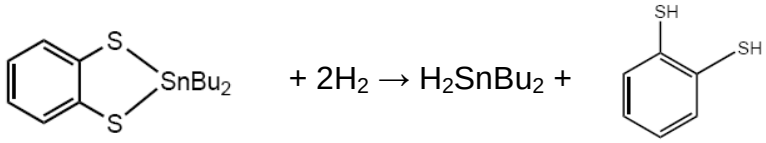	23.8	27.6
	5.1	16.0

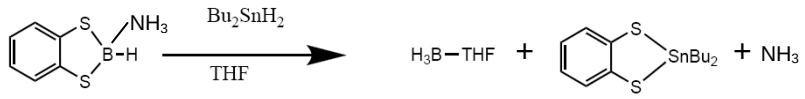

9.2 9.5

3.9 14.4

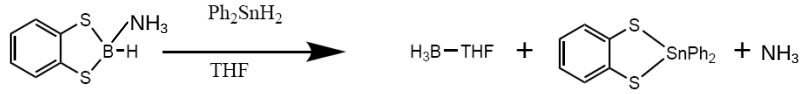

7.9 7.9

6.2 17.9

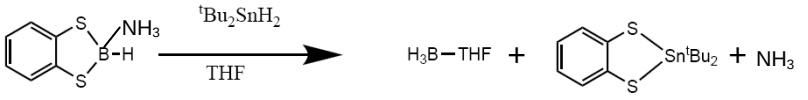

10.3 11.4

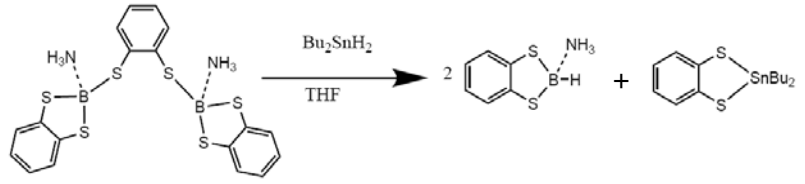

-11.7 -24.0

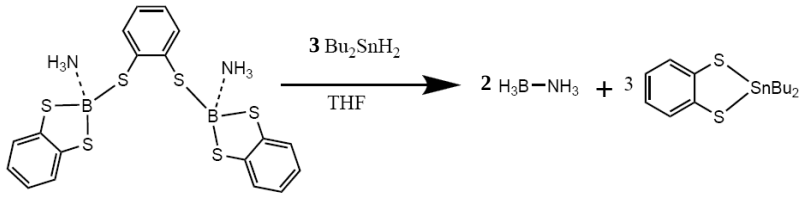

-10.0 -23.4

0.8 0.3

10.9 22.6

9.8 20.1

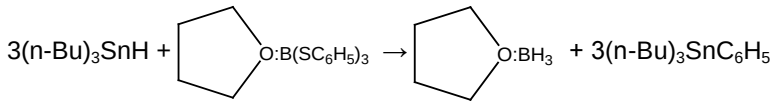

-20.6 -26.5

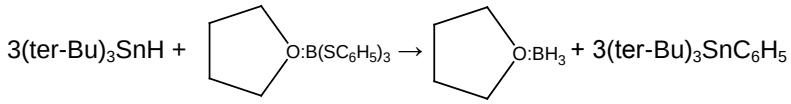

-15.5 -18.9

Table 61. Reaction Enthalpies and Free Energies for Regeneration Reactions of S and Sn Compounds at the B3LYP/DZVP2 Level at 298 K in kcal/mol.

Reaction	**ΔH**	**ΔG**
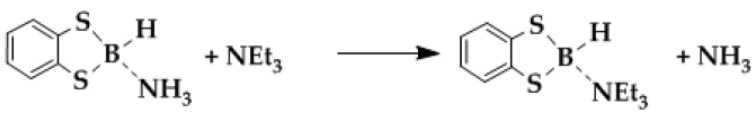	6.2	9.2
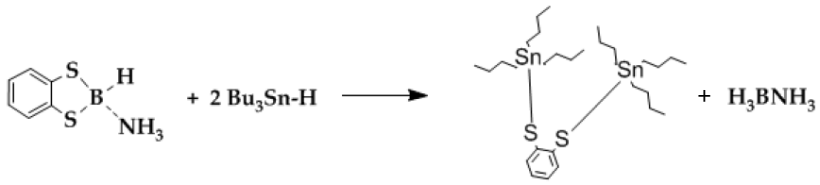	2.8	13.8
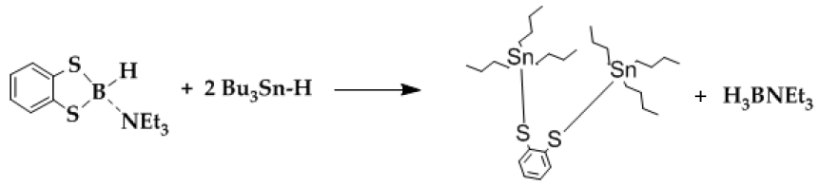	-4.7	5.6
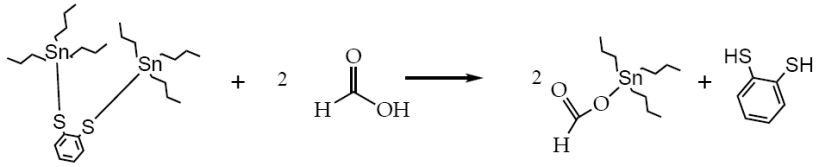	-4.4	-7.7
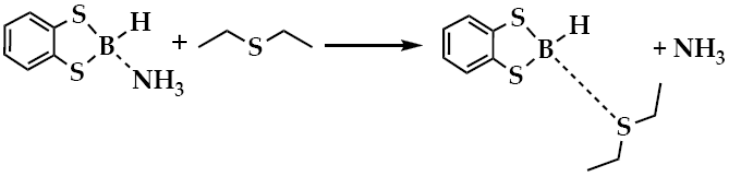		

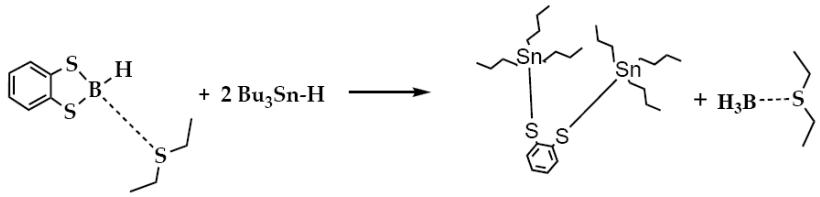

We calculated the heat of formation of $B_{12}N_{12}H_{12}$ in the coronene structure to provide a model for spent fuel thermodynamics from the following isodesmic reaction at the G3(MP2) level in kcal/mol at 298 K.

$$C_{24}H_{12} + 12BNH_4 \rightarrow B_{12}N_{12}H_{12} + 12C_2H_4 \quad (99)$$

The heat of the reaction is -255.8 kcal/mol leading to $\Delta H_f(B_{12}N_{12}H_{12})$ = -569.0 kcal/mol and ΔH_f("BNH", spent fuel) = -47.4 kcal/mol.

We continued our efforts to assess different chemistries for the regeneration processes. Examples of some of the recent scouting work for LANL is shown in Table 62 and Figure 60. Figure 59 shows the energetics of carbodiimide reactions as an alternative to formate/CO_2 chemistry.

Table 62. $2HMR_y + PhS_2BH{:}NH_3 \rightarrow 1,2\ Ph(SMR_y)_2 + BH_3NH_3$

Reaction	**ΔH**	**ΔG**
M = Pb R = CH_3 y=1	-43.4	-31.6
M = Pb R = CH_3 y=3	-0.5	10.5
M = Sn R = CH_3 y=3	3.8	12.5
M = Ge R = CH_3 y=3	9.4	19.0
M = Si R = CH_3 y=3	9.2	20.1
M = In R = CH_3 y=3	-35.2	-21.2
M = Ga R = CH_3 y=3	-31.6	-17.2
M = Al R = CH_3 y=3	-44.3	-30.6
M = Pb R = C_6H_5 y=1	-36.8	-24.9
M = Pb R = C_6H_5 y=3	3.7	14.6
M = Sn R = C_6H_5 y=3	5.8	15.6
M = Ge R = C_6H_5 y=3	11.3	24.0
M = Si R = C_6H_5 y=3	11.0	24.5
M = In R = C_6H_5 y=3	-27.2	-13.8
M = Ga R = C_6H_5 y=3	-22.2	-9.5
M = Al R = C_6H_5 y=3	-36.0	-22.2
M = Pb R = C_6H_{11}-c y=1	-43.4	-28.9
M = Pb R = C_6H_{11}-c y=3	-14.2	-0.6
M = Sn R = C_6H_{11}-c y=3	3.0	10.5
M = Ge R = C_6H_{11}-c y=3	-0.6	12.6
M = Si R = C_6H_{11}-c y=3	14.0	26.0
M = In R = C_6H_{11}-c y=3	-37.4	-20.7
M = Ga R = C_6H_{11}-c y=3	-30.5	-18.7
M = Al R = C_6H_{11}-c y=3	-43.6	-27.8
M = Pb R = C_4H_9 y=1	-43.4	-32.3
M = Pb R = C_4H_9 y=3	-1.7	11.8

M = Sn R = C_4H_9 y=3	3.5	12.8
M = Ge R = C_4H_9 y=3	9.8	21.8
M = Si R = C_4H_9 y=3	10.9	24.1
M = In R = C_4H_9 y=3	-35.2	-22.1
M = Ga R = C_4H_9 y=3	-31.1	-17.0
M = Al R = C_4H_9 y=3	-44.1	-28.9
M = Pb R = C_4H_9-t y=1	-36.0	-22.5
M = Pb R = C_4H_9-t y=3	0.0	8.4
M = Sn R = C_4H_9-t y=3	6.7	18.3
M = Ge R = C_4H_9-t y=3	20.3	33.0
M = Si R = C_4H_9-t y=3	26.1	40.0
M = In R = C_4H_9-t y=3	-23.0	-11.9
M = Ga R = C_4H_9-t y=3	-18.7	-7.3
M = Al R = C_4H_9-t y=3	-91.8	-78.6

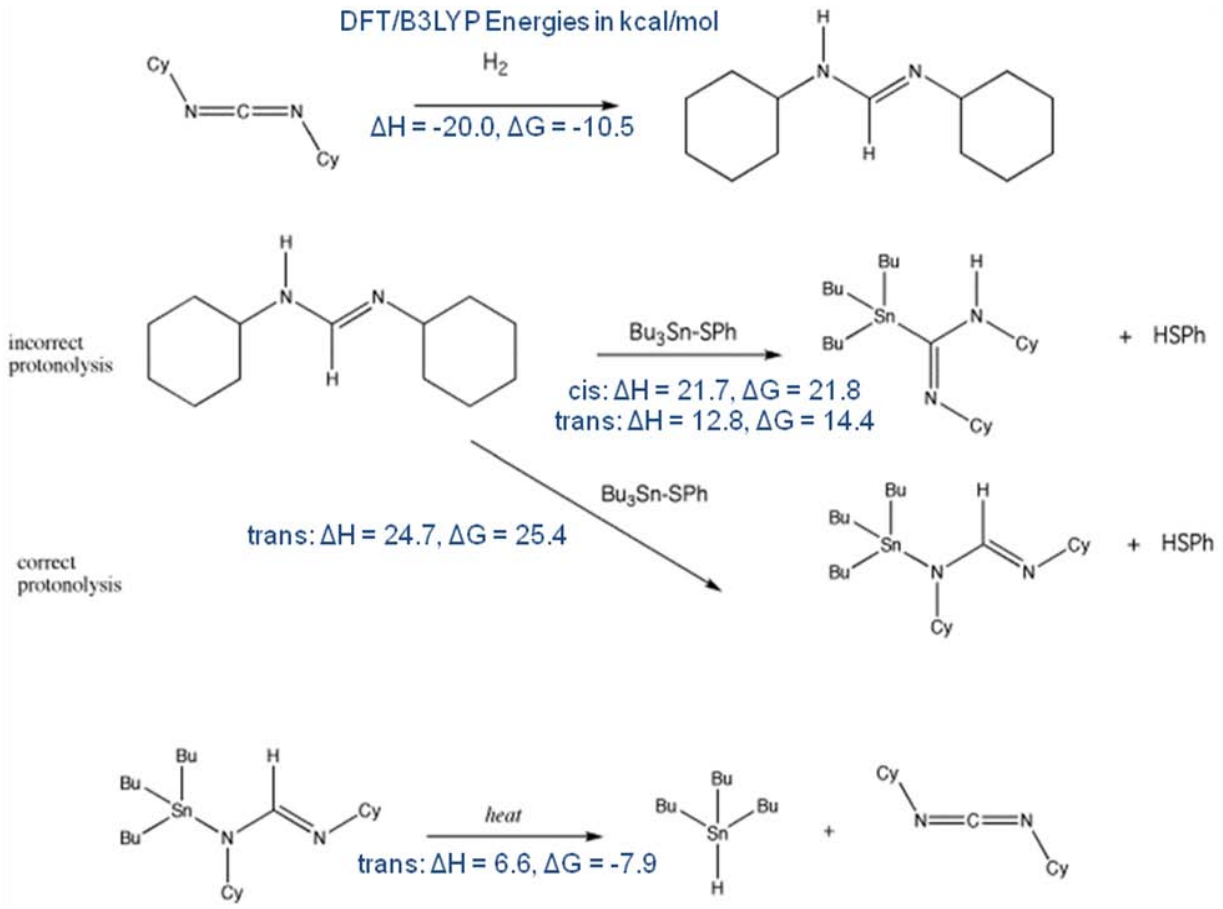

Figure 59. Reaction energetics at the B3LYP level in kcal/mol for potential carbodiimide chemistry

		ΔH(kcal/mol)
Reactor 1:		
Digestion	**(1a)** $BNH + 1.5\ C_6H_4(SH)_2 \rightarrow 0.5\ HB(C_6H_4S_2)\cdot NH_3 + 0.5\ (NH_4)B(C_6H_4S_2)_2$	8.6
Undesirable:	**(1b)** $C_6H_4(SH)_2 + HB(C_6H_4S_2)\cdot NH_3 \rightarrow (NH_4)B(C_6H_4S_2)_2 + H_2$	22.9
Reactor 2:		
Reduction:	**(2a)** $0.5\ (NH_4)B(C_6H_4S_2)_2 + 0.5\ Bu_3SnH \rightarrow 0.5\ HB(C_6H_4S_2)\cdot NH_3 + 0.5\ (C_6H_4)(SH)(SSnBu_3)$	-18.3
Amine Exchange:	**(2b)** $HB(C_6H_4S_2)\cdot NH_3 + Et_2NH \rightarrow HB(C_6H_4S_2)\cdot NHEt_2 + NH_3(g)$	1.6
Reduction:	**(2c)** $HB(C_6H_4S_2)\cdot NHEt_2 + 2\ Bu_3SnH \rightarrow Et_2NHBH_3 + C_6H_4(SSnBu_3)_2$	9.5
Net:	**(2d)** $0.5\ HB(C_6H4S_2)\cdot NH_3 + 0.5\ (NH_4)B(C_6H_4S_2)_2 + Et_2NH + 2.5\ Bu_3SnH \rightarrow Et_2NHBH_3 + NH_3 + 0.5\ (C_6H_4)(SH)(SSnBu_3) + C_6H_4(SSnBu_3)_2$	-7.2
Undesirable:	**(2e)** $C_6H_4(SH)_2 + Bu_3SnH \rightarrow C_6H_4(SH)(SSnBu_3) + H_2$	-13.7
	(2f) $C_6H_4(SH)(SSnBu_3) + Bu_3SnH \rightarrow C_6H_4(SSnBu_3)_2 + H_2$	-5.0
Net:	(2g) $C_6H_4(SH)_2 + 2Bu_3SnH \rightarrow C_6H_4(SSnBu_3)_2 + 2H_2$	-18.7
Reactor 3		
Ammoniation:	(3) $Et_2NHBH_3 + NH_3\ (l) \leftrightarrows H_3NBH_3 + Et_2NH$	-7.3
Reactor 4:		
Metal Recycle:	(4a) $C_6H_4(SSnBu_3)_2 + 2H_2 \rightarrow C_6H_4(SH)_2 + 2\ Bu_3SnH$	18.7
	(4b) $0.5\ C_6H_4(SH)(SSnBu_3) + 0.5\ H_2 \rightarrow 0.5\ C_6H_4(SH)_2 + 0.5\ Bu_3SnH$	6.8

Figure 60. Best reaction energetics in kcal/mol for the LANL recycle process designed by Rohm & Haas.

We predicted the energies at a range of regeneration reactions from the LANL group to look at Sn chemistry and the effects of substituents at the DFT/B3LYP level (Tables 63 to 67) in the gas phase. The ΔH and ΔG for the reaction "Ph(S-H)(S-Sn(Bu_3)) + HCOOH→ Ph -$(SH)_2$ + (Bu_3)Sn-OOCH" calculated at the B3LYP/VDZ-PP (Pb, Sn, Ge, In, Ga)/DZVP2 (H, C, S) level in kcal/mol are 2.4 and 1.1 kcal/mol respectively in the gas phase.

Table 63. Reaction Energies for the Reaction "$(R_3M)(R')N\text{-}HC{=}O \rightarrow HMR_3 + (R')N{=}C{=}O$" Calculated at the B3LYP/VDZ-PP (Sn)/DZVP2 (H, C, N, O) in kcal/mol at 298 K.

Reactions (M = Sn)	**ΔH**	**ΔG**
R = H; R′ = H	17.9	8.3
R = CH_3; R′ = H	19.2	9.5
R = CH_3; R′ = CH_3	17.9	5.2
R = CH_3; R′ = n-Bu	16.3	4.1
R = CH_3; R′ = t-Bu	10.1	-5.2
R = CH_3; R′ = n-Hex	16.1	4.1
R = CH_3; R′ = c-Hex	7.9	-4.7
R = CH_3; R′ = Ph	14.1	2.2
R = CH_3; R′ = Ph-Cl	14.8	2.7
R = CH_3; R′ = Ph-NO_2	16.3	4.1
R = Et; R′ = H	20.0	11.0
R = Et; R′ = CH_3	18.4	6.8

R = Et; R′ = n-Bu	17.0	5.6
R = Et; R′ = t-Bu	10.1	-3.6
R = Et; R′ = n-Hex	16.8	5.7
R = Et; R′ = c-Hex	8.8	-3.9
R = Et; R′ = Ph	15.1	2.9
R = Et; R′ = Ph-Cl	16.0	4.1
R = Et; R′ = Ph-NO_2	17.6	5.7
R = n-Bu; R′ = H	17.5	7.1
R = n-Bu; R′ = CH_3	19.1	6.2
R = n-Bu; R′ = n-Bu	17.1	6.1
R = n-Bu; R′ = t-Bu	10.2	-3.6
R = n-Bu; R′ = n-Hex	17.0	4.8
R = n-Bu; R′ = c-Hex	8.9	-2.6
R = n-Bu; R′ = Ph	15.4	4.1
R = n-Bu; R′ = Ph-Cl	16.3	5.5
R = n-Bu; R′ = Ph-NO_2	18.1	7.1
R = Ph; R′ = H	19.1	7.1
R = Ph; R′ = CH_3	17.9	3.3
R = Ph; R′ = n-Bu	16.4	2.9
R = Ph; R′ = t-Bu	8.5	-6.9
R = Ph; R′ = n-Hex	16.1	2.4
R = Ph; R′ = c-Hex	7.2	-6.0
R = Ph; R′ = Ph	13.2	-0.3
R = Ph; R′ = Ph-Cl	14.2	0.6
R = Ph; R′ = Ph-NO_2	16.0	2.3

Table 64. Reaction energies for the reaction "(R'_3)SnS-R + RHNHC=O→ (R'_3)Sn-RNHC=O + HSR" calculated at the B3LYP/VDZ-PP (Sn)/DZVP2 (H, C, N, O, S) level in kcal/mol at 298 K.

Reactions	**ΔH**	**ΔG**
R = H; R′ = CH_3	12.0	12.8
R = CH_3; R′ = CH_3	11.2	12.3
R = Ph; R′ = CH_3	15.2	16.7
R = H; R′ = Ph	11.9	13.2
R = CH_3; R′ = Ph	11.6	19.5
R = Ph; R′ = Ph	15.9	19.7

Table 65. Reaction energies for the reaction "$(2R_y)$X-H + PhS_2HB-NH_3 → Ph(S-X$(R_y)_3)_2$ + BH_3NH_3" calculated at the B3LYP/VDZ-PP (Pb, Sn, Ge, In, Ga)/DZVP2 (H, C, S) level in kcal/mol.

Reactions	**ΔH**	**ΔG**
X = Pb; R = CH_3 ; y = 3	3.1	15.4
X = Sn; R = CH_3 ; y = 3	6.1	16.9
X = Ge; R = CH_3 ; y = 3	12.9	21.6

X = Si; R = CH_3 ; y = 3	12.7	22.3
X = In; R = CH_3 ; y = 2	-31.7	-18.9
X = Ga; R = CH_3 ; y = 2	-28.1	-13.0
X = Al; R = CH_3 ; y = 2	-41.4	-26.9

Table 66. Reaction energies for the reaction "(Bu_3)Sn-SPh + H-X → (Bu_3)Sn-X + H-SPh" calculated at the B3LYP/VDZ-PP (Pb, Sn, Ge, In, Ga)/DZVP2 (H, C, S) level in kcal/mol.

Reactions	**ΔH**	**ΔG**
X = Cl	-11.0	-14.6
X = Br	-14.3	-17.0
X = OOCH	1.3	-1.6

Table 67. Reaction energies for the reaction (Bu_3)Sn-X + HCOOH → (Bu_3)Sn-OOCH + H-X" calculated at the B3LYP/VDZ-PP (Pb, Sn, Ge, In, Ga)/DZVP2 (H, C, S) level in kcal/mol.

Reactions	**ΔH**	**ΔG**
X = Cl	12.4	13.0
X = Br	15.6	15.4

Computational Results for B-H Transfer Reactions in Si and Sn Compounds

For regeneration, we predicted B-H transfer reactions in silicon and tin compounds at the B3LYP/6-311++G** level. The general reaction is as follows:

$HSiR_3 + BX_3 \rightarrow XSiR_3 + HBX_2$
with R = CH_3, $C(CH_3)_3$, NH_2, Ph, Ph-$(NH_2)_2$ and X = F, Cl, Br, OH, OCH_3, SPh_3

Table 68. Reaction Enthalpies and Free-Energy Calculated at the B3LYP/6-311++G** level in kcal/mol at 298K

Reaction	**ΔH**	**ΔG**
$HSi(CH_3)_3 + BF_3 \rightarrow FSi(CH_3)_3 + HBF_2$	-2.0	-2.8
$HSi(CH_3)_3 + BCl_3 \rightarrow ClSi(CH_3)_3 + HBCl_2$	-7.6	-8.4
$HSi(CH_3)_3 + BBr_3 \rightarrow BrSi(CH_3)_3 + HBBr_2$	-10.4	-11.2
$HSi(CH_3)_3 + B(OH)_3 \rightarrow (OH)Si(CH_3)_3 + HB(OH)_2$	8.3	6.6
$HSi(CH3)_3 + B(OCH_3)_3 \rightarrow (OCH_3)Si(CH_3)_3 + HB(OCH_3)_2$	7.9	6.2
$HSi(CH3)_3 + B(SPh)_3 \rightarrow (SPh)Si(CH_3)_3 + HB(SPh)_2$	-2.1	-4.0
$HSn(CH_3)_3 + BF_3 \rightarrow FSn(CH_3)_3 + HBF_2$	12.9	11.6
$HSn(CH_3)_3 + BCl_3 \rightarrow ClSn(CH_3)_3 + HBCl_2$	-8.8	-9.5
$HSn(CH_3)_3 + BBr_3 \rightarrow BrSn(CH_3)_3 + HBBr_2$	-15.5	-16.3
$HSn(CH_3)_3 + B(OH)_3 \rightarrow (OH)Sn(CH_3)_3 + HB(OH)_2$	24.0	21.8
$HSn(CH_3)_3 + B(OCH_3)_3 \rightarrow (OCH_3)Sn(CH_3)_3 + HB(OCH_3)_2$	24.0	22.0
$HSn(CH_3)_3 + B(SPh)_3 \rightarrow (SPh)Sn(CH_3)_3 + HB(SPh)_2$	-4.9	-6.3
$HSi(C(CH_3)_3)_3 + BF_3 \rightarrow FSi(C(CH_3)_3)_3 + HBF_2$	-1.5	-1.8
$HSi(C(CH_3)_3)_3 + BCl_3 \rightarrow ClSi(C(CH_3)_3)_3 + HBCl_2$	-6.2	-6.2
$HSi(C(CH_3)_3)_3 + BBr_3 \rightarrow BrSi(C(CH_3)_3)_3 + HBBr_2$	-8.0	-8.0
$HSi(C(CH_3)_3)_3 + B(OH)_3 \rightarrow (OH)Si(C(CH_3)_3)_3 + HB(OH)_2$	9.8	8.4

$HSi(C(CH_3)_3)_3 + B(OCH_3)_3 \rightarrow (OCH_3)Si(C(CH_3)_3)_3 + HB(OCH3)_2$	12.0	11.2
$HSi(C(CH_3)_3)_3 + B(SPh)_3 \rightarrow (SPh)Si(C(CH_3)_3)_3 + HB(SPh)_2$	5.8	5.7
$HSn(C(CH_3)_3)_3 + BF_3 \rightarrow FSn(C(CH_3)_3)_3 + HBF_2$	10.2	9.2
$HSn(C(CH_3)_3)_3 + BBr_3 \rightarrow BrSn(C(CH_3)_3)_3 + HBBr_2$	-17.7	-19.8
$HSn(C(CH_3)_3)_3 + B(OH)_3 \rightarrow (OH)Sn(C(CH_3)_3)_3 + HB(OH)_2$	22.3	19.6
$HSi(Si(CH_3)_3)_3 + BF_3 \rightarrow FSi(Si(CH_3)_3)_3 + HBF_2$	8.0	6.5
$HSi(Si(CH_3)_3)_3 + BCl_3 \rightarrow ClSi(Si(CH_3)_3)_3 + HBCl_2$	-3.1	-4.6
$HSi(Si(CH_3)_3)_3 + BBr_3 \rightarrow BrSi(Si(CH_3)_3)_3 + HBBr_2$	-7.5	-7.9
$HSi(Si(CH_3)_3)_3 + B(OH)_3 \rightarrow (OH)Si(Si(CH_3)_3)_3 + HB(OH)_2$	18.1	13.8
$HSi(Si(CH_3)_3)_3 + B(OCH_3)_3 \rightarrow (OCH_3)Si(Si(CH_3)_3)_3 + HB(OCH_3)_2$	18.1	16.9
$HSi(Si(CH_3)_3)_3 + B(SPh)_3 \rightarrow (SPh)Si(Si(CH_3)_3)_3 + HB(SPh)_2$	5.8	5.7
$HSi(NH_2)_3 + BF_3 \rightarrow FSi(NH_2)_3 + HBF_2$	-4.6	-5.5
$HSi(NH_2)_3 + BCl_3 \rightarrow ClSi(NH_2)_3 + HBCl_2$	-7.7	-8.5
$HSi(NH_2)_3 + BBr_3 \rightarrow BrSi(NH_2)_3 + HBBr_2$	-10.0	-10.8
$HSi(NH_2)_3 + B(OH)_3 \rightarrow (OH)Si(NH_2)_3 + HB(OH)_2$	4.8	4.1
$HSi(NH_2)_3 + B(OCH_3)_3 \rightarrow (OCH_3)Si(NH_2)_3 + HB(OCH_3)_2$	4.6	3.7
$HSi(NH_2)_3 + B(SPh)_3 \rightarrow (SPh)Si(NH_2)_3 + HB(SPh)_2$	-2.1	-4.0
$HSi(Ph)_3 + BF_3 \rightarrow FSi(Ph)_3 + HBF_2$	-1.0	-1.5
$HSi(Ph)_3 + BCl_3 \rightarrow ClSi(Ph)_3 + HBCl_2$	-6.3	-6.2
$HSi(Ph)_3 + BBr_3 \rightarrow BrSi(Ph)_3 + HBBr_2$	-8.6	-8.3
$HSi(Ph)_3 + B(OH)_3 \rightarrow (OH)Si(Ph)_3 + HB(OH)_2$	8.1	7.4
$HSi(Ph)_3 + B(OCH_3)_3 \rightarrow (OCH_3)Si(Ph)_3 + HB(OCH_3)_2$	7.7	7.6
$HSi(Ph)_3 + B(SPh)_3 \rightarrow (SPh)Si(Ph)_3 + HB(SPh)_2$	-1.1	-0.7
$HSn(Ph)_3 + BF_3 \rightarrow FSn(Ph)_3 + HBF_2$	14.2	12.9
$HSn(Ph)_3 + BCl_3 \rightarrow ClSn(Ph)_3 + HBCl_2$	-7.5	-8.9
$HSn(Ph)_3 + BBr_3 \rightarrow BrSn(Ph)_3 + HBBr_2$	-14.0	-14.8
$HSi(Ph\text{-}NH_2)_3 + BF_3 \rightarrow FSi(Ph\text{-}NH_2)_3 + HBF_2$	-2.1	-2.2
$HSi(Ph\text{-}NH_2)_3 + BCl_3 \rightarrow ClSi(Ph\text{-}NH_2)_3 + HBCl_2$	-7.5	-7.2
$HSi(Ph\text{-}NH_2)_3 + BBr_3 \rightarrow BrSi(Ph\text{-}NH_2)_3 + HBBr_2$	-9.9	-10.0
$HSi(Ph\text{-}NH_2)_3 + B(OH)_3 \rightarrow (OH)Si(Ph\text{-}NH_2)_3 + HB(OH)_2$	7.7	7.4
$HSi(Ph\text{-}NH_2)_3 + B(OCH_3)_3 \rightarrow (OCH_3)Si(Ph\text{-}NH_2)_3 + HB(OCH_3)_2$	7.4	7.7
$HSi(Ph\text{-}NH_2)_3 + B(SPh)_3 \rightarrow (SPh)Si(Ph\text{-}NH_2)_3 + HB(SPh)_2$	-1.9	-1.7
$HSn(Ph\text{-}NH_2)_3 + BF_3 \rightarrow FSn(Ph\text{-}NH_2)_3 + HBF_2$	12.9	11.8
$HSn(Ph\text{-}NH_2)_3 + BCl_3 \rightarrow ClSn(Ph\text{-}NH_2)_3 + HBCl_2$	-8.8	-9.7
$HSn(Ph\text{-}NH_2)_3 + BBr_3 \rightarrow BrSn(Ph\text{-}NH_2)_3 + HBBr_2$	-15.3	-17.6

Computational Results for B-O to B-H Conversions

The thermodynamics of the following disproportionation and conproportionation equilibria for alkoxyboron compounds were investigated at the B3LYP/6-311++G** level. All energies are in kcal/mol.

Table 69. Reaction Enthalpies and Free-Energy Calculated at the B3LYP/6-311++G** level in kcal/mol at 298K

$2HB(OCH_3)_3^- \rightarrow H_2B(OCH_3)_2^- + B(OCH_3)_4^-$	$\Delta E = -1.4$
$HB(OCH_3)_3^- + H_2B(OCH_3)_2^- \rightarrow H_3B(OCH_3)^- + B(OCH_3)_4^-$	$\Delta E = -4.2$

$HB(OCH_3)_3^- + H_3B(OCH_3)^- \rightarrow B(OCH_3)_4^- + BH_4^-$ $\Delta E = -11.4$

$2HAl(OCH_3)_3^- \rightarrow H_2Al(OCH_3)_2^- + Al(OCH_3)_4^-$ $\Delta E = 0.3$

$HAl(OCH_3)_3^- + H_2Al(OCH_3)_2^- \rightarrow H_3Al(OCH_3)^- + Al(OCH_3)_4^-$ $\Delta E = -0.4$

$HAl(OCH_3)_3^- + H_3Al(OCH_3)^- \rightarrow Al(OCH_3)_4^- + AlH_4^-$ $\Delta E = -3.3$

$HSi(CH_3)_3 + B(OCH_3)_4^- \rightarrow (CH_3)_3Si(OCH_3) + HB(OCH_3)_3^-$ $\Delta E = 6.2$

$HSi(OCH_3)_3 + B(OCH_3)_4^- \rightarrow Si(OCH_3)_4 + HB(OCH_3)_3^-$ $\Delta E = 2.1$

$HAl(OCH_3)_2 + B(OCH_3)_4^- \rightarrow Al(OCH_3)_3 + HB(OCH_3)_3^-$ $\Delta E = 16.5$

$HAl(CH_3)_2 + B(OCH_3)_4^- \rightarrow (CH_3)_2Al(OCH_3) + HB(OCH_3)_3^-$ $\Delta E = 12.8$

$HSi(CH_3)_3 + Al(OCH_3)_4^- \rightarrow (CH_3)_3Si(OCH_3) + HAl(OCH_3)_3^-$ $\Delta E = 10.6$

$HSi(OCH_3)_3 + Al(OCH_3)_4^- \rightarrow Si(OCH_3)_4 + HAl(OCH_3)_3^-$ $\Delta E = 6.5$

$HAl(OCH_3)_2 + Al(OCH_3)_4^- \rightarrow H_2Al(OCH_3)_3 + HAl(OCH_3)_3^-$ $\Delta E = 20.9$

$HAl(CH_3)_2 + B(OCH_3)_4^- \rightarrow (CH_3)_2Al(OCH_3) + HAl(OCH_3)_3^-$ $\Delta E = 17.2$

Hydride exchange involving the alkoxyboron compounds and silicon metal hydrides were also investigated at the above level. The generic reaction (in kcal/mol) for the hydride exchange is:

$HSiR_3 + BX_3 \rightarrow XSiR_3 + HBX_2$ for R/X = CH_3, CH_2CH_3, F, Cl, Br, and OCH_3

Table 70. Reaction Enthalpies and Free-Energy Calculated at the B3LYP/6-311++G** level in kcal/mol at 298K

$HSiF_3 + BF_3 \rightarrow SiF_4 + HBF_2$ $\Delta E = 3.3$

$HSiCl_3 + BCl_3 \rightarrow SiCl_4 + HBCl_2$ $\Delta E = 0.4$

$HSiBr_3 + BBr_3 \rightarrow SiBr_4 + HBBr_2$ $\Delta E = -1.9$

$HSi(OCH_3)_3 + B(OCH_3)_3 \rightarrow Si(OCH_3)_4 + HB(OCH_3)_2$ $\Delta E = 3.7$

$HSi(CH_3)_3 + BF_3 \rightarrow FSi(CH_3)_3 + HBF_2$ $\Delta E = -2.4$

$HSi(CH_3)_3 + BCl_3 \rightarrow ClSi(CH_3)_3 + HBCl_2$ $\Delta E = -7.8$

$HSi(CH_3)_3 + BBr_3 \rightarrow BrSi(CH_3)_3 + HBBr_2$ $\Delta E = -10.5$

$HSi(CH_3)_3 + B(OCH_3)_3 \rightarrow (OCH_3)Si(CH_3)_3 + HB(OCH_3)_2$ $\Delta E = 8.2$

$HSi(CH_2CH_3)_3 + BF_3 \rightarrow FSi(CH_2CH_3)_3 + HBF_2$ $\Delta E = -2.1$

$HSi(CH_2CH_3)_3 + BCl_3 \rightarrow ClSi(CH_2CH_3)_3 + HBCl_2$ $\Delta E = -8.3$

$HSi(CH_2CH_3)_3 + BBr_3 \rightarrow BrSi(CH_2CH_3)_3 + HBBr_2$ $\Delta E = -11.0$

$HSi(CH_2CH_3)_3 + B(OCH_3)_3 \rightarrow (OCH_3)Si(CH_2CH_3)_3 + HB(OCH_3)_2$ $\Delta E = 9.4$

$HSi(OCH_3)_3 + BF_3 \rightarrow FSi(OCH_3)_3 + HBF_2$ $\Delta E = -2.7$

$HSi(OCH_3)_3 + BCl_3 \rightarrow ClSi(OCH_3)_3 + HBCl_2$ $\Delta E = -5.9$

$HSi(OCH_3)_3 + BBr_3 \rightarrow BrSi(OCH_3)_3 + HBBr_2$ $\Delta E = -7.8$

$HSi(OCH_3)_3 + B(OCH_3)_3 \rightarrow Si(OCH_3)_4 + HB(OCH_3)_2$ $\Delta E = 3.7$

The thermodynamics of the following new disproportionation/conproportionation equilibria for alkoxyboron compounds were investigated at the B3LYP/6-311++G** level. All energies are in kcal/mol.

Table 71. Reaction Enthalpies and Free-Energy Calculated at the B3LYP/6-311++G** level in kcal/mol at 298K

$2HGa(OCH_3)_3^- \rightarrow H_2Ga(OCH_3)_2^- + Ga(OCH_3)_4^-$	$\Delta E = 2.7$
$HGa(OCH_3)_3^- + H_2Ga(OCH_3)_2^- \rightarrow H_3Ga(OCH_3)^- + Ga(OCH_3)_4^-$	$\Delta E = 2.6$
$HGa(OCH_3)_3^- + H_3Ga(OCH_3)^- \rightarrow Ga(OCH_3)_4^- + GaH_4^-$	$\Delta E = 1.6$
$HSi(CH_3)_3 + Ga(OCH_3)_4^- \rightarrow (CH_3)_3Si(OCH_3) + HGa(OCH_3)_3^-$	$\Delta E = -7.0$
$HSi(OCH_3)_3 + Ga(OCH_3)_4^- \rightarrow Si(OCH_3)_4 + HGa(OCH_3)_3^-$	$\Delta E = -11.1$
$HGe(CH_3)_3 + B(OCH_3)_4^- \rightarrow (CH_3)_3Ge(OCH_3) + HB(OCH_3)_3^-$	$\Delta E = 19.4$
$HGe(OCH_3)_3 + B(OCH_3)_4^- \rightarrow Ge(OCH_3)_4 + HB(OCH_3)_3^-$	$\Delta E = 19.0$
$HGe(CH_3)_3 + Al(OCH_3)_4^- \rightarrow (CH_3)_3Ge(OCH_3) + HAl(OCH_3)_3^-$	$\Delta E = 23.8$
$HGe(OCH_3)_3 + Al(OCH_3)_4^- \rightarrow Ge(OCH_3)_4 + HAl(OCH_3)_3^-$	$\Delta E = 23.4$
$HGe(CH_3)_3 + Ga(OCH_3)_4^- \rightarrow (CH_3)_3Ge(OCH_3) + HGa(OCH_3)_3^-$	$\Delta E = 6.2$
$HGe(OCH_3)_3 + Ga(OCH_3)_4^- \rightarrow Ge(OCH_3)_4 + HGa(OCH_3)_3^-$	$\Delta E = 5.8$
$HSn(CH_3)_3 + B(OCH_3)_4^- \rightarrow (CH_3)_3Sn(OCH_3) + HB(OCH_3)_3^-$	$\Delta E = 21.7$
$HSn(OCH_3)_3 + B(OCH_3)_4^- \rightarrow Sn(OCH_3)_4 + HB(OCH_3)_3^-$	$\Delta E = 25.5$
$HSn(CH_3)_3 + Al(OCH_3)_4^- \rightarrow (CH_3)_3Sn(OCH_3) + HAl(OCH_3)_3^-$	$\Delta E = 26.1$
$HSn(OCH_3)_3 + Al(OCH_3)_4^- \rightarrow Sn(OCH_3)_4 + HAl(OCH_3)_3^-$	$\Delta E = 29.9$
$HSn(CH_3)_3 + Ga(OCH_3)_4^- \rightarrow (CH_3)_3Sn(OCH_3) + HGa(OCH_3)_3^-$	$\Delta E = 8.5$
$HSn(OCH_3)_3 + Ga(OCH_3)_4^- \rightarrow Sn(OCH_3)_4 + HGa(OCH_3)_3^-$	$\Delta E = 12.4$

Hydride exchange involving the alkoxyboron compounds and silicon metal hydrides were also investigated at the B3LYP/6-311++G** level. The generic reaction for the hydride exchange is:

$HSiR_3 + BX_3 \rightarrow XSiR_3 + HBX_2$ for R/X = CH_3, CH_2CH_3, F, Cl, Br, and OCH_3 in kcal/mol:

Table 72. Reaction Enthalpies and Free-Energy Calculated at the B3LYP/6-311++G** level in kcal/mol at 298K

$HAl(OCH_3)_2 + Ga(OCH_3)_4^- \rightarrow H_2Al(OCH_3)_3 + HGa(OCH_3)_3^-$	$\Delta E = 3.4$
$HAl(CH_3)_2 + Ga(OCH_3)_4^- \rightarrow (CH_3)_2Al(OCH_3) + HGa(OCH_3)_3^-$	$\Delta E = -0.4$
$HGa(OCH_3)_2 + B(OCH_3)_4^- \rightarrow Ga(OCH_3)_3 + HB(OCH_3)_3^-$	$\Delta E = 18.8$
$HGa(CH_3)_2 + B(OCH_3)_4^- \rightarrow (CH_3)_2Ga(OCH_3) + HB(OCH_3)_3^-$	$\Delta E = 11.7$
$HGa(OCH_3)_2 + Al(OCH_3)_4^- \rightarrow H_2Ga(OCH_3)_3 + HAl(OCH_3)_3^-$	$\Delta E = 23.2$
$HGa(CH_3)_2 + Al(OCH_3)_4^- \rightarrow (CH_3)_2Ga(OCH_3) + HAl(OCH_3)_3^-$	$\Delta E = 16.1$
$HGa(OCH_3)_2 + Ga(OCH_3)_4^- \rightarrow H_2Ga(OCH_3)_3 + HGa(OCH_3)_3^-$	$\Delta E = 5.6$
$HGa(CH_3)_2 + Ga(OCH_3)_4^- \rightarrow (CH_3)_2Ga(OCH_3) + HGa(OCH_3)_3^-$	$\Delta E = -1.5$

We completed the calculations of all of the compounds requested by LANL for modeling the thermodynamics of disproportionation/conproportionation equilibria for alkoxyboron compounds at the B3LYP/6-311++G** level.

Computational Predictions of Boron and Silicon Chemistry

We performed calculations on a number of reactions involving the exchange of BH/SiH bonds and predicted the B-H and Si-H bond strengths in B-Si compounds. The B3LYP energies for the following reactions are at 0 K in kcal/mol:

$HSi(Ph)_3 + BF_3 \rightarrow FSi(Ph)_3 + HBF_2$ $\Delta E = -1.4$ (100)

$HSi(Ph)_3 + BCl_3 \rightarrow ClSi(Ph)_3 + HBCl_2$ $\Delta E = -6.6$ (101)

$HSi(Ph)_3 + BBr_3 \rightarrow BrSi(Ph)_3 + HBBr_2$ $\Delta E = -8.8$ (102)

$HSi(Ph)_3 + B(OCH_3)_3 \rightarrow (OCH_3)Si(Ph)_3 + HB(OCH_3)_2$ $\Delta E = 7.5$ (103)

To serve as benchmark, we have also calculated the following absolute bond energies at 0 K in kcal/mol in the model compounds, as well as predict the hydride affinity at the CCSD(T)/CBS level plus additional corrections.

$BH_2SiH_3 \rightarrow HBSiH_3 + H$ $\Delta E = 99.4$ (104)

$BH_2SiH_3 \rightarrow H_2BSiH_2 + H$ $\Delta E = 77.8$ (105)

$BH_2SiH_3 + H^- \rightarrow H_3BsiH_3$ $\Delta E = -90.2$ (106)

The heats of formation for the molecules BH_2SiH_3, $HBSiH_3$, H_2BSiH_2, and $H_3BSiH_3^-$ CCSD(T)/CBS method with additional corrections have been calculated. The properties of the compounds at 0K in kcal/mol are given below. Given these accurately calculated heats of formation in addition to the heats of formation of some small boron/silicon hydrides would allow the predictions of the heats of formation of other larger boron/silicon clusters, which would be too computationally expensive to calculated at the CCSD(T) level, through isodesmic reactions. The reaction energies were calculated at the B3LYP/DZVP2 level to obtain heats of formation at 0K. In addition, G3MP2 values are given in parentheses to also serve as comparison to the composite MP2 method, and we note that there is excellent agreement between the two methods in most cases.

Table 73. Reaction Enthalpies and Free-Energy Calculated at the B3LYP/6-311++G** level in kcal/mol at 298K

Molecule	**ΔH_f**	**D_e(B-H)**	**D_e(Si-H)**	**Hydride Affinity**
		CCSD(T)/CBS		
BH_2SiH_3	41.4	101.1	76.4	90.6
$HBSiH_3$	90.8			
H_2BSiH_2	66.2			
$H_3BSiH_3^-$	-14.9			
		Isodesmic reactions		
$BH(SiH_3)_2$	55.4	96.4(95.5)	76.0(74.6)	
$B(SiH_3)_2$	100.2			
$HB(SiH_3)(SiH_2)$	79.7			
$B(SiH_3)_3$)	68.7		74.9(73.2)	
$B(SiH_3)_2(SiH_2)$	91.9			
$H_2Si(BH_2)_2$	72.2	76.2(69.8)	71.9(71.9)	
$HSi(BH_2)_2$	92.4			

$H_2Si(BH_2)(BH)$	96.7		
$HSi(BH_2)_3$	100.4	101.0(100.2)	70.8(72.9)
$Si(BH_2)_3$	119.6		
$HSi(BH_2)_2(BH)$	149.8		
$Si(BH_2)_4$	131.1	99.9(99.3)	
$Si(BH_2)_3(BH)$	179.3		

Reactions Involving Release of CO and CO_2

We also studied the following reactions where CO and CO_2 are released:

$$R_2BOC(O)H \rightarrow R_2BOH + CO \quad (107)$$

$$R_2BOC(O)H \rightarrow R_2BH + CO_2 \quad (108)$$

where R = H, CH_3, CH_2CH_3, OCH_3, OPh

We calculated the heats of formation of the following compounds $H_2BOC(O)H$, H_2BOH, and BH_3 at the CCSD(T)/CBS level including additional core-valence, scalar-relativistic, and atomic spin orbit corrections and at the G3(MP2) levels for comparison, which allows us to calculation the reaction energies as shown below.

Table 74. Reaction Energy based on Heats of Formation Calculated at the CCSD(T)/CBS and G3(MP2) Levels in kcal/mol.

Reaction	**G3MP2 ΔH_r(298K)**	**CCSD(T) ΔH_f (298K)**
$H_2BOC(O)H \rightarrow H_2BOH + CO$	-1.4	-1.1
$H_2BOC(O)H \rightarrow BH_3 + CO_2$	21.3	21.2

In order to predict the heats of formation of the other compounds, our approach is based on isodesmic reactions, where the heats of formation of the known compounds are either experimental or from highly accurate theoretical calculations (CCSD(T)/CBS + additional corrections). The reaction energies at 0K and 298K were calculated at the B3LYP/DZVP2, MP2/aug-cc-pVTZ, and G3(MP2) levels.

Table 75. Heats of Formation at 298K based on Reaction Energies Calculated at the B3LYP/DZVP2, MP2/aug-cc-pVTZ, and G3(MP2) levels in kcal/mol at 298 K.

Molecule	**B3LYP**	**MP2** [a]	**G3(MP2)**
$(OH)_2BOC(O)H$	-264.0	-264.0	-263.6
$(CH_3)_2BOC(O)H$	-121.5	-123.5	-123.0
$(CH_3)_2BOH$	-96.5	-98.3	-98.0
$(CH_3)_2BH$	-7.7	-8.6	-8.4
$(CH_3CH_2)_2BOC(O)H$	-124.8		
$(CH_3CH_2)_2BOH$	-100.5		
$(CH_3CH_2)_2BH$	-11.2		
$(OCH_3)_2BOC(O)H$	-245.7	-251.9	-249.0
$(OCH_3)_2BOH$	-218.8	-225.1	-221.8
$(OCH_3)_2BH$	-136.2	-140.1	-138.6
$(OPh)_2BOC(O)H$	-187.3		
$(OPh)_2BOH$	-161.7		

$(OPh)_2BH$	-79.5

[a] For R = OCH_3, reaction energies were calculated at the MP2/aug-cc-pVDZ level.

Table 76. Energies for Reactions (107) and (108) at the B3LYP, MP2, and G3(MP2) levels in kcal/mol at 298 K.[a]

R	B3LYP	MP2	G3(MP2)
H (1)	-1.1	-1.1	-1.5
H (2)	19.1	19.2	18.7
OH (1)	-1.4	-1.2	-1.4
OH (2)	19.8	20.9	20.6
CH_3 (1)	-2.1		
CH_3 (2)	19.6		
CH_3CH_2 (1)	0.5	0.4	0.8
CH_3CH_2 (2)	15.5	17.7	16.4
OCH_3[b] (1)	-1.1	-1.1	-1.5
OCH_3[b] (2)	19.1	19.2	18.7
OPh (1)	6.9		
OPh (2)	16.8		

[a] For each specific R group, the first row corresponds to Reaction 1 while the second row corresponds to Reaction 2. [b] For R = OCH_3, the reaction energies at the MP2 level were calculated with an aug-cc-pVDZ basis set.

We additionally studied the reactions where CO and CO_2 are released from the heavier homologues of $H_2XOC(O)H$ with X = Al and Ga.

$$H_2XOC(O)H \rightarrow H_2XOH + CO \quad (109)$$

$$H_2XOC(O)H \rightarrow XH_3 + CO_2 \quad (110)$$

The heats of formation of the following compounds AlH_3, GaH_3, H_2AlOH, H_2GaOH, and $H_2AlOC(O)H$ at the CCSD(T)/CBS level with effective core potential correlation-consistent basis sets for Ga including additional core-valence, scalar-relativistic, and atomic spin orbit corrections. Calculations were also performed at the G3(MP2) level, where possible, for comparison.

Table 77. Heats of Formation of AlH_3, GaH_3, H_2AlOH, H_2GaOH, and $H_2AlOC(O)H$ at 0 K and 298 K in kcal/mol.

Molecule	G3(MP2) ΔH_f		CCSD(T) ΔH_f	
	(0 K)	(298 K)	(0 K)	(298 K)
AlH_3	32.7	31.2	31.9	30.3
H_2AlOH	-56.0	-58.1	-57.5	-59.7
$H_2AlOC(O)H$	-84.9	-87.0	-85.6	-87.8
GaH_3			36.8	34.8
H_2GaOH			2.2	-0.6

Based on the accurately calculated heats of formation, we predicted the varies reactions energies for releasing CO and CO_2 at various levels, where they can be comparted to the CCSD(T)/CBS values.

Table 78. Reaction Energies Calculated at the B3LYP/DZVP2, MP2/aug-cc-pVTZ-PP, G3(MP2), and CCSD(T)/CBS Levels in kcal/mol at 298 K.[a]

Reaction	B3LYP	MP2	G3MP2	CCSD(T)
$H_2AlOC(O)H \rightarrow H_2AlOH + CO$	10.0	2.9	1.5	1.7
$H_2AlOC(O)H \rightarrow AlH_3 + CO_2$	24.6	23.5	23.3	24.1
$H_2GaOC(O)H \rightarrow H_2GaOH + CO$	8.9	6.8		
$H_2GaOC(O)H \rightarrow GaH_3 + CO_2$	-2.5	12.3		

[a] For the Ga series, the DFT calculations were performed with the DZVP basis set.

Computational Predictions of Thermodynamics for Recycle

In response to requests from Center partners, we studied different processes for the regeneration of spent fuel. We have used computational chemistry methods to predict the thermodynamics of a series of reactions such as digestion of spent fuel by thiol reagents and the subsequent reduction by tin hydrides, as suggested by our collaborators at Los Alamos National Laboratory. The main purpose of this kind of regeneration schemes is to regenerate borazine ($B_3N_3H_6$) into ammonia borane BH_3NH_3, from reaction 110 with a ΔH of 4.7 kcal/mol.

$$\tfrac{1}{3}\ B_3N_3H_6\ (s) + 2\ H_2\ (g) \rightarrow BH_3NH_3\ (s) \qquad (111)$$

In order to minimize the environmental impact of the proposed processes, some of the reactions are focused on the recycling and recovery of all of the products in the minimum number of steps with the highest efficiency. This study is critical to our understanding of how toregenerate other B-N derived spent fuels.

Scheme 1: **Sn hydrides with production of CO_2**

Reaction	ΔH
1) $\tfrac{1}{3}\ B_3N_3H_6\ (l) + C_6H_4(SH)_2\ (l) \rightarrow C_6H_4S_2BH{:}NH_3\ (l)$	-7.6
2) $\tfrac{1}{2}\ HB(C_6H_4S_2){:}NH_3\ (l) + \tfrac{1}{2}\ C_6H_4(SH)_2\ (l)$ $\rightarrow \tfrac{1}{2}\ [NH_4][B(C_6H_4S_2)_2]\ (s) + \tfrac{1}{2}\ H_2\ (g)$	9.9
3) $\tfrac{1}{2}\ [NH_4][B(C_6H_4S_2)_2]\ (s) + \tfrac{1}{2}\ Bu_3SnH\ (l)$ $\rightarrow \tfrac{1}{2}\ HB(C_6H_4S_2){:}NH_3\ (l) + \tfrac{1}{2}\ C_6H_4SH(SSnBu_3)\ (l)$	-34.3
4) $HB(C_6H_4S_2)NH_3\ (l) + H_2SnBu_2\ (l) \rightarrow BH_3NH_3\ (s) + (C_6H_4S_2)SnBu_2\ (l)$	-4.5
5) $(C_6H_4S_2)SnBu_2\ (l) + 2\ HCOOH\ (l) \rightarrow C_6H_4(SH)_2\ (l) + (HOOC)_2SnBu_2\ (l)$	54.2
6) $(HOOC)_2SnBu_2\ (l) \rightarrow 2\ CO_2\ (g) + H_2SnBu_2\ (l)$	-22.7
7) $\tfrac{1}{2}\ C_6H_4(SH)(SSnBu_3)\ (l) + \tfrac{1}{2}\ HCOOH\ (l)$ $\rightarrow \tfrac{1}{2}\ C_6H_4(SH)_2\ (l) + \tfrac{1}{2}\ (HCOOH)SnBu_3\ (l)$	21.7
8) $\tfrac{1}{2}\ (HOOC)SnBu_3\ (l) \rightarrow \tfrac{1}{2}\ CO_2\ (g) + \tfrac{1}{2}\ Bu_3SnH\ (l)$	6.4
9) $^5/_2\ CO_2\ (g) + {}^5/_2\ H_2\ (g) \rightarrow {}^5/_2\ CO\ (g) + {}^5/_2\ H_2O\ (l)$	-1.7
10) $^5/_2\ CO\ (g) + {}^5/_2\ CH_3OH\ (l) \rightarrow {}^5/_2\ CH_3COOH\ (l)$	-80.4
11) $^5/_2\ CH_3COOH\ (l) + {}^5/_2\ H_2O\ (l) \rightarrow {}^5/_2\ HCOOH\ (l) + {}^5/_2\ CH_3OH\ (l)$	63.3
	Efficiency: 43%

Note: Steps 9 to 11 are those for the commercial synthesis of formic acid from CO_2.

Scheme 2: **Sn hydrides without production of CO_2**

Reaction	ΔH
1) $\tfrac{1}{3}\ B_3N_3H_6\ (l) + C_6H_4(SH)_2\ (l) \rightarrow C_6H_4S_2BH{:}NH_3\ (l)$	-7.6
2) $\tfrac{1}{2}\ HB(C_6H_4S_2){:}NH_3\ (l) + \tfrac{1}{2}\ C_6H_4(SH)_2\ (l)$	

$\rightarrow$ ½ $[NH_4][B(C_6H_4S_2)_2]$ (s) + ½ H_2 (g) 9.9

3) ½ $[NH_4][B(C_6H_4S_2)_2]$ (s) + ½ Bu_3SnH (l)
$\rightarrow$ ½ $HB(C_6H_4S_2):NH_3$ (l) + ½ $C_6H_4SH(SSnBu_3)$ (l) -34.3

4) $HB(C_6H_4S_2)NH_3$ (l) + H_2SnBu_2 (l) $\rightarrow$ BH_3NH_3 (s) + $(C_6H_4S_2)SnBu_2$ (l) -4.5

5) $(C_6H_4S_2)SnBu_2$ (l) + 2 H_2 (g) $\rightarrow$ $C_6H_4(SH)_2$ (l) + H_2SnBu_2 (l) 16.4

6) ½ $C_6H_4(SH)(SSnBu_3)$ (l) + H_2 (g) $\rightarrow$ ½ $C_6H_4(SH)_2$ (l) + ½ $HSnBu_3$ (l) 24.3

Efficiency: 62%

Scheme 3: **Diethylamine as a ligand with production of CO_2**

Reaction	ΔH
1) ⅓ $B_3N_3H_6$ (s) + $C_6H_4(SH)_2$ (l) $\rightarrow$ $HB(C_6H_4S_2):NH_3$ (l)	-7.6
2) $HB(C_6H_4S_2):NH_3$ (l) + Et_2NH (l) $\rightarrow$ $HB(C_6H_4S_2):NHEt_2$ (l) + NH_3 (g)	18.3
3) $HB(C_6H_4S_2)\cdot NHEt_2$ (l) + 2 Bu_3SnH (l) $\rightarrow$ Et_2NHBH_3 (s) + $C_6H_4(SSnBu_3)_2$ (l)	11.1
4) Et_2NHBH_3 (s) + NH_3 (g) $\rightarrow$ H_3NBH_3 (s) + Et_2NH (l)	-16.9
5) $C_6H_4(SSnBu_3)_2$ (l) + 2 HCOOH (l) $\rightarrow$ $C_6H_4(SH)_2$ (l) + 2 CO_2 (g) + 2 Bu_3SnH (l)	14.5
6) 2 CO_2 (g) + 2 H_2 (g) $\rightarrow$ 2 CO (g) + 2 H_2O (l)	-1.4
7) 2 CO (g) + 2 MeOH (l) $\rightarrow$ 2 MeCOOH (l)	-64.3
8) 2 MeCOOH (l) + 2 H_2O (l) $\rightarrow$ 2 HCOOH (l) + 2 MeOH (l)	50.6

Efficiency: 60%

Note: Steps 6 to 7 are those for the commercial synthesis of formic acid from CO_2.

Scheme 4: **Diethylamine as a ligand**

Reaction	ΔH
1) ⅓ $B_3N_3H_6$ (s) + $C_6H_4(SH)_2$ (l) $\rightarrow$ $HB(C_6H_4S_2):NH_3$ (l)	-7.6
2) $HB(C_6H_4S_2):NH_3$ (l) + Et_2NH (l) $\rightarrow$ $HB(C_6H_4S_2):NHEt_2$ (l) + NH_3 (g)	18.3
3) $HB(C_6H_4S_2)\cdot NHEt_2$ (l) + 2 Bu_3SnH (l) $\rightarrow$ Et_2NHBH_3 (s) + $C_6H_4(SSnBu_3)_2$ (l)	11.1
4) Et_2NHBH_3 (s) + NH_3 (g) $\rightarrow$ H_3NBH_3 (s) + Et_2NH (l)	-16.9
5) $C_6H_4(SSnBu_3)_2$ (l) + 2 H_2 (g) $\rightarrow$ $C_6H_4(SH)_2$ (l) + 2 Bu_3SnH (l)	-0.6

Efficiency: 83%

A summary of this scheme is shown in Fig. 60.

Scheme 5: **Trimethylphosphine as a ligand with production of CO_2**

Reaction	ΔH
1) ⅓ $B_3N_3H_6$ (l) + $C_6H_4(SH)_2$ (l) $\rightarrow$ $HB(C_6H_4S_2):NH_3$ (l)	-7.6
2) $HB(C_6H_4S_2):NH_3$ (l) + $P(CH_3)_3$ (l) $\rightarrow$ $HB(C_6H_4S_2):P(CH_3)_3$ (l) + NH_3 (g)	0.5
3) $HB(C_6H_4S_2):P(CH_3)_3$ (l) + 2 Bu_3SnH (l) $\rightarrow$ $(CH_3)_3PBH_3$ (s) + $C_6H_4(SSnBu_3)_2$ (l)	16.9
4) $(CH_3)_3PBH_3$ (s) + NH_3 (g) $\rightarrow$ H_3NBH_3 (s) + $P(CH_3)_3$ (l)	-4.8
5) $C_6H_4(SSnBu_3)_2$ (l) + 2 HCOOH (l) $\rightarrow$ $C_6H_4(SH)_2$ (l) + 2 CO_2 (g) + 2 Bu_3SnH (l)	14.5
6) 2 CO_2 (g) + 2 H_2 (g) $\rightarrow$ 2 CO (g) + 2 H_2O (l)	-1.4
7) 2 CO (g) + 2 MeOH (l) $\rightarrow$ 2 MeCOOH (l)	-64.3
8) 2 MeCOOH (l) + 2 H_2O (l) $\rightarrow$ 2 HCOOH (l) + 2 MeOH (l)	50.6

Efficiency: 63%

Note: Steps 6 to 7 are those for the commercial synthesis of formic acid from CO_2.

Scheme 6: Trimethylphosphine as a ligand

Reaction	ΔH

1) ⅓ $B_3N_3H_6$ (l) + $C_6H_4(SH)_2$ (l) → $HB(C_6H_4S_2):NH_3$ (l) -7.6
2) $HB(C_6H_4S_2):NH_3$ (l) + $P(CH_3)_3$ (l) → $HB(C_6H_4S_2):P(CH_3)_3$ (l) + NH_3 (g) 0.5
3) $HB(C_6H_4S_2):P(CH_3)_3$ (l) + 2 Bu_3SnH (l) → $(CH_3)_3PBH_3$ (s) + $C_6H_4(SSnBu_3)_2$ (l) 16.9
4) $(CH_3)_3PBH_3$ (s) + NH_3 (g) → H_3NBH_3 (s) + $P(CH_3)_3$ (l) -4.8
5) $C_6H_4(SSnBu_3)_2$ (l) + 2 H_2 (g) → $C_6H_4(SH)_2$ (l) + 2 Bu_3SnH (l) -0.6

Efficiency: 89%

Scheme 7: Compounds with metals

Reaction	ΔH
1) $NH_4B(OMe)_4$ (s) + NH_4Cl (s) + $LiAlH_4$ (s) → NH_3BH_3 (s) + $Al(OMe)_3$ (l) + MeOH (l) + H_2 (g) + LiCl (s) + NH_3 (g)	-68.5
2) NaCl (s) + electricity → Na (s) + ½ Cl_2(g)	98.2
3) ½ Cl_2 (g) + ½ H_2 (g) → HCl (g)	-22.1
4) HCl (g) + NH_3 (g) → NH_4Cl (s)	-42.1
5) $Al(OMe)_3$ (l) + $^3/_2$ H_2 (g) + electricity → Al (s) + 3 MeOH (l)	49.9
6) Na (s) + Al (s) + 2 H_2 (g) → $NaAlH_4$ (s)	-27.6
7) LiCl (s) + $NaAlH_4$ (s) → $LiAlH_4$ (s) + NaCl (s)	2.4

Efficiency: 50%

Scheme 7 is present to show a competing route. In general, those processes with CO_2 production are less efficient than the corresponding process without CO_2 production.

The heat of formation of benzenethiol (liquid) was taken from Pedley's compilation (ΔH_f(l) = 15.22 ± 0.19 kcal/mol). The heat of formation of benzenedithiol (liquid) was obtained from the gas phase value for o-$C_6H_4(SH)_2$ obtained from an isodesmic reaction scheme and the calculated heat of vaporization (ΔH_f(l) = 29.7 kcal/mol). The heat of formation of $(C_6H_5S)_2BH(NH_3)$ (liquid) was calculated from a gas phase heat of formation from isodesmic reactions and a calculated heat of vaporization (ΔH_f(l) = 2.6 kcal/mol). The heat of formation of $C_6H_4S_2BH(NH_3)$ (liquid) was estimated from a gas phase reaction energy and the calculated heat of vaporization (ΔH_f(l) = -19.1 kcal/mol). The heat of formation of Bu_3SnH (liquid) and Bu_2SnH_2 (liquid) were estimated from the calculated heats of vaporization and the gas phase heats of formation from isodesmic reactions ($\Delta H_f(Bu_3SnH,l)$ = -45.3 kcal/mol; $\Delta H_f(Bu_2SnH_2,l)$ = -21.8 kcal/mol). We obtained the heats of formation of $C_6H_4(SSnBu_3)_2$ (liquid), $C_6H_4S_2SnBu_2$ (liquid), and $C_6H_4(SH)(SSnBu_3)$ (liquid) ($\Delta H_f(C_6H_4(SSnBu_3)_2,l)$ = -76.7 kcal/mol; ($\Delta H_f(C_6H_4S_2SnBu_2,l)$ = -14.0 kcal/mol; $\Delta H_f(C_6H_4(SH)(SSnBu_3),l)$ = -23.6 kcal/mol). The heat of formation of the salt $NH_4B(C_6H_4S_2)_2$(s) was estimated from the $\Delta H_f(NH_4^+)$ = 150.9 kcal/mol and $\Delta H_f((C_6H_4S_2)_2B^-)$ in the gas phase from isodesmic reactions and the lattice energy to obtain the heat of formation of the solid salt ($\Delta H_f(NH_4B(C_6H_4S_2)_2,s)$ = 24.7 kcal/mol, $U_{L,298K}$ = 106.8 kcal/mol).

For the metal regeneration scheme, the heat of formation of $NH_4B(OMe)_4$ (s) was estimated from the $\Delta H_f(NH_4^+)$ and $\Delta H_f(B(OMe)_4^-)$ in the gas phase from isodesmic reactions and the lattice energy to get the solid salt ($\Delta H_f(NH_4B(OMe)_4,s)$ = -256.2 kcal/mol, $U_{L,298K}$ = 121.1 kcal/mol). The heat of formation of $Al(OMe)_3$ (l) was obtained from isodesmic reactions and the calculated heat of vaporization ($\Delta H_f(Al(OMe)_3,l)$ = -216.1 kcal/mol). The heat of formation of MeOH (l)

was taken from Pedley and the heats of formation of the remaining solids from Wagman et al. or the NIST website.

NMR Calculations

Calculations at the DFT level with the B3LYP exchange-correlation functional and the Ahlrichs VTZ + P basis set were performed to predict the chemical shift of boron atoms in the following structures:

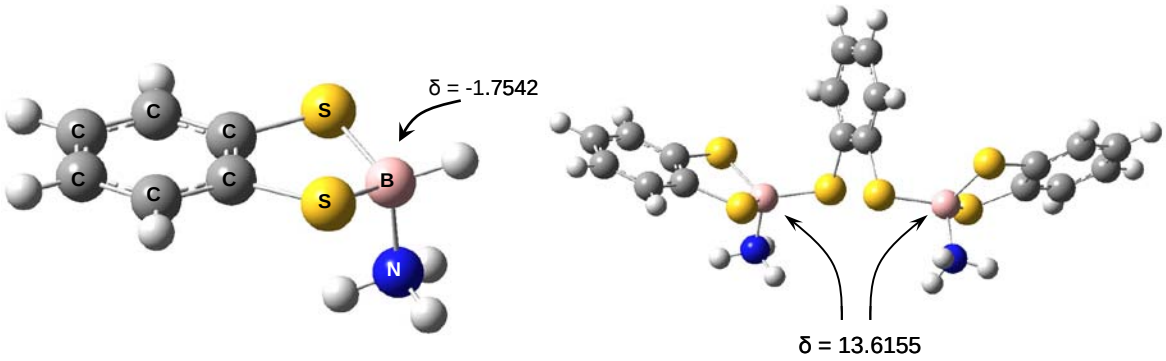

Our results are in good agreement with those found by LANL Hydrogen Storage Research Group.

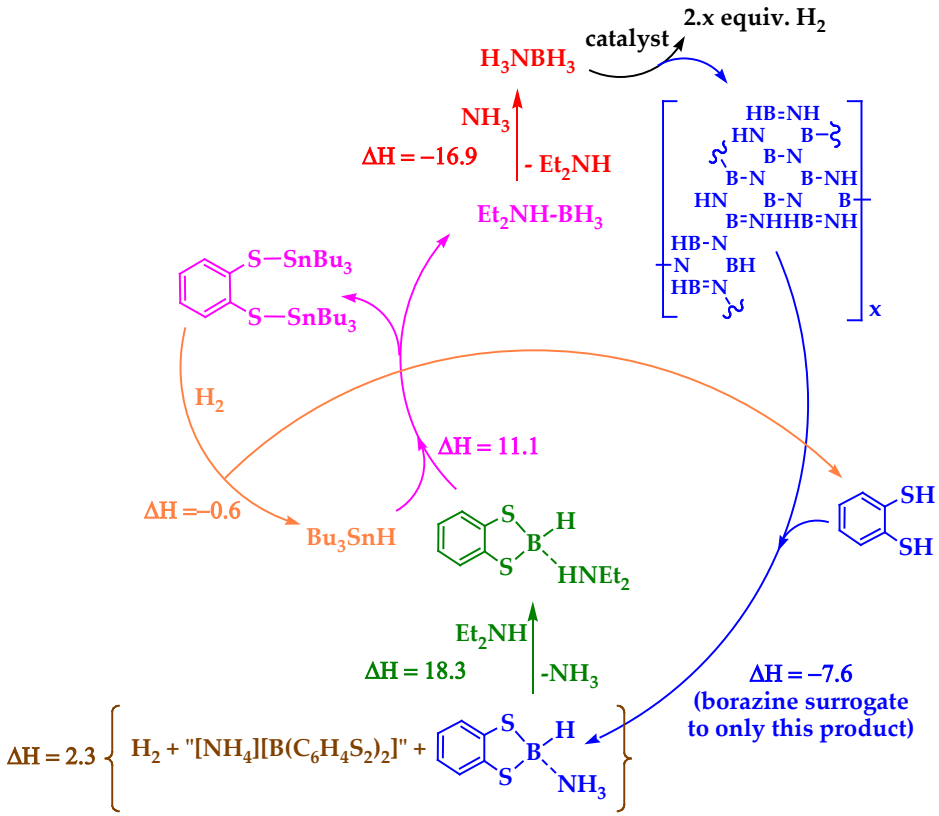

Figure 61. Summary of potential regeneration scheme with Et_2NH.

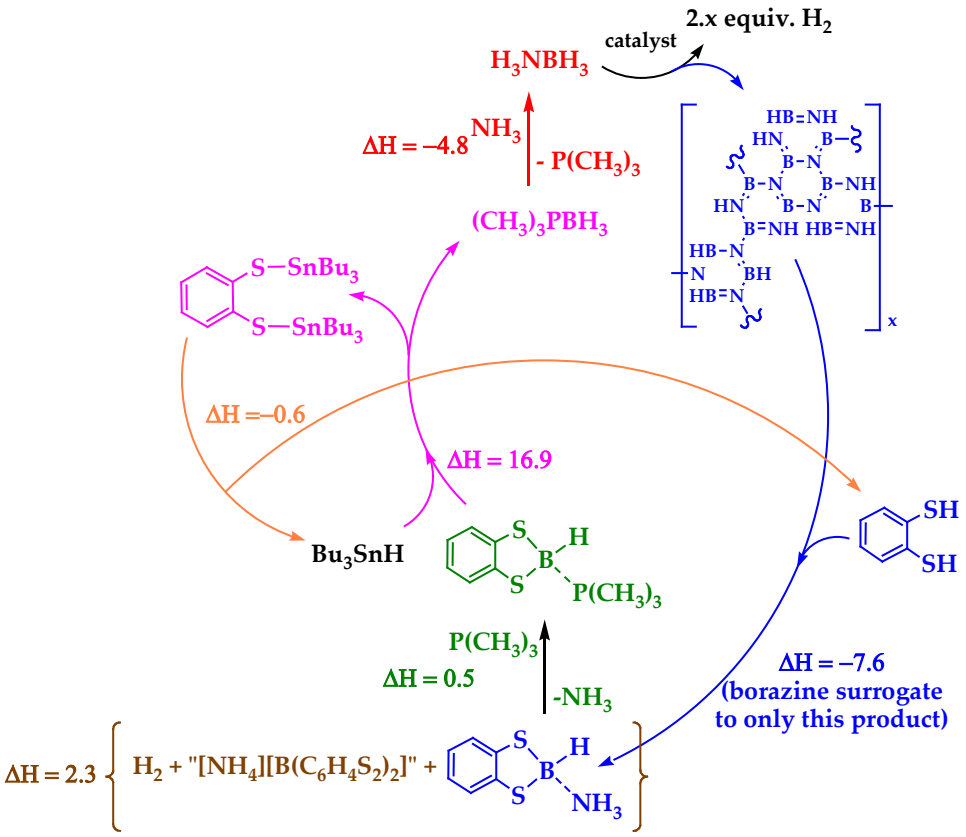

Figure 62. Summary of potential regeneration scheme with $P(CH_3)_3$.

Boiling Point Calculations

A critical aspect of the reactions that we are studying is that many take place in the liquid so we have developed an approach to estimate the heat of formation in the liquid. We have developed an approach to predict the condensed phase heats of formation from the corresponding gas phase values for the compounds involved in the regeneration schemes. We have developed an approach to the estimation of heats of vaporization to convert our calculated gas phase heats of formation to condensed heats of formation. The gas phase calculations were carried out with the Gaussian03 program using density functional theory (DFT) with the B3LYP hybrid exchange-correlation functional and the DZVP2 basis set, except for Sn where the cc-pVDZ-PP basis set with an effective core potential was used. The calculations are done with the COSMO-RS implementation in ADF 2007. COSMO-RS is used to predict the boiling point and then the heat of vaporization is estimated from the Rule of Pictet and Trouton with $\Delta H_{vap} = T_{BP}\Delta S$, where T_{BP} is the calculated boiling point and ΔS = 22 cal/mol -K for the phase change. The electronic densities were calculated with the Becke Perdew exchange-correlation functional and the TZ2P basis set. Relativistic corrections were included at the ZORA level for heavier elements such as Sn. The inclusion of such effects introduced a negligible change. We developed new van der Waals radii and scaling factors and also tested the effects of different DFT exchange-correlation functionals.

The gas phase heats of formation are given in Table 79 and the isodesmic reaction schemes used to obtain these values are given in Table 80. Our intital test set is shown in Table 81 and a

comparison with literature data shows reasonable agreement with experiment for the types of compounds of interest.. We found that the boiling points were not strongly affected by the functional as shown in Table 82. Thus the heats of vaporization and liquid heats of formation are not strongly affected.

We developed an improved approach to predict the boiling points. Two parameterizations of the COSMO-RS method were used to predict the boiling points: (1) combi2005 and (2) Klamt. The calculated boiling points with the combi2005 parameters were within ~3 ºC for ethanol and ~9 ºC for for diethylamine. The boiling points predicted with the Klamt parameters differed from experiment by a significantly larger amount. The results for larger molecules relevant to the regeneration scheme are in Table 83. It was noticed, however, that although some compounds were still within ~ 15 ºC, some compounds containing ring atoms were off by over 100 ºC with the combi2005 parameters and by a varying amounts with the Klamt parameters. An additional COSMO-RS parameter is the Nring parameter, which is essentially the number of ring atoms in the molecule. Use of this parameter fixed the accuracy issues for benzene and phenol. Use of the Nring parameter only fixed the boiling points for non-sulfur containing compounds. The COSMO-RS parameterization uses dispersion coefficients for the non-bonded interactions in the calculation the boiling point. Cosmo-RS parameters are available elements such as H, C, N, O, and Cl but not for S. Estimates for the COSMO-RS dispersion coefficient for S of -0.0400 gave calculated boiling points in good agreement with experiment. The process was then repeated for the dispersion coefficient for B (Table 87), Al, and Sn (B = -0.026, Al = -0.033, and Sn = -0.050 in the COSMO units). The boiling points of the compounds were recalculated using the new parameters. At a phase change, the free energy $\Delta G = 0$. Thus, for example, $\Delta H_{vap} = T_{BP}\Delta S_{vap}$. Given T_{BP} and the fact that ΔS_{vap} is approximately a constant for many compounds, one can get reliable estimates of ΔH_{vap}. This was originally done by Pictet and Trouton who found values of 0.021 to 0.021 kcal/mol-K for a set of small molecules. Larger values of ΔS_{vap} are found for larger molecules and more complex expressions have been derived. Table 88 shows calculated entropies of vaporization for molecules whose enthalpy of vaporization has been reported. From this table, one can see that there are errors in the experimental ΔH_{vap} of $Sn(CH_3)_3$(t-Bu) and in the experimental TBP of $Sn(C_3H_7)_4$. The table shows that for the larger molecules, ΔS_{vap} is 25 to 26 e.u. (cal/mol-K). The final boiling points, vaporization enthalpies for different ΔS_{vap}, and calculated heat capacity data from the B3LYP/aVDZ-PP calculations are given in Table 89.

Table 79. B3LYP/DZVP2 level and B3LYP/cc-pVDZ-PP for Sn and Gas Phase Heats of Formation at 298.15 K (values in kcal/mol).[a]

Molecule	**$\Delta H_f°$**
BH_3NH_3	-14.6 ± 1.0[b]
$B_3N_3H_6$	-118.8 ± 1.0[c]
C_6H_5SH	26.60 ± 0.31[d]
$C_6H_4(SH)_2$	36.7[e]
$C_6H_4S_2BH$	12.9[e]
$C_6H_4S_2BH(NH_3)$	-4.9[e]
$(C_6H_5S)_2BH(NH_3)$	19.7[e]
$(C_6H_4S_2)_2B^-$	-19.4[e]
$HSnBu_3$	-31.0[e]
H_2SnBu_2	-11.6[e]

$C_6H_4(SSnBu_3)_2$	-47.1[e]
$C_6H_4S_2SnBu_2$	1.3[e]
$C_6H_4(SH)(SSnBu_3)$	-8.0
H_2S	-4.9 ± 0.1[f]
$HB(SH)_2$	-21.4[g]
CH_3SH	-5.46 ± 0.14[f]
CH_4	-17.89[f]
NH_3	-10.98 ± 0.084[f]
BH_3	24.4 ± 0.7[b]
BH_4^-	-14.6 ± 0.7[b]
C_5H_{12}	-35.08 ± 0.14[f]
C_2H_6	-20.04 ± 0.07[f]
$HSn(CH_3)_3$	5.0[h]
$SnBu_4$	-52.2 ± 1.8[i]
CH_3OH	-48.2 ± 0.05[d]
$Al(OCH(CH_3)_2)_3$	-257.6
$HOCH(CH_3)_2$	-65.19[f]
$Al(OCH_3)_3$	-205.9[e]
H_2O	-57.7978 ± 0.0096[f]
$B(OH)_4^-$	-321.9[j]
$B(OCH_3)_4^-$	-285.9[e]
H_2	0.0

[a] E_{elec} = electronic energy; E_{ZPE} = zero point energy; $E_0 = E_{elec} + ZPE$; R = gas constant; T = temperature, in this case, at 298.15 K. Bu = $–CH_2CH_2CH_2CH_3$. [b] Ref. 3. [c] Ref. 8. [d] Ref. 17. [e] This work. [f] Chase, M. W., Jr.; NIST-JANAF Tables, 4th Edition, *J. Phys. Chem. Ref. Data*, Mono. 9, Suppl. 1, 1998. [g] D. J. Grant and D.A. Dixon, *J. Phys. Chem. A*, 2008. [h] Ref. 40. [i] Ref. 41. [j] D. J. Grant and D.A. Dixon, CCSD(T)/CBS value.

Table 80. Gas Phase Energies of Isodesmic and Regular Reactions used to Obtain Condensed Phase Results. Values in kcal/mol at the B3LYP/DZVP2 Level and B3LYP/cc-pVDZ-PP for Sn.[a]

Molecule in condensed phase; Isodesmic/Regular Reaction	**ΔH_{rxn} (298 K)**
$C_6H_5SH + CH_3SH \rightarrow C_6H_4(SH)_2 + CH_4$	-2.3
$HB(SH)_2 + C_6H_4(SH)_2 \rightarrow C_6H_4S_2BH + 2\ H_2S$	-12.2
$C_6H_4S_2BH + BH_3NH_3 \rightarrow C_6H_4S_2BH(NH_3) + BH_3$	21.2
$C_6H_4S_2BH(NH_3) + C_6H_5SH + CH_4 \rightarrow (C_6H_5S)_2BH(NH_3) + CH_3SH$	10.5
$HSn(CH_3)_3 + 3\ C_5H_{12} \rightarrow HSnBu_3 + 3\ C_2H_6$	9.1
$2\ HSnBu_3 \rightarrow H_2SnBu_2 + SnBu_4$	-1.8
$C_6H_4(SH)_2 + 2\ HSnBu_3 \rightarrow C_6H_4(SSnBu_3)_2 + 2\ H_2$	-21.8
$C_6H_4(SH)_2 + H_2SnBu_2 \rightarrow C_6H_4S_2SnBu_2 + 2\ H_2$	-23.8
$C_6H_4(SH)_2 + HSnBu_3 \rightarrow C_6H_4(SH)(SSnBu_3) + H_2$	-13.7
$BH_4^- + 2\ C_6H_4S_2BH \rightarrow (C_6H_4S_2)_2B^- + 2\ BH_3$	17.1
$3\ CH_3OH + Al(OCH(CH_3)_2)_3 \rightarrow Al(OCH_3)_3 + 3\ HOCH(CH_3)_2$	0.1
$B(OH)_4^- + 4\ CH_3OH \rightarrow B(OCH_3)_4^- + 4\ H_2O$	-3.4

Table 81. Estimated and Experimental Boiling Points (in K) and Heats of Vaporization (in kcal/mol) for Ethanol, Ethylamine, and Sn Compounds.

Compound	BP_{cosmo}	BP_{expt}[a]	$\Delta H_{vap,cosmo}$	ΔH_{vap1}[a]	ΔH_{vap2}[b]	$\Delta\Delta H_1$[c]	$\Delta\Delta H_2$[d]
$H_2Sn(CH_3)_2$	226	-	5.0	-	-	-	-
$Sn(C_4H_9)_4$	802	-	17.6	-	19.8	-	-2.17
$Sn(C_2H_5)_4$	466	454	10.2	10.0	12.2	0.26	-1.95
$Sn(CH_3)_4$	336	351	7.4	7.7	7.9	-0.34	-0.51
$Sn(C_3H_7)_4$	626	501	13.8	11.0	16.0	2.74	-2.23
$Sn(CH_3)_3(C_2H_5)$	372	-	8.2	-	8.9	-	-0.70
$HSn(CH_3)_3$	283	-	6.2	-	-	-	-
$Sn(CH_3)_3$(t-Bu)	414	-	9.1	-	12.9	-	-3.80
Ethanol	355	351	7.8	7.7	-	0.07	-
Diethylamine	320	329	7.0	7.2	-	-0.19	-

[a] CRC Handbook. [b] From Pedley or Cox and Wagman. [c] $\Delta H_{vap,cosmo} - \Delta H_{vap1}$. [d] $\Delta H_{vap,cosmo} - \Delta H_{vap2}$.

Table 82. Boiling Points (K) for Compounds for Testing and Recycle for Different DFT Gradient Corrected Functionals.

Compound Name	BP_{B88P86}	BP_{PBE}	BP_{BLYP}	BP_{PW91}	BP_{expt}
Ethanol	354.7	353.3	351.6	354.1	351.4
Diethylamine	320.0	319.9	313.4	319.4	328.7
$Al(OCH_3)_3$	439.0	437.8	436.4	438.4	
$H_2Sn(CH_3)_2$	302.8	302.8	301.8	302.5	
$H_2Sn(C_4H_9)_2$	530.8	530.5	526.8	530.0	
$HSn(CH_3)_3$	335.8	336.2	333.7	335.8	
$HSn(C_4H_9)_3$	682.7	682.8	676.5	682.1	
$Sn(CH_3)_4$	367.3	368.2	364.3	368.0	351.2
$Sn(C_2H_5)_4$	475.3	476.0	470.8	475.7	454.2
$Sn(C_3H_7)_4$	635.1	640.4	633.9	640.0	501.2
$Sn(C_4H_9)_4$	803.9	808.8	800.4	808.1	
$Sn(CH_3)_3(C_2H_5)$	396.8	397.7	393.3	397.4	
$Sn(CH_3)_3$(t-Bu)	431.6	432.2	427.1	431.9	
$BH_3NH_2CH_3$	558.6	557.6	557.0	556.9	
$BH_3NH(C_2H_5)_2$	541.8	540.8	540.3	538.6	
$B_3N_3H_9(CH_3)_3$	645.8	645.0	640.2	643.6	
$NH_3BH(SPh)_2$	1016.1	1016.8	1004.4	1015.2	
C_6H_6	353.3	355.6	348.7	356.1	353.2
C_6H_5SH	431.0	433.3	426.2	433.3	442.3
1, 2-$C_6H_4(SH)_2$	518.0	521.9	502.5	521.7	511.7
1,2-$C_6H_4S_2BH:NH_3$	842.8	841.9	827.9	840.0	
1,2-$C_6H_4S_2BH:NH(C_2H_5)_2$	876.5	877.4	869.3	877.1	
1,2-$C_6H_4S_2Sn(C_4H_9)_2$	927.1	930.7	921.3	930.4	
1,2-$C_6H_4(SH)(SSn(C_4H_9)_3)$	1028.2	1030.3	1020.3	1030.1	
1,2-$C_6H_4(SSn(C_4H_9)_3)_2$	1512.9	1515.0	1499.8	1513.2	
CH_3I	308.0	306.1	303.4	305.8	315.7

CH_2I_2	440.6	439.4	438.5	439.0	455.2
C_2H_5I	348.7	347.2	344.2	346.8	345.7
$C_2H_4I_2$	483.2	480.0	480.2	479.8	-
C_6H_5I	493.1	494.9	489.3	495.0	461.6
CH_3Br	275.8	275.1	273.4	275.2	276.7
CH_2Br_2	365.6	-	364.7	364.5	370.2
C_2H_5Br	315.6	314.6	312.7	314.6	311.7
$C_2H_4Br_2$	408.4	407.0	408.1	407.2	404.8
C_6H_5Br	457.0	458.2	453.3	458.5	429.2
CH_3Cl	249.7	249.2	247.9	249.1	249.1
CH_2Cl_2	314.9	313.8	314.4	313.7	313.2
C_2H_5Cl	288.2	287.3	285.7	287.1	285.5
$C_2H_4Cl_2$	354.5	353.1	354.4	353.2	356.7
C_6H_5Cl	426.2	427.3	422.7	427.2	404.9

Table 83. Comparing Methods Within COSMO-RS. The Enthalpies of Formation were calculated by multiplying the Boiling Points (BP) by 0.022 kcal/mol.K. BP in K and ΔH_{vap} in kcal/mol.

Compound	$BP_{cosmo-RS, combi2005}$	$BP_{cosmo-RS, Klamt}$	$BP_{exp,CRC}$	$BP_{exp, NIST}$	$\Delta H_{vap,cosmo-RS, combi2005}$	$\Delta H_{vap,cosmo-RS, Klamt}$	$\Delta H_{vap,exp, CRC}$	$\Delta H_{vap, exp, Pedley/Cox \& Pilcher, Wagman}$	$\Delta H_{vap, exp, NIST}$
Ethanol	354.7	427.2	351.4	351.5	7.80	9.40	7.73	10.1 ± 0.1	10 ± 0.6
Diethylamine	320.0	405.1	328.6	328.7	7.04	8.91	7.23	7.5 ± 0.3	7.5
$H_2Sn(CH_3)_2$	226.3	285.6			4.98	6.28		6.5	6.8
$Sn(C_4H_9)_4$	801.6	999.3			17.63	21.98		19.8 ± 0.5	19.8 ± 0.5
$Sn(C_2H_5)_4$	465.9	578.4	454.2	473.1	10.25	12.72	9.99	12.2 ± 0.5	12.1 ± 0.5
$Sn(CH_3)_4$	336.1	421.3	351.2	351.0	7.39	9.27	7.73	7.9 ± 0.3	7.6 ± 0.2
$Sn(C_3H_7)_4$	626.0	779.8	501.2		13.77	17.16	11.03	16.0 ± 0.5	15.6 ± 0.6
$Sn(CH_3)_3(C_2H_5)$	372.5	466.2			8.20	10.26		9.0 ± 0.4	9.0 ± 0.4
$HSn(CH_3)_3$	283.0	356.2			6.23	7.84		7.1	7.2
$Sn(CH_3)_3$(t-Bu)	413.7	519.4			9.10	11.43		12.9 ± 1.0	

Table 84. Comparing Methods with and without the Nring Parameter in COSMO-RS. BP in K.

Compound	$BP_{noNring, combi2005}$	$BP_{Nring, combi2005}$	$BP_{noNring, Klamt}$	$BP_{Nring, Klamt}$	$BP_{exp, NIST}$	$BP_{exp, CRC}$
PhSH	290.70	356.24	359.20	431.88	441.90	442.25
1, 2 $Ph(SH)_2$	319.63	383.02	396.29	467.38	511.70	511.65
1, 3 $Ph(SH)_2$	304.09	366.85	379.75	450.71	518.20	518.15
C_6H_6	286.16	353.30	347.46	420.66	353.3 ± 0.1	353.24
C_6H_6O	402.50	456.45	503.74	571.19	455.0 ± 0.6	455.02

Table 85. Comparing Methods Within COSMO-RS on Compounds that are to be used in the Regeneration Scheme. The Enthalpies of Formation were alculated by multiplying the Boiling Points by 0.022 kca/mol.K. BP in K and ΔH_{vap} in kcal/mol.

Compound	$BP_{noNring, combi2005}$	$BP_{noNring, Klamt}$	$BP_{Nring, combi2005}$	$BP_{Nring, Klamt}$	$\Delta H_{vap,noNring, combi2005}$	$\Delta H_{vap,noNring, Klamt}$	$\Delta H_{vap,Nring, combi2005}$	$\Delta H_{vap,Nring, Klamt}$
$Al(OCH_3)_3$	465.52	603.97	-	-	10.24	13.29	-	-
PhS_2BHNH_3	641.93	795.58	736.39	901.56	14.12	17.50	16.20	19.83

$HSn(C_4H_9)_3$	649.14	812.18	-	-	14.28	17.87	-	-
$PhSHSSn(C_4H_9)_3$	830.71	1054.63	902.29	1130.87	18.28	23.20	19.85	24.88
$H_2Sn(C_4H_9)_2$	464.12	584.59	-	-	10.21	12.86	-	-
$PhS_2Sn(C_4H_9)_2$	695.26	887.76	765.39	963.26	15.30	19.53	16.84	21.19
$NH_3BH(SPh)_2$	779.90	992.87	911.28	1139.09	17.16	21.84	20.05	25.06
$Ph(SSn(C_4H_9)_3)_2$	1348.39	1717.28	1420.85	1794.23	29.66	37.78	31.26	39.47

Table 86. Comparing Dispersion Coefficient Parameters for Sulfur Containing Compounds. BP in K.

Compound	**$BP_{combi2005}$**	**$BP_{combi2005, -0.0333}$**	**$BP_{combi2005, -0.0366}$**	**$BP_{combi2005, -0.0400}$**	**$BP_{exp, NIST}$**	**$BP_{exp, CRC}$**
PhSH	356.24	418.46	424.68	431.09	441.90	442.25
1, 2 $Ph(SH)_2$	383.02	495.07	506.36	518.03	511.70	511.65
1, 3 $Ph(SH)_2$	366.85	489.48	501.87	514.67	518.20	518.15

Table 87. Comparing Dispersion Coefficient Parameters for Boron Containing Compounds.

Compound	**$BP_{combi2005}$**	**$BP_{combi2005, -0.0184}$**	**$BP_{combi2005, -0.0224}$**	**$BP_{combi2005, -0.0264}$**	**$BP_{exp, NIST}$**
$B_3N_3H_6$	295.65	322.23	328.08	333.91	326.15
$B(C_2H_5)_2$	346.90		349.36		321.81
BCl_3	325.05		329.83		285.65

Table 88. Comparison of ΔS_{vap} obtained from $\Delta HS_{vap} = T\Delta S_{vap}$ in cal/mol-K.

Compound	ΔH_{vap} kcal/mol	ΔS_{vap} $BP_{cosmo\text{-}RS,}$ combi2005	ΔS_{vap} BP_{CRC} Handbook
$H_2Sn(CH_3)_2$	6.5	22.7*	-
$Sn(C_4H_9)_4$	19.8	24.7	-
$Sn(C_2H_5)_4$	12.2	26.2	25.8
$Sn(CH_3)_4$	7.9	23.5	22.5
$Sn(C_3H_7)_4$	16.0	25.6	31.9
$Sn(CH_3)_3(C_2H_5)$	9.0	24.2	-
$HSn(CH_3)_3$	7.1	25.1	-
$Sn(CH_3)_3$(t-Bu)	12.9	31.2	-
Ethanol	10.1	28.5	28.7
Diethylamine	7.5	23.4	22.8
C_6H_6	8.0 ± 0.2	22.6	22.6

*T = 285.6

Table 89. Compounds for Regeneration Scheme with the Best Calculated BP's and Different Values of the Entropy of Vaporization. BP in K, ΔH_{vap} in kcal/mol, C_v and ΔS_{vap} in cal/mol-K.

Compound	$BP_{cosmo\text{-}RS}$	$\Delta H_{vap,\ cosmo\text{-}RS,}$ $\Delta S_{vap} = 22$	$\Delta H_{vap,\ cosmo\text{-}RS,}$ $\Delta S_{vap} = 25$	$\Delta H_{vap,\ cosmo\text{-}RS,}$ $\Delta S_{vap} = 26$	C_v
$Al(OCH_3)_3$	487.1	10.7	12.2	12.7	33.8
PhS_2BHNH_3	854.8	18.8	21.4	22.2	36.9
$HSn(C_4H_9)_3$	672.3	14.8	16.8	17.5	70.0
$PhSHSSn(C_4H_9)_3$	1027.9	22.6	25.7	26.7	102.4
$H_2Sn(C_4H_9)_2$	511.5	11.3	12.8	13.3	51.2
$PhS_2Sn(C_4H_9)_2$	891.6	19.6	22.3	23.2	76.8
$NH_3BH(SPh)_2$	1017.7	22.4	25.4	26.5	59.7
$Ph(SSn(C_4H_9)_3)_2$	1502.8	33.1	37.6	39.1	175.5
$H_2Sn(CH_3)_2$	280.8	6.2	7.0	7.3	22.3
$Sn(C_4H_9)_4$	808.8	17.8	20.2	21.0	87.4
$Sn(C_2H_5)_4$	472.4	10.4	11.8	12.3	54.5
$Sn(CH_3)_4$	353.0	7.8	8.8	9.2	35.8
$Sn(C_3H_7)_4$	632.6	13.9	15.8	16.4	73.6
$Sn(CH_3)_3(C_2H_5)$	386.7	8.5	9.7	10.1	40.5
$HSn(CH_3)_3$	318.5	7.0	8.0	8.3	29.1
$Sn(CH_3)_3$(t-Bu)	421.9	9.3	10.5	11.0	51.7
Ethanol	354.7	7.8	8.9	9.2	14.2
Diethylamine	320.0	7.0	8.0	8.3	30.9
PhS_2BHNH_3	854.8	18.8	21.4	22.2	36.9
$PhS_2BHNH(C_2H_5)_2$	871.8	19.2	21.8	22.7	56.2
$CH_3NH_2BH_3$	586.7	12.9	14.7	15.3	16.2
$B_3N_3H_9(CH_3)_3$	668.7	14.7	16.7	17.4	42.9

$BH_3NH(C_2H_5)_2$	557.2	12.3	13.9	14.5	31.0

The efficiency calculations shown in Table 90 are for the preferred LANL route and represent an update from previous work. The efficiency is above 60% even with no heat recovery. The efficiency of the only competing scheme published in the literature is under 50%.

Table 90. Equations used to Assess Regeneration Efficiency in kcal/mol.

Current Demonstrated Scheme	**ΔH**
⅓ $B_3N_3H_6$ (l) + $C_6H_4(SH)_2$ (l) → $C_6H_4S_2BH(NH_3)$ (l)	-6.8
½ $C_6H_4S_2BH(NH_3)$ (l) + ½ $C_6H_4(SH)_2$ (l) → ½ $[NH_4][B(C_6H4S_2)_2]$ (s) + ½ H_2 (g)	7.0
½ $[NH_4][B(C_6H4S_2)_2]$ (s) + ½ Bu_3SnH (l) → ½ $C_6H_4S_2BH(NH_3)$ (l) + ½ $C_6H_4(SH)(SSnBu_3)$ (l)	-12.4
$C_6H4S_2BH(NH_3)$ (l) + H_2SnBu_2 (l) → BH_3NH_3 (s) + $C_6H_4S_2SnBu_2$ (l)	-9.7
$C_6H_4S_2SnBu_2$ (l) + 2 H_2 (g) → $C_6H_4(SH)_2$ (l) + H_2SnBu_2 (l)	21.9
½ $C_6H_4(SH)(SSnBu_3)$ (l) + ½ H_2 (g) → ½ $C_6H_4(SH)_2$ (l) + ½ $HSnBu_3$ (l)	5.3
Overall reaction: ⅓ $B_3N_3H_6$ (l) + 2 H_2 (g) → BH_3NH_3 (s)	**5.4**
Sum of exothermicities	*-28.9*
Sum of endothermicities	*34.3*
Efficiency with 0% heat recovery	65%
Efficiency with 20% heat recovery	67%

Regeneration Scheme (Ramachandran, P. V.; Gagare, P. D. *Inorg. Chem.* 2007, *46*, 7810)	**ΔH**
$NH_4B(OMe)_4$ (s) + NH_4Cl (s) + $LiAlH_4$ (s) → NH_3BH_3 (s) + $Al(OMe)_3$ (l) + MeOH (l) + H_2 (g) + LiCl (s) + NH_3 (g)	-62.4
NaCl (s) + electricity → Na (s) + ½ Cl_2 (g)	98.2
½ Cl_2 (g) + ½ H_2 (g) → HCl (g)	-22.1
HCl (g) + NH_3 (g) → NH_4Cl (s)	-42.1
$Al(OMe)_3$ (l) + 3/2 H_2 (g) + electricity → Al (s) + 3 MeOH (l)	45.0
Na (s) + Al (s) + 2 H_2 (g) → $NaAlH_4$ (s)	-27.6
LiCl (s) + $NaAlH_4$ (s) → $LiAlH_4$ (s) + NaCl (s)	2.4
Overall reaction: $NH_4B(OMe)_4$ (s) + 3 H_2 (g) → NH_3BH_3 (s) + 4 MeOH (l)	**-8.6**
Sum of exothermicities	*-154.2*

Sum of endothermicities	*145.6*
Efficiency with 0% heat recovery	46%
Efficiency with 20% heat recovery	50%

Oxidation of $B_3N_3H_6$ & $B_3N_3H_{12}$

We have previously calculated the heat of formation of $B_3N_3H_6$ and $B_3N_3H_{12}$ in the gas and condensed phases The oxidation processes of $B_3N_3H_6$ and $B_3N_3H_{12}$ at 298 K are found in Table 91 using the following heats of formation: $\Delta H_{f,298K}$(BO) = 71.4 kcal/mol (new result); $\Delta H_{f,298K}$(NO) = 22.3 kcal/mol; $\Delta H_{f,298K}$($B_3N_3H_6$, gas) = -115.5 kcal/mol; $\Delta H_{f,298K}$($B_3N_3H_6$, liquid) = -122.6 kcal/mol; $\Delta H_{f,298K}$($B_3N_3H_6$, solid) = -123.6 kcal/mol; $\Delta H_{f,298K}$($B_3N_3H_{12}$, gas) = -96.6 kcal/mol; $\Delta H_{f,298K}$($B_3N_3H_{12}$, solid) = -120.5 kcal/mol; $\Delta H_{f,298K}$(H_2O, gas) = -58.1; and $\Delta H_{f,298K}$(H_2O, liquid) = -68.3.

Table 91. Accurate Reaction Energies at 298 K for the Oxidation of $B_3N_3H_6$ and $B_3N_3H_{12}$ in kcal/mol.

Reaction	**ΔH_{298K}**
$B_3N_3H_6$ (g) + 3 O_2 (g)→ 3 BO (g) + 3 NO (g) + 3 H_2 (g)	396.6
$B_3N_3H_6$ (l) + 3 O_2 (g)→ 3 BO (g) + 3 NO (g) + 3 H_2 (g)	403.7
$B_3N_3H_6$ (s) + 3 O_2 (g)→ 3 BO (g) + 3 NO (g) + 3 H_2 (g)	404.7
$B_3N_3H_6$ (g) + 9/2 O_2 (g) → 3 BO (g) + 3 NO (g) + 3 H_2O (g)	222.3
$B_3N_3H_6$ (l) + 9/2 O_2 (g) → 3 BO (g) + 3 NO (g) + 3 H_2O (l)	198.8
$B_3N_3H_6$ (s) + 9/2 O_2 (g) → 3 BO (g) + 3 NO (g) + 3 H_2O (l)	199.8
$B_3N_3H_{12}$ (g) + 3 O_2 (g)→ 3 BO (g) + 3 NO (g) + 6 H_2 (g)	377.7
$B_3N_3H_{12}$ (s) + 3 O_2 (g)→ 3 BO (g) + 3 NO (g) + 6 H_2 (g)	401.6
$B_3N_3H_{12}$ (g) + 6 O_2 (g) → 3 BO (g) + 3 NO (g) + 6 H_2O (g)	29.1
$B_3N_3H_{12}$ (s) + 6 O_2 (g) → 3 BO (g) + 3 NO (g) + 6 H_2O (l)	-8.2

We found that $B_3N_3H_6$, the product resulting from loss of H_2 from BH_3NH_3, is not readily oxidized in the gas phase or in condensed phase. A similar result can be found for the $B_3N_3H_{12}$ when 3 equivalents of O_2 are used and H_2 is one of the products. However, the endothermicity of the gas phase process can be greatly reduced when 6 equivalents of O_2 are used and H_2O is produced. Furthermore, the oxidation of $B_3N_3H_{12}$ by 6 O_2, in the condensed phase, was found to be an exothermic process.

Hydrazine Chemistry

There is substantial interest in the development of new chemical approaches to regeneration of spent fuel. LANL has developed an approach based on using hydrazine. We have been exploring the chemistry of this novel reactant. Potential energy surfaces for H_2 release from hydrazine interacting with borane, alane, diborane, dialane and borane-alane were constructed from MP2/aVTZ geometries and zero point energies with single point energies at the CCSD(T)/aug-cc-pVTZ level. With one borane or alane molecule, the energy barrier for H_2-

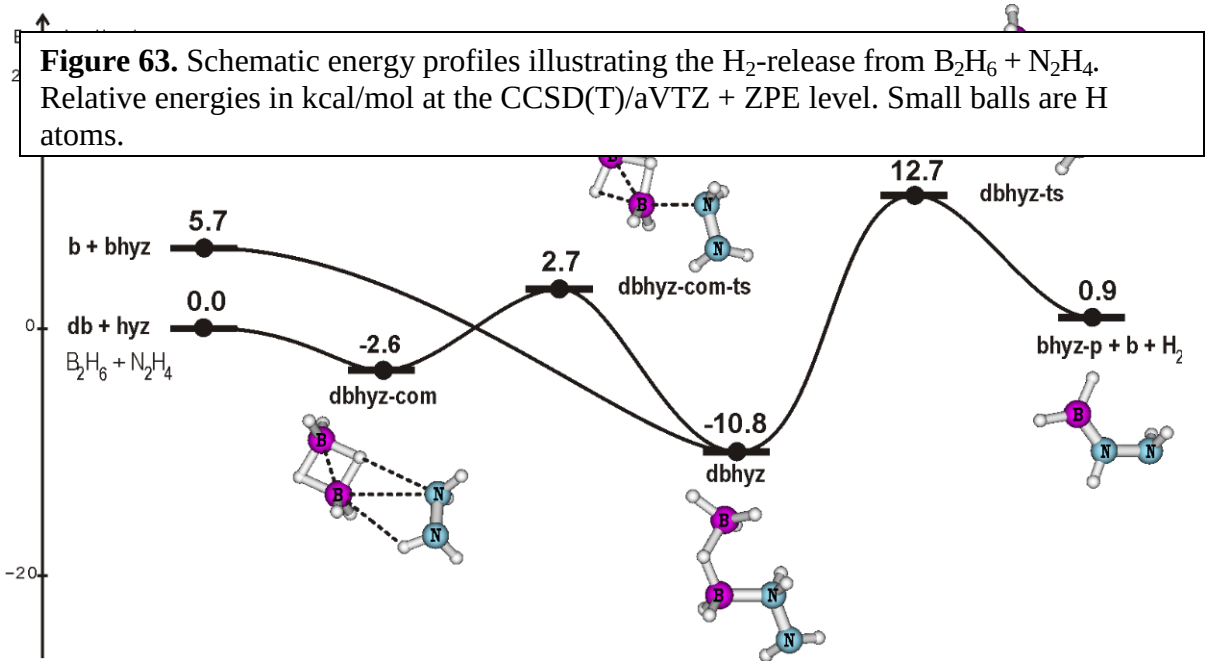

Figure 63. Schematic energy profiles illustrating the H_2-release from $B_2H_6 + N_2H_4$. Relative energies in kcal/mol at the CCSD(T)/aVTZ + ZPE level. Small balls are H atoms.

loss of ~38 or 30 kcal/mol does not compete with the B–N or Al-N bond cleavage (~30 or ~28 kcal/mol). The second borane or alane molecule can play the role of a bifunctional catalyst. The barrier energy for H_2 elimination is reduced from 38 to 23 kcal/mol, or 30 to 20 kcal/mol in the presence of diborane or dialane, respectively. The mixed borane-alane dimer reduces the

barrier energy for H_2 release from hydrazine to ~17 kcal/mol. A systematic comparison with the reaction pathways from ammonia borane shows that hydrazine could be alternative for ammonia in producing borane amine derivatives.

The results show a significant effect of the NH_2 substituent on the relevant thermodynamics. The B-N dative bond energy of 31 kcal/mol in $NH_2NH_2BH_3$ is ~5 kcal/mol larger than that of the parent BH_3NH_3. the condensation reaction of hydrazine with either borane or diborane is similar to that of ammonia with borane or diborane. The terminal amino group induces a small substitutent effect, but does not actively participate in the H-atom transfer relay and thus does not modify qualitatively the energetic landscape. Comparison with H_2-elimination from **dbhyz** (diborane) or **dalhyz** (dialane) shows that H_2-release from the mixed adduct **balhyz** is the most favored in terms of the lowest energy barriers and optimal heats of reaction.

The process involving two alane molecules will be less useful due to the high exothermicity and the inability to regenerate the alane. The condensation of borane and alane forming the mixed dimer BH_3AlH_3 is a better choice for H_2-release from hydrazine. In both cases, the presence of alane improves the reaction kinetics for H_2-release from borane amine derivatives. The mechanism for H_2-release from reactions of hydrazine with either borane or alane or a mixture is similar to that of ammonia with the H_2 being eliminated across the B-N or Al-N bonds. Substitution of an H atom of ammonia by an amino group induces a quantitative effect on the reaction energetics, by stabilizing both the dative adduct and TS for H_2-release. The additional amino group acts as a substituent and does not actively participate in the H atom transfer relay which occurs across the B-N or Al-N bonds. The best process is for $AlH_3 + BH_3$

+ N_2H_4 where the BH_3 adds to the hydrazine and the AlH_3 catalyzes the removal of H_2 across the B-N bond and is readily regenerated with an overall weakly exothermic process.

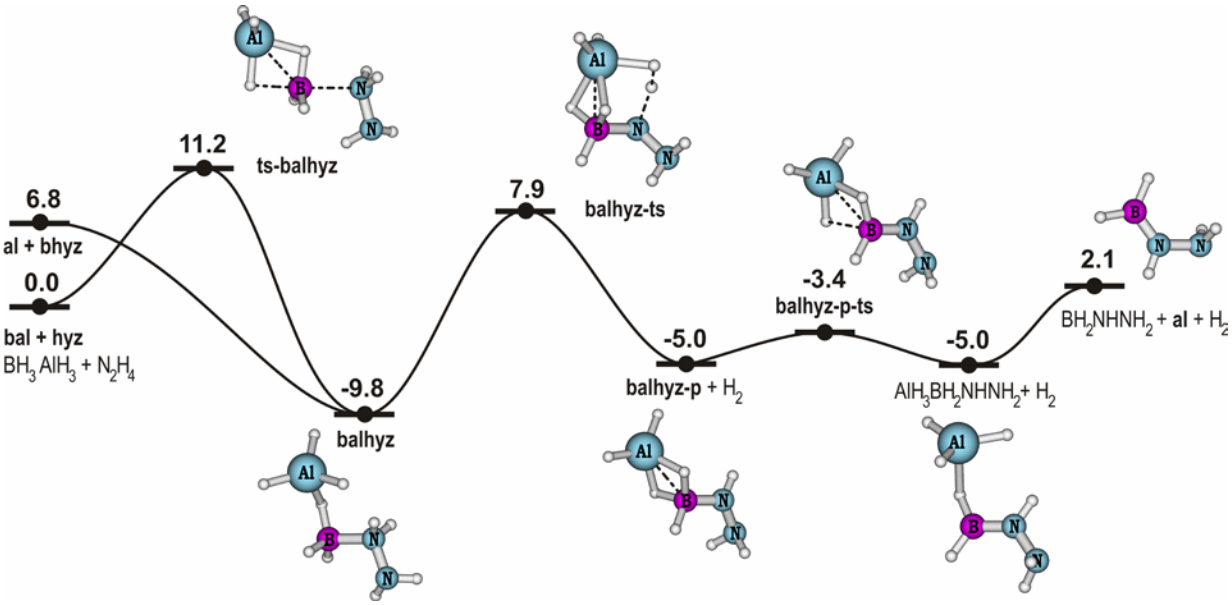

Figure 64. Energy profiles showing the pathways for H_2-release from AlH_3 + BH_3 + N_2H_4. Relative energies in kcal/mol at the CCSD(T)/aVTZ + ZPE level. Small balls are H atoms.

On the basis of the above results, we have studied models of spent fuel reacting with N_2H_4. We have studied the 1st step of the reaction with BNH_2 and BNH_x, $1<x<2$ models of spent fuel as shown in Figure 65. These models of spent fuel can be considered to be the equivalent of benzene ($B_3N_3H_6$), naphthalene ($B_5N_5H_8$) and pyrene ($B_8N_8H_{10}$).

The reaction of $B_3N_3H_6$ with N_2H_4 showed the novel result that breaking the N-N bond in N_2H_4 and adding NH_2 at two different B-H sites leads to cleavage of the $B_3N_3H_6$ ring so that the reaction is proceeding to generate the compounds much closer to BH_3NH_3. This reaction is substantially exothermic.

The reaction of N_2H_4 at the bridgehead B position in the naphthalene-like model after splitting the N-N bond and reacting with the other B-H groups does not lead to ring breaking and the reaction is exothermic. Initial reaction at the B-H group does not lead to any different processes with the NH_2 group migrating to the bridgehead B. Reaction at the other symmetry unique B-H group also leads to exothermic cleavage of the N-N bond but does not lead to ring cleavage.

For the pyrene model, the addition of the N_2H_4 to the 1 B-H position leads to ring cleavage as in the $B_3N_3H_6$ case and is a highly exothermic process. The other exothermic processes for cleaving the N-N bond do not lead to ring cleavage and are less exothermic.

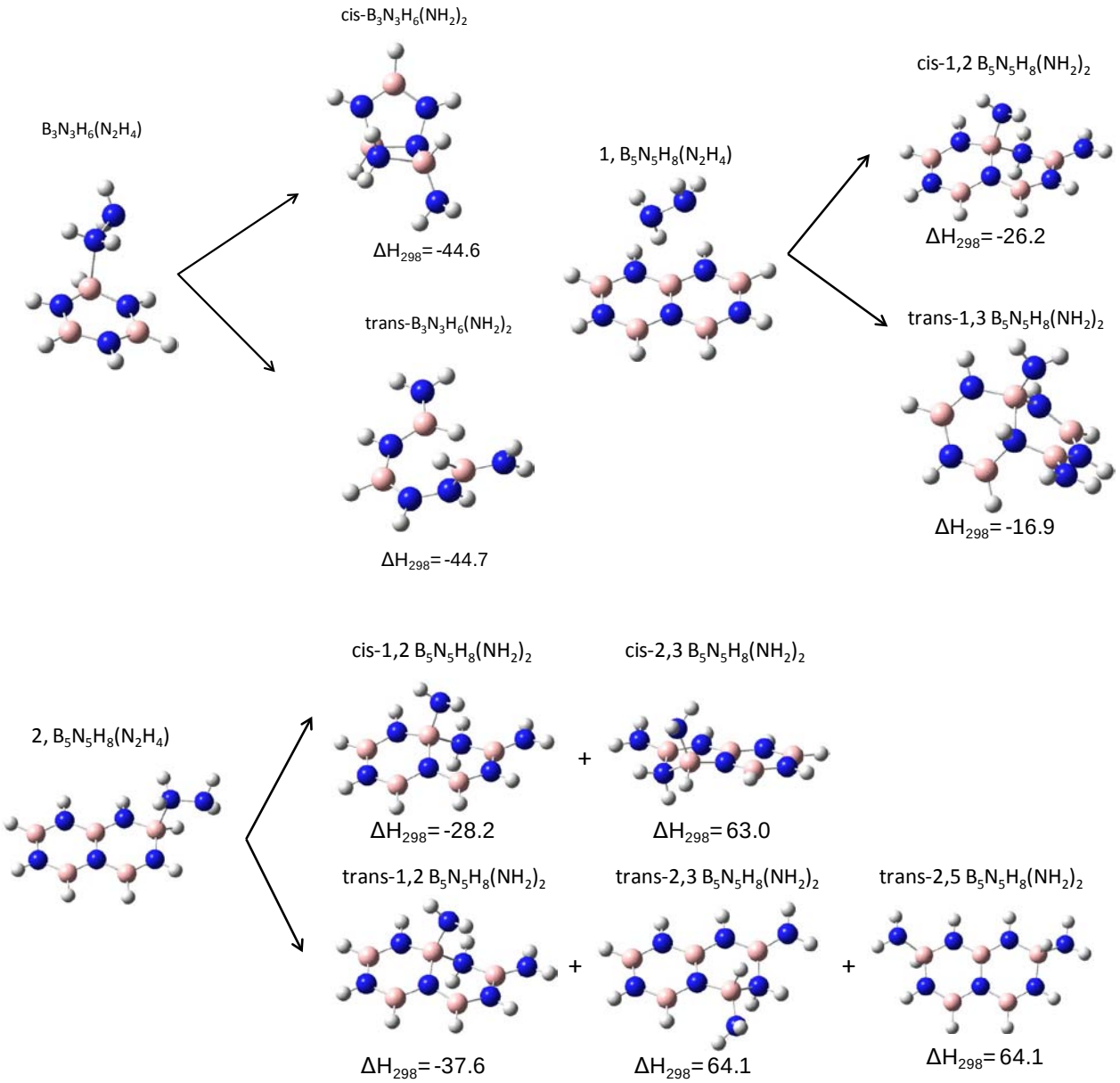
cis-$B_3N_3H_6(NH_2)_2$
$B_3N_3H_6(N_2H_4)$
ΔH_{298}= -44.6
trans-$B_3N_3H_6(NH_2)_2$
ΔH_{298}= -44.7
1, $B_5N_5H_8(N_2H_4)$
cis-1,2 $B_5N_5H_8(NH_2)_2$
ΔH_{298}= -26.2
trans-1,3 $B_5N_5H_8(NH_2)_2$
ΔH_{298}= -16.9
2, $B_5N_5H_8(N_2H_4)$
cis-1,2 $B_5N_5H_8(NH_2)_2$
ΔH_{298}= -28.2
cis-2,3 $B_5N_5H_8(NH_2)_2$
ΔH_{298}= 63.0
trans-1,2 $B_5N_5H_8(NH_2)_2$
ΔH_{298}= -37.6
trans-2,3 $B_5N_5H_8(NH_2)_2$
ΔH_{298}= 64.1
trans-2,5 $B_5N_5H_8(NH_2)_2$
ΔH_{298}= 64.1

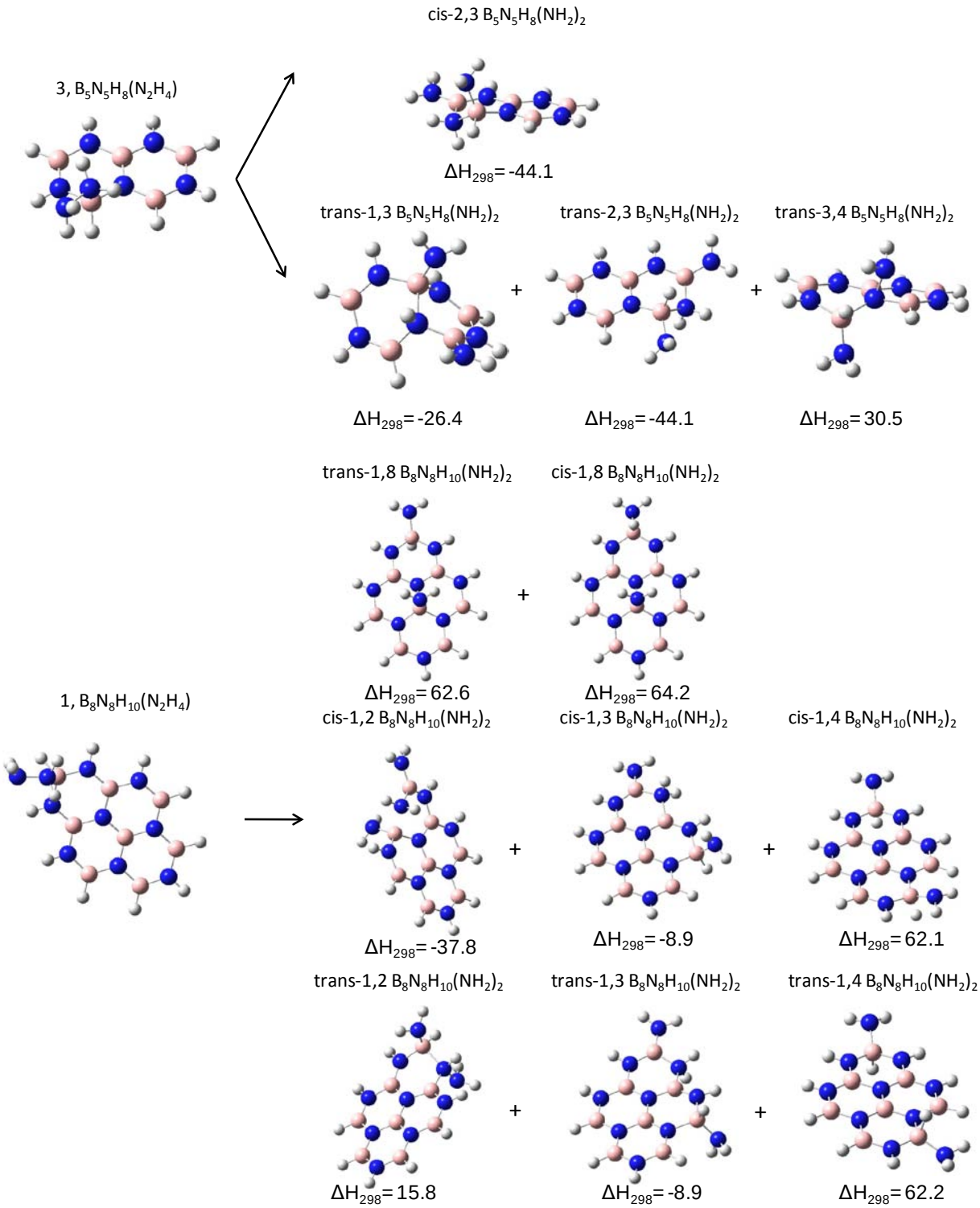

Figure 65. Thermodynamic values at 298K for the 1st step reaction enthalpies in kcal/mol for the addition of N_2H_4 to models of spent fuel.

We have also calculated the B-N bond dissociation energies (BDEs) for different amines relative to hydrazine (N_2H_4) for LANL's new regeneration pathway. These are shown in the following tables. Table 92 shows the benchmarking of the different methods for the simplest B-N bonds for BH_3 binding to NH_3 and N_2H_4. Table 93 shows all of the different amines and energies studied with pictures below. The B-N BDE to BH_3 for hydrazine is about 5 kcal/mol stronger than for NH_3. The G3MP2 BDE is good within 1.5 kcal/mol and B3LYP is reasonable within 3.0 kcal/mol.

Table 92. Calibration of Methods for the B-N BDE in BH_3-NH_2NH_2 and BH_3-NH_3 in kcal/mol

BDE	**CCSD(T)/CBS**		**B3LYP/DZVP22**		**G3MP2**	
	0K	**298K**	**0K**	**298K**	**0K**	**298K**
BH_3-NH_2NH_2	31.0	32.2	28.2	29.6	32.2	33.6
BH_3-NH_3	26.1	27.7	23.4	25.2	26.0	27.7

Table 93. Hz-BH_3+Amine → R-BH_3+Hz (Hz = hydrazine) Relative Reaction Energies and Absolute BDEs in kcal/mol. Absolute BDEs Obtained Relative to CCSD(T) Values for $BH_3NH_2NH_2$ given above

Amine	**B3LYP ΔΔH(rel BDE)**		**G3MP2 ΔΔH(Rel BDE**		**B3LYP BDE absolute rel to CCSD(T) NH_2NH_2**		**G3MP2 BDE absolute rel to CCSD(T) NH_2NH_2**	
	0K	**298K**	**0K**	**298K**	**0K**	**298K**	**0K**	**298K**
$NH_2(CH_2)_2NH_2$	0.6	0.7	0.6	0.8	31.6	32.9	31.6	33.0
$NH_2(CH_2)_2NH_2BH_3$	3.1	3.3	3.0	3.3	34.1	35.5	34.0	35.5
1,2-NH_2 cyclohexane	-2.9	-2.9	-2.7	-2.5	28.1	29.3	28.3	29.7
1,2-NH_2BH_3 cyclohexane	3.8	3.7	2.6	2.7	34.8	35.9	33.6	34.9
1,3-NH_2 cyclohexane	0.6	0.9	0.4	0.7	31.6	33.1	31.4	32.9
1,3-NH_2BH_3 cyclohexane	2.7	2.9	2.3	2.6	33.7	35.1	33.3	34.8
1,4-NH_2 cyclohexane	2.0	2.1	1.5	1.8	33.0	34.3	32.5	33.9
1,4-NH_2BH_3 cyclohexane	2.3	2.6	2.0	2.2	33.3	34.8	33.0	34.4
2,6-luthidine	3.4	3.4	2.8	2.8	34.4	35.6	33.8	35.0
2,6-diMe-N-cyclohexane	3.4	3.6	0.7	1.0	34.4	35.8	31.7	33.2
4-diMeAminoPy	1.2	1.2	0.4	0.5	32.2	33.4	31.4	32.7
Ph-NH_2	8.0	8.2	7.0	7.3	39.0	40.4	38.0	39.5
2.6.diMePhNH_2	7.7	8.0	6.5	6.7	38.7	40.2	37.5	38.9
Et_2PhN	7.0	6.9	1.7	1.7	38.0	39.1	32.7	33.9
Me_2PhN	8.7	8.5	2.9	2.7	39.7	40.7	33.9	34.9
$(C_8H_{18})_3N$	3.0	2.9			34.0	35.1		
allylNH_2	0.4	0.5	0.3	0.5	31.4	32.7	31.3	32.7
Et_3N	3.3	3.0	-1.9	-2.0	34.3	35.2	29.1	30.2
Et_2NH	0.8	0.9	-1.5	-1.5	31.8	33.1	29.5	30.7
EtMeNH	-0.7	-0.6	-2.6	-2.5	30.4	31.6	28.4	29.7

Me_3N	-0.9	-0.8	-4.4	-4.4	30.1	31.4	26.6	27.8
Me_2NH	-1.6	-1.5	-3.3	-3.3	29.5	30.7	27.7	28.9
NH_3	4.7	4.4	6.2	5.9	35.7	36.6	37.2	38.1
Me_2S	9.4	9.8	7.8	8.3	40.4	42.0	38.8	40.5
Et_2S	8.8	9.2	6.9	7.4	39.8	41.4	37.9	39.6
Ph_2S	14.4	14.8	12.1	12.7	45.7	47.0	43.1	44.9
Me_2O	14.5	14.7	13.4	13.8	45.5	46.9	44.4	46.0

Diagrams for Molecules Presented in Table 93 Above.

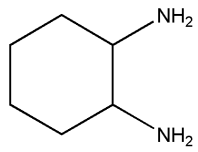	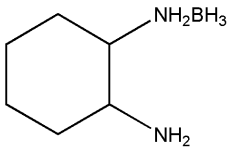	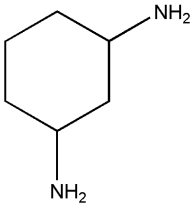	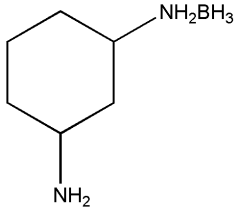
1,2-NH_2 cyclohexane	1,2-NH_2BH_3 cyclohexane	1,3-NH_2 cyclohexane	1,3-NH_2BH_3 cyclohexane
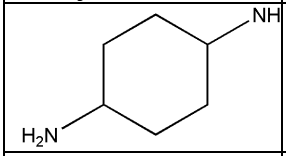	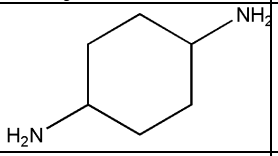	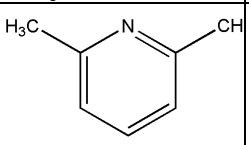	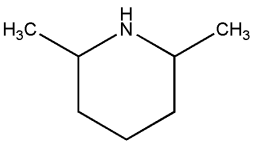
1,4-NH_2 cyclohexane	1,4-NH_2BH_3 cyclohexane	2,6-luthidine	2,6-diMe-N-cyclohexane
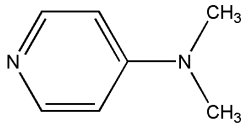	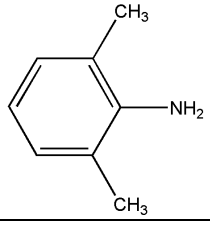	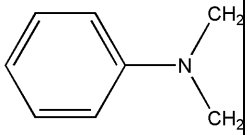	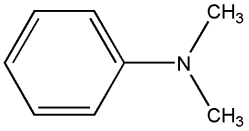
4-diMeAminoPy	2.6.diMePhNH_2	Et_2PhN	Me_2PhN

The B3LYP B-N BDEs are within a couple of kcal/mol for all compounds except for the tri-substituted ones at N where they are about 5 to 6 kcal/mol too strongly bonded as compared to the G3MP2 values, so the $(C_8H_{18})_3N$ B3LYP B-N BDE is probably overbound by about 5 kcal/mol.

We also looked at the following reaction of hydrazine with a current component of spent fuel.

$C_6H_4S_2BHNH_3 + NH_2NH_2 \rightarrow C_6H_4S_2BHNH_2NH_2 + NH_3$
$\Delta H(0K, B3LYP) = -4.4$ $\Delta H(298K, B3LYP) = -4.0$ kcal/mol
$\Delta H(0K, G3MP2) = -7.2$ $\Delta H(298K, G3MP2) = -6.8$ kcal/mol (112)

We continued to explore the chemistry of this novel reactant, hydrazine by extending our study, we have continued to investigate models of spent fuel reacting with N_2H_4. Calculations using the G3MP2B3 method have been done for the first addition and trans second and third

additions of N_2H_4 to $B_3N_3H_6$. The NMR ^{11}B chemical shifts do not change because the optimized geometries are practically the same for the DFT/B3LYP and G3MP2B3 methods. The resulting G3MP2B3 reaction energies differ by up to about 4 kcal/mol from the DFT/B3LYP values. Table 94 compares the difference between the heats of formation for the DFT/B3LYP and the G3MP2B3 methods. The B3LYP geometries were critical to this study as the HF and MP2 geometries used in G3MP2 are often giving different, higher energy structures. Figure 66 more clearly shows how many different products and pathways there potentially are for the addition of N_2H_4 to $B_3N_3H_6$ while Figure 67 shows how many products and pathways there are after just one addition of N_2H_4 to a larger $B_xN_xH_y$ molecule such as BNH.

Table 94. DFT/B3LYP ΔH_{298} Compared to G3MP2B3 ΔH_{298} for Compounds in Figure 66.

Reactions	**DFT/B3LYP**	**G3MP2B3**
$B_3N_3H_6 + N_2H_4 \rightarrow B_3N_3H_6(N_2H_4)$	4.5	0.3
$B_3N_3H_6(N_2H_4) \rightarrow$ cis-$B_3N_3H_6(NH_2)_2$	5.0	5.6
$B_3N_3H_6(N_2H_4) \rightarrow$ trans-$B_3N_3H_6(NH_2)_2$	-2.3	-1.1
i1, (trans-$B_3N_3H_6(NH_2)_2)N_2H_4 \rightarrow$ cis-o1,2 (trans-$B_3N_5H_{10})(NH_2)_2$	-18.7	-22.9
i1, (trans-$B_3N_3H_6(NH_2)_2)N_2H_4 \rightarrow$ cis-o1,3 (trans-$B_3N_5H_{10})(NH_2)_2$	-54.9	-52.8
i1, (trans-$B_3N_3H_6(NH_2)_2)N_2H_4 \rightarrow$ trans-i1,2 (trans-$B_3N_5H_{10})(NH_2)_2$	-19.0	-22.1
i1, (trans-$B_3N_3H_6(NH_2)_2)N_2H_4 \rightarrow$ trans-i1,3 (trans-$B_3N_5H_{10})(NH_2)_2$	-50.8	-53.0
i1, (trans-$B_3N_3H_6(NH_2)_2)N_2H_4 \rightarrow$ trans-o1,3 (trans-$B_3N_5H_{10})(NH_2)_2$	1.7	-0.6
cis-o1,3 (trans-$B_3N_5H_{10})(NH_2)_2 + N_2H_4 \rightarrow$ 1a, cis-o1,3 trans-$B_3N_7H_{14}(N_2H_4)$	-6.0	-7.8
1a, cis-o1,3 trans-$B_3N_7H_{14}(N_2H_4) \rightarrow$ 1a, 2a cis-o1,3 trans-$B_3N_7H_{14}(NH_2)_2$	-6.8	-8.1
1a, cis-o1,3 trans-$B_3N_7H_{14}(N_2H_4) \rightarrow$ 1a, 2b cis-o1,3 trans-$B_3N_7H_{14}(NH_2)_2$	-18.7	-19.8
1a, cis-o1,3 trans-$B_3N_7H_{14}(N_2H_4) \rightarrow$ 1a, 3a cis-o1,3 trans-$B_3N_7H_{14}(NH_2)_2$	-42.6	-40.9
1a, cis-o1,3 trans-$B_3N_7H_{14}(N_2H_4) \rightarrow$ 1a, 3b cis-o1,3 trans-$B_3N_7H_{14}(NH_2)_2$	-52.1	-48.3

Table 95. NMR ^{11}B σ values for Compounds in Figure 66.

Molecule	**σ_{B1}**	**σ_{B2}**	**σ_{B3}**
$B_3N_3H_6$	26.1	26.1	26.1
$B_3N_3H_6(N_2H_4)$	25.0	3.2	25.4
cis-$B_3N_3H_6(NH_2)_2$	24.4	-5.0	23.6
trans-$B_3N_3H_6(NH_2)_2$	24.5	-5.0	25.9
i1, (trans-$B_3N_3H_6(NH_2)_2)N_2H_4$	24.2	25.5	-1.3
cis-o1,2 (trans-$B_3N_5H_{10})(NH_2)_2$	26.1	24.3	-0.9
cis-o1,3 (trans-$B_3N_5H_{10})(NH_2)_2$	22.2	22.9	-7.6

trans-i1,2 (trans-$B_3N_5H_{10}$)$(NH_2)_2$	25.1	-2.5	25.5
trans-i1,3 (trans-$B_3N_5H_{10}$)$(NH_2)_2$	0.2	24.2	22.8
trans-o1,3 (trans-$B_3N_5H_{10}$)$(NH_2)_2$	4.3	26.2	-9.6
1a (cis-o1,3 trans-$B_3N_7H_{14}$)N_2H_4	-7.3	22.6	23.7
1a,2a (cis-o1,3 trans-$B_3N_7H_{14}$)$(NH_2)_2$	22.9	-1.9	-0.3
1a,2b (cis-o1,3 trans-$B_3N_7H_{14}$)$(NH_2)_2$	22.9	-2.1	23.8
1a,3a (cis-o1,3 trans-$B_3N_7H_{14}$)$(NH_2)_2$	-3.9	21.5	-2.9
1a,3b (cis-o1,3 trans-$B_3N_7H_{14}$)$(NH_2)_2$	1.5	23.2	22.3

We have added a third N_2H_4 to the results of the first and second addition of $B_3N_3H_6$ at the B3LYP/DZVP2 level. We have also calculated the addition of a first and second N_2H_4 to $B_3N_3H_6$ at the G3MP2 level. This led to a very large number of structures for addition to $B_3N_3H_6$ at the B3LYP/DZVP2 level but quite a few less at the G3MP2 level. This is because of greater fragmentation predicted by the G3MP2 method. The NMR ^{11}B chemical shifts for the first addition and trans 2nd and 3rd additions for the DFT optimizations have also been done and a few examples are given in Figure 69.

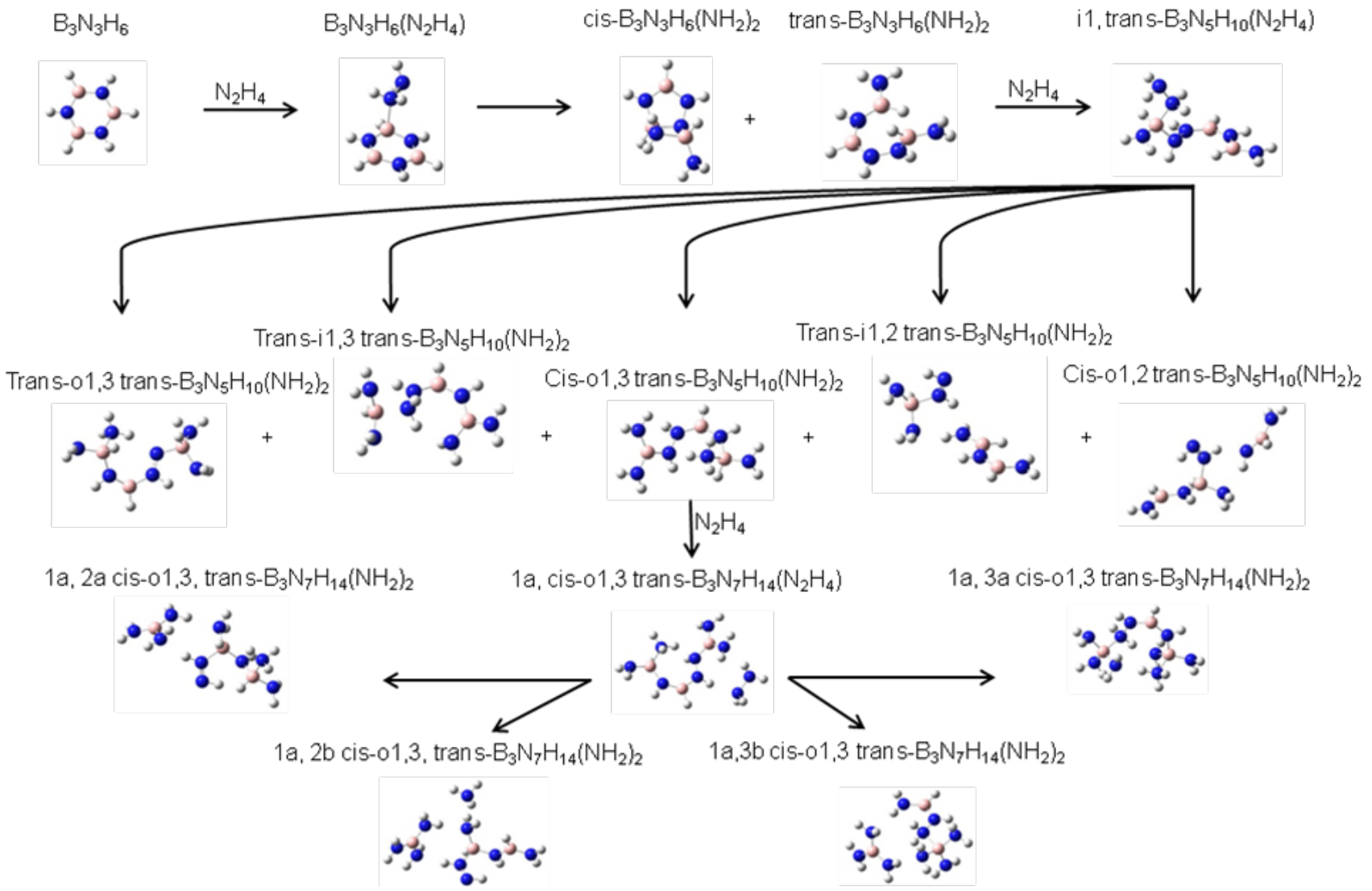

Figure 66. One of ten 2nd addition products of trans-$B_3N_3H_6(NH_2)_2$ and a limited view of its third addition products of BNH_2.

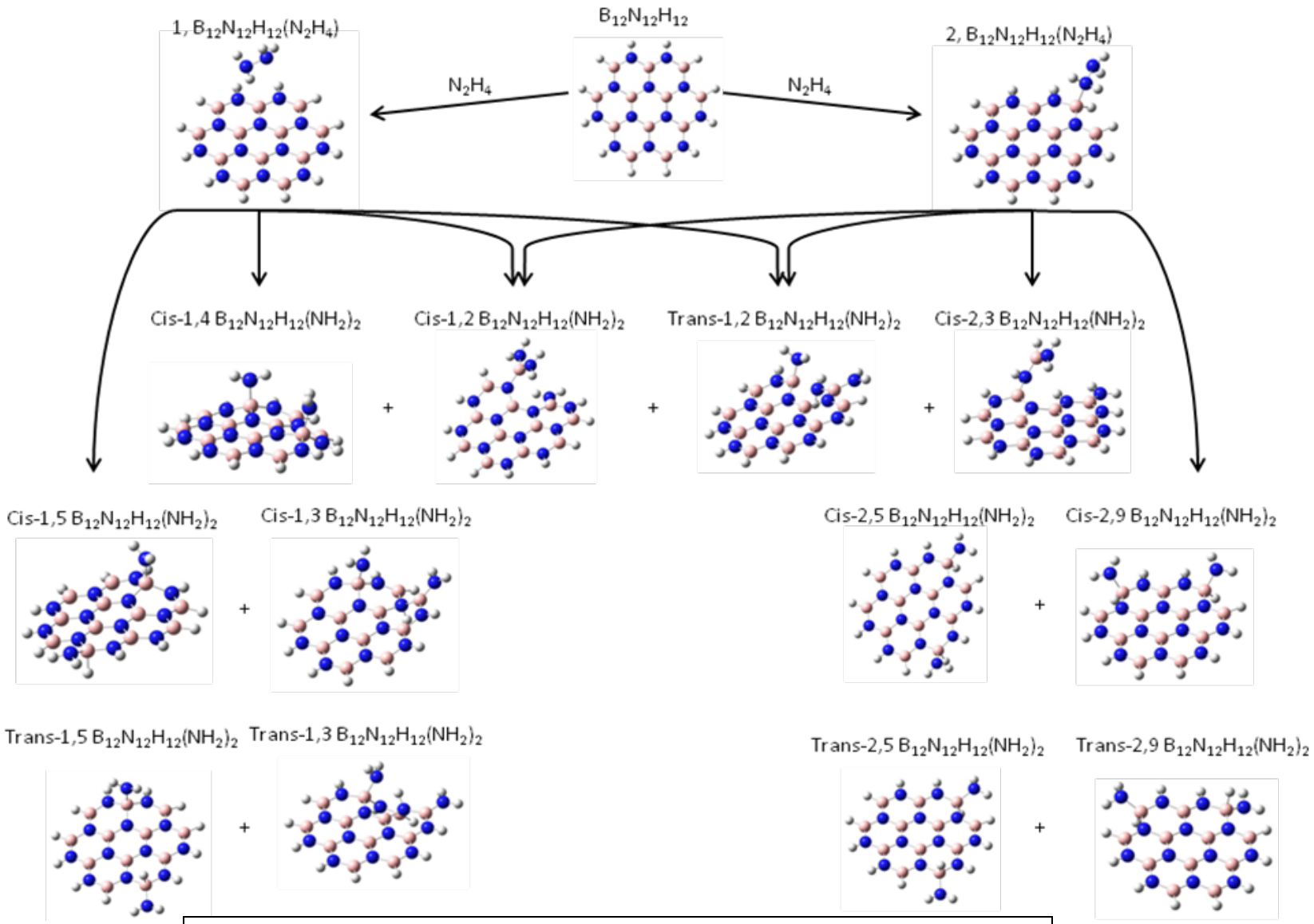

Figure 67. Possible outcomes after only a single addition of hydrazine to BNH.

$B_3N_3H_6$ 1st addition ΔH_{298}

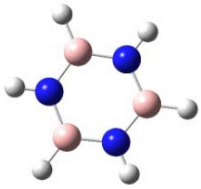

+ N_2H_4

$B_3N_3H_6(N_2H_4)$

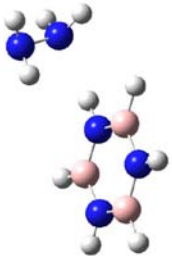

ΔH_{298}= -6.5

cis-$B_3N_3H_6(NH_2)_2$

ΔH_{298}= -45.4

cis-$B_3N_3H_6(NH_2)_2$

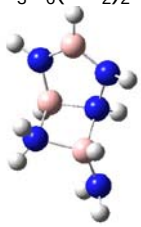

ΔH_{298}= 5.2

trans-$B_3N_3H_6(NH_2)_2$

ΔH_{298}= -44.9

trans-$B_3N_3H_6(NH_2)_2$

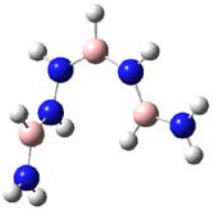

ΔH_{298}= 3.5

Trans-B3N5H10 2nd addition ΔH_{298} on "boron 1"

trans-$B_3N_3H_6(NH_2)_2$

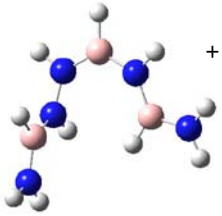

+ N_2H_4

o1.trans-B3N5H10.N2H4

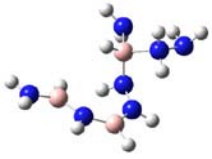

ΔH_{298}=-2.5

cis-o1.3.trans-B3N5H10.NH2.2

ΔH_{298}=-6.4

trans-o1.3.trans-B3N5H10.NH2.2

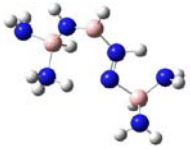

ΔH_{298}=-1.52

trans-i1.3.trans-B3N5H10.NH2.2

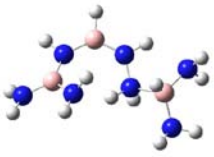

ΔH_{298}=-60.30

Trans-B3N5H10 2nd addition ΔH_{298} on "boron 2"

trans-$B_3N_3H_6(NH_2)_2$ + N_2H_4

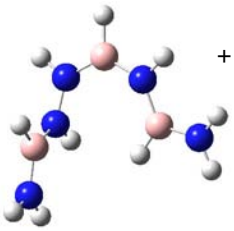

trans-3.2.trans-B3N5H10.NH2.2

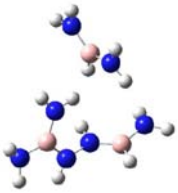

ΔH_{298}=-63.0

cis-3.2.trans-B3N5H10.NH2.2

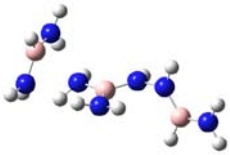

ΔH_{298}=-61.9

u2.trans-B3N5H10.N2H4

ΔH_{298}=-6.4

Trans-B3N5H10 2nd addition ΔH_{298} on "boron 2"

trans-$B_3N_3H_6(NH_2)_2$ + N_2H_4

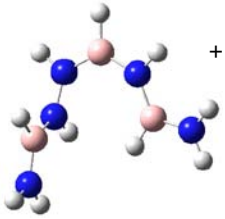

trans-3.2.trans-B3N5H10.NH2.2

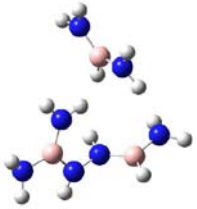

ΔH_{298}=-61.3

cis-3.2.trans-B3N5H10.NH2.2

ΔH_{298}=-60.2

d2.trans-B3N5H10.N2H4

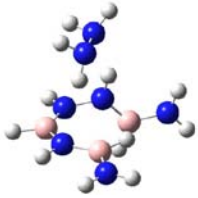

ΔH_{298}=-8.1

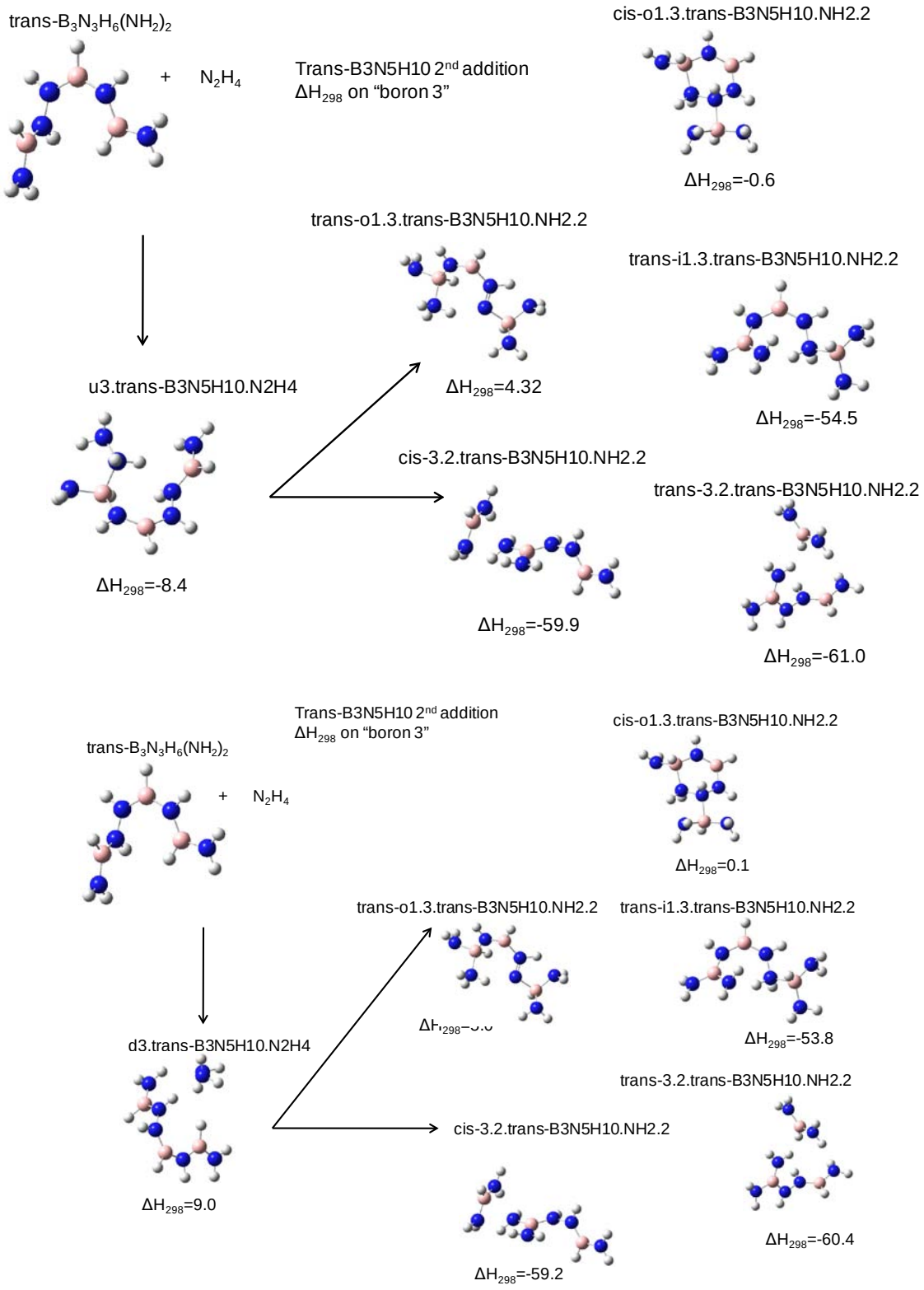

Figure 68. Thermodynamic values at 298K in kcal/mol for the 1st and 2nd addition of N_2H_4 to models of spent fuel BNH_2 at the G3MP2 level.

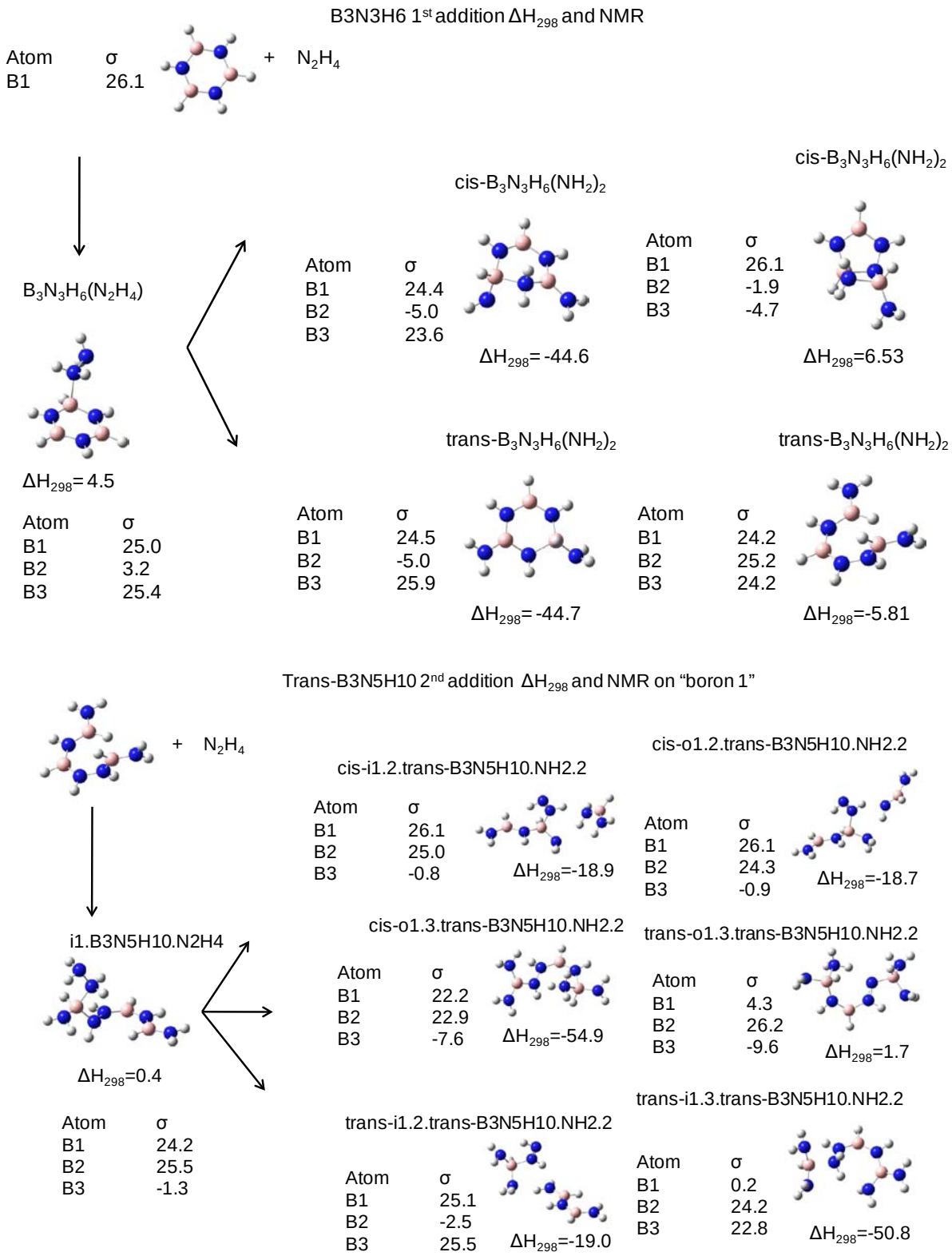

Figure 69. Examples of NMR ^{11}B chemical shift calculations for some of the 1st and 2nd addition of N_2H_4 to models of spent fuel BNH_2.

Thermodynamics of Carbene Chemistry

There has been real excitement due to the discovery that stable carbenes (imidazol-2-ylidenes and/or imidazolin-2-ylidnenes, often called the "Arduengo-type" carbene) can be made and stored for long times. This has led to a significant increase in the use of these species for a wide range of chemical applications, including H_2 storage systems. In developing new uses for such species, it is important to have basic thermodynamic information about their stability. However, for the simplest unsubstituted model compound **1** (See below) which can then be used as a basis for the prediction of heats of formation of substituted species through the use of appropriately chosen isodesmic reactions, the heat of formation is not available. In addition, the ability of the carbene to bind other species is of interest, e.g., a proton to determine its basicity, a hydride, or H_2.

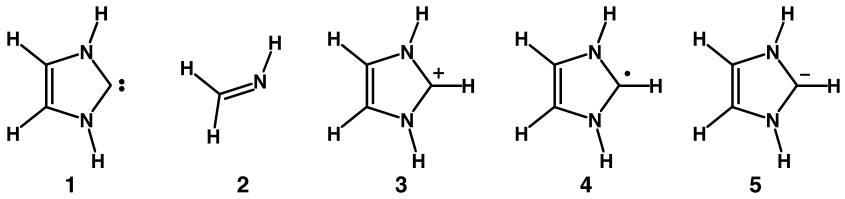

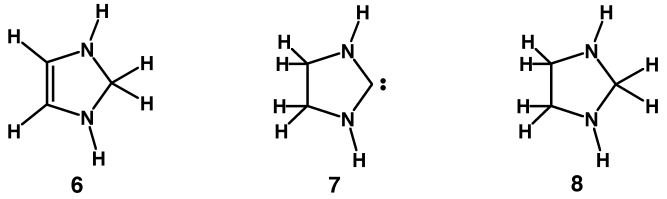

The heats of formation of the saturated and unsaturated diamino carbenes (imadazol(in)-2-ylidenes) have been calculated by using high levels of *ab initio* electronic structure theory. The calculations were done at the coupled cluster level through noniterative triple excitations with augmented correlation consistent basis sets up through quadruple. In addition, four other corrections were applied to the frozen core atomization energies, (1) a zero point vibrational correction: (2) a core/valence correlation correction; (3) a scalar relativistic correction; and (4) a first order atomic spin-orbit correction. The value of ΔH_f^{298} for the unsaturated carbene **1** is calculated to be 56.4 kcal/mol. The value of ΔH_f^{298} for the unsaturated triplet carbene ^{3}**1** is calculated to be 142.8 kcal/mol giving a singlet-triplet splitting of 86.4 kcal/mol. Addition of a proton to **1** forms **3** with ΔH_f^{298}(**3**) = 171.6 kcal/mol with a proton affinity for **1** of 250.5 kcal/mol at 298 K. Addition of a hydrogen atom to **1** forms **4** with ΔH_f^{298}(**4**) = 72.7 kcal/mol and a C-H bond energy of 35.8 kcal/mol at 298K. Addition of H- to **1** gives **5** with ΔH_f^{298}(**5**) = 81.2 kcal/mol and **5** is not stable with respect to loss of an electron to form **4**. Addition of H_2 to the carbene center forms **6** with ΔH_f^{298}(**6**) = 41.5 kcal/mol and a heat of hydrogenation at 298 K of -14.9 kcal/mol. The value of ΔH_f^{298} for the saturated carbene **7** (obtained by adding H_2 to the C=C bond of **1**) is 47.4 kcal/mol. Hydrogenation of **7** to form the fully saturated imidazolidine, **8**, gives ΔH_f^{298}(**8**) = 14.8 kcal/mol and a heat of hydrogenation at 298 K of -32.6 kcal/mol. The estimated error bars for the calculated heats of formation are ±1.0 kcal/mol. The heats of hydrogenation and dehydrogenation of imidazole-derived molecules related to "Arduengo-type" carbenes indicate that with appropriate substitution these heterocycles should make excellent materials for employment as hydrogen storage media. The heats and free energies of reaction lie in a range where one can anticipate easily reversible reactions through employment of mass action effects. Our approach is to first reliably predict the thermodynamic properties before searching for kinetically accessible paths and appropriate catalysts.

The hydrogenation energies of the carbenes at the carbene center in Table 97 provide information on the stability of the "Arduengo-type" carbenes. Based on the smallest heats of hydrogenation, we would expect that carbenes **1** and **7** are the most stable carbenes as is found experimentally. The fact that the hydrogenation energy for **7** is larger than that of **1** is consistent with the fact that molecules like **7** are more reactive than molecules based on the framework of **1**. It is clear that CH_2 is unstable based on the large heat released upon hydrogenation. We can also calculate the hydrogenation energy of the triplet state of **1** and its value is comparable to that of CH_2 showing that ^{3}**1** is similar in stability to CH_2. The hydrogenation energy of the carbene CF_2 can be calculated from the available literature data and it is intermediate between the energies of carbene **1** and CH_2 as would be expected as CF_2 is a singlet carbene that is moderately stable although it cannot be isolated and stored under normal conditions. We note that the hydrogenation energy of $^3CF_2$ can be estimated to be ~108 kcal/mol, comparable to that of CH_2.

Table 96. Calculated Heats of Formation at 0 and 298 K (kcal/mol) and Calculated Entropies at 298K.

Molecule	**ΔH_f(0K)**	**ΔH_f(298K)**	**S (298K)**
1	60.3	56.4	63.8
^{3}**1**	146.4	142.8	69.4
3	176.5	171.6	63.9
4	77.2	72.7	68.8
5	85.7	81.2	67.6
6	47.1	41.5	67.5
7	52.8	47.4	67.3
8	22.2	14.8	70.4

Table 97. Hydrogenation Energies (kcal/mol) of Carbenes.

Reaction	**-ΔH_{rxn}(298K)**
1 + H_2 → **6**	14.9
7 + H_2 → **8**	32.6
$^1CF_2 + H_2 \rightarrow CF_2H_2$	62.2
^{3}**1** + H_2 → **6**	101.3
$^3CF_2 + H_2 \rightarrow CF_2H_2$	108.2
$^3CH_2 + H_2 \rightarrow CH_4$	110.9

We have also studied the thermodynamics for the hydrogen elimination from diaminocarbenes and N-methyl substituted diaminocarbenes, as shown in (113):

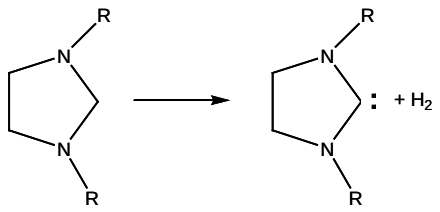

(113)

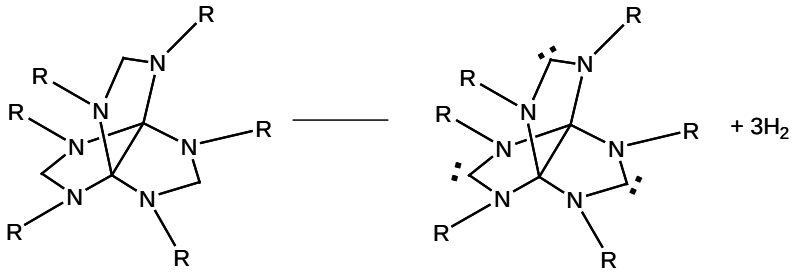

(114)

where R = H or CH_3. The analysis on reaction (114) involves three steps, in each one hydrogen molecule is lost one of the $–CH_2$- groups. The energetics including enthalpies of activation for H_2 elimination is given in Table 98. We are using the B3LYP/DZVP2 level of calculation.

Table 98. Carbenes Reaction Energies in kcal/mol.

Reaction	**R**	**ΔH(298K)**	**ΔG**	**$\Delta H^{\ddagger}$**
112	H	31.1	22.3	68.2
	CH_3	26.7	17.6	60.4
113 (step 1)	H	34.4	25.4	67.8
	CH_3	32.5	22.1	63.5
113 (step 2)	H	37.1	27.8	70.2
	CH_3	32.4	22.7	63.2
113 (step 3)	H	41.0	30.7	78.2
	CH_3	30.7	22.0	63.6

Methylation reductes in the activation barrier by 4.3, 7.0, and 14.6 kcal/mol for steps 1, 2, and 3. We continued to study stable carbenes (imidazol-2-ylidenes and/or imidazolin-2-ylidnenes) for H_2 storage systems. The carbene reaction energetics were calculated by B3LYP/DZVP2 at 0K (ΔE) and 298K (ΔH) and are in good agreement with the results of much higher levels where available. The hydrogens of the nitrogen atoms were not drawn for the tris-carbenes.

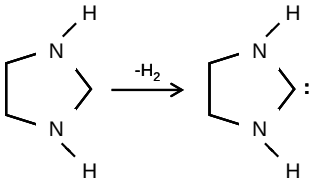

ΔH = 30.1 (115)

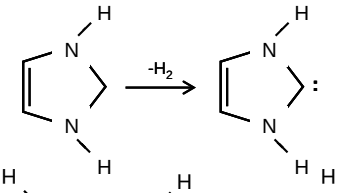

ΔH = 16.6 (116)

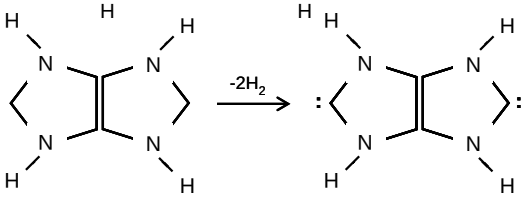

ΔH = 55.0 (117)

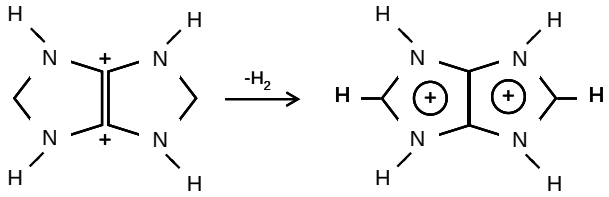

$\Delta H = 19.8$ (118)

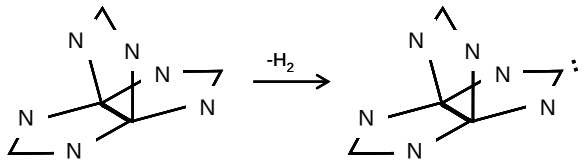

$\Delta H = 34.4$ (119)

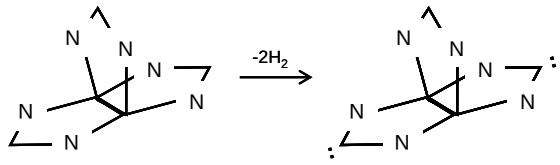

$\Delta H = 71.4$ (120)

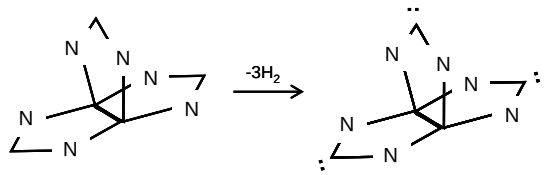

$\Delta H = 112.5$ (121)

Cyanocarbon Chemistry

We are interested in derivatives of cyanocarbons for chemical H_2 storage systems. However, there is little thermodynamic data available for these species. The heats of formation of N_2H, diazene (*cis*- and *trans*-N_2H_2), N_2H_3, and hydrazine (N_2H_4), as well as their protonated species (diazenium, $N_2H_3^+$, and hydrazinium, $N_2H_5^+$), have been calculated by using high level electronic structure theory. Energies were calculated by using coupled cluster theory with a perturbative treatment of the triple excitations (CCSD(T)) and employing augmented correlation consistent basis sets (aug-cc-pV*n*Z) up to quintuple-ζ, in order to perform a complete basis set extrapolation for the energy. Geometries were optimized at the CCSD(T) level with the aug-cc-pVDZ and aug-cc-pVTZ basis sets. Core-valence and scalar relativistic corrections were included, as well as scaled zero point energies. We find the following heats of formation (kcal/mol) at 0(298) K: $\Delta H_f(N_2H) = 60.8(60.1)$; $\Delta H_f(cis\text{-}N_2H_2) = 54.9(53.2)$; $\Delta H_f(trans\text{-}N_2H_2) = 49.9(48.1)$ *versus* $\geq 48.8 \pm 0.5$ (expt., 0 K); $\Delta H_f(N_2H_4) = 26.6(23.1)$ *versus* 22.8 ± 0.2 (expt., 298 K); $\Delta H_f(N_2H_3) = 56.2(53.6)$; $\Delta H_f(N_2H_3^+) = 231.6(228.9)$; and $\Delta H_f(N_2H_5^+) = 187.1(182.7)$. In addition, we calculated the heats of formation of CH_3NH_2, CH_3NNH, and $CH_3HNNHCH_3$ by using isodesmic reactions and at the G3(MP2) level.

$N_2 + H_2 \rightarrow N_2H_2$	$\Delta H = 48.2$	(122)
$N_2H_2 + H_2 \rightarrow N_2H_4$	$\Delta H = -25.1$	(123)
$N_2H_2 \rightarrow 2NH$	$\Delta H = 123.7$	(124)
$N_2H_4 + H_2 \rightarrow 2NH_3$	$\Delta H = -43.0$	(125)
$N_2H_4 \rightarrow 2NH_2$	$\Delta H = 66.1$	(126)

Isodesmic reactions (showed below with their corresponding MP2/CBS enthalpies of reaction at 298K), were used to estimate the heats of formation of *trans*-$CH_3N{=}NH$, *trans*-$CH_3N{=}NCH_3$ and $CH_3HNNHCH_3$ (in a twisted configuration), $\Delta H_f^{298}(CH_3N{=}NH)$ = 41.9 kcal/mol, $\Delta H_f^{298}(CH_3N{=}NCH_3)$ = 36.0 kcal/mol, and $\Delta H_f^{298}[(CH_3)HNNH(CH_3)]$ = 22.2 kcal/mol.

$CH_3NH_2 + N_2H_2 \rightarrow CH_3N{=}NH + NH_3$	ΔH = -12.2	(127)
$2CH_3NH_2 + N_2H_2 \rightarrow CH_3N{=}NCH_3 + 2NH_3$	ΔH = -24.0	(128)
$2CH_3NH_2 + N_2H_4 \rightarrow CH_3HNNHCH_3 + 2NH_3$	ΔH = -12.7	(129)

These values provide the following hydrogenation energies in kcal/mol at 298K:

$(CH_3)HNNH(CH_3) \rightarrow (CH_3)N{=}N(CH_3) + H_2$	ΔH = 13.8	(130)
$2CH_4 + N_2H_2 \rightarrow (CH_3)N{=}N(CH_3) + 2H_2$	ΔH = 23.6	(131)
$2CH_4 + N_2H_4 \rightarrow (CH_3)HNNH(CH_3) + 2H_2$	ΔH = 34.9	(132)
$C_2H_6 + N_2H_2 \rightarrow (CH_3)N{=}N(CH_3) + H_2$	ΔH = 7.4	(133)
$C_2H_6 + N_2H_4 \rightarrow (CH_3)HNNH(CH_3) + H_2$	ΔH = 19.3	(134)

In addition, G3MP2 heats of formation at 298K were also calculated, giving: $\Delta H_f^{298}(N_2H_2)$ = 49.0 kcal/mol, $\Delta H_f^{298}(N_2H_4)$ = 25.3 kcal/mol, $\Delta H_f^{298}(CH_3NH_2)$ = -4.2 kcal/mol, $\Delta H_f^{298}(CH_3N{=}NH)$ = 43.4 kcal/mol, $\Delta H_f^{298}(CH_3N{=}NCH_3)$ = 38.2 kcal/mol, and $\Delta H_f^{298}[(CH_3)HNNH(CH_3)]$ = 24.5 kcal/mol. These results are ~2 kcal/mol higher than those obtained by CCSD(T)/CBS or isodesmic reactions estimations, and ~3 kcal/mol higher than the experimental results. We have also obtained the G3MP2 heats of formation (kcal/mol) for the following molecules: ΔH_f^{298}(c-C_6H_6) = 18.4; ΔH_f^{298}(c-C_6H_{12}) = -20.0; $\Delta H_f^{298}(C_3N_3H_3)$ = 54.7; $\Delta H_f^{298}(C_3N_3H_9)$ = 29.3; $\Delta H_f^{298}(C_6H_5NH_2)$ = 20.0; $\Delta H_f^{298}(C_6H_{11}NH_2)$ = -24.7; $\Delta H_f^{298}(C_3N_3H_2NH_2)$ = 42.2; $\Delta H_f^{298}(C_3N_3H_8NH_2)$ = 18.7; $\Delta H_f^{298}[(C_3N_3H_2)N{=}N(C_3N_3H_2)]$ = 173.1; $\Delta H_f^{298}[(C_3N_3H_2)HNNH(C_3N_3H_2)]$ = 122.0; $\Delta H_f^{298}[(C_3N_3H_8)N{=}N(C_3N_3H_8)]$ = 97.3; $\Delta H_f^{298}[(C_3N_3H_8)HNNH(C_3N_3H_8)]$ = 76.2; $\Delta H_f^{298}(C_8H_8)$ = 56.9; $\Delta H_f^{298}(C_8H_{10})$ = 2.4

These heats of formation were used to benchmark the B3LYP/DZVP2 method (good to ± 3 kcal/mol) used in the following hydrogenation reactions:

Reaction	**ΔE(0K)**	**ΔG(298K)**
c-$C_6H_{12} \rightarrow$ c-$C_6H_6 + 3H_2$	43.3	21.5
$C_3N_3H_9 \rightarrow$ 1,3,5-triazine ($C_3N_3H_3$) + $3H_2$	18.2	-4.5
Cyclohexanamine ($C_6H_{11}NH_2$) → Aniline ($C_6H_5NH_2$) + $3H_2$	38.1	16.3
$C_3N_3H_8NH_2 \rightarrow$ 2-amino-1,3,5-triazine ($C_3N_3H_2NH_2$) + $3H_2$	13.8	-8.8
$2C_6H_6 + N_2H_2 \rightarrow (C_6H_5)N{=}N(C_6H_5) + 3H_2$	38.1	16.3
$2C_6H_{12} + N_2H_2 \rightarrow (C_6H_{11})N{=}N(C_6H_{11}) + 2H_2$	14.0	19.4
$2C_3N_3H_6 + N_2H_2 \rightarrow (C_3N_3H_5)N{=}N(C_3N_3H_5) + 2H_2$	15.0	20.2
$2C_3N_3H_9 + N_2H_2 \rightarrow (C_3N_3H_8)N{=}N(C_3N_3H_8) + 2H_2$	13.1	17.0
$2C_6H_6 + N_2H_4 \rightarrow (C_6H_5)HNNH(C_6H_5) + 2H_2$	17.6	23.8
$2C_6H_{12} + N_2H_4 \rightarrow (C_6H_{11})HNNH(C_6H_{11}) + 2H_2$	27.4	34.1
$2C_3N_3H_3 + N_2H_4 \rightarrow (C_3N_3H_2)HNNH(C_3N_3H_2) + 2H_2$	-8.2	-1.9
$(C_6H_5)HNNH(C_6H_5) \rightarrow (C_6H_5)N{=}N(C_6H_5) + H_2$	15.7	8.5
$(C_6H_{11})HNNH(C_6H_{11}) \rightarrow (C_6H_{11})N{=}N(C_6H_{11}) + H_2$	13.2	5.5

$(C_3N_3H_5)HNNH(C_3N_3H_5) \rightarrow (C_3N_3H_5)N{=}N(C_3N_3H_5) + H_2$	49.8	42.2
$(C_3N_3H_8)HNNH(C_3N_3H_8) \rightarrow (C_3N_3H_8)N{=}N(C_3N_3H_8) + H_2$	19.7	12.6
o-xylene $(C_8H_{10}) \rightarrow$o-xylylene $(C_8H_8) + H_2$	54.9	48.5

The calculations on the hydrogenation energies of small cyanocarbons is shown in Table 99. The calculations show interesting behavior in terms of which sites will by hydrogenated.

Table 99. G3MP2 Hydrogenation of Cyanocarbon Compounds.

Reaction	**ΔH (298 K)**	**ΔG (298 K)**
$NCCN + H_2 \rightarrow HN\text{-}CC\text{-}NH$	23.5	30.9
$HN\text{-}CC\text{-}NH + H_2 \rightarrow HN\text{-}HCCH\text{-}NH$	-53.4	-44.5
$HN\text{-}HCCH\text{-}NH + H_2 \rightarrow H_2N\text{-}HCCH\text{-}NH_2$	-18.3	-10.6
$H_2N\text{-}HCCH\text{-}NH_2 + H_2 \rightarrow H_2N\text{-}H_2CCH_2\text{-}NH_2$	-23.5	-14.7
$(CN)_2CC(CN)_2 + H_2 \rightarrow (CN)_2CHCH(CN)_2$	-24.5	-15.9
$(CN)_2CC(CN)_2 + H2 \rightarrow (CN)_2CC(CN)CHNH$	-15.6	-7.4

The calculated results for the hydrogenation reaction $RNNR + H_2 \rightarrow RHNNHR$ show that substitution of an organic substituent for H improve the energetics suggesting that these types of compounds may be possible to use in a chemical hydrogen storage system.

Thermodynamics of P-substituted Rings

It is generally thought that C-H bonds are too strong to be easily used for H_2 storage systems in terms of the addition and release of H_2 under ambient conditions. Our approach is to change the paradigm that C-H bonds are too strong so that they cannot be readily activated for use in H_2 storage systems. This is based on the recent discovery in our laboratory of a system where H_2 can be added at room temperature and pressure to carbon atoms as in scheme below. This system can be considered to be related to the conversion between bicyclo[1.1.0]butane and cyclobutane in terms of H_2 addition/release. The energetics for the bicyclo[1.1.0]butane/cyclobutane system are predicted to be ~45 kcal/mol at the G3(MP2) level which is too large. Thus, we have to use substituents to tune the energetics for this system. Fundamental studies on these unusual molecules were recently extended to the radical cation derived from I. Thus we have a model system in hand to study H_2 regeneration.

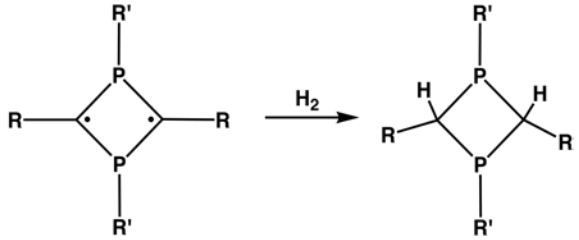

We used the DFT method at the B3LYP/DZVP2 level to predict hydrogen regeneration reactions for singlet and triplet radicals for the four-member PCPC rings with different symmetries and substituents (kcal/mol):

Table 100. Reaction Energies for H_2 Addition in kcal/mol to PCPC Rings in kcal/mol.

Reaction	**ΔH(0 K)**	**ΔH(298 K)**
CHPHCHPH (C_i) + H_2 → CH_2PHCH_2PH	-75.0	-77.1
CHPHCHPH (C_i, triplet) + H_2 → CH_2PHCH_2PH	-78.9	-81.2
CHPHCHPH (C_{2v},triplet) + H_2 → CH_2PHCH_2PH	-81.5	-83.8
CHPHCHPH (C-C bond)* + H_2 → CH_2PHCH_2PH	-43.9	-45.6
$CHP(CH_3)CHP(CH_3)$ (C_i) + H_2 → $CH_2P(CH_3)CH_2P(CH_3)$	-68.7	-70.8
$CHP(CH_3)CHP(CH_3)$ (C-C bond)* + H_2 → $CH_2P(CH_3)CH_2P(CH_3)$	-45.8	-47.6
$CHP(CH_3)CHP(CH_3)$ (C_i, triplet) + H_2 → $CH_2P(CH_3)CH_2P(CH_3)$	-75.2	-77.5
$CHP(CH_3)CHP(CH_3)$ (C_{2v}, triplet) + H_2 → $CH_2P(CH_3)CH_2P(CH_3)$	-79.2	-81.4
$CHP(CH_3)CHP(CH_3)$ (from C-C bond)* + H_2 → $CH_2P(CH_3)CH_2P(CH_3)$	-51.2	-52.9
$C(Ph)P(CH_3)C(Ph)P(CH_3)$ (C_i) + H_2 → $CH(Ph)P(CH_3)CH(Ph)P(CH_3)$	-51.8	-54.2
$C(Ph)P(CH_3)C(Ph)P(CH_3)$ (C_{2h}, triplet) + H_2 → $CH(Ph)P(CH_3)CH(Ph)P(CH_3)$	-49.3	-51.6
$C(Ph)P(CH_3)C(Ph)P(CH_3)$ (C-C bond)* + H_2 → $CH(Ph)P(CH_3)CH(Ph)P(CH_3)$	-46.3	-48.1
$C(Ph(CH_3)_3)P(CH_3)C(Ph(CH_3)_3)P(CH_3)$ (C_i) + H_2 → $CH(Ph(CH_3)_3)P(CH_3)CH(Ph(CH_3)_3)P(CH_3)$ (*trans*-R,R)	-49.8	-52.1
$C(Ph(CH_3)_3)P(CH_3)C(Ph(CH_3)_3)P(CH_3)$ (C_i, triplet) + H_2 → $CH(Ph(CH_3)_3)P(CH_3)CH(Ph(CH_3)_3)P(CH_3)$ (*trans*-R,R)	-50.0	-52.2
$C(Ph(CH_3)_3)P(CH_3)C(Ph(CH_3)_3)P(CH_3)$ (C-C bond)* + H_2 → $CH(Ph(CH_3)_3)P(CH_3)CH(Ph(CH_3)_3)P(CH_3)$ (*trans*-R,R)	-43.9	-45.8
$C(Ph(CH_3)_3)P(CH_3)C(Ph(CH_3)_3)P(CH_3)$ (C_i) + H_2 → $CH(Ph(CH_3)_3)P(CH_3)CH(Ph(CH_3)_3)P(CH_3)$ (*cis*-R,R)	-36.8	-39.4
$C(Ph(CH_3)_3)P(CH_3)C(Ph(CH_3)_3)P(CH_3)$ (C_i, triplet) + H_2 → $CH(Ph(CH_3)_3)P(CH_3)CH(Ph(CH_3)_3)P(CH_3)$ (*cis*-R,R)	-37.0	-39.5
$C(Ph(CH_3)_3)P(CH_3)C(Ph(CH_3)_3)P(CH_3)$ (C-C bond)* + H_2 → $CH(Ph(CH_3)_3)P(CH_3)CH(Ph(CH_3)_3)P(CH_3)$ (*cis*-R,R)	-31.0	-33.1
$C(Mes)P(CH_3)C(Mes)P(CH_3)$ +H_2 → $CH(Mes)P(CH_3)CH(Mes)P(CH_3)$	-59.2	-62.2
$C(Mes)P(CH_3)C(Mes)P(CH_3)$ (C-C bond)* +H_2 → $CH(Mes)P(CH_3)CH(Mes)P(CH_3)$	-61.2	-64.0

* Note that C-C bond structures are not radicals.

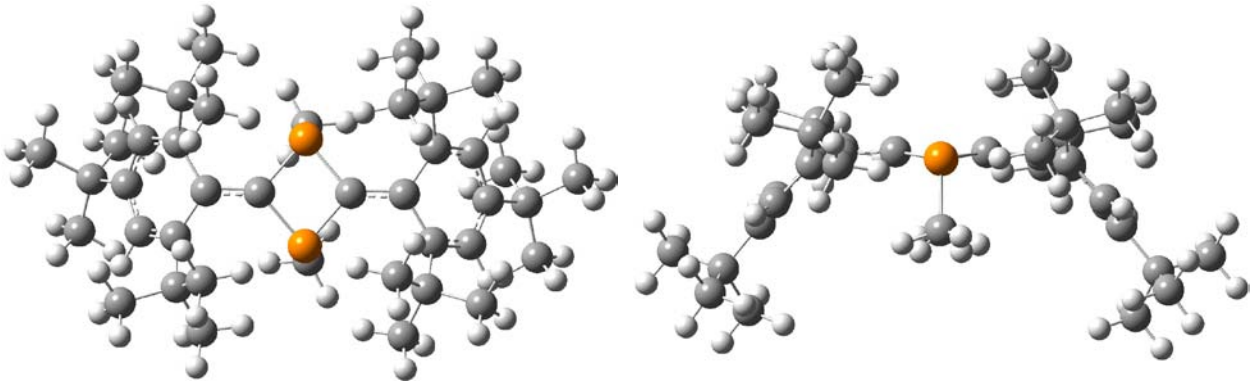

Figure 70. Two views of the cyclic PCPC radical with R=Mes (2,4,6-tri-*tert*-butylphenyl) and R'=CH_3.

Thermodynamics of Additional Phosphorus-Based Compounds

As a follow on to on previous work on compounds derived from cyano compounds containing N-N bonds, we expanded our study to compounds with P-P bonds. The heats of formation of diphosphene (*cis*- and *trans*-P_2H_2), phopshinophosphinidene (singlet and triplet H_2PP) and diphosphine (P_2H_4), as well as the P_2H, P_2H_3 radicals derived from PH bond cleavages, have been calculated by using high level electronic structure theory (CCSD(T)) extrapolated to the complete basis set limit. We find the following heats of formation (kcal/mol) at 0[298] K: $\Delta H_f(P_2H)$ = 54.4[53.4]; ΔH_f(*cis*-P_2H_2) = 33.9[32.0] ; ΔH_f(*trans*-P_2H_2) = 30.6[28.7]; $\Delta H_f(H_2PP)$ = 55.6[53.7]; $\Delta H_f(^3H_2PP)$ = 66.1[64.2]; $\Delta H_f(P_2H_3)$ = 34.8[32.3]; $\Delta H_f(P_2H_4)$ = 9.1[5.7] (expt., 5.0 ± 1.0 298 K); and $\Delta H_f(CH_3PH_2)$ = -1.4[-5.0]. These values have a ±1.0 kcal/mol of error. From these heats of formation we can calculate the energetics of the following reactions (kcal/mol):

Table 101. P_2 Reaction Energetics in kcal/mol.

Reaction	**ΔH(298 K)**	**ΔG(298 K)**
$P_2 + H_2 \rightarrow P_2H_2$	-6.1	1.0
$P_2H_2 + H_2 \rightarrow P_2H_4$	-23.1	-15.5
$P_2H_4 + H_2 \rightarrow 2PH_3$	-3.6	-4.8
$P_2H_2 + 2H_2 \rightarrow 2PH_3$	-26.7	-20.3
$CH_3PH_2 + H_2 \rightarrow PH_3 + CH_4$*	-11.8	-12.4

* CH_4 values taken from: Frenkel, M; Marsh, K. N.; Wilhoit, R. C.; Kabo, G. J.; Roganov, G. N. *Thermodynamics of Organic Compounds in the Gas State*; Thermodynamics Research Center, College Station: Texas, 1994.

In addition, we calculated the heats of formation of the methylated derivatives CH_3PPH, CH_3HPP, $(CH_3)_2PPH_2$ and $CH_3HPPHCH_3$ by using isodesmic reactions MP2/CBS level. The calculated results for the hydrogenation reactions RPPR + H_2 → RHPPHR and $R_2PP + H_2 \rightarrow R_2PPH_2$ show that substitution of an organic substituents, such as bulky alky or aryl groups for H, improve the energetics suggesting that these types of compounds are potential candidates for use in a chemical hydrogen storage system.

$$CH_3PH_2 + P_2H_2 \rightarrow CH_3PPH + PH_3 \quad (135)$$

$CH_3PH_2 + P_2H_4 \rightarrow CH_3HPPH_2 + PH_3$ (136)
$2CH_3PH_2 + P_2H_2 \rightarrow CH_3PPCH_3 + 2PH_3$ (137)
$2CH_3PH_2 + P_2H_4 \rightarrow CH_3HPPHCH_3$ (C_2 symmetry) $+ 2PH_3$ (138)
$2CH_3PH_2 + P_2H_4 \rightarrow CH_3HPPHCH_3$ (C_s symmetry) $+ 2PH_3$ (139)
$2CH_3PH_2 + P_2H_4 \rightarrow (CH_3)_2PPH_2 + 2PH_3$ (140)
$CH_3PH_2 + H_2PP \rightarrow CH_3HPP + PH_3$ (141)
$2CH_3PH_2 + H_2PP \rightarrow (CH_3)_2HPP + 2PH_3$ (142)

Table 102. Substituted P_2 Reaction Energetics in kcal/mol.

Molecule	From Reaction	ΔH_f (0 K) isodesmic	ΔH_f^0 (298 K) isodesmic
trans-CH_3PPH	134	22.6	19.4
CH_3HPPH_2	135	2.8	-1.9
trans-CH_3PPCH_3	136	15.3	10.9
$CH_3HPPHCH_3$ (C_2)	137	-4.1	-8.7
$CH_3HPPHCH_3$ (C_s)	138	-1.7	-7.7
$(CH_3)_2PPH_2$	139	-6.7	-12.7
CH_3HPP	140	43.1	39.8
$(CH_3)_2HPP$	141	-74.9	-61.2

Experimental Results

Fundamentally, all experimental work on hydrogen storage materials at The University of Alabama has centered on activated polarized σ- or π-bonded frameworks that hold the potential for ready dihydrogen activation, uptake, and eventually release. To this end, a large number of non-traditional valence systems including carbenes, cyanocarbons, and C-B and and B-N systems were examined. During the course of these studies an important lead also arose from the novel valency of a class of stable organic singlet bi-radical systems.

A new coupled bis(imidazolium) dication was discovered that facilitated studies on hydrogen uptake and release from carbene and C-N systems in general. The bicyclic bis(1,1'-formamidinium) salt (**I**) was synthesized and structurally characterized. The dication **I** is closely related to the fused imidazolo-imidazolium ion (**II**) which has also recently been synthesized in our laboratory. The relationship between salts **I** and **II** is that of hydrogen uptake or release with **II** being a "reduced," (stored hydrogen) analog version of **I**. We accomplished the oxidation of **II** to **I** and additional studies were undertaken to find conditions under which hydrogen may be re-added to **I** to reform **II**. The X-ray were determined structures in our laboratories for the cations **I** and **II** for the first time and these are shown as space-filling models.

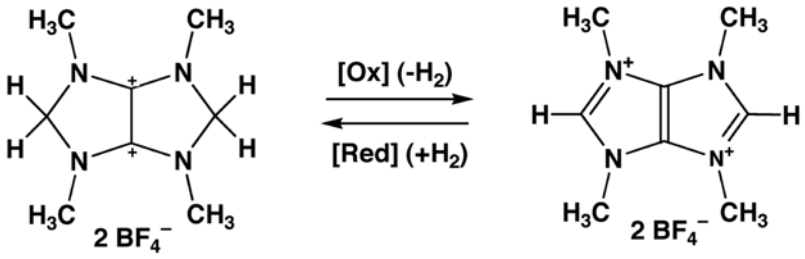

II **I**

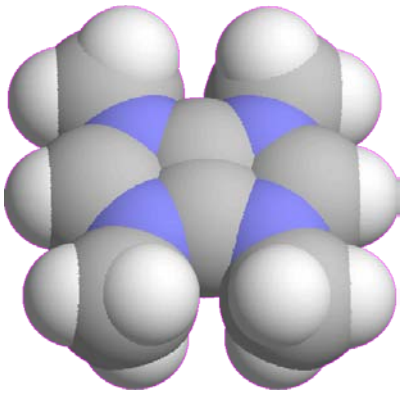

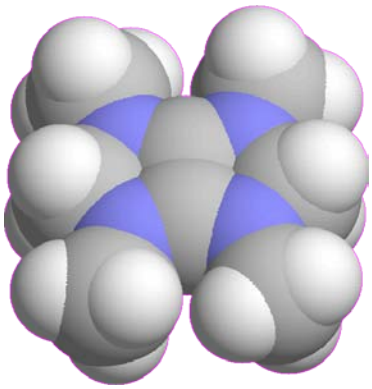

Space-filling models of **I** and **II**.

We were also successful in extension of the 5,5-fused ring systems to other moieties that allowed the introduction of charge separation to facilitate the addition and activation of dihydrogen. One such pair is [3.3.0]-bicyclic system represented structures **III** and **IV**.

Substituents effects are were studied for new derivatives of the zwitterion, **III.** For this zwitterion Lewis acid base pair, we were able to prove the existence and stability of a reduced form **IV** that has incorporated the ele-ments of dihydrogen. Uncatalyzed oxidation of **IV** was not directly observed, but oxidation with reagents such as O_2 and chloranil offer hope that substituent effects may hold the key.

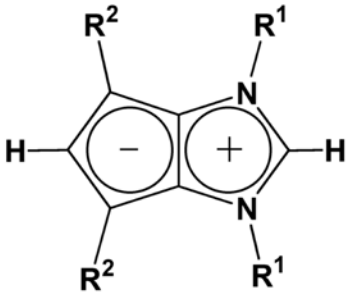

III

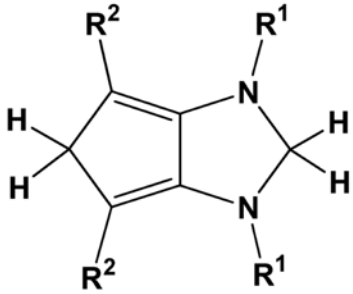

IV

Studies on the bicyclic rings systems were extended to tricyclic systems which incorporated more active hydrogen storage centers per molecular volume (and weight). The [3.3.3]-tricyclic ring system (**V**) with three active methylene (animal) centers for hydrogen storage was synthesized and a range of chemistry relevant to chemical hydrogen storage was studied including related ureas, thioureas, chlorouronium chlorides, organometallic derivatives and corresponding carbenes. Six new X-ray structures on these functionalized compounds were completed.

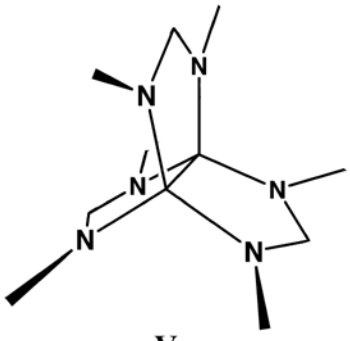

V

An axial oligomerization route for the tricyclic compound was attempted and some progress was achieved although high-degree oligomerization or polymerization needs further development work. The basic axial oligomer is represented by the structure below.

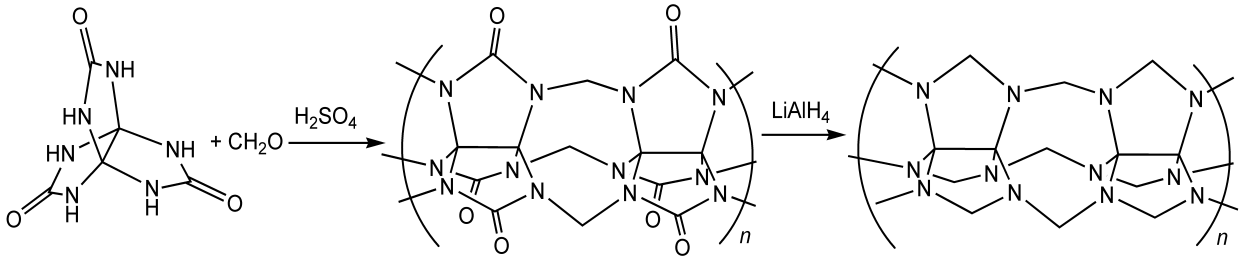

In addition to the axial oligomerization route, a "linear" structure was developed that more readily produced cyclic oligomers as illustrated in the following synthetic scheme. The bridging positions in these oligomeric structures also become potential sites for chemical hydrogen storage and activation. The fully hydrogen depleted material actually achieves the same overall carbon-nitrogen composition as tetracyanoethylene (the basic cyano olefin central to the cyanocarbon storage materials developed and studied as a part of this project.

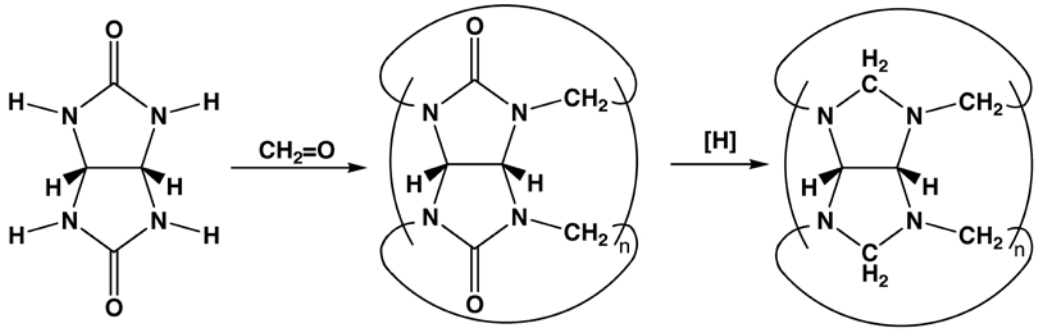

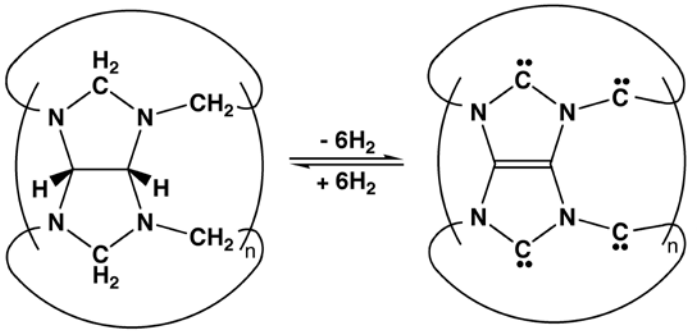

$C_6N_4H_{12}$ C_6N_4 (TCNE Oligomer)

Derivatives of cyanocarbons are excellent candidates for chemical H_2 storage systems. Work on cyanocarbon polymeric systems proved especially promising with special attention given to 5-amino-3,4-dicyanopyrazole (**VI**) and 1,2,5-triamino-3,4-dicyanopyrrole (**VII**) systems. Syntheses of both of these high-heteroatom (nitrogen) content ring systems were accomplished and studies on coupling and polymerization reactions completed. Both ring systems are available from a common precursor, TCNE·H_2 ($C_6N_4H_2$).

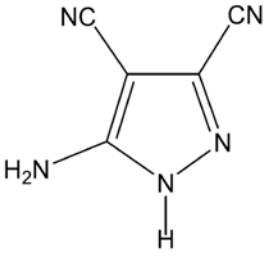

VI

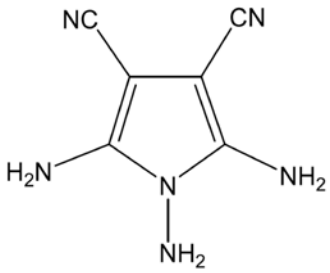

VII

A number of new cyanocarbon oligomers (**VIII**-**X**) allowed us to combine our effort on carbene/imidazolium ion activators for dihydrogen with a charged cyanocarbon fragment for hydrogen storage. Our preliminary work in this highly conjugated system suggested that several stable compositions exist. The most promising candidates were used for more detailed studies. All of the new candidates were fully characterized including X-ray structures on these unprecendented molecular systems. Hydrogen uptake could be relatively easily achieved in the unusual valency cyanocarbon fragments with the more extended frameworks reacting easily. Unfortunately, hydrogen release proved problematic possibly due to skeletal rearrangements on hydrogen uptake and there is a need for new catalyst development.

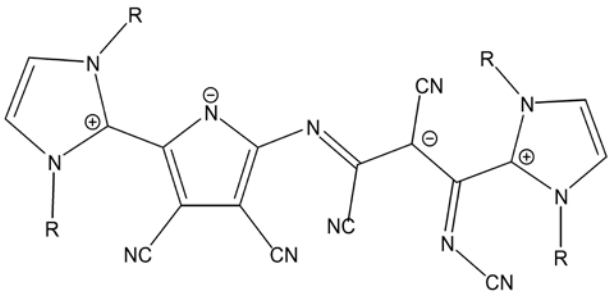

VIII

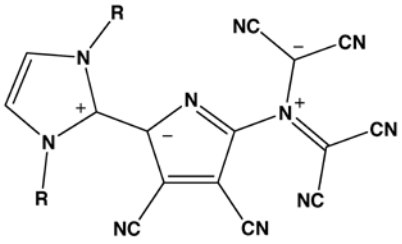

2:1 Adduct

IX

A final interesting variant on the carbene-based hydrogen storage paradigms involved reactions with water. Although the use of water as a "hydrogen source" in these reactions is quite attractive, there was a potential problem in that reaction of the diaminocarbenes with water (**XI** → **XII**) leads to ring opening and the reverse reaction (**XII** → **XI**; ring closure & H_2 elimination) was unknown. We discovered conditions to reverse the ring-opening reaction and recover H_2 (**XII** → **X**). Ultimately, system deterioration on repeated recycling lead to a degradation in performance. In collaboration with the Bertrand group at the University of California-Riverside, it was shown that "CAAC" carbenes could also function in this carbene storage role (Frey, G D.; Lavallo, V; Donnadieu, B; Schoeller, W W.; Bertrand, G. "Facile splitting of hydrogen and ammonia by nucleophilic activation at a single carbon center." *Science* **2007**, *316(5823)*, 439-441.).

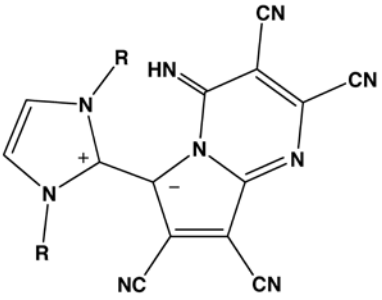

1.75:1 Adduct

X

Work on hydrazine-networked triazine (cyanocarbon) polymers was initiated as a variant on our original cyanocarbon paradigm. Model compounds bearing a single hydrazine unit flanked by two triazine units were synthesized (structure **XIII**). The oxidized diazene was also synthesized and was available for use in the red-ox studies associated with hydrogen uptake and liberation. Synthetic improvements and scale-up were necessary for hydrogen uptake and release on these model

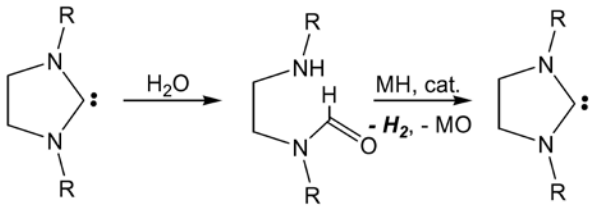

XI **XII** **XI**

systems and proved problematic. Interfacial polymerization was studied as a method for polymer preparation but the attempts at polymer synthesis were unsyccessful on larger scales. This chemistry resembles that used in the synthesis of the structural polymer melamine suggesting that, if successful, hydrogen storage systems could also provide additional structural integrity to the automotive frame. Further work beyond the scope of this current project is needed.

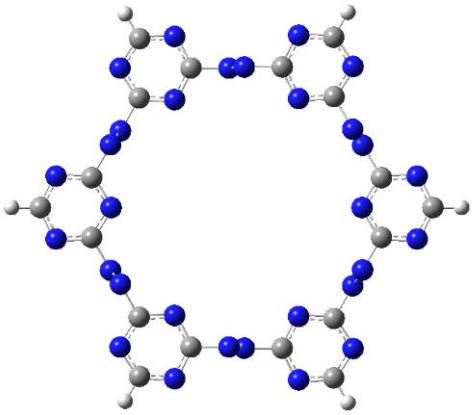

XIII

Work on the hydrazine-networked triazine (cyanocarbon) polymers led to the extension to the unusual valency that arises in a hydrazine-boron system (**XIV**). Interfacial polymerization methodology for polymer preparation proved to be difficult in the parent melamine-like system (**XIII**) so we are also studying this boron-centered triazine polymer offered new possibilities. This novel boron system offers the potential for higher percent weight hydrogen content and experience with this boron polymer system also provided additional insight into the cyanocarbon-hydrazine polymers as well as to borane-amine chemistry to which it is related.

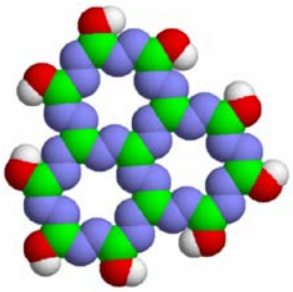

XIV

Experimentally, we separated a B-C bond (in a carbene-borane adduct, **XVI**) by reductive cleavage with hydrogen (hydrogen uptake). Further reduction of B-O (or B-N) bonds at the boron center resulted in even greater hydrogen uptake. New syntheses of imidazolium alkoxy-borates (and imidazolium amino-borates) were necessary to study hydrogen uptake to form imidazolium borohydrides (**XVII**). A promising new synthetic approach has been found in the reaction of carbene-alkoxyborates (or carbene aminoborates) with one additional equivalent of alcohol (or amine), **XVI** → **XVIII**.

Results from collaborators of the Arduengo Group at the Technical University in Braunschweig, Germany demonstrated that dihydrogen can be activated (stored) through the actions of frustrated Lewis acid-base pairs involving imidazole-type carbenes. This is an exciting new step in dihydrogen activation, but is somewhat misleading with regard to the scope of such reactions. Results from our laboratory at The University of Alabama demonstrated that the Lewis acid-base pairs need not be frustrated in their reactivity and that transition metal Lewis acids like iron pentacarbonyl can activate dihydrogen

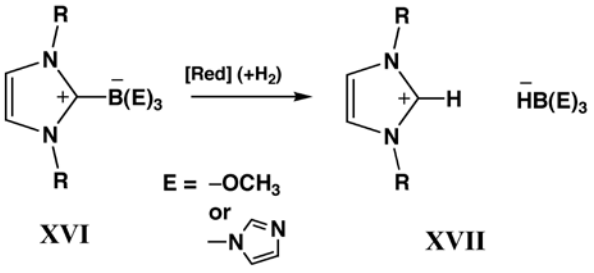

XVI **XVII**

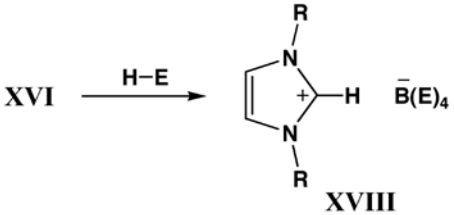

XVIII

smoothly at temperatures as low as -80 ºC (**XIX** to **XX**). This activation system appears to be a complicated sequence of competing reactions (e.g. the room temperature reaction **XIX** to **XXI**). In the absence of dihydrogen at room temperature, a completely different reaction sequence is followed by the Lewis acid-base pair and leads to the formation of an imidazolium acylferrate zwitterion, **XXI**.

Interest in the development of new H_2 activation catalysts, especially for the regeneration of spent fuel, is ongoing. Examples include the use of transition metal hydrides and boron-based Lewis bases at PNNL as well as the processes discussed above in the computational section led by LANL. We discovered a dihydrogen activation step in the presence of carbenes that is a dark-reaction and does not require light (*vide supra*) This reaction was run with $Fe(CO)_5$. Successful reactions with other electrophiles, and our increased understanding of the optimal reaction conditions for the iron system led us to postulate that the dihydrogen-electrophile interaction is a key first step in the activation process. We succeeded in identifying and demonstrating a catalyst to add dihydrogen (H_2) to a carbene center (reversibly). Our work on dihydrogen activation by carbene-electrophile pairs enabled this advance. The dihydrogen addition sequence shown in the first reaction (**XXII** to **XXIII**) demonstrates a catalyst type that is effective in this reaction. The equilibria shown in the lower sequence of reactions indicates all of the steps involved in this addition (storage) - elimination (release) reaction. All of the proposed intermediates (**XXII**, **XXIII**, & **XXIV**) have now been isolated and characterized and their further transformation along equilibria pathways verified. This transformation

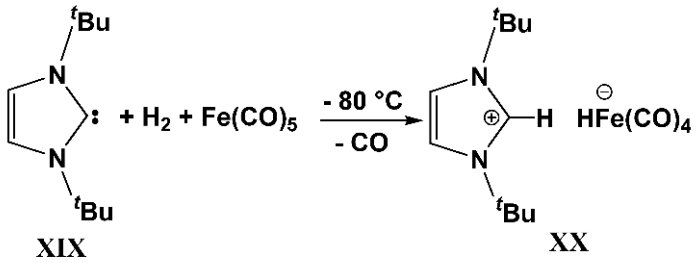

XIX XX

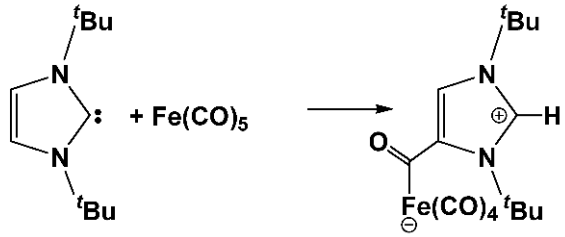

XIX XXI

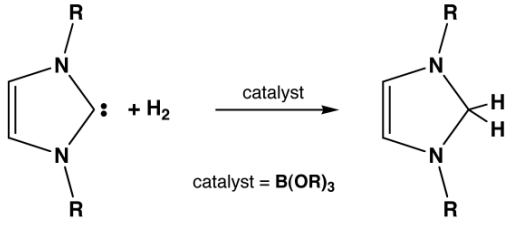

XXII XXIII

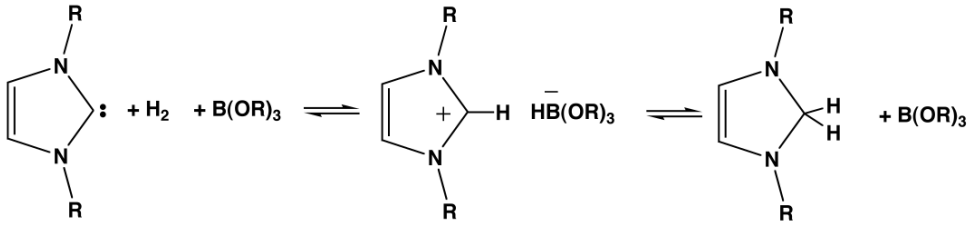

XXIV

provides the first experimental verification for carbenes of the thermodynamic paradigm that we proposed earlier in support of our targets for hydrogen storage research.

A new lead has arisen that effectively amounts to a “masked” carbene. The spiroketal, **XXV**, represents an unprecedented bonding arrangement in which a stable ketal is formed at a urea (imidazolone) center. Spiroketal **XXV** can also be viewed in terms of its valence tautomer (a bicyclic peroxy-carbene) which reveals the competent oxidizing ability of the compound and its ability to be reduced by hydrogen to the zwitterionic imidazolium alkoxide, **XXVI**. Several varients of this novel system were isolated (including E=Cl, E=Ph and E=H) and the solid state X-ray structure of **XXVI** (E=Cl) was determined as shown to the right along with that of a benzo-fused analog.

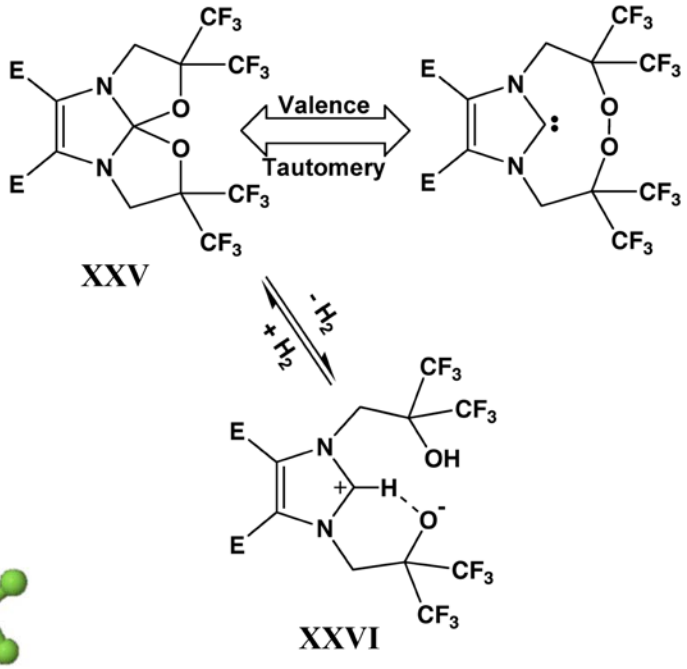

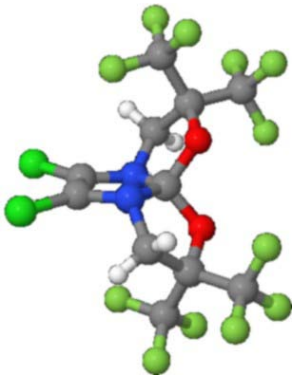

Experimental work on “non-frustrated” acid base pairs continues was pursued with other functionally fuse ring systems. Substituents effects were studied for derivatives of the the new zwitterion, **XXVII.** For this zwitterion Lewis acid base pair, we proved the existence and stability of a reduced form **XXVIII** that has incorporated the elements of dihydro-gen. Uncatalyzed oxidation of **XXVIII** could not be optimized within the scope of this project, but oxidation with reagents such as O_2 provided a key to a reaction sequence through an alternative pathway.

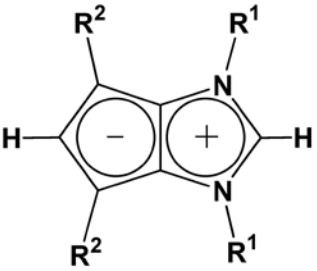

XXVII

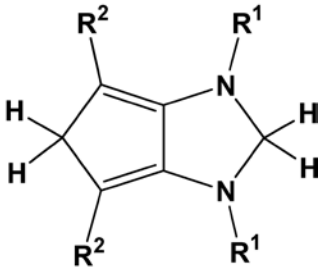

XXVIII

A photochemical catalysis cycle based on an arylmethane dye (methylene blue) was developed for the activation of dihydrogen for storage. The key part of the catalytic, light-activated, storage cycle is illustrated below. The cycle begins with a catalytic quantity of a cyanocarbon anion and large excess of the hydrogen acceptor (in the illustrated case this would be a cyanocarbon, but it could be any hydrogen accepting material). Light reduces the methylene blue cation to leuco-methylene blue by hydride addition and the initial (cyanocarbon) anion is protonated. In a subsequent step leuco-methylene blue transfers a hydride to to the protonated anion to accomplish hydrogen storage while the initially formed H_2-Cyan radical anion (not illustrated) reduces a neutral cyanocarbon to its anion by electron transfer and restarts the cycle. Only the proof of concept could be completed under this project.

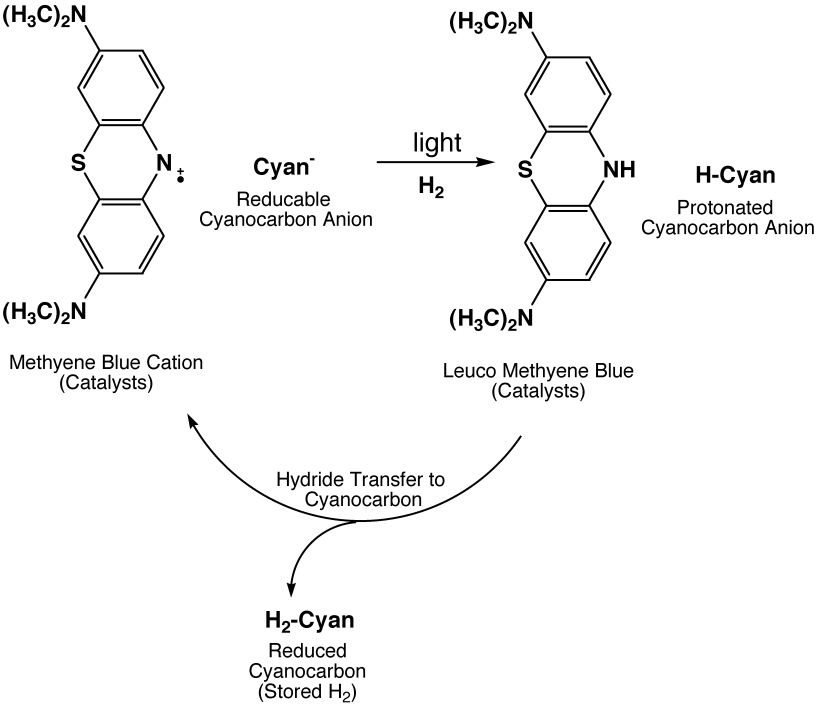

In addition to the photochemical catalysis cycle based on methylene blue for the activation of dihydrogen for storage (*vide supra*), we explored the structural range of dyes that are capable of participating in these reactions. Particular attention is being given to aryl methane dyes (such as *methyl violet 2B*) because we believe that these hold the greatest potential for providing the type of reversible transformation (hydrogenation) that will be required for hydrogen storage systems. It will be important that the dye oxidation and reduction be developed into a catalytic role for hydrogen storage.

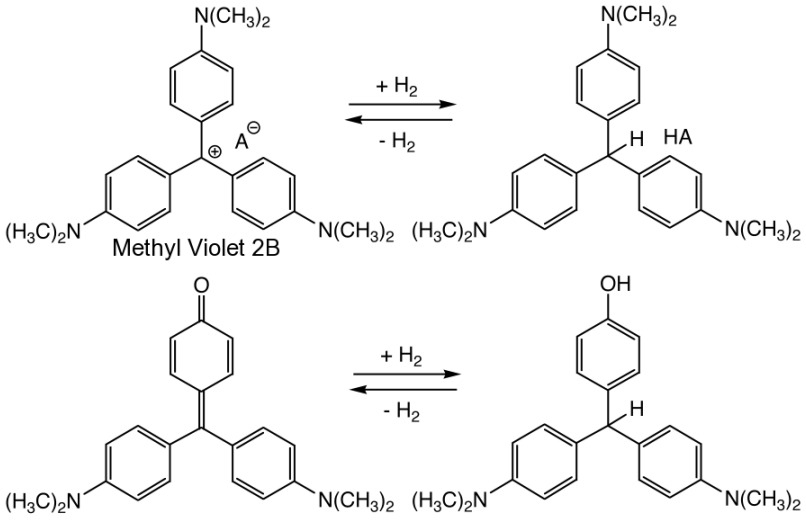

In addition to the carbene and cyanocarbon related systems, work on a diphosphacyclobutadiendiyl proved quite effective for hydrogen storage. The initial phase of this work was reported by us, and further work is being pursued to move the kinetics of this model system into a useful range. Remarkably, even though the biradical is a carbon center single-biradical system hydrogen uptake occures at the phosphorus atoms of this unusual valence system.

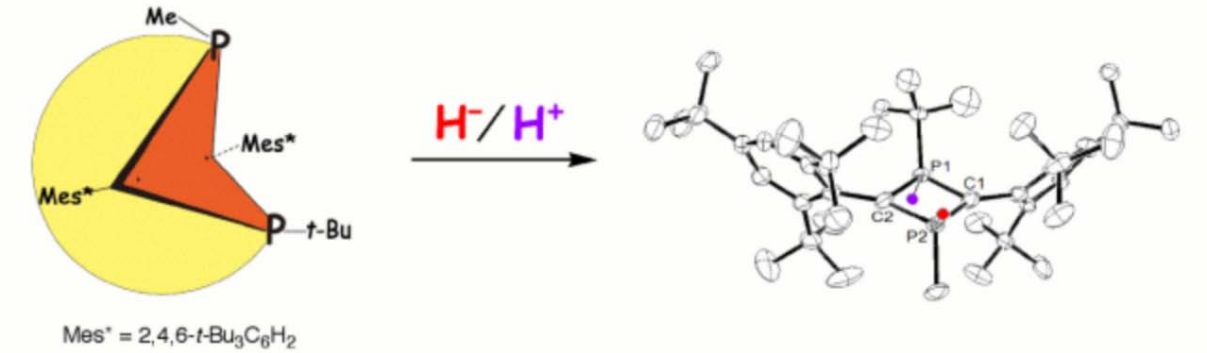

Publications

1. "Thermodynamic Properties of Molecular Borane Amines and the $[BH_4^-][NH_4^+]$ Salt for Chemical Hydrogen Storage Systems from Ab Initio Electronic Structure Theory," D. A. Dixon and M. Gutowski, *J. Phys. Chem. A*, **2005**, *109*, 5129
2. "Thermodynamic Properties of the C_5, C_6, and C_8 n-Alkanes from Ab Initio Electronic Structure Theory," L. Pollack, T. L. Windus, and W. A. de Jong, and D.A. Dixon, J. Phys. Chem. A, **2005**, *109*, 6934.
3. "Thermodynamic Properties of Molecular Borane Phosphines, Alane Amines, and Phosphine Alanes as well as the $[BH_4^-][PH_4^+]$, $[AlH_4^-][NH_4^+]$, and $[AlH_4^-][PH_4^+]$ Salts for Chemical Hydrogen Storage Systems from Ab Initio Electronic Structure Theory," D. J. Grant and D. A. Dixon, *J. Phys. Chem. A*, **2005**, *109*, 10138.
4. "Heats of Formation of the Arduengo Carbene and Various Adducts Including H_2 from Ab Initio Molecular Orbital Theory," D. A. Dixon and A. J. Arduengo, III, *J. Phys. Chem., A.* **2006**, *110*, 1968.
5. "Heats of Formation and Singlet-Triplet Separations of Hydroxymethylene and 1-Hydroxyethylidene," M. H. Matus, M. T. Nguyen, and D. A. Dixon, *J. Phys. Chem., A.* **2006**, *110*, 8864
6. "The lowest energy states of the Group IIIA – Group VA heteronuclear diatomics: BN, BP, AlN, and AlP from Full Configuration Interaction Calculations," Z. Gan, D. J. Grant, R. J. Harrison, and D. A. Dixon, *J. Chem. Phys.* **2006**, *125*, 124311.
7. "The Heats of Formation of Diazene, Hydrazine, $N_2H_3^+$, $N_2H_5^+$, N_2H, and N_2H_3 and the Methyl Derivatives, CH_3NNH, CH_3NNCH_3, and $CH_3HNNHCH_3$," by Myrna H. Matus, Anthony J. Arduengo, III, and David A. Dixon, J. Phys. Chem. A, **2006**, *110*, 10116.
8. "σ- and π-Bond strengths in Main Group 3-5 Compounds," D. Grant and D. A. Dixon, *J. Phys. Chem. A*, **2006**, *110*, 12955.
9. "Oxidation of 2,4-Diphosphacyclobutane-1,4-diyl with Ammoniumyl Antimonate and EPR Study of the Corresponding Cation Radical," Kikuchi, M.; Yoshifuji, M.; Arduengo, III, A. J.; Konovalova, T. A.; Kispert, L. Ito, S.; *Chem. Lett.* **2006**, *35(10)*, 1136
10. "Acid Initiation of Ammonia-Borane Dehydrogenation for Hydrogen Storage" F. H. Stephens, R. T. Baker, M. H. Matus, D. J. Grant, and D. A. Dixon, *Angew Chem. Int. Ed.*, **2007**, *46*, 746 (Cover and VIP article).
11. "Theoretical Prediction of the Heats of Formation of $C_2H_5O^{\bullet}$ Radicals Derived from Ethanol and of the Kinetics of *β*-C–C Scission in the Ethoxy Radical," M. H. Matus, M. T. Nguyen, and D. A. Dixon, *J. Phys. Chem. A*, **2007**, *111*, 113.
12. "Molecular Mechanism for H_2 Release from Amine Borane, BH_3NH_3, Including the Catalytic Role of the Lewis Acid BH_3," M. T. Nguyen, V. S. Nguyen, M. H. Matus, G. Gopakumar, D. A. Dixon, *J. Phys. Chem. A*, **2007**, *111*, 679.
13. "Heats of Formation of Diphosphene, Phosphinophosphinidene, Diphosphine and their Methyl Derivatives, and Mechanism of the Borane-Assisted Hydrogen Release," Myrna H. Matus, Minh Tho Nguyen, and David A. Dixon, *J. Phys. Chem. A*, **2007**, *111*, 1726

14. "Reliable Predictions of the Thermochemistry of Boron-Nitrogen Hydrogen Storage Compounds: $B_xN_xH_y$, x = 2, 3," M. H. Matus, K. D. Anderson, D. M. Camaioni, S. T. Autrey, and D. A. Dixon, *J. Phys. Chem A.*, **2007**, *111*, 4411**.**

15. "Computational Study of the Release of H_2 from Ammonia Borane Dimer $(BH_3NH_3)_2$ and Its Ion Pair Isomers," V. S. Nguyen, M. H. Matus, D. J. Grant, M. T. Nguyen, and D. A. Dixon, *J. Phys. Chem A.*, **2007**, *111*, 8844.

16. "Ammonia Triborane: Theoretical Study of the Mechanism of Hydrogen Release," V, S. Nguyen, M. H. Matus, M. T. Nguyen, and D. A. Dixon, *J. Phys. Chem A.*, **2007**, *111*, 9603.

17. "Heats of Formation of Boron Hydride Anions and Dianions and their Ammonium Salts $[B_nH_m^{y-}][NH_4^+]_y$ with y =1 - 2," M. T. Nguyen, M. H. Matus, and D. A. Dixon, *Inorg. Chem*, **2007**, *46*, 7561

18. "Energetics and Mechanism of the Decomposition of Trifluoromethanol" M. T. Nguyen, M. H. Matus, V. T. Ngan, R. Haiges, K. O. Christie, and D. A. Dixon, *J. Phys. Chem. A*, **2008**, *112*, 1298.

19. "Heats of formation of triplet ethylene, ethylidene, and acetylene," M. T. Nguyen, M. H. Matus, W. A. Lester, Jr., and D. A. Dixon, *J. Phys. Chem. A*, **2008**, *112*, 2082.

20. "Thermochemical Properties of CHFO, CF_2O, and CFO" by M. H. Matus, M. T. Nguyen, D. A. Dixon, and K.O. Christe, *J. Phys. Chem. A* **2008**, *112*, 4973.

21. "Theoretical Study of the Hydrogen Release from Ammonia Alane and the Catalytic Effect of Alane," V. S. Nguyen, M. H. Matus, V. T. Ngan, M. T. Nguyen, and D. A. Dixon, *J. Phys. Chem. C*, **2008**, *112*, 5662.

22. "Reactions of Diborane with Ammonia and Ammonia Borane: Catalytic Effects in Multiple Pathways for Hydrogen Release," V. S. Nguyen, M. H. Matus, M. T. Nguyen, and D. A. Dixon, *J. Phys. Chem.*, **2008**, *112*, 9946-9954.

23. "Quantum Chemical Studies of Alane and Phosphine Derivatives for Chemical Hydrogen Storage," M. T. Nguyen, S. V. Nguyen, M. H. Matus, D. J. Grant, S. Swinnen, and D. A. Dixon, *Prepr. Pap.-Am. Chem. Soc., Div. Fuel Chem*. **2008**, *53 (1)*, 141.

24. "Computational Studies on Regeneration of Boron-Nitrogen Compounds for Hydrogen Fuel Cells," M. H. Matus, D. J. Grant, J. R. Switzer, B**.** L. Davis, F**.** H. Stephens, and D**.** A. Dixon**,** *Prepr. Pap.-Am. Chem. Soc., Div. Fuel Chem*. **2008**, *53 (1)*, 115.

25. "Computational advances in predicting molecular properties for alternative energy solutions," D. A. Dixon, M. T. Nguyen, M. H. Matus, and S. Li, *Prepr. Pap.-Am. Chem. Soc., Div. Fuel Chem*. **2008**, *53 (1)*, 105.

26. "Coordination of aminoborane, NH_2BH_2, dictates selectivity and extent of H_2 release in metal-catalysed ammonia borane dehydrogenation.," V. Pons, R. T. Baker, N. K. Szymczak, D. J. Heldebrant, J. C. Linehan, M. H. Matus, D. J. Grant, D. A. Dixon, *Chem Comm*., **2008**, 6597.

27. "Heats of Formation and Bond Energies of the $H_{(3-n)}BX_n$ compounds for (X = F, Cl, Br, I, NH_2, OH, and SH)," D. J. Grant and D.A. Dixon *J. Phys. Chem. A*, **2009**, *113*, 777.

28. “Diammoniosilane: Computational Prediction of the Thermodynamic Properties of a Potential Chemical Hydrogen Storage System,” D. J. Grant, A. J. Arduengo, III, and D. A. Dixon, *J. Phys. Chem. A*, **2009**, *113*, 750.

29. “Poly(Biradicals): Oligomers of 1,3-Diphosphacyclobutane-2,4-diyl Units” Masaaki Yoshifuji, A.J. Arduengo, III, Shigekazu Ito, Joji Miura, and Noboru Morita) *Angew. Chemie, Int. Ed. Engl.*, **2008**, *47*, 6418.

30. “A Hybrid Organic/Inorganic Benzene,” A. J. V. Marwitz, M. H. Matus, L. N. Zakharov, D. A. Dixon, and S.-Y. Liu, *Angew. Chem. Int. Ed.*, **2009**, *48*, 973.

31. “Thermochemistry and Electronic Structure of Small Boron and Boron Oxide Clusters and Their Anions,” M. T. Nguyen, M. H. Matus, V. T. Ngan, D. J. Grant, and D. A. Dixon, *J. Phys. Chem. A*, **2009**, *113*, 4895

32. “Thermochemistry for the Dehydrogenation of Methyl Substituted Ammonia Borane Compounds,” D. J. Grant, M. H. Matus, K. D. Anderson, D. M. Camaioni, S. Neufeldt, C. F. Lane, and D. A. Dixon, *J. Phys. Chem. A*, **2009**, *113*, 6121.

33. “Efficient Regeneration of Partially Spent Ammonia Borane Fuel,” B. L. Davis, D. A. Dixon, E. B. Garner, J. C. Gordon, M. H. Matus, and F. H. Stephens, *Angew. Chem.*, **2009**, *48*, 6812 (inside cover art)

34. “The Effect of the NH_2 Substituent on NH_3: Hydrazine as an Alternative for Ammonia in Hydrogen Release with Presence of Borane and Alane,” V. S. Nguyen, S. Swinnen, M. H. Matus, M. T. Nguyen, and D. A. Dixon, *Phys. Chem. Chem. Phys.*, **2009**, *11*, 6339

35. “The Hydride and Fluoride Affinities of the $H_{3-n}BX_n$ compounds for (X = F, Cl, Br, I, NH_2, OH, and SH) from High Level Electronic Structure Calculations,” D. J. Grant, D.A. Dixon, R. G. Potter, D. Camaioni, and K.O. Christe, *Inorg. Chem* **2009**, *48*, 8811.

36. “Fundamental Themochemical Properties of Ammonia Borane and Dehydrogenated Derivatives (BNH_n, $n = 1 – 6$),” M. H. Matus, D. J. Grant, M. T. Nguyen, and D. A. Dixon, *J. Phys. Chem. C*, **2009**, *113*, 16553.

37. “Computational Study of Molecular Complexes Based on Ammonia Alane for Chemical Hydrogen Storage,” V. S. Nguyen, S. Swinnen, M. T. Nguyen and D. A. Dixon, *J. Phys. Chem. C* **2009**, 113, 18914.

38. **“**Fused polycyclic nucleophilic carbenes – synthesis, structure, and function,” A. J. Arduengo, III and Luigi I. Iconaru, *Dalton Trans.*, **2009**, 6903.

39. Modeling the Direct Activation of Dihydrogen by a P2C2 Cyclic Biradical: Formation of a Cyclic Bis(P-H λ^5-phosphorane). S. Ito, J. Miura, N. Morita, M. Yoshifuji, and A. J. Arduengo, III, *Inorg. Chem.*, **2009**, *48*, 8063.

40. “Catenation of 1,3-diphosphacyclobutane-2,4-diyl units having 2,4,6-tri-tert-butylphenyl protecting groups and a P-sec-butyl group in the ring,” S. Ito, J. Miura, N. Morita, M. Yoshifuji, and A. J. Arduengo, III, *Z. Anorg. Allg. Chem.*, **2009**, *635*, 488

41. “Dehydrogenation Reactions of Cyclic $C_2B_2N_2H_{12}$ and C_4BNH_{12} Isomers,” Myrna H. Matus, Shih-Yuan Liu, and David A. Dixon, *J. Phys. Chem. A*, **2010**, *114*, 2644

42. "Thermochemical Properties and Electronic Structure of Boron Oxides B_nO_m (n = 5-10, m = 1-2) and Their Anions," T. B. Tai, M. T. Nguyen, and D. A. Dixon, *J. Phys. Chem. A*, **2010**, *114*, 2893.

43. "Thermochemistry and Electronic Structure of Small Boron Clusters (B_n, n = 5 - 13) and Their Anions," T. B. Tai, D. J. Grant, M. T. Nguyen, and D. A. Dixon, *J. Phys. Chem. A*, **2010**, *114*, 994

44. "Hydrogen Storage by Boron-Nitrogen Heterocycles: A Simple Route for Spent Fuel Regeneration," P. G. Campbell, L. N. Zakharov, D. J. Grant, D. A. Dixon, and S.-Y. Liu, *J. Am. Chem. Soc.*, **2010**, *132*, 3289.

45. "Diverse reactions of sterically-protected 1,3-diphosphacyclobutane-2,4-diyls with hydride," Ito, Shigekazu; Miura, Joji; Morita, Noboru; Yoshifuji, Masaaki; Arduengo, Anthony J., III. *Dalton Trans.*, **2010**, *39*, 8281.

Presentations

D. A. Dixon, Invited Lecture, Structure and Function in Chemistry and Biology, Symposium Celebrating the 85th Birthday of Prof. William N. Lipscomb, Shanghai, China, August, 2005

D. A. Dixon, Invited Lecture, Computational Chemistry at the Teraflop and Beyond Symposium, ACS National Meeting, Washington, DC, Aug. 2005

D. A. Dixon, "Computational Studies of Catalytic Reactions," Invited Lecture, XVI Undergraduate Research Symposium, Nanotechnology, Computational Chemistry, and Computational Biology Workshop, San Juan, Puerto Rico, Sept., 2005

D. A. Dixon, "Free Energies of Solvation Based on Molecular Clusters," Invited Presentation, Symposium on Clusters from the Gas Phase to the Bulk, Pacificchem 2005, December 2005, Honolulu, HI.

D. A. Dixon, "Computational Inorganic Fluorine Chemistry," Invited Presentation, Symposium on Advances in Inorganic Fluorine Chemistry, Pacificchem 2005, December 2005, Honolulu, HI.

D. A. Dixon, Invited Lecture, "Computational Thermochemistry," Quantitative Quantum Chemistry, Symposium in honor Thom Dunning, Santa Fe, March, 2006.

D. A. Dixon, Invited Lecture, "Computational Approaches to the prediction of reaction kinetics for catalysis and chemical hydrogen storage," Solvay Three Day Symposium on Chemical Reactivity, Brussels, April, 2006.

D. A. Dixon, Tutorial on Hydrogen Storage, "Computational Chemistry for H_2 Storage: Theoretical Background and Applications," Materials Research Society Annual Spring Meeting, April, 2006.

D. A. Dixon, Invited Lecture, "High level computational approaches to the prediction of the thermodynamics of chemical hydrogen storage systems," Symposium on Advances in Hydrogen Storage, Materials Research Society Annual Spring Meeting, April, 2006.

D. A. Dixon, Invited Lecture, "High level computational approaches to the prediction of the thermodynamics of chemical hydrogen storage systems," Theory Focus Session on Hydrogen Storage Materials, U.S. DOE H_2 Review Meeting, Crystal City, VA, May, 2006.

Arduengo, III, A. J.; Dolphin, J. Gurau, G.; Yamamoto, Y.; Yamamichi, H. Invited Lecture, "Unusual Valence States of Carbon and other Main-Group Elements" 2nd International Symposium of Core-to-Core Program on Main Group Chemistry", Tokyo, the University of Tokyo, Japan, Aug. 26 -28, 2006.

D. A. Dixon, Invited Lecture, New Aspects of Computational Main Group Chemistry," 2nd International Symposium of Core-to-Core Program on Main Group Chemistry", Tokyo, the University of Tokyo, Japan, Aug. 26 -28, 2006.

D. A. Dixon, Invited Lecture, "Computational Studies of Solvation Processes: Acid-Base Chemistry," XVII Undergraduate Research Symposium, September 15-16, 2006, San Juan, Puerto Rico

D. A. Dixon, Invited Lecture, "High Level Computational Chemistry Approaches to the Prediction of the Properties of Chemical Hydrogen Storage Systems," First Joint NEDO/AIST/LANL Workshop on Fuel Cells and Hydrogen Storage, Santa Fe, August 28 -30, 2006.

M. H. Matus, D. J. Grant, M. T. Nguyen, and D. A. Dixon, Poster: "Computational Study of Boron-Amine Compounds for Chemical Hydrogen Storage," 35th Annual Conference of the Southeast Theoretical Chemists' Association, May 19 and 20, 2006. Emory University, Atlanta, GA.

M. T. Nguyen, G. Gopakumar, Vinh S. Nguyen, Myrna H. Matus, and David A. Dixon, Poster: "BH_3 as a Catalyst for H_2-Generation Reactions: Theoretical Study of the Molecular Mechanism," 35th Annual Conference of the Southeast Theoretical Chemists' Association, May 19 and 20, 2006. Emory University, Atlanta, GA.

D. J. Grant, J. Switzer, M. H. Matus, Z. Gan, R. J. Harrison and D. A. Dixon, Poster: **"**Structure, Bond Energies and Heats of Formation of Group IIIA – Group VA Molecules for Chemical Hydrogen Storage," 5th Annual Conference of the Southeast Theoretical Chemists' Association, May 19 and 20, 2006. Emory University, Atlanta, GA.

V. S. Nguyen, M. T. Nguyen, G. Gopakumar, M. H. Matus, and D. A. Dixon, Poster, **"**BH_3 as a Catalyst for H_2-Generation Reactions: Theoretical Study of the Molecular Mechanism," Faraday Discussion 135, September 4 to 6, 2006. Manchester University, United Kingdom. (no DOE travel funds used)

A. J. Arduengo, *Novel Architectures Involving Imidazol-2-ylidenes: Structure and Chemistry*, Chemistry Department, University of Zurich, Switzerland, Nov. 2007.

A. J. Arduengo, *Novel Architectures Involving Imidazol-2-ylidenes: Structure and Chemistry*, Chemistry Department, University of Bonn, Germany, Nov. 2007.

A. J. Arduengo, *Novel Architectures Involving Imidazol-2-ylidenes: Structure and Chemistry*, Chemistry Department, Technical University of Braunschweig, Germany Dec. 2007.

D. A. Dixon, Invited Lecture, *Recent Advances in Computational Inorganic Chemistry*, Loker Hydrocarbon Research Institute and Department of Chemistry Symposium Honoring Professor Karl O. Christe on the Occasion of his 70th Birthday, University of Southern California, Los Angeles, CA, Jan. 2007

D. A. Dixon, Invited Lecture, *Recent Advances in Computational Inorganic Chemistry*, Chemical Engineering Department, Mississippi State, Starksville, MS, Jan. 2007.

D. A. Dixon, Invited Lecture: *Recent Advances in Computational Inorganic Chemistry*, Physical Chemistry Division, Chemistry Department, University of Maryland, College Park, MD, Feb. 2007.

D. A. Dixon, Invited Lecture: *Recent Advances in Computational Inorganic Chemistry*, Inorganic Division, Chemistry Department, Florida State University, Tallahassee, FL, March, 2007

M. H. Matus, Talk, *Computational Results for Regeneration*, Regeneration Team Meeting, Los Alamos National Laboratory, NM, February, 2007.

M. H. Matus, Seminar, *Computational Modeling of Boron-Nitrogen Compounds for Chemical Hydrogen Storage*, Modeling/Simulation Talks, Department of Computer Science, University of Alabama, Tuscaloosa, AL, March, 2007.

D. A. Dixon, "Computational Advances in Predicting the Behavior of Inorganic Compounds," 20th Coulson Lecture, Department of Chemistry, The University of Georgia, Athens GA, April, 2007.

D. A. Dixon and A.J. Arduengo, III, "Main Group Element and Organic Chemistry for Hydrogen Storage and Activation," Presentation, DOE Hydrogen Review, Arlington VA, May, 2006.

M. T. Nguyen, M.H. Matus, V.S. Nguyen, and D.A. Dixon, Talk, *Molecular Mechanism of Hydrogen Release Reactions from Boron – Nitrogen Compounds*, Southeastern Theoretical Chemistry Association (SETCA) Annual Meeting, Virginia Tech, Blacksburg, VA, May 2007.

M. H. Matus, K.D. Anderson, Donald M. Camaioni, S. T. Autrey, and D. A. Dixon, Poster Presentation, *Computational Studies on Boron-Nitrogen Compounds and Methylated Derivatives For Chemical Hydrogen Storage*, Southeastern Theoretical Chemistry Association (SETCA) Annual Meeting, Virginia Tech, Blacksburg, VA, May 2007.

M. H. Matus, D. J. Grant, S. V. Nguyen, K. D. Anderson, M. T. Nguyen, D. M. Camaioni, S. T. Autrey, and D. A. Dixon Invited Presentation, *High Accuracy Computational Studies Of Boron-Nitrogen Compounds For Chemical Hydrogen Storage*, American Chemical Society (ACS), Division of Fuel Chemistry, Fall National Meeting, Boston, MA, August 2007

D. A. Dixon, Plenary lecture, Alternative energy workshop OASCR, Rockville, MD, September, 2007

M. H. Matus, Presentation, *The University of Alabama's Updates on Regen/First Fuel Load*, Chemical Hydrogen Storage Center Annual Meeting, Denver, CO, November, 2007.

M. H. Matus and D. A. Dixon, Presentation, *Estudios Computacionales de Compuestos de Boro y Nitrógeno para el Almacenamiento Químico de Hidrógeno*, "Computational Studies Of Boron-Nitrogen Compounds For Chemical Hydrogen Storage", VI Reunión Mexicana de Fisicoquímica Teórica, San Miguel Regla, Hgo., Mexico, November, 2007.

A. J. Arduengo, "The Evolution of Nucleophilic Carbene Chemistry," Anthony J. Arduengo, III Abschlusskolloquium of the DFG-Schwerpunktprogramm, Münster, Germany, September 28-30, 2007.

A. J. Arduengo, "Die jüngsten Carben-Werkzeuge" Anthony J. Arduengo, Heidelberg, Germany, December 17, 2007.

A. J. Arduengo, "New Structural Units Based on Imidazol(in)-2-ylidenes - Ligands for Transition Metals and Main Group Elements" Anthony J. Arduengo, Hannover, Germany, December 18, 2007.

A. J. Arduengo, "Modifications of Imidazole-Derived Carbenes" Anthony, J. Arduengo, III, Bonn, Germany, December 13, 2007

M. H. Matus, Presentation, *The University of Alabama's Updates on Regen/First Fuel Load*, Chemical Hydrogen Storage Center Annual Meeting, Denver, CO, November, 2007.

M. H. Matus and D. A. Dixon, Presentation, *Estudios Computacionales de Compuestos de Boro y Nitrógeno para el Almacenamiento Químico de Hidrógeno,* "Computational Studies Of Boron-Nitrogen Compounds For Chemical Hydrogen Storage", VI Reunión Mexicana de Fisicoquímica Teórica, San Miguel Regla, Hgo., Mexico, November, 2007.

A. J. Arduengo, "The Evolution of Nucleophilic Carbene Chemistry," Anthony J. Arduengo, III Abschlusskolloquium of the DFG-Schwerpunktprogramm, Münster, Germany, September 28-30, 2007.

A. J. Arduengo, "Die jüngsten Carben-Werkzeuge" Anthony J. Arduengo, Heidelberg, Germany, December 17, 2007.

A. J. Arduengo, "New Structural Units Based on Imidazol(in)-2-ylidenes - Ligands for Transition Metals and Main Group Elements" Anthony J. Arduengo, Hannover, Germany, December 18, 2007.

A. J. Arduengo, "Modifications of Imidazole-Derived Carbenes" Anthony, J. Arduengo, III, Bonn, Germany, December 13, 2007

M. H. Matus, D. J. Grant, J. R. Switzer, B. L. Davis, F. H. Stephens, and D. A. Dixon, "Computational Studies on Regeneration of Boron-Nitrogen Compounds for Hydrogen Fuel Cells," 37th Annual Conference of the Southeast Theoretical Chemists' Association, May, 2008, The University of Alabama.

D. J. Grant, J. R. Switzer, M. H. Matus, and D. A. Dixon, "Computational studies of the thermodynamics of PF_xO_y and SF_xO_y compounds: bond energy relationships," Poster, 37th Annual Conference of the Southeast Theoretical Chemists' Association, May, 2008, The University of Alabama.

D. A .Dixon, organizer, 37th Annual Conference of the Southeast Theoretical Chemists' Association, May, 2007, The University of Alabama (~70 attendees).

D. A. Dixon and A.J. Arduengo, "Main Group Element Chemistry in Service of Hydrogen Storage and Activation,"DOE Hydrogen Annual Review, Crystal City, June, 2008.

D. A.. Dixon, "Fuel Cell & Hydrogen Research at UA," presentation to the Honorable Jeff Sessions, U.S. Senator (AL, R), The University of Alabama, Tuscaloosa AL, June, 2008.

A. J. Arduengo, III, "Imidazol-2-ylidene zu polycyclischen Carbenen: Strukturen, die aus der Reihe tanzen," Kolloquium Münchener Chemische Ges., Ludwigs Maximilians Universität München, Germany, July, 2008.

A. J. Arduengo, III, "Die jüngste Carben-Chemie: Polycyclische Imidazol-2-ylidene," Organisch-chemisches Kolloquium, Universität zur Köln, Germany, May 2008.

A. J. Arduengo, III, "Polycyclische Imidazol-2-ylidene: Struckturen, die aus der Reihe tanzten," Anorganisch-chemisches Kolloquium, Universität Hamburg, Germany, May, 2008.

A. J. Arduengo, III, "Die jüngste Chemie von Imidazol-2-ylidene: Reaktivität, die aus der Reihe tanzt," Organisch-chemisches Kolloquium, Universität Oldenburg, Germany, May, 2008.

D. A. Dixon, "Computational Chemistry for Design of Materials for Hydrogen Storage, Activation, and Regeneration," D.A. Dixon, Invited presentation, Joint LANL-NEDO Workshop on Hydrogen Storage and Fuel Cells, San Diego, Sept. 2008.

D. A. Dixon, "UA Computational Work for the Center of Excellence," Annual Meetig of the DOE Center of Excellence in Chemical Hydrogen Storage, Nov. 8-9, 2008, Denver CO

D. A. Dixon, "New Concepts in the Energetics of Main Group Compounds," Invited Presentation, Main Group and f-Element Chemistry Symposium, Southeastern Regional Meeting of the American Chemical Society (SERMACS), November 14, 2008, Nashville, TN

D. A. Dixon, "Recent UA Computational Work for the DOE Center of Excellence in Chemical Hydrogen Storage," Invited Presentation to the DOE Center of Excellence in Metal Hydrides Meeting, Dec. 18, 2008, California Institute of Technology, Pasadena CA.

A.J. Arduengo, III, "Poly(imidazol(in)ylidene) und Chelatisierende Imidazol(in)ylidene:

Entwicklungen aus der Carben-Chemie," Organisch-Chemisches-Kolloquium International, Marburg, Germany (December, 2008)

A.J. Arduengo, III, "Neue Ringsysteme und Chelatstrukturen aus Imidazol(in)ylidene," Organic Colloqium International, Gieβen, Germany (December, 2008)

D.A. Dixon, invited presentation, "Prediction of Reliable Bond Energies and Molecular Properties for Fluorinated Compounds," 19th Winter Fluorine Conference, St. Petersburg Beach, FL, Jan. 2009.

D.A. Dixon, plenary lecture, "Prediction of Reliable Heats of Formation and Bond Dissociation Energies," 49th Sanibel Symposium, Feb. 2009, St. Simons Island, Georgia

D.A. Dixon, Invited lecture, "Computational chemistry for catalysis, hydrogen storage, and the stratosphere," Mississippi State University, March, 2009, Starkville, MS

D.A. Dixon, "Computational Chemistry Support for the DOE CoE in Chemical Hydrogen Storage," Tech Team Review, March 2009, Detroit MI.

M. Vasiliu, A. J. Arduengo III, and D. D. Dixon, "Acidity and basicity for azole.xBH_3 compounds for chemical hydrogen storage," 38th Annual Conference of the Southeast Theoretical Chemists' Association, May, 2009, Duke University, Durham NC.

E. B Garner III, D. J. Grant, M. H. Matus, D.A Dixon, and K. A. Peterson, "Prediction of Thermodynamic Properties for H_2 Spent Fuel Regeneration Schemes and Heats of Formation of IOOX Compounds," 38th Annual Conference of the Southeast Theoretical Chemists' Association, May, 2009, Duke University, Durham NC

D.A. Dixon and A.J. Arduengo, "Main Group Element and Organic Chemistry for Hydrogen Storage and Activation,"DOE Hydrogen Annual Review, Crystal City, May, 2009.

D.A. Dixon, Co-chair with T. Autrey of American Chemical Society Fuels Division, National Meeting, Washington D.C., August, 2009 Symposium, "Advances in Experimental and Computational Studies of Materials for Hydrogen Storage"

D. A. Dixon, E. B. Garner, M. H. Matus, and D. M. Camaioni **"**Computational approaches for the prediction of molecular properties for chemical hydrogen systems: release and regeneration," American Chemical Society Fuels Division, National Meeting, Washington D.C., August, 2009 Symposium, "Advances in Experimental and Computational Studies of Materials for Hydrogen Storage"